LIQUID ELECTRON MICROSCOPY FOR BIOMATERIALS CHARACTERIZATION

STRATEGIES FOR LIQUID ELECTRON MICROSCOPY OF BIOMATERIALS: CHARACTERIZING HYDRATED STRUCTURES & DYNAMIC PROCESSES

By LIZA-ANASTASIA DICECCO, B.A.Sc., M.A.Sc.

A Thesis Submitted to the School of Graduate Studies in Partial Fulfilment of the Requirements for the Degree Doctor of Philosophy

McMaster University

Copyright © by Liza-Anastasia DiCecco, May 2023

Doctor of Philosophy (Materials Engineering)

McMaster University (2023)

Hamilton, ON, Canada

TITLE:	Strategies for Liquid Electron Microscopy of Biomaterials: Characterizing Hydrated Structures & Dynamic Processes
AUTHOR:	Liza-Anastasia DiCecco, B.A.Sc., M.A.Sc. (McMaster University)
SUPERVISOR:	Prof. Dr. Kathryn Grandfield
NUMBER OF PAGES:	xxvi, 163

Dedication

To Anne, thank you for helping raise me to be the independent woman I am today.

Love & miss you always.

Thesis Lay Abstract

In the electron microscopy (EM) community, there is a need for improved methodologies for high-resolution liquid imaging of biological materials and dynamic processes. Imaging biological structures and reactions in hydrated biomimetic environments improves our understanding of their true nature, thus providing better insight into how they behave in the human body. While liquid EM methods have surged in publications recently, the field is still in its infancy; limited works present best practice strategies, and several challenges remain for their effective implementation. To address these shortcomings, this thesis aims to strategically explore the improvement of liquid EM of biomaterials and real-time dynamic processes through two key methods: room temperature ionic liquid treatment for scanning EM and liquid cell transmission EM. Using these novel techniques, the research explores the characterization of hard-tissue systems relevant to bone and seeks to provide new means of exploring structurally biological culprits behind diseases like COVID-19.

Abstract

Advances in micro/nano-fabrication, thin electron transparent materials, holder designs, and acquisition methods have made it possible to perform meaningful experiments using liquid electron microscopy (liquid EM). Liquid EM provides researchers with micro-to-nano scale tools to explore biomaterials in liquid environments capable of capturing dynamic *in situ* reactions, providing characterization means in mimetic conditions to the human body. However, these emerging techniques remain in their infancy; limited work presents best practice strategies, and several challenges remain for their effective implementation, particularly for beam-sensitive, soft biological materials. This thesis seeks to address these shortcomings by exploring strategies for liquid EM of biomaterials and real-time dynamic processes using two key methods: room temperature ionic liquid (RTIL) treatment for scanning EM (SEM) and liquid cell transmission EM (TEM). With these techniques, the research explores the characterization of hard-tissue systems relevant to bone and seeks to provide new methods of exploring structurally biological culprits behind diseases like COVID-19. Research in this thesis is presented by increasing complexity, touching on three themes: (i) *exploring* liquid EM for the first time using RTILs for SEM of biological samples notably bone (*static, micro-scale*), (ii) *developing* new methods for high-resolution liquid biological TEM of viruses (*static, nano-scale*), and (iii) *applying* novel liquid TEM to dynamic biomineralization systems (*dynamic, nano-scale*).

After review articles serve as introductory material in Chapter 2, in Chapter 3, healthy and pathological bone was *explored* in hydrated conditions with liquid SEM using a new workflow involving RTIL treatment, demonstrated to be highly efficient for biological SEM. Moving to the nanoscale, Chapter 4 presents a commercial liquid TEM option and a new liquid TEM clipped enclosure *developed* for imaging biological specimens, specifically virus assemblies such as Rotavirus and SARS-CoV-2. Combined with automated acquisition tools and low-dose direct electron detection, enclosures resolved high-resolution structural features in the range of ~3.5 Å – 10 Å and were correlatively used for cryo TEM. Chapter 5 *applies* these liquid TEM methods to study collagen mineralization, revealing in high-resolution the presence of precursor calcium phosphate mineral phases, important transitional phases to mineral platelets found in mineralized tissues. But – dynamic reactions were not captured, attributed to confinement effects, lack of heating functionality, and cumulative beam damage experienced. Chapter 6 overcomes these challenges by optimizing collagen-liquid encapsulation within a commercial liquid TEM holder mimicking physiological conditions at 37°C. *Dynamic* nanoscale interactions were highlighted, where evidence of the coexistence of amorphous precursor phases involving polymer-induced liquid as well as particle attachment was presented within this model. Several liquid TEM challenges remain particularly beam sensitivity and distribution for biomaterials, providing many exciting avenues in future to explore. Taken together, this thesis is advancing characterization through the development and applied use of new liquid EM strategies for studying biomaterials and dynamic reactions. Insights on these reactions and structures anticipate leading to a better understanding of diseases and treatment pathways, the key to moving Canada's health care system forward.

Acknowledgements

There are many people to whom I must express my appreciation and acknowledge for their support during my doctoral studies at McMaster University. For my doctoral success, first and foremost, I would like to express my sincerest and deepest gratitude to my advisor Dr. Kathryn Grandfield for her guidance, mentorship, and continuous support throughout my graduate studies. Kathryn has been one of my biggest cheerleaders to date, always pushing me toward exciting opportunities for my betterment. I would like to extend a big thank you to my committee members, Dr. Leyla Soleymani and Dr. Kyla Sask, for their support, helpful feedback, and insightful suggestions. I thank my external examiner, Dr. Joe Patterson, for agreeing to take part in my thesis defence and for contributing to my Ph.D. journey. I would also like to thank all the wonderful collaborators I have had the chance to work with over the years, most notably Dr. Deborah F. Kelly and Dr. Eli D. Sone for their support, informative research discussions, training, and expert insights into my research.

Notably, I must thank my family and friends next for their love and support throughout my studies, especially during a global pandemic when I needed it the most. The biggest thank-you of all goes out to my partner Anthony Gudisey, for all the love and support he has given me throughout my studies. Every hug, kiss, and sweet nothing helped bring me forward each step, making me feel like the luckiest person alive and not like a miserable graduate student. Another big thank you goes out to my twin sister Alexa, who has proofread more papers of mine than I can count and I have always been able to count on.
I would like next express my sincerest gratitude to my research colleagues, particularly Alyssa Williams, Chiara Micheletti, Alessandra Merlo, Dakota Binkley, Samantha Berry Dr. Tengteng (Toni) Tang, Dr. Joseph Deering, Dr. Bryan Lee, Dr. Shane Scott, Dr. Jing Zhang, and the GRG undergraduate students I have worked with over the years. I truly appreciate all the support, guidance, training, and company that you have provided me in my studies, but I appreciate most all joy you have brought to my life at McMaster.

A special thanks go out to all the hard-working and amazing staff members that I have worked with at McMaster University, who have gone above and beyond to help support me in my research endeavours. Particularly, I have more thanks than I can offer to the staff of the Canadian Centre for Electron Microscopy who helped flame my passion for microscopy, especially Carmen Andrei, Natalie Hamada, Jhoynner Martinez, Chris Butcher, Travis Casagrande, Marcia Reid, Samantha Stambula, and Brian Langelier. Thank you to Dr. Hatem Zurob, our Materials Science and Engineering Department Chair, for being an advocate for me and helping make McMaster feel more like home.

Lastly, I would like to acknowledge support from the Natural Sciences and Engineering Research Council of Canada through the Vanier Canada Graduate Scholarship. Many others have positively impacted me along this journey, for anyone that I may have overlooked and for readers taking the time to go through this, I thank you!

Table of Content

List of Figures

List of Tables

List of All Abbreviations and Symbols

2D	Two-dimensional or two-dimensions
3D	Three-dimensional or three-dimensions
AAV	Adeno-associated virus
ACC	Amorphous calcium carbonate
ACP	Amorphous calcium phosphate
BF	Bright field
[BMI][BF_4]	1-butyl-3-methyl imidazolium tetrafluoroborate
BSE	Backscattered electron
$CaCO_3$	Calcium carbonate
CaOx	Calcium oxalate
CaP	Calcium phosphate
COVID-19	Coronavirus disease of 2019
Cryo	Cryogenic
DE	Direct electron
DED	Direct electron detector
DQE	Detective quantum efficiency
EDX	Energy-dispersive X-ray spectroscopy
EELS	Electron Energy Loss Spectroscopy
EM	Electron microscopy
[EMI][BF_4]	1-ethyl-3-methylimidazolium tetrafluoroborate
HA	Hydroxyapatite
HAADF	High-angle annular dark-field
HIV	Human immunodeficiency virus
HR	High-resolution
HRTEM	High-resolution TEM
Liquid EM	Liquid electron microscopy
Liquid ET	Liquid electron tomography
LLPS	Liquid-liquid phase separation
Na-Cit	Sodium citrate
NCP	Non-collagenous protein
pAsp	Poly-L-aspartic acid
LAsp	L-aspartic acid
PAA	Sodium poly-acrylate
PDB	Protein database
PILP	Polymer-induced liquid precursor
PNCs	Pre-nucleation clusters
PSS	Polystyrene sulphonate
ROI	Region of interest
RTIL	Room-temperature ionic liquid
SAED	Selective area electron diffraction
SE	Secondary electron
SEM	Scanning transmission electron microscopy
SiN/SiNx	Silicon nitride
TEM	Transmission electron microscopy

Declaration of Academic Achievement

The major components of my doctoral thesis are published, submitted, and/or in manuscript form with the intent to publish in scholarly peer-reviewed journals. The thesis is developed as a sandwich thesis based upon the following papers, listed in sequence and referred to in the text by their chapter numbers as follows:

(Ch. 3) **DiCecco, L.-A.,** D'Elia, A., Quenneville, C., Soleymani, L., and Grandfield, K. Ionic liquid treatment for efficient sample preparation of hydrated bone for scanning electron microscopy. 2022. *Micron,* Vol 15 (103192). DOI: 10.1016/j.micron.2021.103192

Contributions: The work conducted in Chapter 3 was conceptualized and planned by myself with insights from Kathryn Grandfield, where I proposed the idea of using the specific ionic liquids to image unfixed, hydrated healthy and osteoporotic bone structures. Cheryl Quenneville was our consulting bone expert and provided the samples used in this study. Data curation and formal analysis were primarily done by myself. Andrew D'Elia assisted with the preparation of bone samples for this work and contributed insights into what treatment to use for experiments as well as the manuscript review. The manuscript was primarily written and reviewed by myself, with editing from all the listed contributing authors. This manuscript has been published in the journal *Micron.*

(Ch. 4) **DiCecco, L.-A.*,** Berry, S.*, Jonaid, G.*, Solares, M.J., Kaylor, L., Gray, J.L., Bator, C., Dearnaley, W.J., Spilman, M., Dressel-Dukes, M.J., Grandfield, K., McDonald Esstman, S. M., and Kelly, D.F. Advancing high-resolution imaging of virus assemblies in liquid and ice. 2022. *Journal of Visualized Experiments,* 2022 Jul (185). DOI: 10.3791/63856 [Invited]
** Indicates equal contribution.*

Contributions: The work conducted in Chapter 4 was conceptualized by myself and Deborah F. Kelly, to create an article highlighting liquid electron microscopy techniques for virus imaging and correlative methods for cryo imaging. A major focus of the work is on a new clipping-based liquid transmission electron microscopy enclosure method, which I developed with Deborah F. Kelly and Jennifer L. Gray. I came up with the concept of trying to freeze these enclosures in liquid nitrogen, which was successfully imaged and a novelty of these clipped liquid enclosures. The article focuses on three high-resolution virus datasets imaged in cryo and liquid conditions, where I focused on data curation and analysis. I made the liquid enclosures and imaged two-thirds of the virus structures featured, notably the Rotavirus and SARS-CoV-2 particle datasets, with assistance from Carol Bator, Jennifer L. Gray, and Deborah F. Kelly. Carol Bator, Jennifer L. Gray, and Deborah F. Kelly imaged the AAV datasets. I did the reconstruction data image analysis of the Rotavirus sample and assisted Samantha Berry with the SARS-CoV-2 particle datasets; GM Jonaid did the data analysis for the AAV sample. Sarah M. McDonald Esstman was our consulting expert in virology and provided some of the samples while

Samantha Berry, Maria Solares, and Liam Kaylor did the wet-lab sample purification and preparation. William J. Dearnaley's primary focus was data management while Madeline J. Dressel-Dukes and Michael Spilman were our consulting experts and collaborators for liquid electron microscopy and direct-electron detector data acquisition, respectively. The manuscript was primarily written and reviewed by myself and Deborah F. Kelly, with minor writing and editing contributions from all the listed contributing authors. This manuscript has been published in the *Journal of Visualized Experiments*, which includes a freely accessible video tutorial on the methods described within the article.

(Ch. 5) **DiCecco, L.-A.,** Gao, R., Kelly, D.F., Sone, E.D., and Grandfield, K. Liquid transmission electron microscopy for probing collagen biomineralization. *In submission format.*

Contributions: The work conducted in Chapter 5 was conceptualized by myself, where I proposed the idea of using the novel clipped liquid enclosures developed in Chapter 4 to investigate collagen mineralization processes in hydrated conditions. Here, I prepared mineralization experiments and primarily led the data curation and formal analysis. Eli D. Sone and Kathryn Grandfield provided insights into the analysis and helped guide directions for the research. Ruixin Gao provided collagen samples and mineralization reagents for the mineralization experiments, where Ruixin Gao and Eli D. Sone together with their team optimized separately the calcium phosphate poly-L-aspartic acid *in vitro* collagen mineralization model used in this paper. Deborah F. Kelly aided as a consulting expert on the liquid EM experiments and provided the imaging and technical resources to conduct these experiments. The manuscript was primarily written and reviewed by myself, with editing from all the listed contributing authors. The manuscript is in submission format.

(Ch. 6) **DiCecco, L.-A.,** Gao, R., Sone, E.D., and Grandfield, K. Towards Understanding Dynamics Behind Collagen Mineralization Through *In Situ* Liquid TEM – Trials and Tribulations. *In submission format.*

Contributions: The work conducted in Chapter 6 was conceptualized by myself with feedback from my advisor Kathryn Grandfield and collaborator Eli D. Sone, where first-time collagen biomineralization dynamics were captured using an *in situ* liquid heating holder. Here, I prepared mineralization experiments and primarily led the data curation and formal analysis. Eli D. Sone and Kathryn Grandfield provided insights into the analysis and helped guide directions for the research. Ruixin Gao provided collagen samples and mineralization reagents for the mineralization experiments, where Ruixin Gao and Eli D. Sone together with their team optimized separately the calcium phosphate poly-L-aspartic acid *in vitro* collagen mineralization model used in this paper. The manuscript was primarily written and reviewed by myself, with editing from all the listed contributing authors. The manuscript is currently in submission format.

Apart from the published and submitted works featured in the main text of my doctoral thesis mentioned above, I have *other authorship contributions* that relate themes on the development of strategies for performing liquid electron microscopy of biomaterials and real-time dynamic processes *in situ.* These articles are referenced in the main body of my thesis. Notably, I have three separate review articles associated with each of the works presented as distinct introductory sections within Chapter 2 of this thesis. These provide a clear background to the field and review the current state-of-the-art to contextualize the importance of this doctoral research while also providing clear insights into future directions of the field and applications. These articles are provided as a literature review section of my thesis in Chapter 2 and are presented as follows for context to the thesis:

(Ch. 2.1) **DiCecco, L.-A.,** D'Elia, A., Miller, C., Sask, K.N., Soleymani, L., and Grandfield, K. Electron Microscopy Imaging Applications of Room Temperature Ionic Liquids in the Biological Field: A Review. 2021. *ChemBioChem,* Vol. 22(15), pp. 2488-2506. DOI: 10.1002/cbic.202100041

Contributions: This review provides a complementary perspective on the applied use of room-temperature ionic liquids for preparing biological samples for electron microscopy imaging applications. At the time that this was researched, there was no comprehensive review specifically on the topic of room-temperature ionic liquids for biological applications and the technique was still emerging as a method for preparing hydrated samples for electron microscopy imaging. The literature review article was primarily conducted and drafted by myself, with some research and writing assistance from Andrew D'Elia and Chelsea Miller. All the authors contributed to the review and editing of the final draft. This manuscript has been published in the *ChemBioChem*.

(Ch. 2.2) Kelly, D.F., **DiCecco, L.-A.,** Jonaid, G., Dearnaley, W.J., Spilman, M.S., Gray, J.L, and Dressel-Dukes, M.J. Liquid-EM goes viral – visualizing structure and dynamics. 2022. *Current Opinion in Structural Biology*, Vol. 75(102426). DOI: 10.1016/j.sbi.2022.102426 [Invited]

Contributions: This invited review and opinion article critically overviews the current state-of-the-art in the field of liquid electron microscopy for biological applications, specifically for the study of virions. It is complementary to Chapter 4 and provides further detailed insights into crucial strategies and techniques used for liquid electron microscopy of biological samples. The literature review article was primarily conducted and drafted by Deborah F. Kelly and myself, with insights and suggestions provided by all authors. All the authors contributed to the review and editing of the final draft. This manuscript has been published in the journal *Current Opinion in Structural Biology*.

(Ch. 2.3) **DiCecco, L.-A.,** Tengteng, T., Kelly, D.F., Sone, E.D., and Grandfield, K. Exploring biomineralization processes using *in situ* liquid transmission electron microscopy: *A review*. *In submission format.*

Contributions: This invited review is comprehensive of current liquid electron microscopy research related to biomineralization. It is complementary to Chapter 5 and the review of the literature presented was foundational to the execution of my *in situ* liquid transmission electron microscopy biomineralization and other research. The literature review article was primarily conducted and drafted by myself with guidance provided by Kathryn Grandfield. Tengtang Tang, Deborah F. Kelly, and Eli D. Sone all provided their insights and suggestions throughout the writing process. All the authors contributed to the review and editing of the final draft. The manuscript is currently in submission format.

In addition, the following is a list of 10 other relevant journal and conference publications representing significant research contributions by myself during the time of my doctoral studies. These works relate to themes presented within this thesis and further build upon the motivation and objectives outlined in Chapter 1, but are not included for evaluation.

- **DiCecco, L.-A.,** Gao, R., Gray, J.L., Kelly, D.F., Sone, E.D., and Grandfield, K. Liquid Transmission Electron Microscopy of Organic-Inorganic Interfaces: Exploring Hydrated Collagen Mineralization Processes. 2023. *Microscopy and Microanalysis*, Accepted for publication ID: 1474959.
- **DiCecco, L.-A.,** Gao, R., Athanasiadou, D., Chan, R.L., Carneiro, K.M.M., Kelly, D.F., Sone, E.D., and Grandfield, K. Exploring Calcium Phosphate Biomineralization Systems Using *In Situ* Liquid Phase Electron Microscopy. 2022. *Microscopy and Microanalysis* Vol. 28 (S1), pp. 1818-1820. DOI: 10.1017/S1431927622007176
- Berry, S., **DiCecco, L.-A.,** Dearnaley, W.J., Solares, M.J., Gray, J.L., and Kelly, D.F. Utilizing Liquid-Electron Microscopy to Visualize SARS-CoV-2 Assemblies from COVID-19 Patients. 2022. *Microscopy and Microanalysis* Vol. 28 (S1), pp. 1384-1386. DOI: 10.1017/S1431927622005645
- Micheletti, C., **DiCecco, L.-A.,** Wexell, C.L., Binkley, D.M., Palmquist, A., Grandfield, K., and Shah, F.A. Multimodal and Multiscale Characterization of the Bone-Bacteria Interface in a Case of Medication-Related Osteonecrosis of the Jaw. 2022. *Journal of Bone and Mineral Research*, Vol. 6 (12). DOI: 10.1002/jbm4.10693
- Casasanta, M.A., Jonaid, G., Kaylor, L., Luqiu, W.Y., **DiCecco, L.-A.,** Solares, M.J., Berry, S., Dearnaley, W.J., and Kelly, D.F. Structural Insights of the SARS-CoV-2 Nucleocapsid Protein: Implications for the Inner-workings of Rapid Antigen Tests. 2022. *Microscopy and Microanalysis*, ID: ozac036. DOI: 10.1093/micmic/ozac036
- Merlo, A., Gonzalez-Martinez, E., Saad, K., Gomez, M., Grewal, M., Deering, J, **DiCecco, L.-A**., Hosseinidoust, Z., Sask, K., Moran-Mirabal, J., and Grandfield, K. Functionalization of 3D printed scaffolds using polydopamine and silver nanoparticles for bone-interfacing applications. 2023. *Journal of ACS Applied Bio Materials*, Vol. 6 (3), pp. 1161-1172. DOI: 10.1021/acsabm.2c00988
- Deering, J.*, Dowling, K.I.*, **DiCecco, L.-A.,** McLean, G.D., Yu, B., and Grandfield, K. Selective Voronoi tessellation as a method to design anisotropic and

biomimetic implants. 2021. *Journal of the Mechanical Behavior of Biomedical Materials*, Vol. 116 (104361). DOI: 10.1016/j.jmbbm.2021.104361.

— Lee, B.E.J., **DiCecco, L.-A.,** Exir, H., Weck, A., Sask, K.N., and Grandfield, K. Simultaneous Visualization of Wet Cells and Nanostructured Biomaterials in SEM using Ionic Liquids. 2021. *ChemBioChem*, Vol. 22(3), pp. 571-576. DOI: 10.1002/cbic.202000552

— Abdellah, A.M., Ismail, F., Siig, O.W., Yang, J., Andrei, C.M., **DiCecco, L.-A.**, Rakhsha, A., Salem, K.E., Grandfield, K., Bassim, N., Black, R., Kastlunger, G., Soleymani, L., and Higgins, D. Impact of Palladium/Palladium Hybride Conversion on Electrochemical CO_2 Reduction via In-Situ Transmission Electron Microscopy and Diffraction. *Under Revision – Nature Materials* (ID: NM23030941).

— Micheletti, C., **DiCecco, L.-A.***, Deering, J.*, Chen, W., Ervolino da Silva, A.C., Shah, A.F., Palmquist, A., Okamoto, R., and Grandfield, K. Additively Manufactured Ti-6Al-4V Implant for Local Genistein Delivery in Osteoporosis: Micro-to-Nanoscale Characterization of Osseointegration and Lacuno-Canalicular Network. *Under Revision – PLOS One* (ID: PONE-D-23-06680).

** Indicates equal contribution.*

Chapter 1: Introduction

1.1. Research Motivation

In the past few decades, advances in micro/nanofabrication, thin electron transparent materials, holder designs, and acquisition methods have made it possible to perform meaningful experiments using *liquid electron microscopy* (EM).[1] Since its advent, liquid EM has proven to be a powerful microscopy tool that provides new possibilities to observe soft biological samples at high resolution in native hydrated environments,[2,3] without needing to dehydrate, fix, and/or coat samples often required in conventional EM observations. Moreover, uniquely liquid EM can be used to observe reactions taking place dynamically in real-time in an EM environment, or *in situ*.[4–6] This capability is key for validating long-withstanding theories based on time-stamped observations, or in essence, *seeing is believing.*

However, while these newly developed 21st-century techniques offer novel means of observing biological samples and related dynamic processes, *several challenges exist to these approaches*, notably: understanding electron beam sample interactions and their subsequent influence on the processes observed,[2,3,7] differentiating physical and chemical reactions from inelastic scattering events such as beam-induced crystallization and radiolysis effects,[3,8–11] resolution limitations such as liquid and/or membrane thickness,[3] need for faster imaging rates to limit artifacts due to blurring,[12] artifacts related to system assembly e.g. dewetting, bulging, bubble formation, contamination, etc.,[4,10] and many other general and system-specific challenges. Subsequently, these shortcomings limit the interpretation of liquid phase observations and thus restrict their implementation and broader use in research fields.

Due to the infancy of this field, while there remain many exciting research possibilities and biological specimens to characterize using this powerful platform, limited works are available which provide a comprehensive understanding of best practices. To address these shortcomings, this research is *motivated* to strategically explore the improvement of liquid EM of biomaterials and real-time dynamic processes through two key state-of-the-art high-resolution liquid EM techniques: room temperature ionic liquid (RTIL) treatment for scanning EM (SEM) and liquid cell transmission EM (TEM). The exploration of both techniques addresses a *microscopy need* to improve workflows for liquid EM imaging as well as for real-time approaches to validate theory developed from time stamp observations. In systematically approaching these two techniques, this work *aims to develop an improved framework* that I *hypothesize* will allow for routine and reproducible imaging to advance this field. The liquid EM methods discussed will also be compared to conventional preparation methods to better understand how artifacts related to sample preparation, such as fixation and dehydration, may be influencing the natural morphology of biological structures being observed.

Improving upon these liquid EM techniques is crucial for the biological field, where for many biological systems it presents the only opportunity to validate nanoscale reactions and structural features in a biomimetic hydrated environment. This thesis focuses on researching liquid EM techniques to study the ultrastructure and mineralization of hard tissues, notably bone and collagen, and for structural biological virus research, relevant to the fight against COVID-19. This is *impacting* our current fundamental understanding of these events and structures. Insights on biomineralization and how this occurs can help further understand a variety of hard-tissue conditions that impact millions of Canadians, such as periodontitis and osteoporosis.[13,14] This improved understanding anticipates providing insight into how to better control these processes and reveal new treatment pathways. Additionally, a greater understanding of biomineralization processes will help in improving implant and scaffold designs to better interface with biological systems. Moreover, since the advent of the COVID-19 global pandemic, SARS-CoV-2 remains a grave threat to human health – with over 6.7 million deaths worldwide and devasting global economic impacts.[15,16] The new liquid EM workflows presented are changing our understanding of such virions by revealing never-before-seen features, presenting new opportunities for targeted therapeutics and clinical advantages to fight future culprits.

Herein, the research in this thesis is presented in four articles which represent my research contributions to liquid-EM for biological imaging and capturing dynamic processes. The four works are presented by increasing complexity discussed in the following subsections, touching on themes as follows: *exploring* liquid EM for the first time using RTILs for SEM of biological samples notably bone, (static, micro-scale), *developing* new methods for high-resolution liquid biological TEM of viruses (static, nano-scale), and *applying* novel liquid-TEM to dynamic biomineralization systems (dynamic, nano-scale).

Overall, this work has ***broad implications*** for understanding the native hydrated morphology of biological materials such as bone and virions and can capture dynamic reactions. This is highly relevant to our growing aging population,[17] who are at higher risk of severe symptoms in viral infections and often prevalent victims of hard-tissue mineralization-related health conditions.[18,19] Thus, insights on these reactions and structures anticipate leading to a better understanding of diseases and treatment pathways, key to moving Canada's health care system forward.

1.1.1. Exploring Room Temperature Ionic Liquids to Facilitate Biological SEM

For over the last fifty years, SEM has been among one of the most frequently used tools to study bone's complex hierarchical structure and its relation to many human health concerns,[20] for instance for understanding disease mechanisms such as osteoporosis[21,22] and improving implant osseointegration.[23,24] However, conventional SEM imaging necessitates biomaterial sample preparation involving typically fixation, dehydration, embedding, and/or conductive coatings to visualize these structures in the high-vacuum environment in high-resolution – which together, risk altering their natural morphologies.[25–28] Moreover, for bone structures, these preparation methods are lengthy

and laborious.[29,30] As a solution, alternative preparation methods such as RTILs have been proposed in literature as a new liquid EM-based preparation method for SEM.[31–33] Due to their high conductivity and low vapour pressure, RTILs can be used to stabilize liquid samples in high-vacuum environments for stable SEM imaging.[33,34] However, limited researchers have explored these techniques for biomaterial applications, and no one has optimized its bone treatment. The work presented in Chapter 3 explores the first-time optimization of RTIL treatments for SEM preparation of hydrated, unfixed healthy and osteoporotic bone structures. The refined RTIL treatment was noted to achieve similar imaging quality in comparison to conventional treatments and was suggested to better preserve the natural features of bones. Moreover, it proved to be a much faster and simpler preparation method compared to conventional means, with the downfall that it cannot permanently conserve samples for periods longer than one month. Complemented by the review and suggested best practices provided within Chapter 2.1 for imaging biomaterials with RTILs, the proof-of-concept research in Chapter 3 lays a foundation for the broad application of RTIL-based techniques in the study of wide-ranging biomaterials in natural hydrated conditions.

1.1.2. Developing New Methods for High-Resolution Liquid Biological TEM

The emergence of SARS-CoV-2 triggered tremendous global resources aimed at understanding the features of a minute human pathogen.[15,16,35,36] High-resolution tools, such as cryogenic (cryo) EM, were deployed to shed light on the molecular aspects of SARS-CoV-2. This important structural information was key to identifying new vaccine products and drug therapies to save lives and curb viral transmission.[37–40] However, current technology that led to recent life-saving interventions has only provided limited snapshots of one part of the virus, the outer spike protein, which is the part most subject due to environmental pressures. Liquid EM, the room temperature correlate to cryo EM, is a relatively new imaging technique that provides high-resolution information for dynamic interactions, key to understanding whole virions and protein behaviours while contained in a liquid environment.[2–4,41–50] The work presented in Chapter 4 focuses on the development of liquid-EM protocols for routine virus imaging for SARS-CoV-2 and other viruses, using commercially available specimen holders and a new thin-film-based clipped enclosure.

Structural features from single-particle reconstructions are highlighted which are comparable to resolutions achieved in cryo EM modalities, where structural dynamics can be simulated. The use of automated tools and direct electron detectors in imaging is also highlighted as a novel means to quickly screen samples for optimum thickness and electron dose parameters for high-resolution acquisition. Moreover, the article is accompanied by a video supplemental that will highlight the techniques presented in detail as a tutorial to broaden the accessibility of these techniques to biological communities. Complemented by the critical review of liquid-EM related to viral applications in Chapter 2.2, the innovative research presented in Chapter 4 is anticipated to provide new characterization tools to study dynamic processes in near-atomic detail. This will help us better understand pandemic

pathogens and other specimens encompassing life science, medicine, and materials research.

1.1.3. Applying Novel Liquid-TEM to Dynamic Biomineralization Systems

Biomineralization processes are key to the formation and maintenance of hard tissues, thus essential for many organisms ranging from humans, zebrafish, lobsters, to mussels. For bone, the biomineralization of calcium-phosphate-based minerals in collagen is crucial for its mechanical integrity, where its distribution and extent are key factors to tissue mechanical strength.[51,52] Moreover, the study of biomineralization processes is clinically relevant for medical advancement, where it can provide an improved understanding of conditions such as diseases such as atherosclerosis, dental caries, and osteoporosis and provide new insights for designing bioinspired materials and treatment pathways.[53–57] While collagen biomineralization processes have been studied extensively in literature,[58–64] many competing theories exist on mineral formation and distribution within bone and much is yet to be discovered about its complicated hierarchical micro-to-sub-nano scale structure.

Thus far, traditional and cryo EM modalities have helped reveal time-stamp observations key to making eliciting crucial structural features and theories of mechanistic biomineralization pathways.[59,65–72] However, these methods do not provide a true view of the native liquid state of the structures, where water is an integral part of collagen,[73] and cannot capture dynamics key to validating biomineralization theories. Thus, studying how collagen mineralizes in a liquid environment is essential for understanding its mineralization processes and native structures. The work presented in Chapter 5 and Chapter 6 applies the novel new thin-film liquid TEM enclosure developed in Chapter 4 as well as commercially available liquid TEM holders to study a biomimetic collagen mineralization model for the first time in hydrated conditions. This involves using a calcium-phosphate (CaP) based mineralization solution with poly-L-aspartic acid (pAsp) considered, mimetic to non-collagenous proteins found in hard tissues, and a reconstituted rat-tail tendon collagen model that is similar in structure to type I collagen found in bone.[57,59,74]

TEM acquisition at high resolution highlights key features at early mineralization periods, notably the presence of precursor minerals attached to collagen fibrils, as well as distinctive crystalline nanoscale mineral platelets formed aligned the long axis of collagen fibrils at more mature periods. Complemented by the detailed review of liquid EM techniques and their application in biomineralization research in Chapter 2.3, the novel research presented in Chapter 5 and Chapter 6 provides new techniques to study these systems in native hydrated environments at high resolution, pushing the biomineralization field one step closer to answering how collagen biomineralization occurs.

1.2 Research Objectives

As a general objective, this thesis aims to develop improved strategies for liquid EM methodologies for biological sample characterization and the observation of dynamic, real-time processes. Specifically, this research has considered RTIL treatment and liquid cell TEM means methods to consider and ameliorate to study hard tissues and their mineralization as well as virions. This objective is broken down within Chapters 3-6 into three specific objectives schematically presented in Fig. 1-1. The three works are presented by increasing complexity, touching on themes as follows:

(i) ***To explore liquid SEM for the first time using RTILs for biological samples notably bone (static, micro-scale)***
(ii) ***To develop new methods for high-resolution liquid biological TEM of virions (static, nano-scale)***
(iii) ***To apply novel liquid TEM to dynamic biomineralization systems (dynamic, nano-scale)***

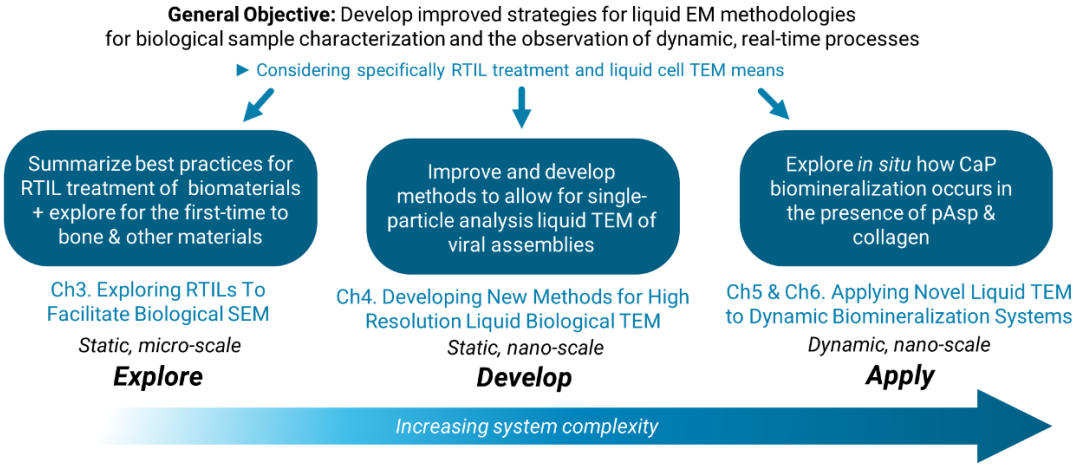

Ch. 1.2 – Figure 1. *Overview of thesis research objectives and three projects presented within this thesis.*

1.3 Thesis Chapter Summary

The following summarizes how the subsequent sections of this thesis are organized:

Chapter 2: Literature Review. This chapter reviews pertinent literature to provide context to the research presented while also elaborating on fundamental principles of the work related to the thesis. This includes a focus on fundamental concepts of EM, a comprehensive overview of the liquid EM field, calcium-phosphate biomineralization processes in bone, and the characterization of viral entities. The work is split into three sections, one related to each theme, presented through two published review articles and a third in manuscript format.

Chapter 3: Ionic Liquid Treatment for Efficient Sample Preparation of Hydrated Bone for Scanning Electron Microscopy. This chapter presents the first-time exploration of RTILs for preparing bone samples for SEM imaging, where healthy and osteoporotic bone is imaged in unfixed, hydrated conditions. The newly established workflow presents a facile manner to image hard tissues and lays a foundation for the study of wide-ranging biomaterials in natural hydrated conditions.

Chapter 4: Advancing High-Resolution Imaging of Virus Assemblies in Liquid and Ice. This chapter presents the development of novel liquid EM and correlative cryo protocols for routine virus imaging for SARS-CoV-2 and other viruses, using commercially available specimen holders and a new thin-film-based clipped enclosure. Using single-particle analysis, structural features at near-atomic resolution were able to be resolved. These new techniques for native hydrated imaging will help us better understand pandemic pathogens and other specimens encompassing life science, medicine, and materials research.

Chapter 5: Liquid Electron Microscopy Techniques for Probing Collagen Biomineralization. This chapter presents the application of the new liquid TEM methods developed in Chapter 4 to the study of collagen biomineralization processes for the first time using a CaP and pAsp-based biomimetic collagen model. High-resolution nanoscale characterization was able to be achieved using these techniques to reveal early and mature mineralization patterns in liquid. This opens new characterization pathways in the study of biomineralization processes, bringing the field closer to controlling these complex mechanisms in clinical applications.

Chapter 6: Towards Understanding Dynamics Behind Collagen Mineralization Through *In Situ* Liquid TEM – Trials and Tribulations. This chapter presents the application of commercially available liquid TEM methods to study the collagen biomineralization processes presented in Chapter 5, where heating is incorporated *in situ.* Using this system, high-resolution nanoscale characterization was able to be achieved and dynamic mineralization of these events was captured. This work is foundational for the study of dynamic biomineralization processes *in situ* and includes strategies to address challenges in the future.

Chapter 7: Concluding Remarks. The final chapter links together the conclusions formalized between the preceding chapters and summarizes key findings and impacts, where future directions for this research are elaborated.

References

[1] N. de Jonge et al., *Nat Nanotechnol* 2011, *6*, 695.
[2] K. He et al., *J Phys Condens Matter* 2019, *31*, 103001.
[3] H. Wu et al., *Adv Mater* 2020, *32*, 2001582.

[4] X. Wang et al., *Commun Chem* 2018, *1*, 80.
[5] P. J. M. Smeets et al., *Nat Mater* 2015, *14*, 394.
[6] J. M. Yuk et al., *Science* 2012, *336*, 61.
[7] P. Abellan et al., *Chem Commun* 2014, *50*, 4873.
[8] H. Wu et al., *Microsc Microanal* 2019, *25*, 63.
[9] T. J. Woehl et al., *Ultramicroscopy* 2013, *127*, 53.
[10] F. M. Ross, *Science* 2015, *350*, aaa9886.
[11] S. Pu et al., *Roy Soc Open Sci* 2020, *7*, 191204.
[12] J. E. Evans et al., *Micron* 2012, *43*, 1085.
[13] C. Cooper et al., *IOF Compendium of Osteoporosis*, International Osteoporosis Foundation, 2019.
[14] M. A. Nazir, *Int J Heal Sci* 2017, *11*, 72.
[15] "WHO Coronavirus (COVID-19) Dashboard," can be found under https://covid19.who.int/, 2023.
[16] A. Sharif et al., *Int Rev Financ Anal* 2020, *70*, 101496.
[17] *World Population Prospects: The 2017 Revision*, United Nations, Department Of Economic And Social Affairs, Population Division, 2017.
[18] *Impact Report 2019-2020*, Osteoporosis Canada, 2020.
[19] *Hip and Knee Replacements in Canada: CJRR Quick Stats, 2019–2020*, Canadian Institute For Health Information, Ottawa, ON: CIHI, 2021.
[20] F. A. Shah et al., *Bone Res* 2019, *7*, 15.
[21] D. W. Dempster et al., *J Bone Miner Res* 1986, *1*, 15.
[22] F. A. Shah et al., *J Biomed Mater Res A* 2018, *106*, 997.
[23] F. A. Shah et al., *Acs Biomater Sci Eng* 2015, *1*, 305.
[24] F. A. Shah et al., *Nanomed Nanotechnol Biology Medicine* 2014, *10*, 1729.
[25] E. Kellenberger et al., *J Microsc-oxford* 1992, *168*, 181.
[26] Y. Li et al., *Exp Cell Res* 2017, *358*, 253.
[27] M. D. McKee et al., *J Bone Miner Res* 1991, *6*, 937.
[28] F. S. Utku et al., *J Struct Biol* 2008, *162*, 361.
[29] J. Tedesco et al., *Int J Dent* 2017, *2017*, 1.
[30] D. M. Binkley et al., *J Struct Biol* 2020, 107615.
[31] L. DiCecco et al., *Chembiochem* 2021, *22*, 2488.
[32] T. Tsuda et al., *Microscopy* 2020, *69*, 183.
[33] S. Kuwabata et al., *Chem Lett* 2006, *35*, 600.
[34] R. Hagiwara et al., *J Fluorine Chem* 2000, *105*, 221.
[35] A. D. Kaye et al., *Best Pract Res Clin Anaesthesiol* 2021, *35*, 293.
[36] "Government of Canada COVID-19 daily epidemiology update," can be found under https://health-infobase.canada.ca/covid-19/epidemiological-summary-covid-19-cases.html, 2021.
[37] L. A. Caldas et al., *Sci Rep-uk* 2020, *10*, 16099.
[38] Z. Ke et al., *Nature* 2020, *588*, 498.
[39] M. Jeyanathan et al., *Nat Rev Immunol* 2020, *20*, 615.
[40] R. Chilamakuri et al., *Cells* 2021, *10*, 206.
[41] M. J. Dukes et al., *J Vis Exp* 2013, 50936.

[42] L.-A. DiCecco et al., *J Vis Exp* 2022, e63856.
[43] G. M. Jonaid et al., *Microsc Microanal* 2022, 1.
[44] L.-A. DiCecco et al., *Microsc Microanal* 2022, *28*, 1818.
[45] M. J. Dukes et al., *Microsc Microanal* 2021, *27*, 19.
[46] G. Jonaid et al., *Adv Mater* 2021, *33*, 2103221.
[47] D. F. Kelly et al., *Curr. Opin. Struct. Biol.* 2022, *75*.
[48] L. M. DiMemmo et al., *Lab Chip* 2017, *17*, 315.
[49] M. J. Dukes et al., *Chem Commun* 2013, *49*, 3007.
[50] A. C. Varano et al., *Chem Commun* 2015, *51*, 16176.
[51] L. C. Palmer et al., *Chem Rev* 2008, *108*, 4754.
[52] Y.-R. Zhang et al., *Int J Oral Sci* 2014, *6*, 61.
[53] S. V. Dorozhkin et al., *Angewandte Chemie Int Ed* 2002, *41*, 3130.
[54] L. He et al., *J Struct Biol* 2019, *207*, 115.
[55] C.-W. (Jeff) Wang et al., *Curr Osteoporos Rep* 2016, *14*, 284.
[56] N. Alexopoulos et al., *Nat Rev Cardiol* 2009, *6*, 681.
[57] A. J. Lausch et al., *Adv Funct Mater* 2018, *28*, 1804730.
[58] A. J. Hodge et al., in *Aspects of Protein Structure* (Ed: G.N. Ramachandran), Academic Press, New York, 1963, pp. 289–300.
[59] F. Nudelman et al., *J Struct Biol* 2013, *183*, 258.
[60] S. R. Stock, *Calcif Tissue Int* 2015, *97*, 262.
[61] W. J. Landis et al., *J Struct Biol* 1993, *110*, 39.
[62] E. A. McNally et al., *Plos One* 2012, *7*, e29258.
[63] J. P. R. O. Orgel et al., *Proc National Acad Sci* 2006, *103*, 9001.
[64] J. P. R. O. Orgel et al., *Structure* 2001, *9*, 1061.
[65] F. Nudelman et al., *Nat Mater* 2010, *9*, 1004.
[66] E. Macías-Sánchez et al., *Adv Funct Mater* 2022, *32*, 2200504.
[67] W. J. Landis et al., *J. Struct. Biol.* 1993, *110*, 39.
[68] H. P. Schwarcz et al., *J Struct Biol* 2014, *188*, 240.
[69] B. E. J. Lee et al., *Adv Biology* 2021, *5*, 2100657.
[70] N. Reznikov et al., *Acta Biomater* 2014, *10*, 3815.
[71] N. Reznikov et al., *Science* 2018, *360*, eaao2189.
[72] B. D. Quan et al., *Bone* 2015, *77*, 42.
[73] A. Masic et al., *Nat Commun* 2015, *6*, 5942.
[74] B. D. Quan et al., *J Roy Soc Interface* 2018, *15*, 20180269.

Chapter 2: Background

Within the last few years, exciting liquid EM and ionic liquid research have emerged showcasing micro-to-nano scale possibilities of observing biological structures in hydrated conditions. The following is an introduction of relevant literature, organized into three review articles published or in manuscript format, key to the thesis research themes.

2.1. Electron Microscopy Imaging Applications of Room Temperature Ionic Liquids in the Biological Field: A Review

2.1.1. Section Introduction (Objective i)

Recently, the use of RTILs has been proposed in literature as an alternative technique to traditional preparation schemes of biological materials for EM involving dehydration and fixation. Provided the low-vapour and highly conductive nature of RTILs, they can be used to treat biomaterials to stabilize them for EM imaging while conserving their naturally hydrated structure. However, the use of RTILs is highly underutilized within the microscopy field and their application has not been widely established. To accomplish objective (i) set out for this thesis involving exploring an RTIL-based method to perform liquid SEM on bone, Section 2.1 provides a comprehensive summary of biological applications of RTILs for EM and best practices for their use. Future research avenues within RTIL liquid EM research were summarised to include: i) RTIL selection and optimization, ii) applications for live cell processes and iii) electron beam and ionic liquid interaction studies. Overall, this work contributes to a foundational understanding of the applied use of RTILs for biological EM and provides working guidelines that are anticipated to lead to wider adoption of these techniques in future.

Authors: **Liza-Anastasia DiCecco**, Andrew D'Elia, Chelsea Miller, Kyla N. Sask, Leyla Soleymani, Kathryn Grandfield.

Publication: This work is published with a full citation provided as follows:

DiCecco, L.-A., D'Elia, A., Miller, C., Sask, K.N., Soleymani, L., and Grandfield, K. Electron Microscopy Imaging Applications of Room Temperature Ionic Liquids in the Biological Field: A Review. 2021. *ChemBioChem,* Vol. 22(15), pp. 2488-2506. DOI: 10.1002/cbic.202100041

Reprinted from the above-listed citation, with permission from *ChemBioChem.* Copyright © 2021 Wiley-VCH GmbH.

ChemBioChem | Reviews
doi.org/10.1002/cbic.202100041
Chemistry Europe
European Chemical Societies Publishing

Electron Microscopy Imaging Applications of Room Temperature Ionic Liquids in the Biological Field: A Review

Liza-Anastasia DiCecco,[a] Andrew D'Elia,[a] Chelsea Miller,[b] Kyla N. Sask,[a, b] Leyla Soleymani,[b, c] and Kathryn Grandfield*[a, b]

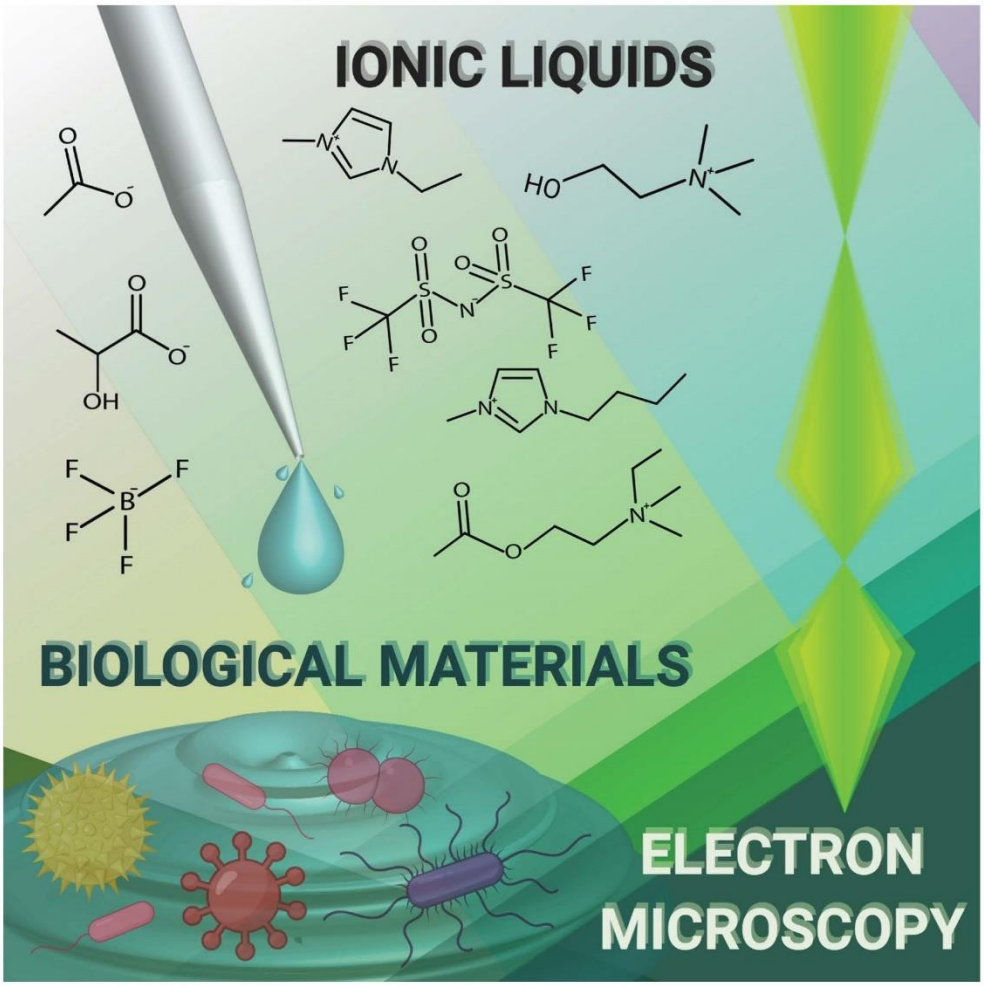

© 2021 Wiley-VCH GmbH

ChemBioChem | Reviews
doi.org/10.1002/cbic.202100041
Chemistry Europe
European Chemical Societies Publishing

For biological imaging using electron microscopy (EM), the use of room-temperature ionic liquids (RTILs) has been proposed as an alternative to traditional lengthy preparation methods. With their low vapor pressures and conductivity, RTILs can be applied onto hard-to-image soft and/or wet samples without dehydration – allowing for a more representative, hydrated state of material and opening the possibility for visualization of *in situ* physiological processes using conventional EM systems. However, RTILs have yet to be utilized to their full potential by microscopists and microbiologists alike. To this end, this review aims to provide a comprehensive summary of biological applications of RTILs for EM to bridge the RTIL, *in situ* microscopy, and biological communities. We outline future research avenues for the use of RTILs for the EM observation of biological samples, notably i) RTIL selection and optimization, ii) applications for live cell processes and iii) electron beam and ionic liquid interaction studies.

Introduction

Room temperature ionic liquids (RTILs), also referred to as molten or fused salts, are composed of ions and short-lived ionic pairs that are liquid at room temperature. They are known for their attractive properties such as low vapour pressure, high ionic conductivity, non-combustibility, and capacity to dissolve many kinds of substances.[1–4] In the last forty years, water-stable RTILs have been studied in a wide range of applications within chemical fields,[1,5,6] such as for biocatalysis and biotransformations,[7–9] electrolytes for electrochemical applications,[10] specifically for batteries[11–13] and electrodeposition,[14] micro-CT imaging,[15] and lubrication,[16] among others. However, only recently has the potential of RTILs as a preparation method for biological sample imaging in electron microscopy (EM) been explored.[17–21] Applications of RTILs in the place of conductive coatings,[10,22,23] provide comparable resolution and contrast to that of conventional preparation methods for biological EM imaging.[21] Notably, their low vapour pressures enable samples wetted with ionic liquid solutions to be imaged under high vacuum conditions.[18] Combined, the unique properties of RTILs allow them to play the role of a solvent, a discharging layer for electron charge, and a vacuum-stable solution that enables hydrated EM imaging at high vacuum. While conventional methods of preparing biological samples for EM constitute dehydration and fixation protocols that can significantly alter the structure of these materials,[24–26] preparation methods with RTILs involve simpler and shorter steps.[17–21] The unique properties of RTILs have provided new avenues for EM applications involving soft and/or hydrated biological materials as well as novel mediums for *in situ* EM. However, RTILs in EM have yet to be explored to their full potential by researchers including microscopists and microbiologists.

[a] *L.-A. DiCecco, A. D'Elia, Prof. Dr. K. N. Sask, Prof. Dr. K. Grandfield*
Department of Materials Science and Engineering
McMaster University, 1280 Main Street West, Hamilton, Ontario, L8S 4L7 (Canada)
E-mail: kgrandfield@mcmaster.ca
[b] *C. Miller, Prof. Dr. K. N. Sask, Prof. Dr. L. Soleymani, Prof. Dr. K. Grandfield*
School of Biomedical Engineering
McMaster University, 1280 Main Street West, Hamilton, Ontario, L8S 4L7 (Canada)
[c] *Prof. Dr. L. Soleymani*
Department of Engineering Physics
McMaster University, 1280 Main Street West, Hamilton, Ontario, L8S 4L7 (Canada)

This review paper aims to offer a fresh perspective on the capabilities, challenges, and outlook of using RTILs in the EM study of biological materials. Here, we present the use of RTILs in common preparation schemes for biological samples and highlight their use in a diverse range of applications, summarized in Tables 1&2. We intend this review paper to inspire others working with biological samples to explore the use of RTILs to investigate new avenues for hydrated sample preparation.

Brief Historical Review

Early work produced by Hurley et al. in 1951 highlighted initial research in the field of ionic liquids with the exploration of fused quaternary ammonium salts used for electrodeposition of metals.[53] However, they found the ionic liquid solution was highly sensitive to moisture and unstable at room temperature,[53] which remained a limiting factor in their application for years to come. Further development of RTILs was pioneered by Wilkes et al. starting with their key 1982 published work,[5] though it was the 1992 article produced by Wilkes et al. that revolutionized the field by presenting the first water-stable RTIL, 1-ethyl-3-methylimidazolium tetrafluoroborate or [EMI][BF_4].[1] In parallel to Wilkes, Cooper and O'Sullivan prepared 1-ethyl-3-methylimidazolium with triflate or [EMI][CF_3SO_3], a novel water-stable RTIL.[6]

Previously limited by chemical instability in the presence of moisture, the new generation of water-stable RTILs have received wide acclaim for their synthetic and electrochemical applications, with an electrochemical window of larger than three Volts.[4] Since then a variety of commercially available water-stable ionic liquids have been developed featuring various cationic and anionic combinations, each comprising a unique subset of physicochemical properties. Also referred to as "designer solvents,"[54] ionic liquids can be defined as a material in the liquid state at or below 373 K (100 °C), composed entirely of cations and anions that do not contain a molecular solvent.[4] Those that remain liquid at or below room temperature (298 K) are more specifically referred to as RTILs.[55] Table 1 summarizes select RTILs commonly used in EM applications, their chemical structures, and other properties, such as molecular weight and hydrophobicity.

The first application of RTILs in EM was not shown until 2006 by Kuwabata et al. in their fundamental work which describes the first published observation of RTILs in scanning

© 2021 Wiley-VCH GmbH

ChemBioChem | Reviews doi.org/10.1002/cbic.202100041 | Chemistry Europe European Chemical Societies Publishing

EM (SEM).[22] They featured the use of [EMI][TFSI] applied to the star-shape shells of *Foraminifera*, that post-RTIL treatment exhibited a significant reduction of charging effects in SEM compared to untreated shells.[22] A simple immersion method was used where a sample is directly dipped into an RTIL and excess liquid is removed, which allowed the shell's features to be imaged efficiently and clearly.[22] In electron microscopy, RTILs lend similar electrical conductivity to those of metal or carbon coatings commonly used in EM sample preparation.[10,22,23] Electron ejection from RTILs has been shown to be effective due to the solvation nature of the condensed ions which compose this solution,[43,56] leading to improved electron signal detection in EM.

Further to this, Kuwabata et al. postulated if the morphology of samples is not influenced by replacing water constituents of biological samples with RTILs, they could be used to image hydrated samples in normal high-vacuum EM modes.[22] Subsequent work by Arimoto et al. using both [BMI][TFSI] and [BMI][BF_4] for imaging rehydrated seaweed demonstrated that RTIL treatment could facilitate imaging hydrated specimens through water replacement with RTIL.[23] Arguably, these works[22,23] paved the way for the consideration of RTILs as treatment methods for biological samples in EM studies, with several works since exploring the application of RTILs in EM in the biological field, as discussed in the following subsections. A summary of biological applications of RTILs in EM is presented in Table 2.

Challenges of Biological Sample Imaging in Electron Microscopy and Advantages to RTIL Application

Prior to introducing applications in which RTILs have been used for imaging biological samples, it is important to discuss the current protocols and challenges with biological sample preparation, particularly of soft and/or wet samples for EM. EM generally must be performed under high-vacuum, low moisture conditions on conductive, dry specimens with negligible vapour pressure. Moreover, to probe specimens with high resolution, electron charging effects must be mitigated.

Traditional EM preparation methods for biological materials, such as cells and soft tissue, require hours of work prior to observation. An example of a typical workflow for a traditional cell treatment methodology for SEM is shown in Figure 1A, where a biomaterial disc is considered after being incubated with cells. First, a fixation media such as glutaraldehyde can be applied which creates crosslinks between proteins and fixes membranes for shape preservation. However, through fixation, the soft fluid-like behaviour of the membrane is compromised, proteins lose their function, and cells quickly die.[57] Moreover, the high-vacuum EM necessitates biological samples to be dehydrated to maintain the vacuum, prevent damage to the instrument, and mitigate sample evaporation. This may be accomplished via dehydration in increasing concentrations of ethanol followed by critical-point or freeze-drying. Fixation and subsequent dehydration are known to influence the structure of biological samples, leading to significant morphological changes such as shrinkage or wrinkling and potential imaging artifacts in EM.[57,58] This poses a greater limitation of the observations made with EM methods, being that biological structures observed in EM may not be representative of the naturally hydrated state. In consideration of this, users can alternatively employ more involved critical point drying processes which offer improved preservation of the morphological structures of samples but with the trade-off of increased complexity in preparation.

Biological specimens are most commonly insulators, soft, and composed of low atomic number elements, which render samples susceptible to several chemical and physical electron beam damage phenomena. Relevant damage examples include electrostatic charging effects, burn artifacts, carbon deposition from sample preparation itself or storage, and sample degradation,[59] which can of course be exacerbated further by poor vacuum conditions. To prevent artifacts related to conductivity, samples are often sputter-coated with a metal or carbon to improve surface conductivity. Sputter coating may result in non-uniform thickness over the surface of the substrate, a particular challenge for samples with distinct geometries, such as biological entities. Alternatively, methods that employ heavy metal stains, such as uranyl acetate, lead citrate and osmium tetroxide, can be used with the disadvantages of toxicity, and potential for altering sample morphology.[24,26,60]

Environmental-SEM (ESEM) and Cryogenic-EM (Cryo-EM) have been used as alternative methods to observe biological materials, suspended solutions, and liquid-solid

Liza-Anastasia DiCecco is a Ph.D. candidate in Materials Science and Engineering at McMaster University where she holds a prestigious Vanier Canada Graduate Scholarship, a top doctoral distinction in Canada. She utilizes and develops advanced microscopy techniques to characterize mineralization processes and bone structure. Notably, her research interests centre on liquid-phase imaging methods including liquid-phase transmission electron microscopy and exploring the use of ionic liquids to observe cells, biofilms, bone, and other biological samples in electron microscopy systems.

Kathryn Grandfield received her Ph.D. in Engineering Sciences in 2012 from Uppsala University prior to completing postdoctoral training at the University of California San Francisco. Currently, she is an Associate Professor in Materials Science and Engineering at McMaster University and Canada Research Chair in Microscopy of Biomaterials and Biointerfaces. Her group focuses on the development of biomaterials and multi-scale characterization techniques for biomineralization, osseointegration and live-cell imaging.

 © 2021 Wiley-VCH GmbH

ChemBioChem | Reviews | doi.org/10.1002/cbic.202100041 | Chemistry Europe, European Chemical Societies Publishing

Table 1. Chemical and physical properties of RTILs mentioned in this review.

RTIL index	Chemical name	RTIL [cation][anion]		Molecular weight [g/mol]	Viscosity [cP]	Density [g/cm^3]	Hydrophilicity	Ref.(s)
1	1-ethyl-3-methylimidazolium bis(trifluoromethylsulfonyl)imide	[EMI]	[TFSI]	391.3	56 (293 K)	1.54 (293 K)	Hydrophobic	[27,28]
2	1-butyl-3-methylimidazolium bis(trifluoromethylsulfonyl)imide	[BMI]	[TFSI]	419.4	52 (293 K)	1.44 (293 K)	Hydrophobic	[23,28,29]
3	1-ethyl-3-methylimidazolium tetrafluoroborate	[EMI]	[BF_4]	198.0	37 (298 K)	1.28 (298 K)	Hydrophilic	[21, 30,31]
4	1-ethyl-3-methylimidazolium acetate	[EMI]	[AcO]	170.2	144 (298 K)	1.10 (298 K)	Hydrophobic	[30]
5	1-ethyl-3-methylimidazolium lactate	[EMI]	[Lac]	200.2	184 (303 K)	1.14 (298 K)	Hydrophilic	[33]
6	1-butyl-3-methylimidazolium tetrafluoroborate	[BMI]	[BF_4]	226.0	99 (298 K)	1.20 (298 K)	Hydrophilic	[30,31]
7	2-hydroxy-*N*,*N*,*N*-trimethyl-Ethanaminium 2-hydroxypropionate methylglycolate (choline lactate)	[Ch]	[Lac]	193.2	895 (303 K)	1.14 (298 K)	Hydrophilic	[33]
8	tri-*n*-butylmethylphosphonium dimethylphosphate	[$P_{4,4,4,1}$]	[DMP]	342.4	439 (298 K)	1.03 (303 K)	Hydrophilic	[34]
9	1-hexyl-3-methylimidazolium hexafluorophosphate	[HMI]	[PF_6]	312.2	497 (298 K)	1.29 (298 K)	Hydrophobic	[29]
10	2-carboxylethyldimethylammonium methylsulfonate	[OACh]	[MS]	255.3	–	1.31 (298 K)	Hydrophilic	[35]

© 2021 Wiley-VCH GmbH

ChemBioChem | Reviews | doi.org/10.1002/cbic.202100041 | Chemistry Europe, European Chemical Societies Publishing

Table 1. continued

RTIL index	Chemical name	RTIL [cation][anion]		Molecular weight [g/mol]	Viscosity [cP]	Density [g/cm³]	Hydrophilicity	Ref.(s)
11	2-carboxylethyl-tris(2-hydroxylethyl)ammonium methylsulfonate	[XXCh]	[MS]	289.3	–	1.37 (298 K)	Hydrophilic	[35]
12	Hitachi Ionic Liquid HILEM® IL1000 (2-hydroxyethyl-ethyl-dimethyl-ammonium methylsulfonate)	[MECh]	[MS]	213.3	–	–	Hydrophilic	[35,36,37]
13	1- butyl-1- methylpyrrolidinium dicyanamide	[BMP]	[DCA]	208.3	50 (293 K)	1.02 (293 K)	Hydrophilic	[27]
14	1- butyl-1- methylpyrrolidinium bis(trifluoromethylsulfonyl)imide	[BMP]	[TFSI]	422.4	307 (293 K)	1.46 (293 K)	Hydrophobic	[27]
15	1-ethyl-3-methylimidazolium dicyanamide	[EMI]	[DCA]	177.2	21 (293 K)	1.11 (293 K)	Hydrophilic	[27]
16	1-MEethyl-3-methylimidazolium methylphosphonate	[EMI]	[MP]	316.3	107 (298 K)	1.21 (293 K)	Hydrophilic	[38]
17	1-methoxymethyl-1-methylpyrrolidinium tetrafluoroborate	[(MethoxyMe)MePyr]	[BF_4]	217.0	95 (298 K)	–	Hydrophilic	[39]
18	tributylmethylammonium bis(trifluoromethylsulfonyl)amide	[N_{4441}]	[TFSI]	480.5	551 (298 K)	1.27 (293 K)	Hydrophobic	[39]
19	1-methoxymethyl-1-methylpyrrolidinium bis(trifluoromethylsulfonyl) amide	[(MethoxyMe)MePyr]	[TFSI]	243.2	40 (298 K)	1.46 (293 K)	Hydrophobic	[39]

© 2021 Wiley-VCH GmbH

ChemBioChem | Reviews doi.org/10.1002/cbic.202100041 | Chemistry Europe European Chemical Societies Publishing

Table 1. continued

RTIL index	Chemical name	RTIL [cation][anion]		Molecular weight [g/mol]	Viscosity [cP]	Density [g/cm³]	Hydrophilicity	Ref.(s)
20	tri-n-butyldodecylphosphonium tetrafluoroborate	$[P_{4,4,4,12}]$	$[BF_4]$	458.7	1310	–	Hydrophobic	[20]
21	2-hydroxy-*N*,*N*,*N*-trimethyl-ethanaminium 4-oxopentanoate (choline levulinate)	[Ch]	[Lev]	219.3	–	–	Hydrophilic	[40]

interactions.[61–65] However, shortcomings and limitations to these techniques for hard-to-image soft and/or wet samples[61,66–68] have resulted in the exploration of new methods to facilitate EM observation of biological specimens. In contrast to these established techniques, RTILs leverage properties that, in theory, are better equipped to handle the unique demands of biological specimens. By maintaining the hydrated nature of these specimens, RTIL treatments may be able to preserve delicate morphological structures often damaged through dehydration, providing a means to image samples in a representative state of their true size and morphology.[21] Golding et al. suggest RTILs can provide superior capabilities of conserving the size of microbes while minimizing the effects of cracking and wrinkling.[21] Figure 2 featured from their work provides a visual on how RTIL treatment for imaging various microbes compare to conventional preparation methods, notably sputter coating for SEM and negative staining for TEM imaging.[21] They posit that RTIL treatment can produce images of similar quality to traditional sputter coating in a fraction of the time,[21] without the need of specialized equipment required for ESEM or Cryo-EM.

Applications of Ionic Liquids in Biological Imaging

RTIL treatment can facilitate EM imaging of biological samples by offering an alternative to coatings for conductivity-improvement and the ability to view samples in a hydrated state. With the elimination of dehydration and/or fixation steps, RTIL-based protocols can drastically reduce preparation time.[17,18] Research in this area suggests that RTILs produce a thin, uniform conductive layer on samples for their imaging,[10,22,23] thus their capacity to spread evenly on a wet surface is key in this type of work.

Table 1 summarizes relevant material properties of the RTILs used in EM studies and shows the anions and cations which form these solutions. Table 2 displays a variety of biological samples where RTILs have been used to observe in the literature while also showing the various sample conditions that have been applied to commonly fixed or unfixed and dehydrated or hydrated samples. Two direct and facile RTIL sample preparation protocols for EM are summarized through the illustration in Figure 1B. These include: 1) the addition of an RTIL solution directly to the sample of interest through directly pipetting solution to the sample for a given exposure period (Figure 1B – Scheme 1); and 2) the RTIL solution immersion treatment, an infiltration method where samples are immersed in solution for a given amount of time for sample integration (Figure 1B – Scheme 2).

Most works using RTILs for EM preparation fall within these two schemes, with some variation in protocols and preliminary sample preparation. Typically, the Scheme 1 (Figure 1B) addition method is applied for smaller samples or for quick surface treatment of drier samples while the Scheme 2 (Figure 1B) immersion method may be required with large, hydrous samples that are being impregnated by the RTIL solution.[69] The treatment time associated with solution addition or immersion

 © 2021 Wiley-VCH GmbH

ChemBioChem | Reviews | doi.org/10.1002/cbic.202100041 | Chemistry Europe, European Chemical Societies Publishing

Table 2. Select RTIL treatment for biological material applications (RTIL: room temperature ionic liquid; SE: secondary electron; BSE: backscatter electron; SEM: scanning electron microscopy; S1: RTIL addition method (Figure 1B); S2: RTIL immersion method (Figure 1B); Var.: variable).

Biological material sample observed	RTIL used (Index # from Table 1)	Initial sample condition	Treatment method and time	v/v% RTIL solution (optimal in parenthesis if applicable)	EM observation parameters (optimal in parenthesis if applicable)	Authors, reference, & year
Microbial Studies						
Grains of star sand (*foraminifera* shells)	1	–	S2	100%	20 kV SE-SEM	Kuwabata et al.[22] 2006
Basidiospores (*Laccaria, Lactarius lignyotus,* & *Russula integra*)	3	Fixed, hydrated	S2: 1 minute	Var. 1–100% (5–10%)	15 kV SE-SEM	Yanaga et al.[19] 2012
Aspergillus fumigatus, mixed culture yeast (*Saccharomyces cerevisiae*) and bacteria (bac)	12	–	–	Var. (10%)	10 kV SE-SEM, 2–3 kV FESEM, 15 kV for VP-SEM	Joubert and McDonald[36] 2016
Protists (*Paramecium caudatum, Thalassiosira,* & *Dinophysis*)	6	Fixed, hydrated	S2: 15 minutes	2%	BSE-SEM, low vacuum	Ishida et al.[41] 2016
Staphylococcus aureus	6, 12	Unfixed, hydrated	S2: 5 minutes	50%	15 kV SEM	Kawai et al.[42] 2013
Leptospira biflexa, Salmonella Senftenberg, vaccinia, and Ebola virus	6	Unfixed, hydrated	S1: 60 seconds	2.5%	4 kV SE-SEM	Golding et al.[21] 2016
Streptococcus mutans biofilm	2, 4, 7, 20	Unfixed and fixed, hydrated	S1: 10 minutes	Var. 1–20% (RTILs 7 & 4–10%)	Var. 1–20 kV SE-SEM (5 kV), 200 kV TEM	Asahi et al.[20] 2015
Herpes simplex virus 1	3–7, 21	Unfixed, hydrated	S1: 3 minutes	2%	TEM	Tsuda et al.[40] 2018
Cellular Biology						
A549 (adenocarcinomic human alveolar basal epithelial cells) cells on wrapping film & Panc-1 (pancreatic carcinoma)	2, 3, 6, 14, 17,18,19	Fixed and/or treated with 50X diluted colloidal gold labelled IgG for improved contrast	S1: 60 second	Var. 0–75% (RTILs 3 & 6-10-25%)	Var. kV SE-SEM (0.9–1.2 kV)	Ishigaki et al.[39,43,44] 2011
Mouse-derived fibroblast L929 cells	5, 7	Unfixed, hydrated	S2: RTIL 5 for 60 seconds; RTIL 7 for 10 seconds	0.5%	SE-SEM	Tsuda, et al.[18] 2011
Chinese Hamster Ovary (CHO) cells	12	–	7 –	10%	10 kV SE-SE4 M, 2–3 kV FESEM, 15 kV for VP-SEM	Joubert and McDonald[36] 2016
Indian muntjac spread chromosomes and polyamine (PA) isolated human chromosomes from HeLa cell line	3, 5, 6	Fixed, hydrated	S1: 1 minute	Var. 0.1–3% (RTIL 6–0.1-1%)	Var. 1.5–10 kV SE-SEM (1.5 kV), high and low vacuum	Dwiranti et al.[45] 2012
Forelimb buds of embryonic mice	12	Fixed, hydrated	S2: 60 seconds	–	SE-SEM	Iezaki et al.[46] 2018
Human osteoblast-like Saos-2 cells on untreated and laser-modified Ti surfaces	3	Live, unfixed, hydrated	S2: 5 minutes	5%	BSE-SEM, low vacuum	Lee et al.[47] 2020
Plant Structures						
Seaweed leaf	2, 6	Dried, re-hydrated	S2: 2 hours	100% (RTIL 6)	SE-SEM	Arimoto et al.[23] 2008
Seaweed leaf	2, 6, 10,11,12,	Dried, re-hydrated	S2: 2 hours	100%	15 kV SE-SEM	Kawai et al.[35] 2011
Pollen from a stamen of *Camellia sasanqua (C. sasanqua)*	6, 12	Unfixed, hydrated	S2: 30 minutes	0.5 g	15 kV SEM	Kawai et al.[42] 2013
Pollen from *Lillium* 'Casa Blanca'	2	Unfixed, hydrated	S2: 30 seconds	5%	10 kV SE-SEM	Tsuda, et al.[17] 2011

© 2021 Wiley-VCH GmbH

Table 2. continued

Biological material sample observed	RTIL used (Index # from Table 1)	Initial sample condition	Treatment method and time	v/v% RTIL solution (optimal in parenthesis if applicable)	EM observation parameters (optimal in parenthesis if applicable)	Authors, reference, & year
Microbial Studies						
Pollen from *Primula juliae, Anemone coronaria, Leucoglossum paludosum, and Lathyrus odoratus*	6	Unfixed, hydrated	S2: 600 second	10%	5 kV SE-SEM	Tsuda, et al.[17] 2011
Mature pollen grains of *Lilium* cultivar	7	Unfixed, hydrated	S2: 10 seconds	Var. 1–100% (1 & 5%)	5 kV, SE-SEM	Komai et. al.[48] 2014
Petal and stamen of Asteraceae flower	2	Unfixed, hydrated	S2: 30 seconds	5%	10 kV SE-SEM	Tsuda, et al.[18] 2011
Pelargonium leaf, Pollen grains	12	–	–	Var. (10%)	10 kV SE-SEM, 2–3 kV FES-EM, 15 kV for VP-SEM	Joubert and McDonald[56] 2016
Dried wood (*Cryptomeria japonica*)	4	–	S2: 60 seconds	5%	5 kV SE-SEM	Tsuda et al.[17] 2012
Modern wood (*Cryptomeria Japonica, Larix gmelinii*, Zelkova serrata Makino, *Fagus crenata Blume*) & archaeological wood (*Chamaecyparis obtuse*)	16	Originally dried and then boiled in water	S2: 10 minutes	Var. 1–30% (10%)	10 kV SE-SEM (10 kV)	Yamashita et al.[38] 2018
Modern wood, archaeological wood (violin c. 1750, 18th-century spruce wood, Chinese zither)	1, 13, 14, 15	–	S2: 30 seconds	Var. 5–100% (RTIL 14–7.5%)	5 kV SE-SEM	Lu et al.[27] 2019
Arthropods						
Scaled butterfly wing	1	Unfixed, hydrated	S2: 60 seconds	5%	10 kV SE-SEM	Tsuda et al.[17] 2012
Small Crustaceans (*Gammaridea, Tanaidacea,* and *Myodocopida*)	12	–	S2: 1–3 hours	10%	5 kV SE-SEM	Shiono et al.[37] 2014
Yellow jacket (*Vespula*)	2	Unfixed, hydrated	S2: 60 seconds	5%	10 kV SE-SEM	Tsuda et al.[18] 2011
Live Tick (*Haemaphysalis flava*)	–	Unfixed, live	–	–	SEM	Ishiqaki et al.[49] 2012
Other Biological and Related Specimens						
Bacterial cellulose gel (produced by *acetobacter xylinum*), red king crab shell (tsubugai), Neptune Whelk shell (tsubugai), scallop shell (hotate)	7	Freeze dried	S1: < 30 seconds	Var. 0.1–10% (10%)	5 kV SE-SEM	Abe et al.[50] 2012
Villi of mouse small intestine	3	Unfixed, hydrated	S2: 600 seconds	5%	5 kV SE-SEM	Tsuda et al.[18] 2011
Epithelial and muscular chicken tissue	6, 12	Unfixed, hydrated	S2: 30 minutes	100%	15 kV SE-SEM	Kawai et al.[53] 2011
Liposomes	5, 7	Hydrated	S1	Var. 10–30% (10%)	TEM	Hayakawa et al.[51] 2013
Carbon nanotubes (CNTs), fullerene C_{60} nanocrystals and nanowhiskers	9	–	S1: < 30 seconds	Var. 0.01–0.1% (0.02%)	5 kV SE-SEM	Abe et al.[52] 2013
Hydrous superabsorbent polymer (SAP)	3-8	Dry and hydrous SAP particles (pre-treated with water overnight)	S1: 5 minutes	Var. 10–100% (RTILs 4 & 8–100%)	5 kV SE-SEM	Tsuda et al.[33] 2014

 © 2021 Wiley-VCH GmbH

ChemBioChem | Reviews
doi.org/10.1002/cbic.202100041
Chemistry Europe
European Chemical Societies Publishing

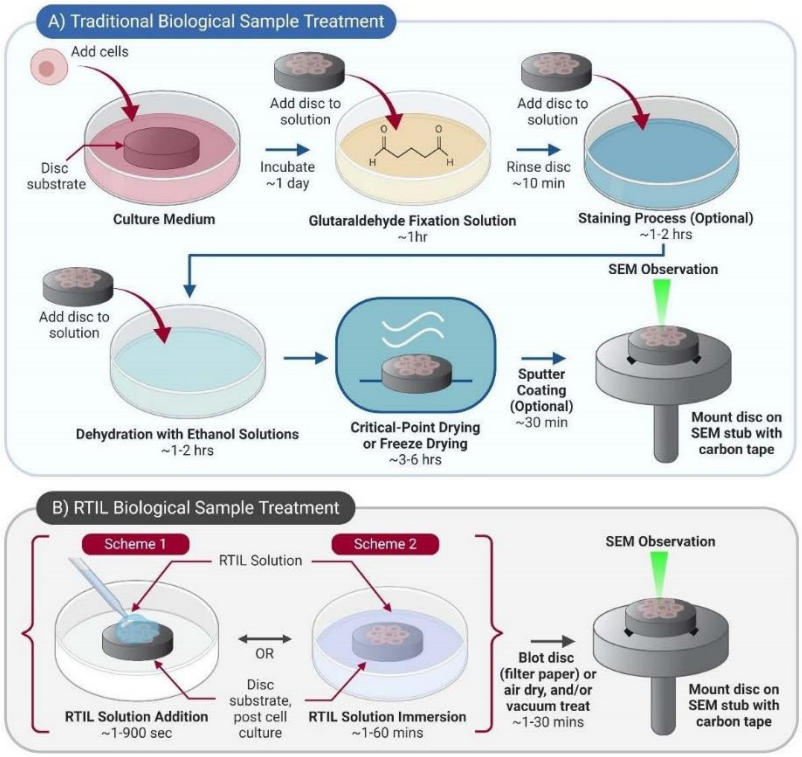

Figure 1. A) Illustration of the traditional biological sample preparation treatment procedure for SEM observation of cells. B) Illustration of RTIL biological sample treatment procedure, highlighting RTIL solution via addition (Scheme 1) or immersion (Scheme 2) techniques to prepare cells for SEM observation. Note the decrease in preparation time from longer than six hours to minutes. Image created with BioRender.com.

is variable in literature, though can be found to normally last under 5 minutes (Table 2). With this minimal exposure time in treatment, an unfixed, hydrated sample may be prepared for EM imaging in under an hour. Heating the solution prior to treatment is recommended, reducing the viscosity of the solution to spread more evenly across a surface and mitigating liquid accumulation on the surface referred to as pooling.[18,23] If high-purity RTILs cannot be obtained, purification methods of RTILs may be considered.[70,71] Post-treatment, samples are typically blotted using filter paper or other means to remove excess liquid, often followed by vacuum treatment in the range of 1–30 mins before SEM observation to evaporate excess liquid from the sample surface. After being appropriately prepared and mounted onto an SEM stub, RTIL-treated biological samples are typically observed using acceleration voltages within the range of 5–10 kV in SEM (Table 2). Similarly, Figure 3 shows how the Scheme 1 (Figure 1B) addition method can be adapted for use in transmission electron microscopy (TEM).

Microbial Studies

Since Kuwabata et al. first observed star sand grains, *Foraminifera* shells, using RTILs,[22] many other microbial-based applications have been explored, outlined within this section. Golding et al. proposed that the RTIL treatment may better conserve microbe size, making it a representative preparation model for studying microbes.[21] Similarities between morphological measurements of the Ebola virus prepared for EM using [BMI][BF_4][21] are noted to Cryo-EM observations,[72] suggesting that the RTIL preparation is a closer representation of the natural hydrated state.[21] This is attributed to the low vapor pressure of [BMI][BF_4], which avoided artifacts in samples such as wrinkling, shrinkage and cracking, as well as the preserved hydrated state of the sample.[21] Traditionally prepared samples were reported to have flattening and collapse of samples due to dehydration.[21]

Microbial samples with pointed or sharp features are often hard to image in SEM due to a phenomenon known as the "edge effect". For samples that have sharp edge-like features,

© 2021 Wiley-VCH GmbH

ChemBioChem | Reviews doi.org/10.1002/cbic.202100041 | Chemistry Europe European Chemical Societies Publishing

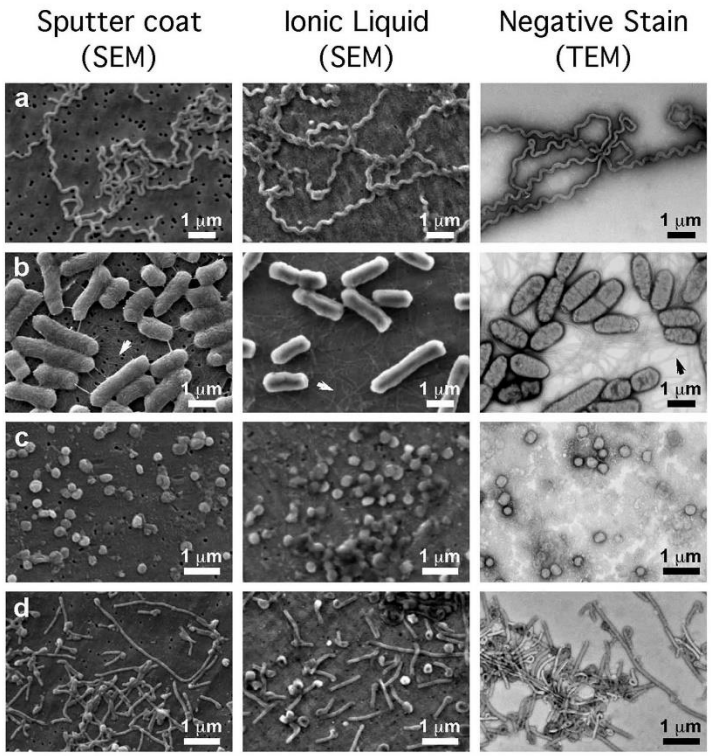

Figure 2. Comparison of conventional sputter coating SEM sample preparation methods (left column) with [BMI][BF_4] RTIL treatment (middle column) and conventional TEM (right column) for the observation of microbes: (a) *Leptospira biflexa*, (b) *Salmonella* Senftenberg, (c) vaccinia, and (d) Ebola virus. Sputter coating was done with gold on plain uncoated filters, RTIL treatment was on pre-coated aluminium filters, and TEM utilized methylamine tungstate negative staining. Image reproduced under the Creative Commons CC BY 4.0 License from Christine G. Golding et al.[21]

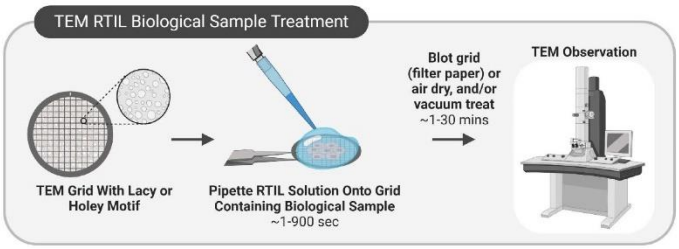

Figure 3. Illustration of sample addition RTIL method for TEM biological sample observation. Image created with BioRender.com.

higher amounts of escaping surface electrons cause charge accumulation in these areas, which can be difficult to mitigate using conventional sample preparation methods apart from using lower electron-beam energies.[73] Yanaga et al. used varying concentrations of [EMI][BF_4] in pure water to study the ultrastructure of various basidiospores, which are highly topographical with pointed features.[19] Notably, at an optimal concentration between 5–10%, imaging artifacts such as electron charging at point tips were mitigated using the RTIL treatment, showing that RTILs present a method to improve imaging of sharp edge-like features.[19] Similarly, Ishida et al. found an optimal treatment of 2–3% [BMI][BF_4] resolved fine

 © 2021 Wiley-VCH GmbH

ChemBioChem
Reviews
doi.org/10.1002/cbic.202100041
Chemistry Europe
European Chemical Societies Publishing

structural details of highly textured protists with minimal amounts of charging.[41] Both works further note that low concentrations outside of these optimal ranges resulted in surface charging while higher concentrations resulted in liquid pooling on the surface.[19,41]

Other applications of RTILs can be found in literature reporting quick and efficient observation of microbes in SEM. In the study of biofilms, Asahi et al. were able to use RTILs to study the native structure of *Streptococcus mutans*, in hydrated fixed and unfixed states.[20] Biofilms are hydrous and otherwise severely impacted by dehydration and harsh fixation steps used in conventional EM preparation.[74,75] Hydrophilic RTILs resulted in better imaging quality for biofilms while highly concentrated RTIL solutions led to liquid pooling on regions of interest.[20] Typical features of conventionally prepared biofilms such as sample cracking and fibrous features of extracellular matrix constituents were not observed in RTIL treatment.[20]

Recently, works produced by Tsuda et al. explored the use of RTILs in TEM imaging applications for microbial research.[40] Following a pipette-based IL treatment protocol (similar to Figure 3), RTILs successfully facilitated the visualization of herpes simplex virus I (HSVI) in TEM.[40] Kamlet-Taft parameters for polarity factors were consulted in evaluating RTILs for TEM imaging, where RTILs such as [EMI][BF_4] and [Ch][Lac] with a high hydrogen bond accepting ability (denoted by parameter β) performed optimally and caused no noticeable damage to specimen morphology.[40] This is one of the few studies to effectively report the successful use of RTILs in TEM, while most available studies use RTIL treatment in SEM.

Cellular Biology

Key works produced in 2011 were the first to collectively explore fundamental concepts of RTIL usage for cellular samples, notably the feasibility of imaging cells with various RTILs at different concentrations, the influence of hydrophilicity, and its application for different cellular samples.[18,39,43,44] Since then, RTIL solutions have been applied to a variety of cellular samples and proposed as a potential medium for live-cell imaging.

Tsuda et al. were the first to describe RTILs as a "facile" treatment in studying a wide range of biological samples, from insects and plants to single-cell observation applications.[18] For cellular studies, Tsuda et al. suggested using biocompatible RTIL candidates that may better preserve cellular structures, where [EMI][Lac] & [Ch][Lac] were identified as the most suitable for imaging mouse-derived L929 cells after evaluating their viability using flow cytometry at different RTIL and cell medium concentrations.[18] While the cells could be quickly imaged using this method, finer cellular features were lost due to low secondary electron contrast and cells appeared flattened, a potential artifact from the drying and/or vacuum conditions.[18] Fixed hydrated samples were found to provide stable and improved imaging quality in their work in comparison to unfixed samples.[18] Joubert and McDonald further note that fixation may allow for better sample preservation when using diluted 10% Hitachi Ionic Liquid HILEM© IL1000 solution to perform single-cell SEM observation of Chinese Hamster Ovarian (CHO) cells.[36]

The influence of RTIL concentration and selection for cellular samples have been explored in great depth for fixed A549 cells, treated with and without gold-conjugated antibodies.[39,43] It was highlighted that RTILs can efficiently facilitate cellular imaging without SEM charge build-up, resolve fine cellular features such as microvilli, and perform optimally at low SEM accelerating voltages of 0.9–1.2 kV (Figure 4).[39,43] Hydrated A549 cell images of exceptional quality are shown using a reported 1-minute [EMI][BF_4] RTIL treatment protocol in Figure 4, which was further improved upon using gold-conjugated antibodies treatment prior to RTIL treatment.[43] In exploring the influence of concentration, similarly to previously presented microbial studies,[19,20,41] it was found that higher concentrated RTILs resulted in solution surface pooling due to their highly viscous nature while low concentration solutions resulted in charge buildup.[39,43] Moreover, the study of these cells helped show that the hydrophobicity of the RTILs greatly affects imaging, with hydrophilic RTILs diluted in aqueous solution giving far superior imaging quality in comparison to hydrophobic RTILs diluted in acetone-based solutions.[39]

The potential of RTILs to image different types of cells and cellular processes was highlighted by Ishigaki et al., who studied the epithelial-mesenchymal transition of A549 as well as Panc-1 (pancreatic carcinoma) cells in the presence of TGF-β1, a transforming growth factor.[44] Fine features such as cell-to-cell bridging as well as filopodia in cells could be observed using a 25% [EMI][BF_4]-aqueous solution in SEM, features that were also observed at lower resolution in their EVOS microscope.[44] Moreover, the authors distinguished key morphological differences between cells with and without TGF-β1 treatment, noting that the number of filopodia reduced in size and number significantly with exposure to TGF-β1, one of the first demonstrations of this novel effect in SEM.[44]

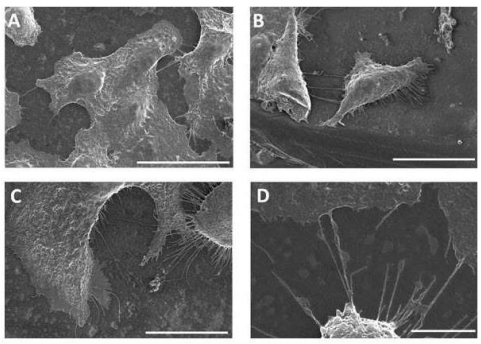

Figure 4. Fixed, hydrated A549 cells observed with [EMI][BF_4], diluted to concentrations within 10—40 v/v%. Fine topographical features and microvilli were resolved with this treatment. Scalebars are 50 μm in panel A, 30 μm in B and C, and 10 μm in D. Image reproduced with permission from Yasuhito Ishigaki et al.[43] (Copyright © 2010 Wiley-Liss, Inc.)

© 2021 Wiley-VCH GmbH

ChemBioChem
Reviews
doi.org/10.1002/cbic.202100041
Chemistry Europe
European Chemical Societies Publishing

A novel application of RTILs in imaging of cellular structures by Dwiranti et al. used combinations of platinum blue (Pt-blue) staining and one of EMI-BF_4 or BMI-BF_4 to image Indian Muntjac and human chromosomes.[45] The optimal concentration of these RTILs for imaging was found to be within the range of 0.1–1%.[45] Notably, phase contrast microscopy of these chromosomes confirmed that the treatment had no detrimental effects on chromosome morphology, indicating that RTILs can be used to image DNA without significantly altering its structure.[45] The results and discussion of this study suggested simply trading traditional methods out for RTILs is insufficient.[45] The use of an ionic liquid comes with its own unique set of parameters to achieve the best results, ranging from sample preparation technique to optimal instrument operating conditions. However, the best practices and operating parameters for SEMs, such as optimal spot size and accelerating voltage, have yet to be fully characterized for the use of ionic liquids.

While RTIL treatment for cells in these works shows promising results due to their comparable imaging quality and resolution to conventional preparation techniques,[18,36,39,43,44] several aspects must still be understood and further studied in this field. Differences in morphological features in RTIL treated samples and conventionally prepared samples have been noted in the literature and should be further explored. Smooth surfaces obtained in platinum-coated cells versus ragged surfaces of those treated with RTIL have been observed as well as different lengths of microvilli of cells.[43] It is unclear as to whether these morphological features are preserved natural structures or artifacts from the treatment itself.

A new avenue explored by a limited number of researchers is the potential of RTILs for studying "live" cell imaging and surface interactions. Recently, Lee et al. featured a new treatment scheme that utilized a 5% [EMI][BF_4] solution in McCoy's 5 A modified medium to image mammalian cells adhered to nanotopographic laser-modified titanium substrates (Figure 5).[47] In Figure 5, low-vacuum backscattered SEM imaging mode is used with the RTIL treatment, where cells appear dark in contrast to the bright titanium substrate. The work compared the influence of untreated titanium substrates (Figure 5A/B) and laser-modified titanium (Figure 5C/D), where sub-micron features induced from the laser-modification appear as thin lines most clearly represented in Figure 5D.[47] Prior to imaging, an optimal percentage of ionic liquid that would cause limited influence on cell viability while maintaining improved imaging in SEM was determined. Human osteoblast-like Saos-2 cells were imaged using SEM and subsequently evaluated using biochemical assays as well as fluorescence microscopy to confirm cell viability.[47] Cells from this specimen were viable after treatment with the RTIL-media solution and after imaging; however, directly irradiated cells were killed due to electron beam damage.[47] This demonstrates treatment applicability to facilitate live imaging of cells in near-native environments while warning that cells are still highly vulnerable to the extreme environment required for EM.

In separate works, the viability of yeast cells in RTIL solutions was explored using hydrophilic [Ch][Lac] and [EMI][AcO] diluted with cell culture medium.[76] Observation characteristic bands

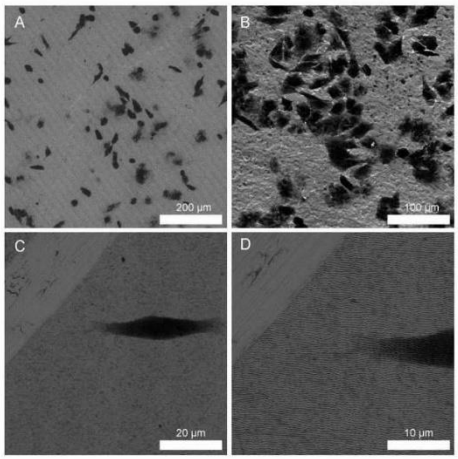

Figure 5. Cells adhered to titanium substrates after 5 minutes of a 5 v/v% aqueous [EMI][BF_4] RTIL treatment. Cells can be observed across the entire substrate of the unmodified sample (A/B) and in detail with respect to sub-micron features from the laser-modification treatment, which appear as fine lines on the metallic substrate (C/D). Image reproduced with permission from Bryan E. Lee et al.[47] (Copyright © 2020 Wiley-VCH GmbH).

following treatment revealed that yeast cells were able to maintain their bioactivity in the presence of RTILs,[76] further highlighting RTILs as a potential medium for live studies. Evidence of blueshift in the Raman spectrum corresponding to [EMI][AcO], however, was reflective of protein denaturation.[76] These results warn that only select RTILs such as [Ch][Lac] may be suitable for the investigation of cellular events that are contingent upon proper protein functioning, an incipient advantage of RTIL-based EM. A choline-like [EHACh][MO] RTIL used in the observation of red blood cells in SEM by Hyono et al. was noted to have minimal effect on the shape and size of cells observed with minimum charging.[77] When observation was attempted using imidazolium-based ionic liquids, no cells could be visualized, speculated due to induced cell lysis with high osmotic pressure on the cell membrane.[77] This suggests that choline-based RTILs could be used to accurately study blood cells without causing significant damage to their structure. Additionally, [Ch][Lac] has been demonstrated to be an effective medium for the analysis of lipid vesicle fusion in TEM.[51] It was posited that ionic liquids induce this process via localization at the water-lipid interface between the vesicles and cytosol, which separates the water layer and promotes fusion of the membrane with the vesicle.[51] With lactate anions, comparison with vesicle fusion induced by [EMI] cations showed that cholinium cations yield smaller vesicles.[51] The observation of these sub-cellular processes *in vitro* and *in vacuo* provides further support for the potential to view live cellular processes in EM through sample preparation methods using choline-based RTILs.

© 2021 Wiley-VCH GmbH

ChemBioChem | Reviews
doi.org/10.1002/cbic.202100041
Chemistry Europe
European Chemical Societies Publishing

Plant Structures

Arimoto et al. were the first to study plant structures in SEM using pure [BMIM][TFSI] and [BMIM][BF_4] to observe water-swelled seaweed through an immersion treatment method.[22] In later works, Kawai et al. further explored seaweed in SEM using bioinspired choline-like RTILs, noting they were more easily integrated through the immersion protocol.[35] Moreover, choline-like solutions better conserved the morphology of the seaweed with higher impregnation rates and size retention of samples.[23] Subsequently, several others have used RTILs to observe plant structures, such as delicate flower petals and stems,[18] leaf structures,[36] pollen,[18,36,42] and wood.[17,27,38]

Pollen specimens have been a key target for RTIL treatment due to their inherently fragile and highly topographical, non-conductive structures. Tsuda et al. featured a variety of pollen specimens (*Primula juliae, Anemone coronaria, Leucoglossum paludosum, and Lathyrus odoratus*) with sharp features that were easily imaged using a 10% [BMI][BF_4]-water solution, shown in Figure 6.[18] Similarly, Joubert and McDonald used a 10% Hitachi Ionic Liquid HILEM© IL1000 solution to observe pollen grains.[36] While fine structures could be observed, excess solution remained on the sample, highlighting the need to further optimize the treatment method.[36] When RTILs are used in pure condition states, the application of choline-type RTILs to study pollen samples has been shown to lead to improved imaging results in comparison to non-choline-like [BMI][BF_4].[42] However, Komai et. al. noted that highly concentrated RTILs can effectively hide surface features from observation and found that low concentrations of 1% and 5% [Ch][Lac]-ethanolic solutions provided improved resolution in imaging hydrated, unfixed mature pollen grains of *Lilium* cultivar in SEM.[48]

The study of wood and its hierarchical structure is another area that researchers have explored the use of RTILs for imaging treatment. Wooden specimens can be difficult to image using

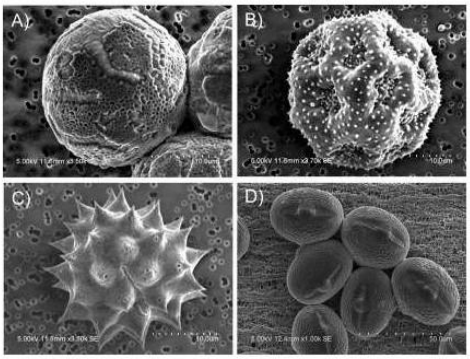

Figure 6. SEM images featuring pollen pretreated using an RTIL immersion-based method using a 10 v/v% [BMI][BF_4] aqueous solution for 600 seconds. Pollen specimens shown are: A) *Primula juliae*, B) *Anemone coronaria*, C) *Leucoglossum paludosum*, and D) *Lathyrus odoratus*. Image reproduced with permission from Tetsuya Tsuda et al.[18] (Copyright © 2011 Wiley-VCH, Weinheim).

EM methods due to their insulating nature, requiring conductive coating for SEM.[78] Often, wood-based structures have complex topographical features due to their hierarchical structure, and sample features such as fractured surfaces can be even more difficult to coat, leading to potential uneven coverage. Tsuda et al. first studied wood (*Cryptomeria japonica*) using [EMI][AcO]. Uniquely, the RTIL was used as a solvent to better understand the mechanism behind wood liquification used for the depolymerization of cellulose[17] as high β value RTILs can easily dissolve cellulose.[79] SEM imaging of samples before and after liquification below 393 K was done to observe morphology changes in samples, exposing them to an immersion-based treatment of [EMI][AcO].[17]

More recently researchers have used RTILs to study a wide variety of modern and unique archaeological woods. Yamashita et al. used varying concentrations of [EMI][MP] ethanolic solutions to study soft, hard, and archaeological wooden specimens.[38] The study found a 10% ethanolic RTIL solution to be ideal for imaging and avoiding surface charging without deforming the fine wooden structures being observed.[38] Lu et al. further explored several RTILs as a means to effectively observe archaeological and spruce wood hierarchical structures, using a "facile" immersion-based treatment to quickly prepare samples and obtain high-quality SEM images (Figure 7).[27] It was noted that hydrophilic RTILs in this study performed better in imaging than hydrophobic solutions and that water content, viscosity, and density of the RTILs were also key parameters that influenced imaging quality.[27] The study found [BMP][DCA] at a 7.5% concentration in an ethanol solution gave the best imaging quality results, which outperformed conventional coatings in this work.[27] Delicate features such as torus/margo of wood pit membranes were imaged at varying temperatures without specimen damage using this scheme.[27] Given proper optimization procedures, RTIL preparation can give high-quality imaging with reduced time and higher throughput in sample preparation, particularly useful for studying precious wooden samples where only small pieces are available for study.

Arthropods

On the mesoscale, in between the macro and micro levels, RTILs have been applied to arthropods. Arthropods can be challenging samples to coat due to their inherent complex structures as well as the occasional presence of exoskeletons which can make it difficult and slow to impregnate with many conventional SEM preparation solutions. While acidified 2,2-dimethoxypropane (DMP) has been proposed as a quick alternative to traditional fixation and dehydration of insects with hard-to-penetrate cuticles, this still requires that conductive coatings be applied post-application.[80] These harsh treatments can also be destructive for fragile and soft insect tissues. Moreover, traditional treatments do not facilitate the observation of wet or soft samples, such as soft-shelled eggs, winged structures, and larvae which, due to high-vacuum SEM conditions, can alter their morphology and appearance, leading to crumpling and wrinkling.

© 2021 Wiley-VCH GmbH

ChemBioChem
Reviews
doi.org/10.1002/cbic.202100041
Chemistry Europe
European Chemical Societies Publishing

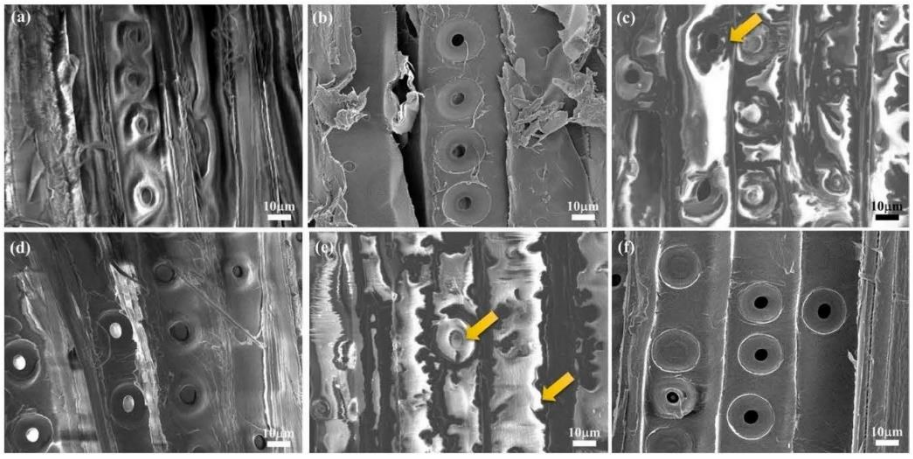

Figure 7. SEM images of modern spruce pretreated with (a) no treatment, (b) platinum sputtering, (c) 5% [EMI][TFSI], (d) 5% [EMI][DCA] (e) 10% [BMP][TFSI], and (f) 7.5% [BMP][DCA]/ethanol solutions. The acceleration voltage is 5 kV. Arrows highlight regions of excess RTIL accumulation. Image reproduced under the Creative Commons CC BY 4.0 License from Bing-Jyun Lu et al.[27]

To address these difficulties, researchers have turned towards alternative preparation techniques using RTILs. Tsuda et al. describe the versatility of RTIL treatment for biological applications and the use of [BMI][TFSI] in a 5% ethanolic solution to efficiently image yellow jacket (*Vespula*) specimens using a 60-second immersion method.[18] Fine features of the yellow jacket, such as its antennal fossae, were able to be imaged as shown in Figure 8.[18] Tsuda et al. show a similar immersion-based technique using [EMI][TFSI] to successfully observe delicate, unfixed scaled butterfly wings.[17] A comparison between the morphological observations of the RTIL treated sample to a glutaraldehyde fixed and gold sputter-coated specimen showed differences in size, shape, and SEM quality.[17] Due to the complex scaled butterfly wing structure and likely uneven coating, charging was observed when gold sputter coating technique was used, and imaging artifacts noted.[17] The avoidance of the fixation step in this work saved several hours of laborious sample preparation and enabled quick observation of these samples.[17] At the macro scale, Shiono et al. use the Hitachi Ionic Liquid HILEM© IL1000 to observe small crustaceans, *Gammaridea*, *Tanaidacea*, and *Myodocopida*, in SEM using an immersion-based RTIL treatment protocol.[37] Notably, the soft and delicate parts of the crustaceans, including the specimen's eggs, could be imaged using this solution without evaporating in the microscope.[37]

Both hydrophobic and hydrophilic ionic liquids have been applied to larger macro-scale observations done in the works of Ishigaki et al. for the observation of live ticks.[49] To reduce the potential of death, ticks were observed in the study at low vacuum conditions of 1.5×10^{3} Pa and lower acceleration voltages in the 2–5 kV range.[49] However, in this application, it was noted that the RTIL treatment techniques did not show significant improvement in imaging and that some RTILs were toxic to the live specimens being observed.[49] This highlights the need for understanding how RTILs may interact with specimens being observed, particularly toxicity effects in live imaging, as well as the need to study dilute solutions to optimize imaging parameters and decrease toxicity.

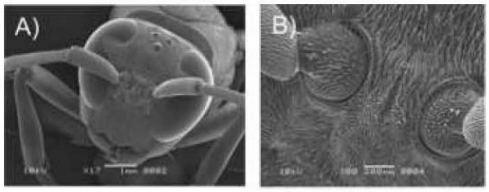

Figure 8. SEM images highlighting the A) head of a yellow jacket and B) antennal fossae of a yellow jacket. Both were treated with a 5 v/v% ethanolic [BMI][TFSI] RTIL solution for 60 seconds. Image reproduced with permission from Tetsuya Tsuda et al.[18] (Copyright © 2011 Wiley-VCH, Weinheim).

Other Biological and Related Specimens

Other works can be highlighted which look at the use of RTILs relevant to unique biological applications. One avenue which has not been discussed is the imaging of soft and mineralized tissue using RTILs.

Kawai et al. showed that immersion-based treatment methods can successfully be applied to soft tissue samples, notably the epithelial and muscular tissue of chicken, by using an immersion-based technique with choline-like RTILs.[35] Contrary

© 2021 Wiley-VCH GmbH

ChemBioChem | Reviews doi.org/10.1002/cbic.202100041 | Chemistry Europe European Chemical Societies Publishing

to imidazolium-based hydrophilic RTIL leaving hydrated samples relatively stiff, specimens treated with choline-based RTILs remained flexible.[35] The sub-standard performance of imidazolium-based ionic liquids in this study is attributed to their relative lipophilicity compared to choline-based ionic liquid, and their inherent structural differences that inhibit cell-mediated movement of the liquid across the membrane.[35] These findings suggest that choline-based ionic liquid treatments may be suitable for the investigation of other soft tissue samples. Using a similar technique, Tsuda et al. were able to image the villi of the small intestine of a mouse, revealing fine details such as microvillus from epithelial cells of the small intestine villi.[18] For successful imaging of soft tissue, longer immersion times can be noted in sample preparation using RTILs compared to other biological materials in Table 2, ranging from 5–10 minutes, allowing the RTIL to better impregnate the soft, wetted tissues considered.

Soft and hard tissue has been successfully imaged in SEM using [Ch][Lac] by Abe et al. to study mineralized shellfish and a soft bacterial cellulose gel.[50] The work achieved similar imaging quality to conventional Pt/Pd sputter coating techniques using [Ch][Lac] at a 10 v/v% concentration in ethanol instead. Energy-dispersed fluorescence X-ray spectroscopy (EDS) and elemental distribution mapping could also be done on RTIL-treated mineralized samples.[50] This suggests that similar preparation techniques could be effectively applied for imaging and analytical analysis of other tissues quickly and efficiently in SEM, a presentable area of growth for RTIL applications.

Research in non-biological sample centred RTIL imaging literature also has implications towards the imaging of biological samples. Carbon nanotubes (CNTs) are highly studied for their unique properties and characteristics. Notably in biomedical studies, CNT structures are being considered for their nanotextured features which may play an important role in protein adsorption and cellular adhesion.[52] To study potential hydrated unfixed samples on CNTs, Abe et al. showed that fine nano-scale features could be resolved in RTIL treatment using [HMI][PF_6], obtaining a resolution below 30 nm in their work and comparable quality to that of conventional Pt/Pd sputtering coating treatment.[52] This has implications not only for imaging CNTs in biological fields at high resolution but also for the potential to study other nanostructured surfaces and their interactions with biological specimens.

Tsuda et al. present a study that uses a variety of RTILs and studies their effectiveness in observing hydrous superabsorbent polymer (SAP) particles through an addition-based treatment method.[33] While not a typical biological material, SAP particles are used for a variety of applications in hygienic products and information from this RTIL study can be used, for instance, to infer the behaviour of RTILs on similarly structured polymers used in biological material scaffolds. The application of several RTILs found [$P_{4,4,4,1}$][DMP] to be the most effective in imaging these SAP samples while commonly used [EMI][BF_4] and [BMI][BF_4] were found to damage particles and lead to a reduction in the size of samples.[33] Potential degradation of [EMI][BF_4] and [BMI][BF_4] through hydrolysis of the [BF_4]$^-$ anion can occur with exposure to water and temperature increase, which could result in the formation of HF by-products.[81,82] Other RTILs studied by Tsuda et al. did not sufficiently integrate into structures and led to a reduction of size in SAP particles.[33] Overall, as exemplified by this work, as well as other applications mentioned, users need to consider how samples interact with the RTIL solutions, and how that may influence their structure and interpretation of images.

Related to the tissue applications mentioned, and the potential of RTILs to study non-conductive polymer-based materials such as SAP particles,[33] the use of RTILs in the application for visualizing substrates such as nanostructured surfaces, scaffolded materials, and polymeric based materials like hydrogels, is a natural point of progression for their application in biological imaging. Particularly, given the number of applications observing hydrated cells and microbes highlighted in Table 2, the use of RTILs for imaging interactions between complex substrates and biological samples holds great potential. In past work, Lee et al. eluded to this application, showing the success of visualizing SAOS-2 osteoblast-like cells imaged in their hydrated state on nanostructured, laser-modified titanium substrates.[47] The titanium substrates were of interest for orthopedic applications and using the RTIL technique, cellular interactions between the submicron features and cells could be elicited.[47] While limited works have been produced in this area, we believe this could be a key area of development for future growth of RTIL biological imaging.

Outlook

Acclaim of the scientific community

While the previous sections presented several examples of RTIL applications facilitating EM imaging for biological samples, the use of these RTILs is limited in comparison to the wide application of conventional EM techniques applied within the biological field. Typically, studies that use RTILs explore the application of RTILs themselves, rather than using RTILs to facilitate the investigation of other research topics. EM imaging presented by Iezaki et al. is one of few studies where RTILs are mentioned solely in the method section of the work and not as a focus of the research itself.[46] This is in part due to a lack of repetition studies as well as the limited availability of standardized treatment protocols for new RTIL users, despite the facile nature of this treatment. Moreover, limited studies exist where RTIL treatments are thoroughly compared to various control preparation methods, which could help identify whether observations are of natural structures or artifacts from the treatment itself. One suggested approach to improve confidence in these techniques would be to explore correlative imaging methods combined with different preparation methods to gain better insight into these methods. The works of Golding et al. do this quite well, where their RTIL treatment was compared to conventional TEM and SEM preparation and structural measurements of samples were correlated to past published Cryo-EM research for technique validation.[21] The expansion of casual RTIL use in biological studies as well as the

 © 2021 Wiley-VCH GmbH

ChemBioChem | Reviews doi.org/10.1002/cbic.202100041 | Chemistry Europe European Chemical Societies Publishing

exploration of these methods against various imaging controls may further encourage the application by others in the field and help establish it as an equivalent method to conventional protocols.

Another challenge to its adaptation, emphasized by Torimoto et al., is the reluctance of microscopists and scientists alike for putting liquid, wetted, and/or hydrated samples in vacuum-based microscopes.[16] This apprehension persists despite several works highlighting the possibility of observing samples hydrated with RTILs and has slowed the adoption and development of this technique, leaving many avenues of research unexplored and the true potential of RTILs insufficiently characterized.

Undoubtedly, using a technique such as this raises concerns of possible water and other contamination to the vacuum system should users not be careful in how they treat samples. To mitigate these risks, we suggest researchers use a minimal amount of RTIL solution where possible to treat samples. Moreover, blotting away excess solution with filter paper and using an intermediate vacuum treatment before EM observation is suggested to minimize the amount of solution being effectively introduced to the EM system. A vacuum station or intermediate vacuum stage that can be monitored is ideal where users can survey the stability of the vacuum and wait for it to stabilize to mitigate EM system risks. Lastly, it is suggested that for users considering samples treated with greater amounts of RTIL solution, observations should be conducted first in low vacuum mode to evaluate the risk of high vacuum operation by visually surveying to note if excess solution has accumulated on the sample surface.

Until RTILs are more widely accepted, traditional biological sample preparation methods are likely to continue and with it the limitations previously discussed. While this has persisted as a challenge, with increasing research in fields of liquid-phase electron microscopy, we expect that researchers will move towards accepting these methods and this reluctance will be alleviated.

RTIL selection and protocol optimization

With limited works available exploring these techniques, strategies need to be optimized to provide scientists guidelines on imaging techniques. Literature has focused more on the synthesis and application of these solutions, but little work has been done to comprehensively summarize and make recommendations on their utilization for biological samples for EM. Typical questions include: What are the optimal concentrations for imaging particular sample types and which RTILs are most suitable? How should the time of ionic liquid immersion change with sample and RTIL types in accordance with osmolarity and RTIL infiltration rate?

Table 1 and Table 2 may act as a good starting point towards identifying these trends; however, significantly more work and meta-analysis must be accomplished in this area. RTILs can vary greatly with respect to their interactions with different samples. Interactions include, but are not limited to, the extent of infiltration, water substitution, changes to sample structure, and changes to sample function in the case of live specimens. Thus, research must be done to establish interaction trends between sample type and the RTILs so that protocols can be designed accordingly. Expansion of statistical analysis of EM-relevant RTILs' Kamlet-Taft parameters[83] and their corresponding performance in EM may help answer part of this question and guide RTIL selection.[40]

Another important consideration relates to the customization of RTILs to yield properties that will work best for each biological sample type. Ganske and Bornscheuer used anion type, a determinant of water-miscibility, to inform their choice of RTIL paired with considerations of bacterial viability.[84] It was found that certain bacteria, such as *E. coli*, are intolerant to ionic liquids while others, such as *Bacillus cereus* and *Pichia pastoris*, experience only mildly toxic effects.[84] These findings suggest RTIL selection may be species-specific, and thus requires extensive investigation to characterize the applicability of each ionic liquid for a variety of specimens.

The suitability of certain RTILs for biological observation is owed in part to their structure, notably their hydrophobicity – with hydrophilic RTILs often performing more optimally for hydrated biological samples.[23,39] The phospholipid bilayer of cells in biological specimens are particularly sensitive to RTILs. Cations with long alkyl side chains are largely hydrophobic and can insert themselves in between phospholipids of the cell membrane.[69] This disturbance in the cell membrane can create artifacts in the morphology of the cell surface.[69] On the method of using RTILs in imaging, the mechanism by which ionic liquids diffuse and substitute water in hydrated samples must also be further characterized. Although the replacement of water by RTILs has been performed in theory,[23] the extent, efficiency, and precision to which RTILs can substitute water is not yet demonstrated experimentally. This is an important consideration for future works, as failure to properly integrate RTILs into hydrated tissues and sufficiently displace water molecules can impact imaging and affect sensitive EM instruments.

RTIL sample longevity and purity

The impermanence of RTIL treatment hinders the long-term viability of samples and is another challenge facing future adopters.[44] The impermanence of the RTIL treatment is generally due to its wetted state, which can accumulate contaminants overtime even with careful storage and lead to reduced imaging quality. Thus, samples pretreated with RTILs should be imaged within the first 6–7 days following treatment, after which samples exhibit charging effects and must be treated again to re-establish conductivity.[43] Careful storage to mitigate dust or contamination could extend hydrophilic RTIL coated samples up to one month.[39] However, little is known about how successive treatments with ionic liquids affect image quality or sample integrity and is an area for further exploration.

In addition, the importance of RTIL purity in yielding high-quality EM images has been noted in various works.[18,45] The

 © 2021 Wiley-VCH GmbH

ChemBioChem | Reviews doi.org/10.1002/cbic.202100041 | Chemistry Europe European Chemical Societies Publishing

purity of an RTIL constitutes various measures, including water, chloride ion, and oxygen contamination.[55] Increasing ionic liquid purity can have profound effects on the clarity of images,[18] with sufficiently high purity (>99%) proven to eliminate the need for additional chemical treatments in some cases.[45] Should highly pure RTILs be unavailable, purification methods are available for RTILs,[70,71] however, these procedures require specialized equipment and related chemistry training. Purity has implications on the viability of RTILs for potential live-cell microscopy avenues. Dilute water-based RTIL solutions may interact with the electron beam to form acidic solutions at high accelerating voltages.[85] If not destroyed by radiation itself, sufficiently high H^+ concentrations from electron beam water interactions may significantly damage cellular structures.[85]

Application of RTIL to live microscopy

Despite preliminary success shown by Lee et al. in maintaining cellular activity in RTIL solutions and placing living cells under low-vacuum conditions in EM,[47] radiation of the electron beam can ultimately swiftly induce cellular and microbial death, a challenge in the investigation of live cellular processes.[86] De Jonge and Pecky stress that live-cell EM is likely impossible due to the difficulties of the method.[86] Principally, they highlight the electron dosage required to yield quality images is much higher than the lethal dose.[86] They argue that certain reports of live cell studies feature questionable interpretations of live/dead assay results.[86] Kennedy et al. presented a strong case refuting these conclusions, with proof showing that *E. coli* could survive up to 90 mins of beam exposure in low electron dose imaging (less than $29e^-/nm^2$) in TEM.[87,88] While live imaging may be possible in EM, its methodologies are difficult and our understanding of assessing "life" at the micro length and time scale is limited. The superposition of these works demonstrates two core challenges in live EM: mitigating the effects of electron dosage and the scientific challenge of the quantification of live cells post EM observation.

A potential solution with respect to creating a more biologically-friendly environment for live cell EM may reside in choline-based RTILs. As mentioned earlier, Kawai et al. demonstrated the ability for choline-based ionic liquids to not only provide adequate conductivity to the surface but also preserve the size and structure of samples by traversing the cell membrane.[35] This conclusion was supported by Hyono et al. in their research on red blood cells and seaweed samples using another choline-like ionic liquid.[77] In possessing a structure similar to precursors of naturally occurring biosynthetic pathways, choline-like RTILs can make use of cellular channels and machinery to better infiltrate the tissues while still preserving the natural structure and flexibility of samples.[35] Although the mechanism of choline-like RTIL impregnation is not yet understood, its resemblance to choline derivatives may permit their movement across the cell membrane via membrane transport mechanisms.[35] This speculation has, in part, been addressed by the work of Sung and Johnstone, who demonstrate that despite a lack of active transport mechanisms, cells can stockpile choline derivatives in accordance with their metabolic needs.[89] These findings and the success of choline-based RTILs in imaging suggest that they may be better suited for creating a less hostile environment for biological sample observation, though more research is required in this field to address this.

In parallel, we must further consider how these materials combined with RTIL treatment behave in EM regarding fundamental electron beam interactions, such as the interaction volume, backscattered electron signals, the potential formation of radiolysis products in these media, and the generation of characteristic X-rays, which rely on deeper sample interactions for their signals. Answers to these questions will help develop an understanding of how instrument parameters, such as accelerating voltage, beam current, and electron dose should be adjusted for different RTIL treatments and samples under investigation, especially considering the assessment of live cells.

Summary

In this review, key works outlining the use of RTILs in biological EM have been identified and reviewed. These studies ranging from applications on microbes, arthropods, cells, and plant structures, highlight the potential advantages of RTILs as EM imaging agents for a wide variety of hard-to-image soft and/or wet samples. RTIL preparation protocols can drastically reduce the time spent preparing samples for EM, enabling users to image unfixed, hydrated samples while providing an equivalent, or even superior, image quality to that of traditional preparation methods.

Currently, RTIL treatment in the literature is highly sample-specific. Limited studies dedicated to protocol optimization are available, and these studies are largely restricted to the comparison of relative hydrophilicity, dilution and viscosity. Broadly, several challenges still exist in the use of RTILs in EM concerning the complexity of the interactions between RTILs, the sample to which they are being applied, and the electron beam they are later subject to.

While the use of RTIL treatment in EM is still in its infancy, it holds promise as a new conventional preparation method in the biological field. Although preliminary trends and conclusions can be drawn for certain subsets of RTILs and samples, overarching principles and best practices for optimal results remain difficult to identify. Standardized protocols for various biological sample types must be developed and shared with biological imaging communities for their consideration. As with any methodology, there exists a positive feedback relationship between knowledge of a method and its acceptance for general use, so it is expected that RTILs will gradually become better characterized as the apprehension over introducing wet samples into high-vacuum EM environments recedes. At this stage, it is paramount that not only successful results and methodologies be documented, but also that key points for failure, every refinement, and every observation leading to these results be identified, documented, and characterized. In doing so, we may eventually identify more definitive trends

 © 2021 Wiley-VCH GmbH

that will inform and shape the use of RTILs as a next-generation imaging treatment in future work.

Author Contributions

Conceptualization: Liza-Anastasia DiCecco, Kathryn Grandfield; Methodology: Liza-Anastasia DiCecco, Andrew D'Elia; Data curation: Liza-Anastasia DiCecco, Chelsea Miller; Formal analysis: Liza-Anastasia DiCecco, Andrew D'Elia, Chelsea Miller; Funding acquisitions and supervision: Kathryn Grandfield, Kyla N. Sask, Leyla Soleymani; Writing: Liza-Anastasia DiCecco, Andrew D'Elia, Chelsea Miller; Review and editing: Kathryn Grandfield, Kyla N. Sask, Leyla Soleymani

Acknowledgements

Financial support provided by the McMaster Faculty of Engineering Big Ideas fund, the Natural Sciences and Engineering Research Council of Canada (NSERC) Discovery Grant Program (RGPIN-2020-05722) and the Vanier Canada Graduate Scholarship (Vanier CGS) program is greatly acknowledged. The Frontispiece image was created with BioRender.com.

Conflicts of Interest

The authors declare no conflict of interest.

Keywords: Ionic Liquids · Electron Microscopy · Biology · Life Science · *in situ* Electron Microscopy · Imaging

[1] J. S. Wilkes, M. J. Zaworotko, *J. Chem. Soc. Chem. Commun.* **1992**, 965–967.
[2] M. J. Earle, P. B. McCormac, K. R. Seddon, *Chem. Commun.* **1998**, 2245–2246.
[3] T. Welton, *Chem. Rev.* **1999**, *99*, 2071–2083.
[4] R. Hagiwara, Y. Ito, *J. Fluorine Chem.* **2000**, *105*, 221–227.
[5] J. S. Wilkes, J. A. Levisky, R. A. Wilson, C. L. Hussey, *Inorg. Chem.* **1982**, *21*, 1263–1264.
[6] E. Cooper, E. J. O. Sullivan, *Proc. Eighth Int. Symp. Molten Salts*, The Electrochemical Society Inc, Pennington, NJ **1992**, pp. 386–393.
[7] C. Roosen, P. Müller, L. Greiner, *Appl. Microbiol. Biotechnol.* **2008**, *81*, 607–614.
[8] H. Pfruender, R. Jones, D. Weuster-Botz, *J. Biotechnol.* **2006**, *124*, 182–190.
[9] A. P. M. Tavares, O. Rodriguez, E. A. Macedo, *Ionic Liquids: New Aspects for the Future* (Ed.: J. Kadokawa), IntechOpen **2013**, pp. 537–556.
[10] S. Arimoto, D. Oyamatsu, T. Torimoto, S. Kuwabata, *ChemPhysChem* **2008**, *9*, 763–767.
[11] L. G. Chagas, S. Jeong, I. Hasa, S. Passerini, *ACS Appl. Mater. Interfaces* **2019**, *11*, 22278–22289.
[12] D. Chen, S. Indris, M. Schulz, B. Gamer, R. Mönig, *J. Power Sources* **2011**, *196*, 6382–6387.
[13] T. Tsuda, A. Imanishi, T. Sano, A. Sawamura, T. Kamidaira, C. Y. Chen, S. Uchida, S. Kusumoto, M. Ishikawa, S. Kuwabata, *Electrochim. Acta* **2018**, *279*, 136–142.
[14] Y. T. Hsieh, T. Tsuda, S. Kuwabata, *Anal. Chem.* **2017**, *89*, 7249–7254.
[15] D. Yamauchi, A. Fukuda, T. Nakai, I. Karahara, M. Takeuchi, D. Tamaoki, T. Tsuda, K. Tsunashima, S. Kuwabata, M. Hoshino, K. Uesugi, A. Takeuchi, Y. Suzuki, Y. Mineyuki, *Microscopy* **2019**, *68*, 92–97.
[16] T. Torimoto, T. Tsuda, K. I. Okazaki, S. Kuwabata, *Adv. Mater.* **2010**, *22*, 1196–1221.
[17] T. Tsuda, E. Mochizuki, S. Kishida, H. Sakagami, S. Tachibana, M. Ebisawa, N. Nemoto, Y. Nishimura, S. Kuwabata, *Electrochemistry* **2012**, *80*, 308–311.
[18] T. Tsuda, N. Nemoto, K. Kawakami, E. Mochizuki, S. Kishida, T. Tajiri, T. Kushibiki, S. Kuwabata, *ChemBioChem* **2011**, *12*, 2547–2550.
[19] K. Yanaga, N. Maekawa, N. Shimomura, Y. Ishigaki, Y. Nakamura, T. Takegami, N. Tomosugi, S. Miyazawa, S. Kuwabata, *Mycol. Prog.* **2012**, *11*, 343–347.
[20] Y. Asahi, J. Miura, T. Tsuda, S. Kuwabata, K. Tsunashima, Y. Noiri, T. Sakata, S. Ebisu, M. Hayashi, *AMB Express* **2015**, *5*.
[21] C. G. Golding, L. L. Lamboo, D. R. Beniac, T. F. Booth, *Sci. Rep.* **2016**, *6*.
[22] S. Kuwabata, A. Kongkanand, D. Oyamatsu, T. Torimoto, *Chem. Lett.* **2006**, *35*, 600–601.
[23] S. Arimoto, M. Sugimura, H. Kageyama, T. Torimoto, S. Kuwabata, *Electrochim. Acta* **2008**, *53*, 6228–6234.
[24] E. Kellenberger, R. Johansen, M. Maeder, B. Bohrmann, E. Stauffer, W. Villiger, *J. Microsc.* **1992**, *168*, 181–201.
[25] M. Ohi, Y. Li, Y. Cheng, T. Walz, *Biol. Proced. Online* **2004**, *6*, 23–34.
[26] Y. Li, L. M. Almassalha, J. E. Chandler, X. Zhou, Y. E. Stypula-Cyrus, K. A. Hujsak, E. W. Roth, R. Bleher, H. Subramanian, I. Szleifer, V. P. Dravid, V. Backman, *Exp. Cell Res.* **2017**, *358*, 253–259.
[27] B. J. Lu, J. R. Li, H. C. Tai, W. Cai, H. H. Tseng, Y. T. Hsieh, *Sci. Rep.* **2019**, *9*.
[28] P. Bonhôte, A. P. Dias, N. Papageorgiou, K. Kalyanasundaram, M. Grätzel, *Inorg. Chem.* **1996**, *35*, 1168–1178.
[29] K. R. Harris, M. Kanakubo, L. A. Woolf, *J. Chem. Eng. Data* **2007**, *52*, 1080–1085.
[30] E. Rilo, J. Pico, S. García-Garabal, L. M. Varela, O. Cabeza, *Fluid Phase Equilib.* **2009**, *285*, 83–89.
[31] E. Rilo, J. Vila, J. Pico, S. García-Garabal, L. Segade, L. M. Varela, O. Cabeza, *J. Chem. Eng. Data* **2010**, *55*, 639–644.
[32] M. G. Freire, A. R. R. Teles, M. A. A. Rocha, B. Schröder, C. M. S. S. Neves, P. J. Carvalho, D. V. Evtuguin, L. M. N. B. F. Santos, J. A. P. Coutinho, *J. Chem. Eng. Data* **2011**, *56*, 4813–4822.
[33] T. Tsuda, E. Mochizuki, S. Kishida, K. Iwasaki, K. Tsunashima, S. Kuwabata, *PLoS One* **2014**, *9*.
[34] K. Yoshii, K. Yamaji, T. Tsuda, K. Tsunashima, H. Yoshida, M. Ozaki, S. Kuwabata, *J. Phys. Chem. B* **2013**, *117*, 15051–15059.
[35] K. Kawai, K. Kaneko, H. Kawakami, T. Yonezawa, *Langmuir* **2011**, *27*, 9671–9675.
[36] L.-M. Joubert, K. McDonald, *Microsc. Microanal.* **2016**, *22*, 1170–1171.
[37] M. Shiono, M. Sakaue, M. Konomi, J. Tomizawa, E. Nakazawa, K. Kawai, S. Kuwabata, *Microsc. Microanal.* **2014**, *20*, 1016–1017.
[38] T. Yamashita, K. Miyamoto, H. Yonenobu, *Microscopy* **2018**, *67*, 259–265.
[39] Y. Ishigaki, Y. Nakamura, T. Takehara, T. Kurihara, H. Koga, T. Takegami, H. Nakagawa, N. Nemoto, N. Tomosugi, S. Kuwabata, S. Miyazawa, *Microsc. Res. Tech.* **2011**, *74*, 1104–1108.
[40] T. Tsuda, K. Kawakami, E. Mochizuki, S. Kuwabata, *Biophys. Rev. Lett.* **2018**, *10*, 927–929.
[41] H. Ishida, Y. Gobara, M. Kobayashi, T. Suzaki, *Int. J. New Technol. Res.* **2016**, *2*, 43-46.
[42] K. Kawai, K. Kaneko, H. Kawakami, T. Narushima, T. Yonezawa, *Colloids Surf. B* **2013**, *102*, 9–12.
[43] Y. Ishigaki, Y. Nakamura, T. Takehara, N. Nemoto, T. Kurihara, H. Koga, H. Nakagawa, T. Takegami, N. Tomosugi, S. Miyazawa, S. Kuwabata, *Microsc. Res. Tech.* **2011**, *74*, 415–420.
[44] Y. Ishigaki, Y. Nakamura, T. Takehara, T. Shimasaki, T. Tatsuno, F. Takano, Y. Ueda, Y. Motoo, T. Takegami, H. Nakagawa, S. Kuwabata, N. Nemoto, N. Tomosugi, S. Miyazawa, *Microsc. Res. Tech.* **2011**, *74*, 1024–1031.
[45] A. Dwiranti, L. Lin, E. Mochizuki, S. Kuwabata, A. Takaoka, S. Uchiyama, K. Fukui, *Microsc. Res. Tech.* **2012**, *75*, 1113–1118.
[46] T. Iezaki, T. Horie, K. Fukasawa, M. Kitabatake, Y. Nakamura, G. Park, Y. Onishi, K. Ozaki, T. Kanayama, M. Hiraiwa, Y. Kitaguchi, K. Kaneda, T. Manabe, Y. Ishigaki, M. Ohno, E. Hinoi, *Stem Cell Rep.* **2018**, *11*, 228–241.
[47] B. E. J. Lee, L.-A. DiCecco, H. Exir, A. Weck, K. Grandfield, *ChemBioChem* **2020**, *22*, 571–576.
[48] F. Komai, K. Okada, Y. Inoue, M. Yada, O. Tanaka, S. Kuwabata, *J. Jpn. Soc. Hortic. Sci.* **2014**, *83*, 317–321.
[49] Y. Ishigaki, Y. Nakamura, Y. Oikawa, Y. Yano, S. Kuwabata, H. Nakagawa, N. Tomosugi, T. Takegami, *PLoS One* **2012**, *7*.
[50] S. Abe, A. Hyono, Y. Machida, F. Watari, T. Yonezawa, *Nano Biomed. Eng.* **2012**, *4*, 18–23.
[51] E. H. Hayakawa, E. Mochizuki, T. Tsuda, K. Akiyoshi, H. Matsuoka, S. Kuwabata, *PLoS One* **2013**, *8*.

 © 2021 Wiley-VCH GmbH

[52] S. Abe, A. Hyono, K. Kawai, T. Yonezawa, *J. Nanosci. Nanotechnol.* **2015**, *15*, 9272–9274.
[53] F. H. Hurley, T. P. J. Wier, *J. Electrochem. Soc.* **1951**, *98*, 203–206.
[54] L. Crowhurst, P. R. Mawdsley, J. M. Perez-Arlandis, P. A. Salter, T. Welton, *Phys. Chem. Chem. Phys.* **2003**, *5*, 2790–2794.
[55] T. Tsuda, C. L. Hussey, *Modern Aspects of Electrochemistry No. 45* (Ed.: R. E. White), Springer, New York **2009**, pp. 337–340.
[56] J. F. Wishart, P. Neta, *J. Phys. Chem. B* **2003**, *107*, 7261–7267.
[57] M. D. McKee, A. Nanci, W. J. Landis, Y. Gotoh, L. C. Gerstenfeld, M. J. Glimcher, *J. Bone Miner. Res.* **1991**, *6*, 937–945.
[58] P. D. Galgano, O. A. El Seoud, *J. Colloid Interface Sci.* **2010**, *345*, 1–11.
[59] R. F. Egerton, P. Li, M. Malac, *Micron* **2004**, *35*, 399–409.
[60] M. Ohi, Y. Li, Y. Cheng, T. Walz, *Biol. Proced. Online* **2004**, *6*, 23–34.
[61] A. Bogner, G. Thollet, D. Basset, P. Jouneau, C. Gauthier, *Ultramicroscopy* **2005**, *104*, 290–301.
[62] J. P. Patterson, Y. Xu, M. A. Moradi, N. A. J. M. Sommerdijk, H. Friedrich, *Acc. Chem. Res.* **2017**, *50*, 1495–1501.
[63] X. Wang, J. Yang, C. M. Andrei, L. Soleymani, K. Grand, *Commun. Chem.* **2018**, *1*.
[64] X. Wang, J. Yang, C. Andrei, L. Soleymani, K. Grandfield, *Microsc. Microanal.* **2019**, *22*, 746–747.
[65] A. M. Donald, *Nat. Mater.* **2003**, *2*, 511–516.
[66] A. Kolmakov, *Liquid Cell Electron Microscopy* (Ed.: F. M. Ross), Cambridge University Press, New York **2019**, pp. 78–105.
[67] T. H. Moser, T. Shokuhfar, J. E. Evans, *Micron* **2019**, *117*, 8–15.
[68] K. He, T. Shokuhfar, R. Shahbazian-Yassar, *J. Phys. Condens. Matter* **2019**, *31*.
[69] T. Tsuda, S. Kuwabata, *Microscopy* **2020**, *69*, 183–195.
[70] M. Freemantle, *An Introduction to Ionic Liquids*, The Royal Society Of Chemistry, Cambridge **2010**.
[71] P. Wasserscheid, T. Welton, Eds., *Ionic Liquids in Synthesis*, Wiley-VCH, Weinheim **2008**.
[72] D. R. Beniac, P. L. Melito, L. Shauna, S. L. Hiebert, M. J. Rabb, L. L. Lamboo, S. M. Jones, T. F. Booth, *PLoS One* **2012**, *7*.
[73] H. Seiler, *J. Appl. Phys.* **1983**, *54*, https://doi.org/10.1063/1.332840.
[74] H. T. Chang, B. E. Rittmann, *Water Res.* **1986**, *20*, 1451–1456.
[75] S. E. Fratesi, F. L. Lynch, B. L. Kirkland, L. R. Brown, *J. Sediment. Res.* **2004**, *74*, 858–867.
[76] A. Matsuda, N. Sakaguchi, S. Shigeto, *J. Raman Spectrosc.* **2019**, *50*, 768–777.
[77] A. Hyono, T. Yonezawa, K. Kawai, S. Abe, M. Fujihara, H. Azuma, S. Wakamoto, *Surf. Interface Anal.* **2014**, *46*, 425–428.
[78] C. R. Cartwright, *Ann. Bot.* **2015**, *116*, 1–13.
[79] H. Ohno, Y. Fukaya, *Chem. Lett.* **2009**, *38*, 2–7.
[80] J. M. Bjerke, T. P. Freeman, A. W. Anderson, *Biotech. Histochem.* **1979**, *54*, 29–31.
[81] M. G. Freire, C. M. S. S. Neves, I. M. Marrucho, J. A. P. Coutinho, A. M. Fernandes, *J. Phys. Chem. A* **2010**, *114*, 3744–3749.
[82] S. Radosavljević, V. Šćepanović, S. Stević, D. Milojković, *J. Fluorine Chem.* **1979**, *13*, 465–471.
[83] D. J. Eyckens, L. C. Henderson, *Front. Chem.* **2019**, *7*.
[84] F. Ganske, U. T. Bornscheuer, *Biotechnol. Lett.* **2006**, *28*, 465–469.
[85] N. M. Schneider, M. M. Norton, B. J. Mendel, J. M. Grogan, F. M. Ross, H. H. Bau, *J. Phys. Chem.* **2014**, *118*, 22373–22382.
[86] N. de Jonge, D. B. Peckys, *ACS Nano* **2016**, *10*, 9061–9063.
[87] E. Kennedy, E. M. Nelson, T. Tanaka, J. Damiano, G. Timp, *ACS Nano* **2016**, *10*, 2669–2677.
[88] E. Kennedy, E. M. Nelson, J. Damiano, G. Timp, *ACS Nano* **2017**, 3–7.
[89] C. Sung, R. M. Johnstone, *Can. J. Biochem.* **1965**, *43*, 1111–1118.

Manuscript received: January 25, 2021
Revised manuscript received: March 8, 2021
Accepted manuscript online: March 9, 2021
Version of record online: ■■, ■■

 © 2021 Wiley-VCH GmbH

2.2. Liquid-EM Goes Viral – Visualizing Structure and Dynamics

2.2.1. Section Introduction (Objective ii)

Interest in liquid EM methods has surged recently, provided its impactful ability to resolve real-time dynamics reactions in liquid environments. This is of particular interest to biological communities, with whom can benefit from the technique with the potential to resolve molecular dynamics at HR. However, the technique remains relatively new for structural biology applications, with limited knowledge of best practices summarized for potential users. To accomplish the objective (ii) set out for this thesis involving developing new methods for HR liquid biological EM of virions, Section 2.2 introduces liquid EM and summarizes research utilizing the technique to explore viral assemblies and host-pathogen interactions. Experimental details such as specimen preparation, data collection, and computing processes that have led to HR liquid EM imaging were concisely summarized. Future possibilities involving the development of high-speed, highly sensitive acquisition detectors and tomography were presented as exciting future avenues for biological imaging. Overall, this work contributes to the advancement of our understanding of these techniques for virus and other biological imaging, highlighting liquid EM as a dynamic complement to current cryo EM methods that can provide a "real-time revolution" in nanoscale imaging.

Authors: Deborah F. Kelly, **Liza-Anastasia DiCecco**, G. M. Jonaid William J. Dearnaley, Michael S. Spilman, Jennifer L. Gray, Madeline J. Dressel-Dukes.

Publication: This work is published with a full citation provided as follows:

Kelly, D.F., **DiCecco, L.-A.**, Jonaid, G., Dearnaley, W.J., Spilman, M.S., Gray, J.L, and Dressel-Dukes, M.J. Liquid-EM goes viral – visualizing structure and dynamics. 2022. *Current Opinion in Structural Biology*, Vol. 75(102426). DOI: 10.1016/j.sbi.2022.102426 [Invited]

Reprinted from the above-listed citation, with permission from *Current Opinion in Structural Biology*. Copyright © 2022 Elsevier Ltd.

Available online at www.sciencedirect.com

ScienceDirect

Current Opinion in Structural Biology

Liquid-EM goes viral – visualizing structure and dynamics

Deborah F. Kelly[1,2,3], Liza-Anastasia DiCecco[1,4], G. M. Jonaid[1,2,5], William J. Dearnaley[1,2,3], Michael S. Spilman[6], Jennifer L. Gray[3] and Madeline J. Dressel-Dukes[7]

Abstract

Liquid-electron microscopy (EM), the room temperature correlate to cryo-EM, is an exciting new technique delivering real-time data of dynamic reactions in solution. Here, we explain how liquid-EM gained popularity in recent years by examining key experiments conducted on viral assemblies and host–pathogen interactions. We describe developing workflows for specimen preparation, data collection, and computing processes that led to the first high-resolution virus structures in a liquid environment. Equally important, we review why liquid-electron tomography may become the next big thing in biomedical research due to its ability to monitor live viruses entering cells within seconds. Taken together, we pose the idea that liquid-EM can serve as a dynamic complement to current cryo-EM methods, inspiring the "real-time revolution" in nanoscale imaging.

Addresses

[1] Department of Biomedical Engineering, Pennsylvania State University, University Park, PA 16802, USA
[2] Center for Structural Oncology, Pennsylvania State University, University Park, PA 16802, USA
[3] Materials Research Institute, Pennsylvania State University, University Park, PA 16802, USA
[4] Department of Materials Science and Engineering, McMaster University, Hamilton, ON L8S 4L7, Canada
[5] Bioinformatics and Genomics Graduate Program, Huck Institutes of the Life Sciences, Pennsylvania State University, University Park, PA 16802, USA
[6] Direct Electron, LP, San Diego, CA 92128, USA
[7] Protochips Inc., Morrisville, NC 27560, USA

Corresponding author: Kelly, Deborah F. (Debkelly@psu.edu)
(Kelly D.F.),
(DiCecco L.-A.),
(Dearnaley W.J.),
(Spilman M.S.),
(Dressel-Dukes M.J.)

Current Opinion in Structural Biology 2022, **75**:102426

This review comes from a themed issue on **Cryo-electron microscopy**

Edited by **Susan M. Lea** and **Pamela A. Williams**

For complete overview of the section, please refer the article collection - Cryo-electron microscopy

Available online 19 July 2022

https://doi.org/10.1016/j.sbi.2022.102426

0959-440X/© 2022 Elsevier Ltd. All rights reserved.

Introduction

For centuries, scientists have longed to view the molecular components that govern life's processes. To satisfy this curiosity, powerful imaging tools, such as electron microscopes, have continued to evolve — capable of revealing exquisite atomic details of biological materials [4,34,64,67]. Using these state-of-the-art instruments, we can better investigate never-before-seen pathogens that threaten human health or cause global pandemics [11,22,33,36,41,42,50,55]. As a complement to the "resolution revolution" that is sweeping the cryo-EM community's interest in liquid-electron microscopy (EM), the room temperature correlated to cryo-EM has skyrocketed in the last decade. It has quickly become a premier technique to analyze macromolecules live in solution providing an excellent complement to cryo-EM studies.

In this review, we track the historical progress of the liquid-EM field while discussing new workflows for specimen preparation, data collection, and computational analysis for the structural biology community. As many recent successes in liquid-EM draw upon

Figure 1

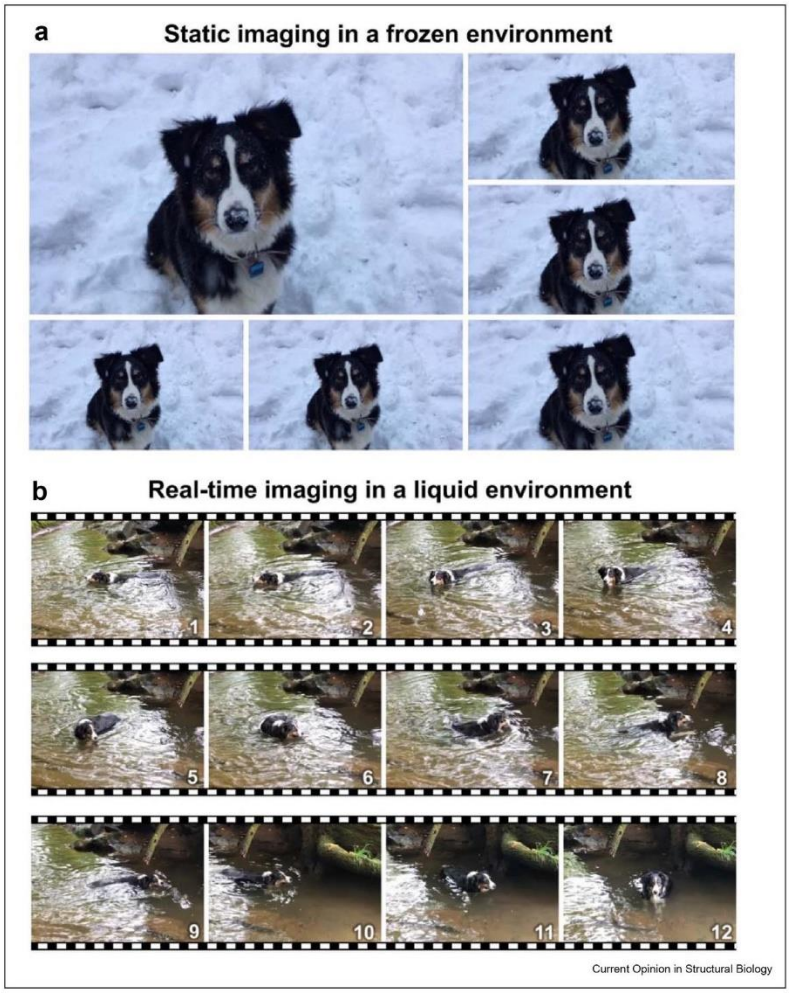

Demonstration of biological samples in static and liquid environments. (a) Gallery of static images of an Australian shepherd in a frozen environment. Panels shown at different magnifications have consistent features. **(b)** Gallery of real-time images of the same specimen in a liquid environment. Movements presented in a dynamic framework complement the structural features displayed at high resolution in the static images.

established routines implemented in the cryo-EM field, here, we focus on specific aspects of solution-based imaging. Broadly speaking, liquid-EM results may not reach the resolution achieved with cryo-EM studies. Its utility is in revealing structural dynamics — permitting scientists to better visualize samples in motion (Figure 1). This feature sets liquid-EM apart from other imaging modalities at the nanoscale.

Undeniable, advances in direct electron detectors and high-throughput data collection have spurred high-resolution observations in both cryo-EM and liquid-EM [3,21,24,40,54,67]. Determining nanoscale features among flexible parts, however, remains a challenge in X-ray crystallography and cryo-EM. While protein crystals and EM specimens are frozen and pristinely preserved during data collection, this step yields mere snapshots of their dynamic subjects. Given enough data, multiple structures may be determined in a time-resolved manner [17–19,49,58]. But what about dynamics? It is often neglected in high-resolution interpretations, yet this important information holds the secret to how biological entities perform their essential duties. For lower molecular weight entities, NMR

studies paired with molecular dynamic simulations are a powerful complement. For larger macromolecules, liquid-EM can fill this gap in dynamic observations to improve our knowledge of the nanoworld.

In materials research, liquid-EM studies have already produced high-resolution results along with dynamic characterizations for hard and soft polymers [1,2,8, 35,46,51,54,65,66]. As applications are now trending toward biomaterials, there is a growing desire to utilize and advance the limits of the technique [25]. For example, there is immense interest from the pharmaceutical industry to observe human viruses in liquid as they would occur in the body. It is, therefore, ideal to pair detailed structural information with live dynamic assessments as many biological events occur within milliseconds. Importantly, the combined knowledge of flexible structures can assist with fighting emerging pathogens including but not limited to SARS-CoV-2, influenza, respiratory syncytial virus, or rotavirus [7,24,30,39,44,60].

Here, we focus on recent liquid-EM imaging results through a series of case studies performed on virus assemblies. Adeno-associated virus subtype 3 (AAV) is the highest resolution structure of a specimen in solution determined using single-particle analysis [24]. This work was possible thanks to direct electron detectors and high-performance computing. Results showed multiple dynamic structures of AAV in solution calculated from real-time movies. In addition to individual viruses, host−pathogen interactions are also discussed using liquid-EM. Bacterium-phage interactions in solution were first described by the Timp team in which phage particles were seen engaging the bacteria surface along with instances of phage entry [27]. This work was foundational for subsequent studies involving liquid-electron tomography (liquid-ET) of bacteria−phage interactions and a new preprint involving human immunodeficiency virus (HIV) entering human cells [10,31]. For each case, we describe specimen preparation, imaging workflow, and biological interpretations of the findings.

Liquid-EM enclosures and imaging workflows

There are numerous protocols to prepare samples in liquid enclosures [10,13,14,25,57,65]. Early work from Parsons and colleagues highlighted first-generation liquid imaging systems using a fitted EM hydration stage [38,48]. While novel at the time, these initial attempts were limited by uncontrollable thick liquid volumes. Nearly thirty years later, the first closed liquid cell configuration was introduced by Williamson et al. with the capability of recording hydrated dynamic observations in thin liquid films [61]. Since its conceptualization, different options have sprung up for liquid enclosures that mimic hydrated environments *in situ* (inside the EM column) [20,26]. Options include microchip assemblies with electron transparent membranes that hermetically seal liquid samples, safely shielding them from the high vacuum of the EM column [8,10,12,47,65]. These more modern assemblies contain engineered spacers ($\sim$0.1−2 microns) and yield thin liquid layers that were difficult to consistently produce with earlier systems. Microchips containing integrated microwells are particularly useful in producing thin liquid specimens for biological imaging studies.

Recent work highlights the capability of microchip methods for high-resolution characterizations comparable to cryo-EM methods (Fig. S1) [24,25]. For liquid-EM, biological specimens are imaged commonly in bright-field TEM, though STEM imaging and elemental analysis are possible [15,16,27,43,57] − an otherwise challenging feat for cryo-EM biological methods due to beam interactions with the vitreous medium. Favored specimen preparation techniques can be narrowed down to two core assembly methods for liquid imaging. Most use either SiN-based microchip assemblies or thin-film hybrid enclosures (Figure 2A). Benefits and drawbacks are elaborated for each enclosure method.

SiN-based microchip assemblies typically require specialized holders, which are costly. These holders offer a wide range of functionalities, such as static and dynamic viewing capabilities, microfluidic flow with mixing, controlled heating, and electrochemistry functions [43,63,68]. Protochips, Hummingbird Scientific, and DENSolutions are among those who have developed powerful platforms for commercial distribution used popularly in research [16,45,52]. Notably, these companies bolster novel gaseous options that can offer new opportunities for atmospheric imaging of biological specimens contained in vapor droplets [6,23,62].

Conversely, recently developed thin-film hybrid enclosures offer an affordable way to perform static, high-resolution experiments without specialized holders. Typically, 5 nm in thickness or less, these thin films are made from amorphous carbon [10,25] or graphene [5,47,65]. For hybrid options, carbon and graphene e closures can be paired with SiN-supporting substrates [5,47,65], while graphene-based enclosures are self-paired with holey support structures [8,47,65]. The flexible enclosures nearly wrap samples and result in very thin liquid layers, facilitating high-resolution data acquisition.

Notably, research suggests that graphene encapsulation can mitigate damage caused by electron beam interactions as it reduces free radical formation thus decreasing radiation damage to the specimen [9,65]. Others have noted that biomaterials imaged in liquid-EM within graphene enclosures exhibited higher dose

Figure 2

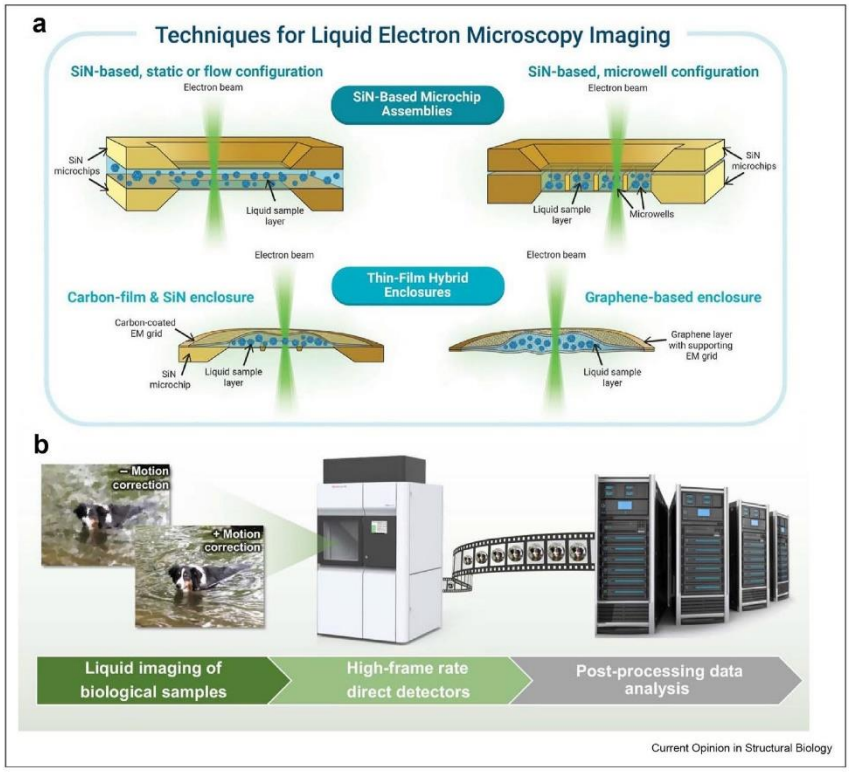

Liquid-EM specimen preparation and general workflow. (a) Paired SiN microchips can be assembled in a static or flow configuration while being hermetically sealed in a commercially available specimen holder. The sealed assemblies may be flat surfaces or milled down to produce microwells. Thin-film hybrid enclosures include SiN microchips paired with carbon-coated EM grids or two EM grids with graphene support films. Using these conventions, liquid layers are sandwiched between the microchips or the carbon-based materials. **(b)** New imaging innovations include *(1)* drift or motion correction in the EM stage; *(2)* high-frame rate direct detectors combined with automated data collection; *(3)* post-processing data analysis or high-throughput computing performed on multi-parallel processors and graphics cards (GPUs). Adapted from Ref. [25].

tolerance than those imaged in cryo-EM [28,29]. A significant drawback to thin-film enclosures is the lack of functional capabilities, such as flow and heating capabilities. Also, graphene films are quite delicate and can crack easily leading to liquid evaporation, and they are notably hydrophobic and thus susceptible to solution dewetting [59]. Standard hydrogen plasma cleaning protocols that impart hydrophilic properties to graphene films can help to minimize dewetting issues.

For hybrid enclosures and graphene-based enclosures, samples can be clipped and sealed using autoloader clipping tools that accompany automated TEM instruments (i.e., Talos series or Titan Krios, Thermo Fisher Scientific). Using autoloader devices, up to 12 sealed samples can be produced and examined in parallel. A key advantage of automated sampling is that many specimens can be rapidly screened for liquid thickness and proper dose conditions. For single-particle analysis, the microchip sandwich technique can compete with high-throughput results obtained with cryo-EM [25].

In terms of imaging and computational advances, automated data collection routines that employ high-frame rate direct detectors are the latest technology in liquid-EM workflows (Figure 2b). Frame averaging processes implemented in programs, such as SerialEM, improve imaging assessments in single-particle structural studies. To enhance real-time imaging for analytical assessments, new stage-correction systems, such as the AXON platform (Protochips, Inc.), control image drift during data collection, as well as inform dose measures at

each pixel during image acquisition. Detailed information for each movie is stored in libraries that can be viewed through machine vision software. Movies can be recorded from seconds to hours with hundreds of frames per second stored in each project library.

Determining biological structures in liquid -- what is possible?

A new AAV-based COVID vaccine candidate was recently imaged in liquid and resolved at high resolution [24]. To accomplish this feat, the Poseidon Select system (Protochips, Inc.) and SiN microchips were used containing integrated microwells. Long-framed movies of diffusing viruses were recorded using a ThermoFisher F200C TEM equipped with a DirectView direct electron detector (Figure 3a). Recordings ranged from 5 s up to 2 min in length. Imaging parameters included a frame rate of 40 fps at a magnification of 92,000× with a final sampling at the specimen level of 1.01 Å/pixel. The beam intensity was 1 electron/pixel/second, and binned movie frames were processed. The optimal movies with limited dose, drift, and damage occurred within ~20-s using a total dose of 20 $e^{-}/Å^{2}$. Individual movie frames were drift-corrected and imported into routine image processing packages, cryoSPARC, and RELION [53,56]. Extracted VP1 protomers that comprise the virus capsid showed features consistent with the VP1 crystal structure (pdb code, 3KIC, A chain (Lerch et al., 2010)) (Figure 3b). The resulting structure was resolved at ~3.22 Å, according to the 0.143-FSC criteria and validation analysis. Slices through the EM map showed expected features along with additional information missing from the slightly truncated crystal structure (Figure 3c). The recent work highlights the first biological assemblies determined at high-resolution in liquid [24].

The liquid-EM data also contained dynamic structures that were not present in cryo-EM data acquired for the same AAV preparation (Figure 3d). While some side chains were resolved in the dynamic structures, disordered regions also persisted presenting a challenge moving forward if atomic details are the project goal. Unresolved regions may be due to Brownian motion or natural dynamics of the virus assemblies. Dynamic structures in the range of 5–7 Å were achieved as a complement to the high-resolution insights. Changes in virus particle diameters during the 20-s time frame indicated an ~5% change with a total dose accumulation of 20 electrons/$Å^{2}$ as viruses diffused in solution (Figure 3e, f). Moving forward, specimen drift correction routines implemented during data collection may complement motion-correction software used in post-processing steps. As beam-induced movement can generally be dealt with computationally, researchers may now observe live protein dynamics in 3D structures while mitigating beam effects to some degree.

Liquid-electron tomography reveals host–pathogen interactions

Bacteriophages are viruses that specifically infect bacteria and they are thought to comprise over half of the carbon mass on earth. The first live recordings of host–pathogen interactions in liquid involved P1 bacteriophage infecting *E.coli* [27]. The researchers used low-dose STEM and microchip assemblies to record real-time movies of the bacteriophage infection process with limited compromise to cellular viability. The study resolved features of the *E.coli* membrane, flagella, and bacteriophage itself at the level of 5 nm using an LD_{50} = 30 electrons/nm^{2}. The LD_{50} value refers to the median lethal dose of electrons required to kill at least half of the bacteria population per experiment. During longer periods with higher dose accumulations, beam damage played a role in diminishing the quality of the obtained structures. Most impressive was that the data revealed the insertion of the viral genome into the bacterium host during short videos while maintaining ~5-nm resolution. This work was the first demonstration of live viral infection visualized at the nanoscale and served as the inspiration for later studies.

Supplementary video related to this article can be found at https://doi.org/10.1016/j.sbi.2022.102426

Beyond movie recordings in two dimensions, liquid samples can be tilted in the TEM for liquid-ET studies in 3D. Tilted EM samples offer direct, higher resolution assessments than optical methods such as confocal microscopy, STORM, or PALM. These techniques rely on fluorescent probes attached to biological entities for spatial interpretations. Stacks of images are recorded at different focus planes, and points of interest are segmented through the images to create 3D representations. In contrast, TEM images of tilted specimen provide a direct visualization of the biological features of interest. Images are recorded at a common origin with varying tilt angles. Resulting EM reconstructions show greater continuity than what is achieved with optical imaging, having less distortions due to the missing wedge of information. Tomographic studies in liquid are especially beneficial, yielding mechanistic insights through dynamic information. Tomographic results may be more limited in cryo-ET assessments in which samples are fixed in vitreous ice.

The work of Dearnaley et al. advanced the field by demonstrating the feasibility of tilting liquid specimens during live recordings [10]. To produce samples that were thin enough to tilt in the column, the team used the hybrid sandwich technique. The assembly consisted of a SiN microchip and one carbon-coated copper EM grid to enclose Agrobacterium sp. H13-3 bacterial host and its natural pathogen, flagellotropic phage (7-7-1). The mechanism of infection involves phage attachment

Cryo-electron microscopy

Figure 3

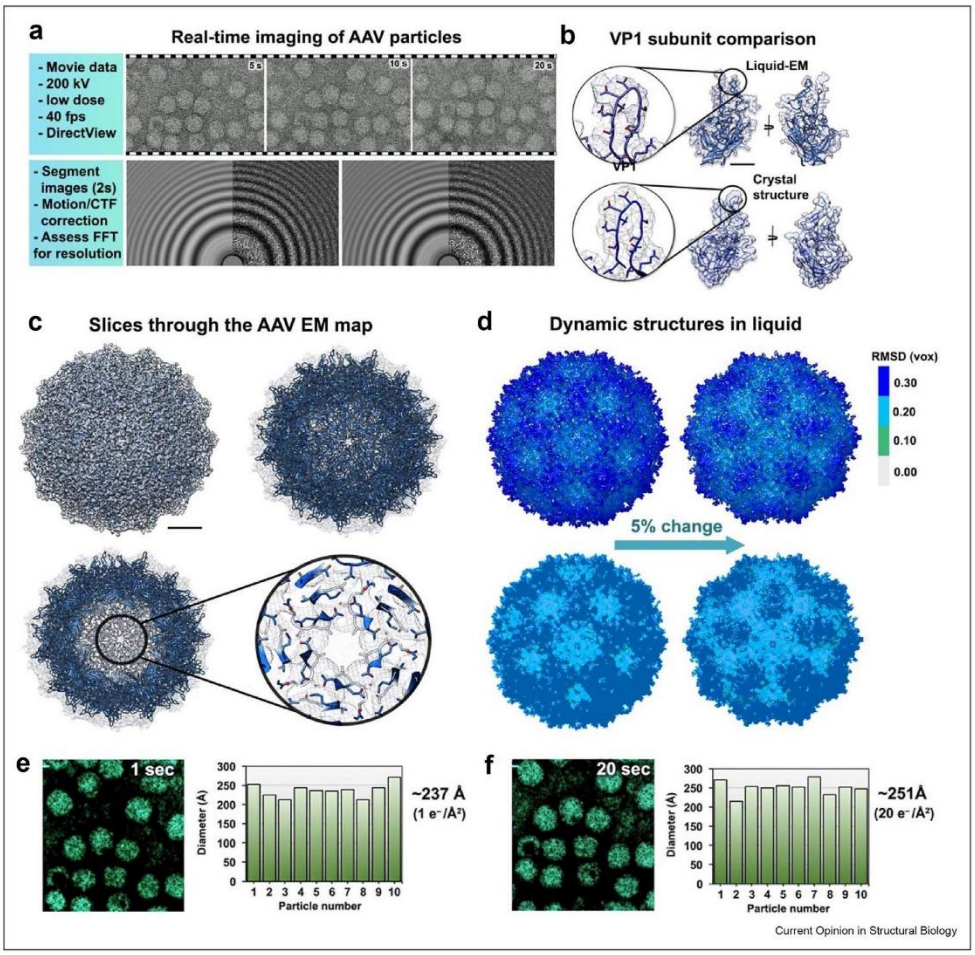

Real-time imaging of AAV in liquid. (a) Data parameters are indicated in cyan panels. Imaged regions at different time intervals and Fourier transforms show nanoscale information. Edge of each panel is ~1/3 Å; left is CTF estimates, right is experimental data. **(b)** VP1 protomers were extracted from the solution structure and compared with the VP1 crystal structure (pdb code, 3KIC, A chain). The magnified loop conveys virus specificity for immune evasion. The model structure was calculated at 3.2 Å and shows good agreement with EM protomer. Scale bar is 10 Å. **(c)** Slices through the AAV map with the atomic model (blue; pdb code, 3KIC) placed in the envelope. A magnified region along the fivefold axis shows density for a few side chains. Scale bar is 5 nm. **(d)** Relative motion in the liquid maps was estimated using the morph map function implemented in the Chimera software package (top panel). The structures show conformational changes representing the ~5% diameter change measured in the movie data. RMSD values in voxels are indicated by the gradations and according to the color scale. Contour maps (bottom panel) of the corresponding structures highlight variations of significance. (**e, f**) Contour maps of images taken at 1 s and 20 s reveal AAV particle diffusion. Scale bar is 5 nm. Changes in representative particle diameters varied between 237 and 251 Å at a cumulative dose of 20 electrons/Å^2. Adapted from Ref. [24].

to the flagellum, and through its natural motion in solution, the phage is brought in close contact to the bacteria cell body. Upon attachment to the cell body, the phage injects its genetic material into the host cell.

To ensure phage contacted the bacteria and were not simply located above or below the host cell, liquid specimens were tilted from 0° ± 45° in the TEM. The liquid-ET data were processed using standard procedures in the IMOD program [32]. Phages with empty capsids resembled ring-like structures in the tomograms and were easily distinguished from whole phage having intact tails (Figure 4a).

Quantitative analysis on multiple tomograms showed that intact phages generally contained genetic material, but many phages that had lost their flagella were devoid of their genome (Figure 4b). Heat maps and contour

Figure 4

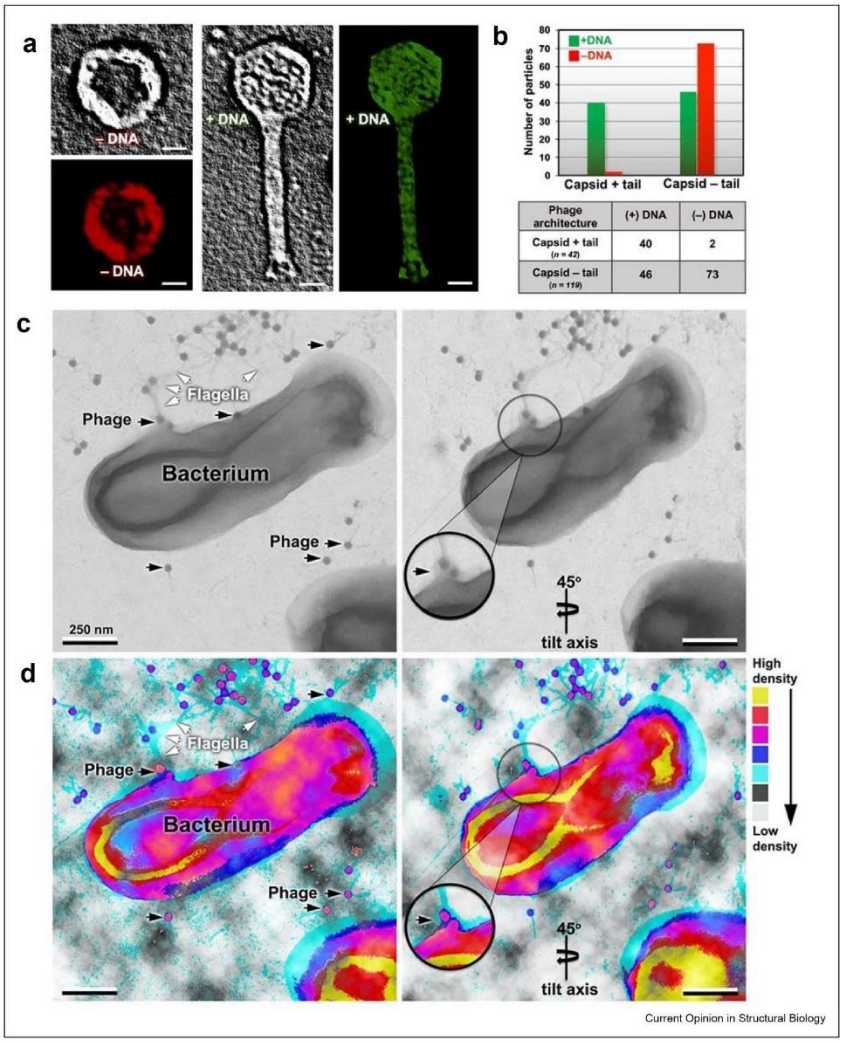

Liquid-electron tomography applications to assess host–pathogen interactions. (a) Tomographic section and reconstruction (red) of an empty phage capsid lacking genetic material and the tail domain (–DNA). Scale bar is 30 nm. Tomographic central section and reconstruction (green) of intact phage (capsid + tail) with genomic material intact (+DNA). Scale bar is 20 nm. **(b)** Quantitative analysis to indicate physical variability in phage architectures. **(c)** EM images of bacterium and phage contained in liquid at different tilt angles (0° and 45°). Black arrows point to individual phage particles while white arrows indicate flagella. **(d)** Colored contour maps of the untilted and tilted images correlate with differences in electron density. Colors range from light gray (1σ) to yellow (4σ). Inset highlights the phage heads (magenta) contacting the outer cell body layer of the bacterium (cyan). Scale bars are 250 nm. Adapted from Ref. [10].

traces of the images collected at higher tilt angles showed the background particles along with phage clearly attached to the bacterium (Figure 4c, d). Overall, this work opened a new avenue for tomographic studies in liquid to decode viral infection steps. It also provided the foundational knowledge for applications involving larger pathogens or cells.

Expanding liquid-ET studies of human viruses, very recent work is being performed on HIV particles infecting human cells [31]. Images of human epithelial adenocarcinoma cells (HeLa cells) with and without HIV particles were acquired using formvar sandwich enclosures. The work methodically compares liquid-EM images to those of matched cryo-EM controls for the

chaperonin, GroEL standard samples on the path to study the HIV infection process. Individual particle electron tomography (IPET) routines originally developed for cryo-EM were applied to the liquid-EM samples, distinguishing nanoparticle uptake from virus particle uptake within the HeLa cells. Ground-breaking results of the tomographic reconstructions reveal HIV and related particles contained within the cells in the range of 6–10 Å resolution. Importantly, this work represents the highest detailed features of viral assemblies contained inside human cells in a native liquid environment. The work also adds to the growing body of knowledge of viral uptake for enveloped viruses lacking protective capsid proteins.

Conclusions and future perspectives

Exciting new results demonstrated that virus particles in liquid were stable under low-dose conditions, producing high-resolution structures with spatial resolutions on par with cryo-EM [24]. As the liquid-EM field continues to grow and develop it is not without challenges along the way. For example, imaging fragile human viruses for extended periods in liquid can damage chemical bonds and limit spatial resolution. To partially mitigate these limitations, high frame rate direct detectors can operate in counting mode, rather than linear mode, to distribute lower beam doses over longer exposure times. Liquid-EM experiments can benefit greatly from high-speed, highly sensitive direct electron detectors in order to minimize the potential effects of electron beam damage and maximize signal-to-noise ratios. Highly sensitive detectors are also advantageous for *in situ* experiments that pair high-resolution structural information with rapid timescale dynamics to observe phenomena in the millisecond -range or faster.

Most commercially available direct electron detectors utilize single electron counting to boost detective quantum efficiency (DQE) but are limited in the number of electrons that can be distinguished before suffering from coincidence loss. A new tool on the horizon is the Apollo detector (Direct Electron), a novel event-based detector that enables high imaging speed while operating in an electron counting mode. For conventional direct detectors, electron counting requires a very sparse signal per frame ($\sim$1 electron per 50 pixels). Individual movie frames are generated by summing many counted frames, which also requires enormous computational power, effectively reducing the time resolution of any data collected. With the Apollo, events occur when pixels are excited by an electron hitting the sensor. These events are counted, thresholded, and centroided in the camera hardware to generate 8192 $\times$ 8192 super-resolution images at 60 frames per second. Combined with automated imaging procedures, data can be acquired at a rate of up to $\sim$200 movies per hour and $\sim$5000 movies per session.

Equally important, the use of automated tools may elevate the liquid-EM field, borrowing from robust practices established for cryo-EM. Programs, such as SerialEM and EPU, that use atlas imaging permit users to identify optimal liquid thickness while supplying thousands of high-quality images per session [37]. Optimal liquid thickness can be determined quantitatively using EELS or EF-TEM measurements. Once this value is empirically determined for each sample, users can select regions having the same thickness measurements using applications already integrated into SerialEM or EPU software systems. These practices are commonly used to screen cryo-EM grids and are easily adapted for liquid-EM samples. In addition, using autoloader devices that work with instruments like the Titan Krios or JEOL Cryo Arm 300, one can acquire thousands of images across multiple samples or imaging sessions.

Looking ahead, as liquid-EM technology continues to evolve, we can expect to decipher new mechanistic insights from real-time movies in solution. Gathering unique information for both structure and function of macromolecules is a true benefit for the technique, which continues to gain popularity in materials and life sciences. By implementing automated tools to improve data collection routines and image processing procedures, the liquid-EM field is primed to assert the "real-time revolution" in nanoscale analysis, providing a dynamic complement to other established techniques.

Conflict of interest

The authors have nothing to declare.

Acknowledgments

The authors thank members of the Kelly Lab and Dr. Carol Bator (PSU, Huck Institutes of the Life Sciences) for useful discussions in the preparation of the work. This work was supported by the National Institutes of Health and the National Cancer Institute [R01CA193578, R01CA227261, R01CA219700 to D.F.K.].

Appendix A. Supplementary data

Supplementary data to this article can be found online at https://doi.org/10.1016/j.sbi.2022.102426.

References

Papers of particular interest, published within the period of review, have been highlighted as:

* of special interest
** of outstanding interest

1. Ahmad N, Wang G, Nelayah J, Ricolleau C, Alloyeau D: **Exploring the formation of symmetric gold nanostars by liquid-cell transmission electron microscopy**. *Nano Lett* 2017, **17**:4194–4201, https://doi.org/10.1021/acs.nanolett.7b01013.

2. Alloyeau D, Dachraoui W, Javed Y, Belkahla H, Wang G, Lecoq H, Ammar S, Ersen O, Wisnet A, Gazeau F, Ricolleau C: **Unravelling kinetic and thermodynamic effects on the growth of gold nanoplates by liquid transmission electron microscopy**. *Nano Lett* 2015, **15**:2574–2581, https://doi.org/10.1021/acs.nanolett.5b00140.

3. Bammes BE, Rochat RH, Jakana J, Chen D-H, Chiu W: **Direct electron detection yields cryo-EM reconstructions at resolutions beyond 3/4 Nyquist frequency**. *J Struct Biol* 2012, **177**: 589–601, https://doi.org/10.1016/j.jsb.2012.01.008.

4. ** Bartesaghi A, Aguerrebere C, Falconieri V, Banerjee S, Earl LA, Zhu X, Grigorieff N, Milne JLS, Sapiro G, Wu X, Subramaniam S: **Atomic resolution cryo-EM structure of β-galactosidase**. *Structure* 2018, **26**:848–856, https://doi.org/10.1016/j.str.2018.04.004. e3.
The first atomic-resolution structure determined through single particle cryo-EM. Defined an optimal workflow and parameters to reach the atomic scale.

5. Blach P, Keskin S, Jonge N de: **Graphene Enclosure of Chemically Fixed Mammalian Cells for Liquid-Phase Electron Microscopy**. *J Vis Exp* 2020, https://doi.org/10.3791/61458.

6. Burke MG, Bertali G, Prestat E, Scenini F, Haigh SJ: **The application of in situ analytical transmission electron microscopy to the study of preferential intergranular oxidation in Alloy 600**. *Ultramicroscopy* 2017, **176**:46–51, https://doi.org/10.1016/j.ultramic.2016.11.014.

7. Casasanta MA, Jonaid GM, Kaylor L, Luqiu WY, Solares MJ, Schroen ML, Dearnaley WJ, Wilson J, Dukes MJ, Kelly DF: **Microchip-based structure determination of low-molecular weight proteins using cryo-electron microscopy**. *Nanoscale* 2021, **13**:7285–7293, https://doi.org/10.1039/d1nr00388g.

8. Chen Q, Smith JM, Park J, Kim K, Ho D, Rasool HI, Zettl A, Alivisatos AP: **3D motion of DNA-Au nanoconjugates in graphene liquid cell electron microscopy**. *Nano Lett* 2013, **13**: 4556–4561, https://doi.org/10.1021/nl402694n.

9. * Cho H, Jones MR, Nguyen SC, Hauwiller MR, Zettl A, Alivisatos AP: **The use of graphene and its derivatives for liquid-phase transmission electron microscopy of radiation-sensitive specimens**. *Nano Lett* 2016, **17**:414–420, https://doi.org/10.1021/acs.nanolett.6b04383.
Graphene liquid cell enclosures show mitigation of beam damage to liquid-EM specimen. Opens the doorway to high resolution imaging in solution.

10. ** Dearnaley WJ, Schleupner B, Varano AC, Alden NA, Gonzalez F, Casasanta MA, Scharf BE, Dukes MJ, Kelly DF: **Liquid-Cell Electron Tomography of Biological Systems**. *Nano Lett* 2019, **19**:6734–6741, https://doi.org/10.1021/acs.nanolett.9b01309.
The first electron-tomography reconstructions of biological entities in liquid. Developed the concept of hybrid enclosures suitable for tilting in the TEM.

11. Deng W, Marshall NC, Rowland JL, McCoy JM, Worrall LJ, Santos AS, Strynadka NCJ, Finlay BB: **Assembly, structure, function and regulation of type III secretion systems**. *Nat Rev Microbiol* 2017, **15**:323–337, https://doi.org/10.1038/nrmicro.2017.20.

12. Dukes MJ, Gilmore BL, Tanner JR, McDonald SM, Kelly DF: **In situ TEM of Biological Assemblies in Liquid**. *J Vis Exp* 2013:50936, https://doi.org/10.3791/50936.

13. Dukes MJ, Thomas R, Damiano J, Klein KL, Balasubramaniam S, Kayandan S, Riffle JS, Davis RM, McDonald SM, Kelly DF: **Improved microchip design and application for in situ transmission electron microscopy of macromolecules**. *Microsc Microanal* 2014, **20**:338–345, https://doi.org/10.1017/s1431927613013858.

14. Dunn G, Adiga VP, Pham T, Bryant C, Horton-Bailey DJ, Belling JN, LaFrance B, Jackson JA, Barzegar HR, Yuk JM, Aloni S, Crommie MF, Zettl A: **Graphene-sealed flow cells for in situ transmission electron microscopy of liquid samples**. *ACS Nano* 2020, **14**:9637–9643, https://doi.org/10.1021/acsnano.0c00431.

15. Evans JE, Jungjohann KL, Wong PCK, Chiu P-L, Dutrow GH, Arslan I, Browning ND: **Visualizing macromolecular complexes with in situ liquid scanning transmission electron microscopy**. *Micron* 2012, **43**:1085–1090, https://doi.org/10.1016/j.micron.2012.01.018.

16. Fan H, Qiu L, Fedorov A, Willinger M-G, Ding F, Huang X: **Dynamic state and active structure of Ni–Co catalyst in carbon nanofiber growth revealed by in situ transmission electron microscopy**. *ACS Nano* 2021, **15**:17895–17906, https://doi.org/10.1021/acsnano.1c06189.

17. * Frank J: **Time-resolved cryo-electron microscopy: recent progress**. *J Struct Biol* 2017, **200**:303–306, https://doi.org/10.1016/j.jsb.2017.06.005.
First detailed analysis of time-resolved imaging using cryo-EM. Defined opportunities and limitations of viewing dynamic systems in vitreous ice.

18. Frank J: *Three-Dimensional Electron Microscopy of Macromolecular Assemblies: Visualization of Biological Molecules in Their Native State*. Oxford University Press; 2006.

19. Frank J, Zhu J, Penczek P, Li Y, Srivastava S, Verschoor A, Radermacher M, Grassucci R, Lata RK, Agrawal RK: **A model of protein synthesis based on cryo-electron microscopy of the E. coli ribosome**. *Nature* 1995, **376**:441–444, https://doi.org/10.1038/376441a0.

20. He K, Shokuhfar T, Shahbazian-Yassar R: **Imaging of soft materials using in situ liquid-cell transmission electron microscopy**. *J Phys Condens Matter* 2019, **31**, 103001, https://doi.org/10.1088/1361-648x/aaf616.

21. Henderson R, Sali A, Baker ML, Carragher B, Devkota B, Downing KH, Egelman EH, Feng Z, Frank J, Grigorieff N, Jiang W, Ludtke SJ, Medalia O, Penczek PA, Rosenthal PB, Rossmann MG, Schmid MF, Schröder GF, Steven AC, Stokes DL, Westbrook JD, Wriggers W, Yang H, Young J, Berman HM, Chiu W, Kleywegt GJ, Lawson CL: **Outcome of the first electron microscopy validation task force meeting**. *Struct Lond Engl 1993* 2012, **20–330**:205–214, https://doi.org/10.1016/j.str.2011.12.014.

22. Hu B, Morado DR, Margolin W, Rohde JR, Arizmendi O, Picking WL, Picking WD, Liu J: **Visualization of the type III secretion sorting platform of Shigella flexneri**. *Proc Natl Acad Sci USA* 2015, **112**: 1047–1052, https://doi.org/10.1073/pnas.1411610112.

23. Hyllested JÆ, Beleggia M: **Investigation of gas-electron interactions with electron holography**. *Ultramicroscopy* 2021, **221**, 113178, https://doi.org/10.1016/j.ultramic.2020.113178.

24. ** Jonaid G, Dearnaley WJ, Casasanta MA, Kaylor L, Berry S, Dukes MJ, Spilman MS, Gray JL, Kelly DF: **High-resolution imaging of human viruses in liquid droplets**. *Adv Mater* 2021, **33**, 2103221, https://doi.org/10.1002/adma.202103221.
First demonstration of high-resolution single particle structure determination of human viruses in liquid.

25. Jonaid GM, Casasanta MA, Dearnaley WJ, Berry S, Kaylor L, Dressel-Dukes MJ, Spilman MS, Gray JL, Kelly DF: **Automated Tools to Advance High-Resolution Imaging in Liquid**. *Microsc Microanal* 2022, **1–10**, https://doi.org/10.1017/s1431927621013921.

26. Jonge N de, Ross FM: **Electron microscopy of specimens in liquid**. *Nat Nanotechnol* 2011, **6**:695–704, https://doi.org/10.1038/nnano.2011.161.

27. ** Kennedy E, Nelson EM, Tanaka T, Damiano J, Timp G: **Live bacterial physiology visualized with 5 nm resolution using scanning transmission electron microscopy**. *ACS Nano* 2016, **10**:2669–2677, https://doi.org/10.1021/acsnano.5b07697.
The work showed real-time host–pathogen interactions in liquid. Movies up to 3s timeframes demonstrate phage engaging bacteria and deposition of genetic material.

28. * Keskin S, Jonge N de: **Reduced Radiation Damage in Transmission Electron Microscopy of Proteins in Graphene Liquid Cells**. *Nano Lett* 2018, **18**:7435–7440, https://doi.org/10.1021/acs.nanolett.8b02490.
Direct imaging comparisons of the same specimen in liquid and in vitreous ice. Dose measurements suggest that liquid environments provide more stable conditions than ice preservation.

29. Keskin S, Kunnas P, Jonge N de: **Liquid-Phase Electron Microscopy with Controllable Liquid Thickness**. *Nano Lett* 2019, **19**:4608–4613, https://doi.org/10.1021/acs.nanolett.9b01576.

30. Kiss G, Chen X, Brindley MA, Campbell P, Afonso CL, Ke Z, Holl JM, Guerrero-Ferreira RC, Byrd-Leotis LA, Steel J, Steinhauer DA, Plemper RK, Kelly DF, Spearman PW, Wright ER: **Capturing enveloped viruses on affinity grids for downstream**

cryo-electron microscopy applications. *Microsc Microanal* 2014, **20**:164–174, https://doi.org/10.1017/s1431927613013937.

31. ** Kong L, Liu Jianfang, Zhang M, Lu Z, Ren A, Liu Jiankang, Li J, Ren G (Gary): **Single-molecule 3D imaging of HIV cellular entry by liquid-phase electron tomography**. *Res Square Preprint V1* 2022, https://doi.org/10.21203/rs.3.rs-1298112/v1.
While still a work in progress, this is the first demonstration of a human viruses entering human cells using liquid-EM and individual particle electron-tomography.

32. Kremer JR, Mastronarde DN, McIntosh JR: **Computer Visualization of Three-Dimensional Image Data Using IMOD**. *J Struct Biol* 1996, **116**:71–76, https://doi.org/10.1006/jsbi.1996.0013.

33. Li Z, Baker ML, Jiang W, Estes MK, Prasad BVV: **Rotavirus architecture at subnanometer resolution**. *J Virol* 2009, **83**: 1754–1766, https://doi.org/10.1128/jvi.01855-08.

34. Liang Y-L, Khoshouei M, Radjainia M, Zhang Y, Glukhova A, Tarrasch J, Thal DM, Furness SGB, Christopoulos G, Coudrat T, Danev R, Baumeister W, Miller LJ, Christopoulos A, Kobilka BK, Wootten D, Skiniotis G, Sexton PM: **Phase-plate cryo-EM structure of a class B GPCR-G protein complex**. *Nature* 2017, **546**:118–123, https://doi.org/10.1038/nature22327.

35. Liao H-G, Zheng H: **Liquid cell transmission electron microscopy study of platinum iron nanocrystal growth and shape evolution**. *J Am Chem Soc* 2013, **135**:5038–5043, https://doi.org/10.1021/ja310612p.

36. Mannar D, Saville JW, Zhu X, Srivastava SS, Berezuk AM, Tuttle KS, Marquez AC, Sekirov I, Subramaniam S: **SARS-CoV-2 Omicron variant: antibody evasion and cryo-EM structure of spike protein–ACE2 complex**. *Science* 2022, **375**:760–764, https://doi.org/10.1126/science.abn7760.

37. * Mastronarde DN: **Advanced data acquisition from electron microscopes with SerialEM**. *Microsc Microanal* 2018, **24**: 864–865, https://doi.org/10.1017/s1431927618004816.
Automated data collection software package that set the stage for high-throughput imaging in TEM.

38. * Matricardi VR, Moretz RC, Parsons DF: **Electron Diffraction of Wet Proteins: Catalase**. *Science* 1972, **177**:268–270, https://doi.org/10.1126/science.177.4045.268.
The work showed the feasibility of imaging biological crystals contained in liquid while isolated from the TEM vacuum system.

39. McDonald SM, McKell AO, Rippinger CM, McAllen JK, Akopov A, Kirkness EF, Payne DC, Edwards KM, Chappell JD, Patton JT: **Diversity and Relationships of Cocirculating Modern Human Rotaviruses Revealed Using Large-Scale Comparative Genomics**. *J Virol* 2012, **86**:9148–9162, https://doi.org/10.1128/jvi.01105-12.

40. Migunov V, Ryll H, Zhuge X, Simson M, Strüder L, Batenburg KJ, Houben L, Dunin-Borkowski RE: **Rapid low dose electron tomography using a direct electron detection camera**. *Sci Rep Uk* 2015, **5**, 14516, https://doi.org/10.1038/srep14516.

41. Murata K, Wolf M: **Cryo-electron microscopy for structural analysis of dynamic biological macromolecules**. *Biochimica Et Biophysica Acta Bba - Gen Subj* 2018, **1862**:324–334, https://doi.org/10.1016/j.bbagen.2017.07.020.

42. Oikonomou CM, Chang Y-W, Jensen GJ: **A new view into prokaryotic cell biology from electron cryotomography**. *Nat Rev Microbiol* 2016, **14**:205–220, https://doi.org/10.1038/nrmicro.2016.7.

43. Omme JT van, Wu H, Sun H, Beker AF, Lemang M, Spruit RG, Maddala SP, Rakowski A, Friedrich H, Patterson JP, Garza HHP: **Liquid phase transmission electron microscopy with flow and temperature control**. *J Mater Chem C* 2020, **8**: 10781–10790, https://doi.org/10.1039/d0tc01103g.

44. Pallesen J, Murin CD, Val N de, Cottrell CA, Hastie KM, Turner HL, Fusco ML, Flyak AI, Zeitlin L, Crowe JE, Andersen KG, Saphire EO, Ward AB: **Structures of ebola virus GP and sGP in complex with therapeutic antibodies**. *Nat Microbiol* 2016, **1**:16128, https://doi.org/10.1038/nmicrobiol.2016.128. 16128.

45. Parent LR, Bakalis E, Ramírez-Hernández A, Kammeyer JK, Park C, Pablo J de, Zerbetto F, Patterson JP, Gianneschi NC: **Directly observing micelle fusion and growth in solution by liquid-cell transmission electron microscopy**. *J Am Chem Soc* 2017, **139**:17140–17151, https://doi.org/10.1021/jacs.7b09060.

46. * Park J, Elmlund H, Ercius P, Yuk JM, Limmer DT, Chen Q, Kim K, Han SH, Weitz DA, Zettl A, Alivisatos AP: **3D structure of individual nanocrystals in solution by electron microscopy**. *Science* 2015a, **349**:290–295, https://doi.org/10.1126/science.aab1343.
High-resolution structures of nanocrystals in graphene enclosures laid the groundwork for advancing liquid-EM to complement cryo-EM frameworks.

47. Park J, Park H, Ercius P, Pegoraro AF, Xu C, Kim JW, Han SH, Weitz DA: **Direct Observation of Wet Biological Samples by Graphene Liquid Cell Transmission Electron Microscopy**. *Nano Lett* 2015b, **15**:4737–4744, https://doi.org/10.1021/acs.nanolett.5b01636.

48. ** Parsons DF: **Structure of wet specimens in electron microscopy**. *Science* 1974, **186**:407–414, https://doi.org/10.1126/science.186.4162.407.
The first environmental TEM stage demonstrated that liquid vapor can be safely contained in a high vacuum system.

49. Penczek PA, Grassucci RA, Frank J: **The ribosome at improved resolution: New techniques for merging and orientation refinement in 3D cryo-electron microscopy of biological particles**. *Ultramicroscopy* 1994, **53**:251–270, https://doi.org/10.1016/0304-3991(94)90038-8.

50. Peng Y, Du N, Lei Y, Dorje S, Qi J, Luo T, Gao GF, Song H: **Structures of the SARS-CoV-2 nucleocapsid and their perspectives for drug design**. *EMBO J* 2020, **39**, e105938, https://doi.org/10.15252/embj.2020105938.

51. Piffoux M, Ahmad N, Nelayah J, Wilhelm C, Silva A, Gazeau F, Alloyeau D: **Monitoring the dynamics of cell-derived extracellular vesicles at the nanoscale by liquid-cell transmission electron microscopy**. *Nanoscale* 2018, **10**:1234–1244, https://doi.org/10.1039/c7nr07576f.

52. * Pohlmann ES, Patel K, Guo S, Dukes MJ, Sheng Z, Kelly DF: **Real-time visualization of nanoparticles interacting with glioblastoma stem cells**. *Nano Lett* 2015, **15**:2329–2335, https://doi.org/10.1021/nl504481k.
Liquid-EM imaging of human cancer cells interacting with therapeutic nanoparticles show the feasibility of real-time at the edge of cellular structures.

53. * Punjani A, Rubinstein JL, Fleet DJ, Brubaker MA: **cryoSPARC: algorithms for rapid unsupervised cryo-EM structure determination**. *Nat Methods* 2017, **14**:290–296, https://doi.org/10.1038/nmeth.4169.
The cryoSPARC program is the roadmap for single particle structure determination of biological specimens.

54. Reboul CF, Heo J, Machello C, Kiesewetter S, Kim BH, Kim S, Elmlund D, Ercius P, Park J, Elmlund H: **SINGLE: Atomic-resolution structure identification of nanocrystals by graphene liquid cell EM**. *Sci Adv* 2021, **7**, eabe6679, https://doi.org/10.1126/sciadv.abe6679.

55. Saville JW, Mannar D, Zhu X, Srivastava SS, Berezuk AM, Demers J-P, Zhou S, Tuttle KS, Sekirov I, Kim A, Li W, Dimitrov DS, Subramaniam S: **Structural and biochemical rationale for enhanced spike protein fitness in delta and kappa SARS-CoV-2 variants**. *Nat Commun* 2022, **13**:742, https://doi.org/10.1038/s41467-022-28324-6.

56. * Scheres SHW: **RELION: implementation of a Bayesian approach to cryo-EM structure determination**. *J Struct Biol* 2012, **180**:519–530, https://doi.org/10.1016/j.jsb.2012.09.006.
The first software packages to provide tools for determining high-resolution structures of biological specimens in the cryo-EM and liquid-EM fields.

57. Serra-Maia R, Kumar P, Meng AC, Foucher AC, Kang Y, Karki K, Jariwala D, Stach EA: **Nanoscale Chemical and Structural Analysis during In Situ Scanning/Transmission Electron Microscopy in Liquids**. *ACS Nano* 2021, **15**:10228–10240, https://doi.org/10.1021/acsnano.1c02340.

58. Shi Y, Giammartino DCD, Taylor D, Sarkeshik A, Rice WJ, Yates JR, Frank J, Manley JL: **Molecular architecture of the**

human pre-mRNA 3′ processing complex. *Mol Cell* 2009, **33**: 365–376, https://doi.org/10.1016/j.molcel.2008.12.028.

59. Textor M, Jonge N de: **Strategies for preparing graphene liquid cells for transmission electron microscopy**. *Nano Lett* 2018, **18**:3313–3321, https://doi.org/10.1021/acs.nanolett.8b01366.

60. Watanabe R, Castillon G, Avalos RD, Ellisman M, Saphire E: **Visualization of intracellular Ebola virus nucleocapsid assembly by cryo-electron tomography**. *Microsc Microanal* 2021, **27**:1708–1711, https://doi.org/10.1017/s1431927621006243.

61. Williamson MJ, Tromp RM, Vereecken PM, Hull R, Ross FM: **Dynamic microscopy of nanoscale cluster growth at the solid–liquid interface**. *Nat Mater* 2003, **2**:532–536, https://doi.org/10.1038/nmat944.

62. Wu YA, Li L, Li Z, Kinaci A, Chan MKY, Sun Y, Guest JR, McNulty I, Rajh T, Liu Y: **Visualizing redox dynamics of a single Ag/AgCl heterogeneous nanocatalyst at atomic resolution**. *ACS Nano* 2016, **10**:3738–3746, https://doi.org/10.1021/acsnano.6b00355.

63. Yang J, Andrei CM, Botton GA, Soleymani L: **In liquid observation and quantification of nucleation and growth of gold nanostructures using in situ transmission electron microscopy**. *J Phys Chem C* 2017, **121**:7435–7441, https://doi.org/10.1021/acs.jpcc.6b10400.

64. ** Yip KM, Fischer N, Paknia E, Chari A, Stark H: **Atomic-resolution protein structure determination by cryo-EM**. *Nature* 2020, **587**: 157–161, https://doi.org/10.1038/s41586-020-2833-4.
The first cryo-EM structures to demonstrate EM maps can resolve atomic features at a similar level as crystallographic methods.

65. ** Yuk JM, Park J, Ercius P, Kim K, Hellebusch DJ, Crommie MF, Lee JY, Zettl A, Alivisatos AP: **High-Resolution EM of Colloidal Nanocrystal Growth Using Graphene Liquid Cells**. *Science* 2012, **336**:61–64, https://doi.org/10.1126/science.1217654.
High-resolution structures of nanocrystals in graphene enclosures using liquid-EM demonstrate dynamic crystal growth at the nanoscale.

66. Zheng H, Smith RK, Jun Y, Kisielowski C, Dahmen U, Alivisatos AP: **Observation of Single Colloidal Platinum Nanocrystal Growth Trajectories**. *Science* 2009, **324**: 1309–1312, https://doi.org/10.1126/science.1172104.

67. Zheng SQ, Palovcak E, Armache J-P, Verba KA, Cheng Y, Agard DA: **MotionCor2: anisotropic correction of beam-induced motion for improved cryo-electron microscopy**. *Nat Methods* 2017, **14**:331–332, https://doi.org/10.1038/nmeth.4193.

68. Zhu G-Z, Prabhudev S, Yang J, Gabardo CM, Botton GA, Soleymani L: **In situ liquid cell TEM study of morphological evolution and degradation of Pt–Fe nanocatalysts during potential cycling**. *J Phys Chem C* 2014, **118**:22111–22119, https://doi.org/10.1021/jp506857b.

2.3. Exploring Biomineralization Processes Using *In Situ* Liquid Transmission Electron Microscopy: *A Review*

2.3.1. Section Introduction (Objective iii)

Biomineralization processes are fundamental in our daily lives, and responsible for important physiological and pathological processes for a wide range of organisms. Liquid TEM techniques are revolutionizing the field of biomineralization by providing new capabilities for visualizing dynamic mineralization reactions in real-time, expanding current knowledge on these complex processes and complementing current characterization techniques for theory validation. However, a review on these topics has yet to be accomplished which summarizes comprehensively the impact that liquid TEM has had on the field. To accomplish the objective (iii) set out for this thesis involving applying novel liquid TEM means to study dynamic biomineralization systems, Section 2.3 summarizes current best practices within the liquid EM community and state-of-the-art research that has used these techniques to study biomineralization-related research. For the works discussed, key preparation and imaging parameters were summarized for reference to provide a foundation for the application of this technique for mineralization research. Several shortcomings of the technique were addressed, where two main challenges which reoccurred in literature involved effects arising from confinement and electron beam. Mitigation strategies for these effects were further summarized, the key to the execution of the research presented in Chapters 5 and 6. Overall, insights from this comprehensive review contribute to an improved understanding of in situ liquid TEM biomineralization applications, which is anticipated to lead to wider adoption of these methods within the field.

Authors: **Liza-Anastasia DiCecco**, Tengteng Tang, Deborah F. Kelly, Eli D. Sone, Kathryn Grandfield.

Publication: This work is to be submitted in 2023.

Exploring Biomineralization Processes Using *In Situ* Liquid Transmission Electron Microscopy: *A Review*

Liza-Anastasia DiCecco[1,2], Tengteng Tang[1], Deborah F. Kelly[2,3], Eli Sone[4-6], Kathryn Grandfield[1,7*]

[1] Department of Materials Science and Engineering, McMaster University, Hamilton, ON, Canada.
[2] Department of Biomedical Engineering, Pennsylvania State University, University Park, PA, USA.
[3.] Center for Structural Oncology, Pennsylvania State University, University Park, PA 16802, USA.
[4] Institute of Biomedical Engineering, University of Toronto, Toronto, ON, Canada.
[5] Faculty of Dentistry, University of Toronto, Toronto, ON, Canada.
[6] Materials Science and Engineering, University of Toronto, Toronto, ON, Canada.
[7] School of Biomedical Engineering, McMaster University, Hamilton, ON, Canada.

[*] Corresponding author:
Prof. Kathryn Grandfield
McMaster University
1280 Main Street West
Hamilton, ON, L8S 4L7
Email: kgrandfield@mcmaster.ca

2.3.2. Abstract

Biomineralization processes are fundamental to life itself and vital for important physiological and pathological processes for a wide range of organisms. For years, a classical view on crystallization pathways dominated theories on biomineralization progression, despite the observations of non-traditional routes involving precursor phases using traditional- and cryo- transmission electron microscopy (TEM). While TEM evidence shifted paradigms towards non-classical theories, the time-stamped evidence remained contended within the field without dynamic proof of mechanisms. With the emergence of novel liquid TEM methods, complex and multifaceted biomineralization processes have been explored with dynamic, real-time resolution, where a variety of classical and non-classical mineralization pathways have been observed for Ca and Fe-based mineral systems. In this review, we provide a summary of recent *in situ* liquid TEM research related to the biomineralization field. Key preparation and imaging parameters are provided as a foundation for the application of this technique for biomineralization research. Challenges and considerations are discussed for those considering liquid TEM. Notably, effects of confinement and electron beam damages are addressed relevant to biomineralization reactions. An outlook on a plethora of opportunities available to those in the biomineralization field is also provided. In future, we anticipate the expansion of liquid TEM biomineralization research will lead to transformative discoveries, providing complimentary dynamic insight on what may be happening in biological systems – *revealing secrets behind life itself.*

Keywords: Liquid electron microscopy, biomineralization, crystallization, biominerals, amorphous precursors

Exploring Biomineralization Processes Using *In Situ* Liquid Transmission Electron Microscopy: *A Review*

2.3.3. Introduction

Broadly, biominerals can be defined as natural composite materials which comprise organic and inorganic phases – produced through living organisms and/or template biomolecules.[1–3] The study of mineralization processes is fundamental to understanding life itself, where organisms from zebra mussels to humans rely on biominerals to reinforce tissues and/or for vital physiological and pathological processes.[4] For marine life, ocean acidification and warming can directly impact the biomineralization of aquatic organisms such as sea urchins, coral, and oysters, and whose study can help understand the impact of climate change.[5–7] For mammals, biomineralization processes are key to the formation, mechanical properties, and maintenance of hard tissues found in the musculoskeletal system such as teeth and bone.[2] Insight into the mechanisms behind these processes can aid in a better understanding of hard tissue diseases, such as osteoporosis and osteoarthritis, as well as possible improvements in the osseointegration of orthopedic and dental implants.[8–11] Biomineralization also plays a relevant role in pathological calcification, such as kidney stones, osteoarthritis, and atherosclerosis [12]. Moreover, for example, iron-based biominerals found in the brain have even been suggested to be associated with neurodegenerative diseases such as Alzheimer's.[13,14] Thus, understanding the fundamental steps behind biomineralization events and the mechanisms controlling these events are instrumental across different fields.

While biologically driven, it is the physical and chemical reactions that contribute to the formation of inorganic biominerals. To elicit mechanistic details on biomineral formation, traditional and cryogenic (cryo) transmission electron microscopy (TEM) have been used extensively in the study of mineralization processes at the micro to sub-nanometer length scales. These studies have led to transformative discoveries in the field, shifting the belief of traditional ion-by-ion crystallization pathways to non-traditional crystallization theories involving precursor mineralization phases.[15–20] As a result, new paradigms regarding biomineralization processes are shifting toward crystallization steps involving more thermodynamically stable precursors that premediate bulk crystal formation, where a variety of possible multiphasic mineralization steps have been proposed (Fig. 1).[20] Some of these precursors include prenucleation clusters (PNCs) and/or an ion-saturated liquid precursor phase through liquid-liquid phase separation (LLPS),[21] where the polymer-induced liquid precursor (PILP) theory has been prominently discussed as an LLPS method for a variety of biomineral systems.[18,22–24] However, traditional and cryo TEM methods only offer time-stamped observations of biomineralizing systems in dried or frozen fixed states, unrepresentative of the dynamic liquid environment in which biomineralization occurs. There is, thus, a great need to validate the theory through visualization of dynamic interactions within the biomineralization systems in real-time.

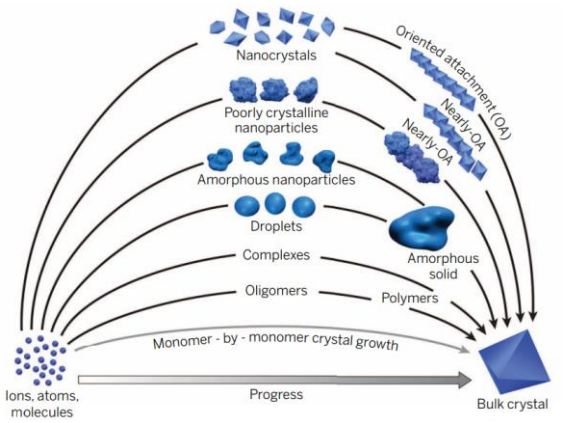

Ch. 2.3 – Figure 1. Pathways to crystallization by particle attachment. *In contrast to monomer-by-monomer addition as envisioned in classical models of crystal growth (gray curve), CPA occurs by the addition of higher-order species ranging from multi-ion complexes to fully formed nanocrystals. The final faceted bulk crystal is a schematic representation of a final single-crystal state, whereby the final crystal can have more complex morphologies. Image reproduced with permission from De Yoreo et al.[20] (Copyright © 2015 American Association for the Advancement of Science).*

In the last few years, manufacturing advances in micro and nano fabrication, thin electron transparent materials, and holder designs, have made it possible to perform meaningful experiments using liquid TEM.[25,26] Liquid TEM is a powerful tool for understanding biological structures and how they interact at high-resolution (HR) in mimetic liquid environments.[27–29] More importantly, it has enabled unique visualization of real-time *in situ* dynamic reactions[29,30] and high-throughput, HR imaging of biological assemblies in hydrated conditions.[31,32] Since the first functional liquid cell TEM enclosure was introduced in 2003,[33] the newly established technique has risen in popularity to characterize reactions and hydrated biological structures, key to determining mechanisms behind complex biomineralization processes.

In this review, we shed light on innovative tools for liquid TEM while exploring research that has utilized this technique to make ground-breaking discoveries in the biomineralization field, including calcium carbonates, calcium phosphates, Fe-based systems and others. We also tabulate and describe essential preparation steps, imaging parameters, experimental considerations, and an outlook on the field. In summarizing experimental parameters and *in situ* biomineralization-related research within this review, we aspire that others will be encouraged to explore this novel imaging methodology for their research to make new biomineralization discoveries and move the field further.

2.3.4. The Liquid Transmission Electron Microscopy Technique

Historically, traditional and cryo TEM modalities have played a dominating role in the characterization of biomineralization mechanisms and structural observations of mineralized tissues.[15–17,34,35] Micro to sub-angstrom scale features revealed through EM,

that could not otherwise be resolved through alternative light microscopy means, have driven theories and helped shape the biomineralization field – from establishing theories on structure-function relationships between tissues and their mineralization to eliciting crucial information on crystallization pathways.[15–20]

Since its emergence, cryo TEM has become one of the most important techniques for structural characterization and the understanding of biomineral synthesis in a near-native state. The process typically involves the fast-freezing of samples using liquid ethane condensed by liquid nitrogen. As such, researchers can observe hydrated specimens that are vitrified in action – immobilizing dynamic reactions for their interpretation at HR and stabilizing a liquid sample for the high-vacuum TEM environment.[36] Moreover, cryo TEM optimizes sample preparation for microscopic analyses and mitigates concerns regarding shrinking and/or solution supersaturation associated with traditional TEM preparation methods involving dehydration, fixation, and/or freeze-drying.[37–40] Nonetheless, some drawbacks to the cryo TEM technique can be elaborated. For one, the vitrification process and sample preparation require extensive trial and error to achieve the desired results, and the related preparation equipment is relatively expensive in comparison to other preparation methods. Moreover, once condensed, the similar densities of the specimens and the vitrified mediums often result in low imaging contrast and low signal-to-noise ratio in cryo TEM.[41] One possible approach to enhance the imaging quality is through contrast agent staining, however, it often employs aggressive heavy elements that can deform soft materials and distort elements of interest in imaging.[41]

While cryo and traditional TEM observations of sample interactions at different timestamps are useful for proposing and hypothesizing theories, dynamic visualization of interactions is required for theory validation. In this context, liquid TEM presents new alternative means to observe wet and/or soft materials, providing the opportunity to visualize dynamic processes with real-time resolution in a mimetic liquid state where many reactions naturally occur.[25,28,42,43] Further, recent endeavours have highlighted the possibility of performing 3D tomography of hydrated specimens using liquid TEM.[44,45] In comparison to cryo TEM, liquid TEM has the advantages of less laborious sample preparation and fewer specialized equipment requirements. However, liquid TEM does not consistently yield the same level of resolution as cryo TEM. This is attributed, in part, to the variable thickness of liquid layers, which scatter electrons more than vitrified ice,[35] and the presence of encapsulating membranes in liquid TEM enclosures, which contribute to increased sample thickness. Nonetheless, recent applications of liquid TEM using single-particle analysis strategies of biological specimens are pushing the resolution boundaries of the technique to sub-nanometer ranges[31,46] while others have achieved atomic-resolution imaging in materials science applications.[47,48] We emphasize liquid TEM provides a complimentary view for research and the validation of theories. It is not meant to be presented herein as a competitive replacement for traditional and cryo TEM methods, where liquid TEM research necessitates extensive correlative *ex situ* and post-mortem or *post situ* analysis to validate findings observed *in situ.*

Most commonly, liquid TEM enclosures involve a cell holder structure with an electron transparent membrane, designed to encapsulate the hermetically sealed samples within the vacuum state for imaging.[45,49–52] Early works by Parsons et al. first inspired those to explore liquid TEM methods for biological imaging,[53–55] though it was not until 2003 that the first functional *in situ* closed cell liquid TEM configuration was published.[33] The cell used sapphire as the electron-transparent membrane to visualize for the first time nanometer scale dynamic copper cluster nucleation and growth at a solid-liquid interface.[33] This was a particularly important development for future studies exploring the particle dynamics at solid-liquid/vapour interfaces, and soon after, other explorations were put forward to develop liquid-cell *in situ* liquid TEM holders for a variety of research applications.[25]

Several liquid cell designs and configurations have been developed since,[27] and they can generally be categorized into 1) silicon-based assemblies that are used in commercially available holders, 2) thin-film configurations that are custom-developed and feature hybrid enclosure options (Fig. 2). These designs are applicable for both TEM and scanning TEM (STEM) modalities supplemented with EELS and EDX elemental/phase characterization.[56–60] This is an advantage of the liquid TEM technique over cryo TEM for biological imaging, as in STEM this is challenging to perform in cryo conditions due to the intensity of the electron beam and its destructive interactions with vitreous media.

Silicon-based liquid TEM assemblies, normally silicon nitride (Si_3N_4; referred to as SiN in text), are mostly widely used in literature (Fig. 2A.-C.). Commercially available SiN configurations offer static and/or dynamic functional capabilities such as microfluidic flow, solution mixing *in situ* from different inlets, heating to various temperature ranges, and electrochemistry functions. This makes liquid TEM a powerful platform to characterize dynamic reactions and hydrated material structures important for understanding biomineralization processes.[59,61,62] Novel adaptations of these commercial holders include the ability to perform atmospheric gaseous imaging in traditional TEMs, which can provide key insights into liquid-vapour dynamic events.[63–65] Popular companies among those who develop liquid TEM systems commercially include Protochips Inc., Hummingbird Scientific, and DENSolutions.[60,66,67] The drawbacks to commercial liquid TEM holders include the investment cost related to its purchase and the thick SiN membranes used, typically ranging from 30-50 nm, which can limit TEM imaging resolution.

More recently, new thin-film configurations have been actively explored (Fig. 2D.-F.). Notably, these methods often require no specialized holder, making them more affordable. Moreover, thin films range in thickness on the order of 5 nm or thinner, and thus are less limiting for HR imaging. The materials used for these thin-film assemblies typically consist of amorphous carbon[45,46] or graphene.[49,51,68,69] Graphene enclosures have been reported to reduce beam damage during imaging by limiting free radical formation and thus provide high electron dose tolerance than samples imaged in cryo TEM.[51,70,71] In applications, the

thin films are described to blanket specimens and lead to small volume liquid pockets with thin liquid regions thus helping improve HR data acquisition.[72] Studies have explored these options using thin-film coated TEM grids paired with SiN microchips (Fig. 2D.),[32,44–46,69] self-paired thin film coated TEM grids that feature a holey supporting material (Fig. 2E.),[49,51] and with thin films which are directly coated onto a SiN support (Fig. 2F.).[68,69]

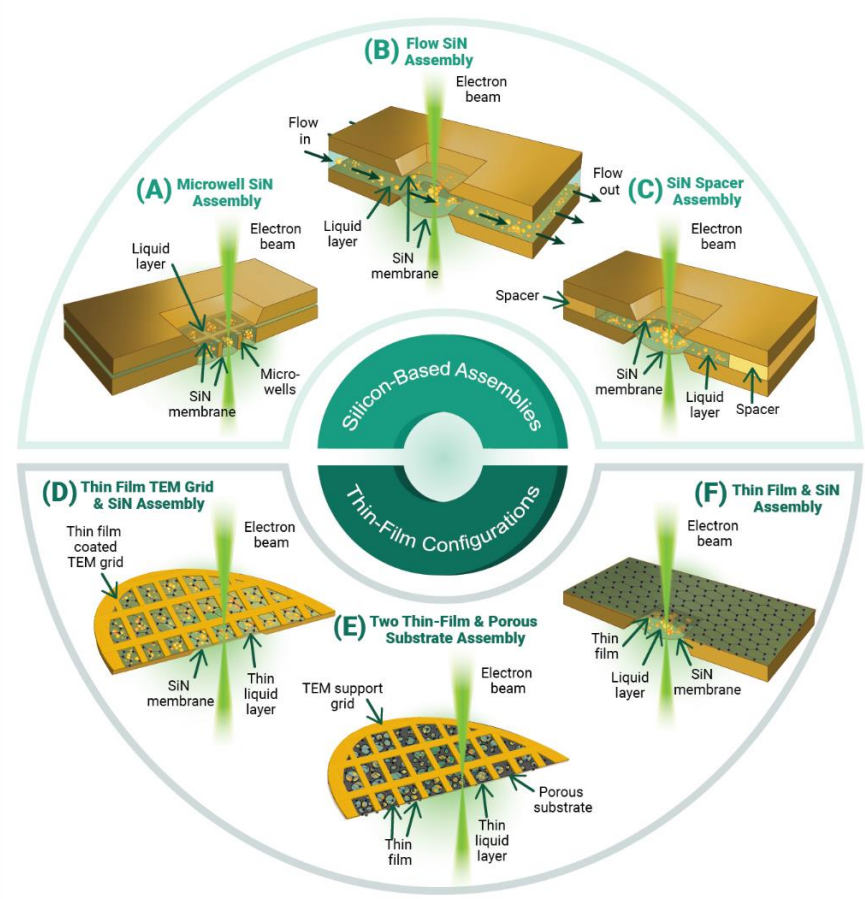

Ch. 2.3 – Figure 2. Representative overview of common liquid TEM assemblies. *A.-C. Commonly used commercial-based options that are silicon nitride (SiN)-based formed of pairing options that can include A. microwells, B. fluidics, and/or C. controlled thickness through the integration of spacers. D.-F. Representative emerging thin-film options, often graphene or amorphous carbon, that can include D. a thin-film coated TEM grid paired with a SiN membrane, E. self-paired thin-films with or without a uniform or non-uniform porous substrate for the controlled formation of liquid pockets, and/or F. a larger support SiN microchip with a thin-film deposited directly onto the membrane.*

Self-paired thin-films (Fig. 2E.), consisting of only thin-film membrane layers paired together to enclose solutions, are reported to achieve the highest spatial resolution to date with the thinnest liquid volumes. However, their fragile membranes can lead to lower reproducibility in a liquid enclosure. In contrast, thin-film assemblies paired with SiN counterparts (Fig. 2D., F.) can benefit from its rigid substrate support to obtain higher

repeatability in a liquid enclosure and accommodate more liquid and larger biological specimens, though with lower imaging spatial resolution. One significant hurdle to these assemblies is reproducing samples with enough liquid volumes captured to observe dynamic reactions due to the thin-film confinement.[72] To address this issue, several recent works within the field have described in detail the optimized preparation methods and facile-to-use commercial options are becoming more widely available.[32,68,73] Another limitation of the thin-film enclosures includes the lack of holistic functionality that commercial holder alternatives offer, such as flow, heating and electrochemistry. A recent work by Dunn et al. using novel graphene flow assemblies using nanochannels for dynamic experiments has opened the possibility of other functional capabilities for these systems in future.[74]

Other alternative assemblies for liquid TEM include single-use enclosures, such as Bio Ma-Tek K-kits, a silicon-based assembly that has been successfully used to image a wide variety of biological samples.[75,76] These fit into the enclosure type shown in Fig. 2C. The benefit of the K-kits is they can fully seal and encapsulate samples quickly and easily, involving usually thirty to sixty minutes of preparation time, and fit into a standard-size TEM grid loop and thus compatible with most standard TEM holders, mitigating the need for a specialized holder.

There are also environmental TEM options that can be used alternatively to enclosures described above to image hydrated specimens, where vapour water is considered for imaging wet and insulating materials in native conditions.[77–79] In this method, materials are viewed in open air, requiring higher pressures and usually a lower vacuum mode to observe wet, uncoated samples. While research has successfully used this technique for studying HR dynamic reactions, one drawback remains as they typically require a specialized microscope system, where there may be challenges to analysis based on the types of imaging and spectroscopy detectors that are available. Noted previously, there are recent emerging environmental TEM option holders, similar to the described commercial liquid TEM holders but for environmental gas-based options which can operate under atmospheric conditions.[63–65] For samples that are not just wet but are rather submerged in liquids like microorganisms, cells, and colloidal nano/micro particle solutions, environmental EM does not allow for depth observations and often provides poor contrast and object drifting while imaging liquid media.[80] Moreover, environmental EM in aqueous conditions can depend on vapour condensation which limits the temperature and pressure achieved in the system.[81] Few applications of environmental EM published in literature studying biomineralization reactions could be found by the authors, though the technique would be useful for studying liquid-solid phase separation and evaporation reactions of biominerals.

Correlatively to TEM, micro-to-nano liquid EM can be done using scanning EM (SEM). Single-use sealable liquid SEM capsules are commercially available that are configurable to most standard SEM holders, such as the QuantomiX WETSEM^{TM} capsules. The capsules allow users to use easily configurable, familiar pin-shaped capsules to observe

soft and wet samples in standard SEM working conditions. Typically, these capsules feature a body with a pressure relief membrane underneath the liquid sample compartment and a liquid media compartment that is encapsulated by an electron transparent membrane such as a polyimide polymer.[81] Researchers have been able to use these WETSEM setups to perform *in situ* SEM experiments such as heating and cooling[82] as well as correlative light microscopy through the introduction of an optical fibre.[83] While these cells have been effective to image wet and soft biological samples,[83] some reported limitations with these capsule designs include the thick viewing membranes that result in lower resolution, poor contrast and resolution, as well as limiting imaging modality in just backscatter electron mode.[84,85] Research is seeking to address these challenges, where for instance one team has explored the design of a microfluidic platform with thin membranes made from graphene for liquid SEM work.[86]

Recently, the use of room temperature ionic liquids (RTILs) has been considered as an alternative method to visualizing hydrated specimens in SEM.[87] RTILs, otherwise known as molten or fused salts, are composed of ions and short-lived ionic pairs and uniquely are known for their low vapour pressure, high ionic conductivity, and non-combustibility.[88,89] Their nearly negligible vapour pressure allows for these liquids to be stable in SEM systems under normal operating conditions, where RTILs behave like conductive coatings and experience limited charge buildup.[90] This provides new capabilities to image wet biological samples with comparable imaging capabilities to conventional methods at a fraction of the preparation time.[40,91] For biomineralization-related research, our team highlights that these tools are quite useful for imaging cellular systems to assess implant surface candidates[92] and can be used to study hard tissues such as bone.[93] Others have noted RTIL application successfully in TEM for biological applications,[94,95] though limited works are available using this as a technique in TEM modalities at HR.

2.3.5. Innovations in Biomineralization Theory Through Liquid Electron Microscopy

Innovations in biomineralization studies through liquid TEM are drastically changing the field to address these debated topics through *in situ* dynamic visualization, providing new avenues to observe the biomineralization processes. The following subsections summarize and discuss selective key works which have investigated biomineralization-related processes using novel *in situ* liquid TEM means. Available published works have primarily focused on studying the formation and mineralization progression of calcium carbonate ($CaCO_3$) and calcium phosphate (CaP) minerals, and few other applications involving iron-based biominerals in literature. The literature reviewed and relevant liquid TEM preparation and acquisition parameters reported in literature are summarized in Table 1 for those seeking to explore the technique.

Ch. 2.3 – Table 3. *Overview of relevant experimental conditions reported for select in situ liquid TEM research related to the biomineralization field, discussed within this section. Acronyms: amorphous calcium carbonate (ACC), pre-nucleation clusters (PNCs), polystyrene sulphonate (PSS), L-aspartic acid (L-Asp), sodium citrate (Na-Cit), sodium poly-acrylate (PAA), poly-L-aspartic acid (pAsp), amorphous calcium phosphate (ACP), hydroxyapatite (HA).*

Product Observed & Study Focus	Liquid TEM Methodology			Liquid TEM Acquisition Variables	Reported Electron Dosage	Ref.
	Enclosure	Membrane Configuration Reported	Assembly (Fig. 2)			
Calcium Carbonates						
$CaCO_3$; nucleation & formation of ACC & vaterite	Hummingbird Scientific liquid flow	SiN, 50 nm membranes, max. imaging area 50 µm × 200 µm,	(B) fluidics; ~10 µL min^{-1}, 250-500 nm spacer	BF TEM, 200 kV, JEOL JEM2100F TEM, 0.1-0.2 s exposures	$5 \pm 3 \times 10^2$ $e^- nm^{-2} s^{-1}$	[96]
$CaCO_3$; formation, dissolution; effect of confinement on mineralization	Poseidon, Protochips	SiN	(B) fluidics; 300 µL min^{-1}	STEM, 200 kV, JEOL 2200 FS, 1.5 pA current, 1 µs dwell time w/ 0.5 s exposures at intervals of 5 s for ~120 s	3-10 × 10 $e^- Å^{-2}$	[97]
$CaCO_3$ w/ PSS; early-stage precipitation, nucleation, growth; globule & ACC formation + calcite & vaterite crystallization	Hummingbird Scientific liquid flow	SiN, 50 nm membranes; max. imaging area 50 µm × 50 µm	(B) fluidics; 100 µL hr^{-1}, 0.5 µL of ultrapure water at start, 250-500 nm spacer	BF TEM, 200 kV, JEOL 2100-F, 5-10 fps acquisition	$1 \pm 0.5 \times 10^3$ $e^- Å^{-2} s^{-1}$; 50-300 $e^- Å^{-2}$	[98]
$CaCO_3$ w/ & w/o L-Asp; early-stage precipitation, nucleation, growth	Poseidon, Protochips	SiN	(B) fluidics; 10 µL hr^{-1}, 5 µL of solution at start	BF S/TEM, 200 kV, JEOL 2100-F, current 50 pA cm^{-2} – 134 pA cm^{-2} in TEM & 7.9 pA cm^{-2} in STEM, 3 fps acquisition	*Not specified.*	[99]
$CaCO_3$ w/ & w/o L-Asp; early-stage precipitation, nucleation, growth	Poseidon, Protochips	SiN, 50 nm thick membranes; 50 µm × 550 µm membrane windows	(B) fluidics; 2.7 µL of fluid passed, 1 µL of solution medium added at start, 150 nm spacer	BF S/TEM, 200 kV, JEOL 2100-F, 10 fps acquisition	*Not specified.*	[100]
$CaCO_3$; early-stage precipitation, nucleation; ACC, embryo, & PNC formation	Poseidon, Protochips	SiN	(B) fluidics; 2 µL min^{-1}, 150 & 500 nm spacers	TEM, 200 kV, Hitachi H-8100, 8-10 fps acquisition	Variable: $1 – 7 \times 10^3$ $e^- nm^{-2} s^{-1}$; reported total dose in one case was 1×10^6 $e^- nm^{-2}$	[101]

Product Observed & Study Focus	Liquid TEM Methodology			Liquid TEM Acquisition Variables	Reported Electron Dosage	Ref.
	Enclosure	Membrane Configuration Reported	Assembly (Fig. 2)			
$CaCO_3$ w/ & w/o Mg^{2+}, Na-Cit, & PAA; nucleation, growth; ACC to $CaCO_3$	Hummingbird Scientific liquid flow	SiN, 50 nm membranes, 30 µm × 200 µm membrane windows	(C) 0.6 µL of liquid place on each microchip, 500 nm spacer	BF TEM, 200kV – Tecnai G^2 F20, 2 s exposure	≤ 3.11 $e^- nm^{-2} s^{-1}$	[102]
$CaCO_3$; nucleation, growth, coalescence; aragonite & calcite formation	Graphene liquid cell	Multilayer graphene membrane transferred onto a quantifoil holey-carbon TEM grid	(E)	DF-TEM & HRTEM, 200kV, Tecnai G^2 F30 S-TWIN, DF-TEM imaging performed at d-spacing of 2.07, 2.43, 2.94 Å	50 $e^- Å^{-2}$ in DF TEM, 837 $e^- Å^{-2} s^{-1}$ in HRTEM	[103]
$CaCO_3$; Early-stage precipitation, nucleation; dense liquid globules & calcite crystallization	Custom setup involving 2D thin-films	SiN w/ two hexagonal boron nitride spacers; few-layer graphene upper & lower membranes; MoS_2 separation mixing layer	N.A. – custom thin-film enclosure with mixing	BF TEM & ADF STEM, 200 kV, Titan G2 80-200 S/TEM *ChemiSTEM*, probe current for STEM 80-160 pA for 2-20 µs	6.8×10^6 $e^- Å^{-2}$ for mixing pore production; 7.3×10^2 $e^- Å^{-2} s^{-1}$ & 1.5×10^3 $e^- Å^{-2} s^{-1}$ for imaging	[69]
Calcium Phosphates						
CaP; nucleation, aggregation growth	Poseidon, Protochips	Microwell SiN – 1) 50 nm membrane paired w/ 2) 8 × 16, 10 µm × 10 µm microwell windows of 30 nm membrane	(A) 2 µL solution added	BF STEM, 200kV, JEOL 2010F TEM	21 $e^- frame^{-1} nm^{-2}$; 2.198×10^3 $e^- Å^{-2} s^{-1}$	[30]
ACP to HA; nucleation, growth pathways	Poseidon, Protochips	SiN, 50 nm membranes	(B) fluidics 300 µl/hour, 150 nm spacer	BF TEM & HAADF-STEM, 200 kV, JEOL JEM-ARM 200CF, 30 fps acquisition	1 $e^- Å^{-2} s^{-1}$ for *in situ*; 17.5, 60 & 1114 $e^- Å^{-2} s^{-1}$ for other imaging	[104]
ACP to HA w/ & w/o Mg^{2+}; nucleation, growth pathways	Hummingbird Scientific liquid flow	SiN, 50 nm membrane, 50 µm × 200 µm membrane windows	(C) 0.4 µL	BF TEM & HAADF STEM, 200 kV, FEI Tecnai G^2 F20, 0.3 s exposure, 10 fps acquisition	0.4 $e^- Å^{-2} s^{-1}$	[105]

Product Observed & Study Focus	Liquid TEM Methodology			Liquid TEM Acquisition Variables	Reported Electron Dosage	Ref.
	Enclosure	Membrane Configuration Reported	Assembly (Fig. 2)			
HA; dissolution & crystallization	Graphene liquid cell	Commercially available single or few-layer chemical vapor deposition-grown graphene on copper	(E) lacey carbon-coated copper TEM grid used as graphene support	LAADF STEM, 80 kV, JEOL JEM-ARM200CF	Variable ranges; reported HA damage threshold noted 24 e^{-} $Å^{-2}$ s^{-1}	[106]
ACP to HA; nucleation, growth pathways	Poseidon, Protochips	SiN, 50 nm membranes	(C) 0.6 µL, 150 nm spacer	BF TEM, 200 kV, JEOL 2100F/Cs(S), 3fps acquisition	Variable range reported ~10-2500 e^{-} nm^{-2} s^{-1}	[107]
CaP w/ pAsp, particle assembly & aggregation growth	Poseidon, Protochips	Microwell SiN – 1) 50 nm membrane paired w/ 2) 8 × 16, 10 µm × 10 µm microwell windows of 30 nm membrane	(A) 0.5-1 µL solution added	BF TEM, 200 kV, Talos 200X, 1 fps acquisition	Variable range 0.4-0.75 e^{-} $Å^{2}$ s^{-1}	[108]
Other Biomineralization Systems						
Iron oxyhydroxide; assembly, growth	Hummingbird Scientific liquid	SiN, 50-100 nm membranes	(C) 450 nm spacer	TEM, 200 kV, JEOL 2100F, 4-10 fps acquisition, current 35 pA cm^{-2}	*Not specified.*	[109]
Iron binding to Mms6 protein; pre-nucleation, nucleation	Hummingbird Scientific liquid flow	SiN	(B) fluidics; 2-5 µL min^{-1}; protein addition onto SiN using Nano eNabler molecular printer	HAADF STEM, 200 kV, FEI Tecnai G^2 F20 (S)TEM	*Not specified.*	[110]
Magnetospirillum magneticum strain AMB-1; structural liquid phase observation	Hummingbird Scientific liquid flow	SiN, 50 nm membrane, 50 µm × 200 µm membranes windows, positive charged either BioPlus biofunctionalized (no spacer) or with poly-L-lysine or (3-Aminopropyl)triethoxysilane (APTES) (spacer)	(B) 10 µL min^{-2} up to 100 µL to freshen media; 100 nm spacer or no spacer	HAADF STEM 200 kV, FEI Tecnai G^2 F20 (S)TEM, 38 pA current, low mag: dwell time 2 µs, higher mag: dwell time 8 µs	Low mag < 0.05 e^{-} $Å^{2}$ s^{-1} High mag 0.1-2.3 e^{-} $Å^{2}$ per scan	[111]

Product Observed & Study Focus	Liquid TEM Methodology			Liquid TEM Acquisition Variables	Reported Electron Dosage	Ref.
	Enclosure	Membrane Configuration Reported	Assembly (Fig. 2)			
Magnetospirillum magneticum strain AMB-1; Structural liquid phase observation	Hummingbird Scientific liquid flow	SiN, 50 nm membrane, 50 μm × 200 μm membranes windows, positive charged functionalized with (3-Aminopropyl)triethoxysilane (APTES)	(B) 1 μL deposition; 100 nm spacer	HAADF STEM, 200 kV, FEI Tecnai G^2 F20 (S)TEM, off-axis electron holography done in FEI Titan 80-300 (S)TEM at 300 kV, Lorentz mode, 6-8 s exposures	1.4-47 e^- $Å^2$ s^{-1}	[112]
Magnetospirillum magneticum; structural liquid phase observation; magnetosome nucleation & growth	Graphene liquid cell	2000 mesh graphene coated copper grids	(E) 1 μL deposition	BF-TEM 80 kV, JEOL 1220 & Hitachi HT7700, 0.1 & 1 sec exposures	200-2000 e^- nm^{-2} per frame	[113]
Ferritin-Iron; formation of iron oxide core inside apoferritin	Graphene liquid cell	Graphene coated lacey grids	(E) 1.5-3.5 μL deposition	HAADF-STEM, 80 kV, JEOL-JEM 200CF 22 mrad semi convergence angle, 90 mrad inner HAAD detector angle, dwell time 31.2 μs for 256 × 256 for imaging	7 e $Å^{-2}$	[114]
Human spleen & heart ferritin; structural liquid phase observation	Graphene liquid cell	Graphene coated lacey gold grids	(E)	STEM 80kV, 80kV Hitachi HT7700 & JEOL-JEM 200CF, 22 mrad semi convergence angle, 90 mrad inner HAAD detector angle, dwell time 31.2 μs for 512 × 512 for imaging	9-181 e $Å^{-2}$	[115]
CaOx w/ & w/o citrate; nucleation, growth, assembly	Graphene liquid cell	Graphene-coated copper grids	(E) 0.5 μL deposition	TEM, 80kV, JEOL 1220 TEM & JEOL ARM 200CF STEM	3×10^9 – 2.24×10^{12} Gy s^{-1}	[116]

Calcium Carbonates

Calcium carbonate ($CaCO_3$) is one of the most broadly studied biomineral compounds and was among some of the first biominerals probed using liquid TEM. $CaCO_3$ is found in a range of substances, such as eggshells, shellfish skeletons, pearls, and sediments, and is used as a medical supplement for calcium.[117–119] While simple in chemical structure, $CaCO_3$ exists in several different stable polymorphic crystalline forms such as calcite, aragonite, and vaterite.[120] Moreover, its formation has been reported to occur through both classical monomer-by-monomer nucleation and non-classical means involving several proposed polyamorphic amorphous calcium carbonate (ACC) forms.[121–124] The reactions behind these processes have been widely debated and remain to be elucidated – which is where dynamic visualization through liquid TEM has been leading discoveries, revealing new evidence to explain these complex pathways.

Early *in situ* liquid TEM work by Nielsen et al. revealed the coexistence of direct and indirect crystallization pathways during $CaCO_3$ nucleation and growth.[96] Using a liquid TEM enclosure that allowed for reagent mixing, the study showed several different concurring pathways involving classical direct nucleation from solution and non-classical processes with ACC formation and crystalline precursors.[96] Direct nucleation of ACC and a vaterite crystalline phase (Fig. 3) was observed in one pathway. Non-classical, precursor-related nucleation from ACC particles was also seen, where aragonite and vaterite were observed to grow within or on the surface of ACC particles, where their growth occurred at the expense of ACC.[96] ACC to calcite transformation was not observed, which aligned with leading theories at the time which hypothesized a classical means to its formation.[96] Particularly, the work challenged the existence of different distinct polyamorphic ACC phases as they might represent different time points of a similar reaction, and proposed instead that ACC as a term represents a variety of structures including ion-dense liquid and anhydrous forms. This important research was the first to visualize mimetic biomineralization reactions in liquid, demonstrating the potential of utilizing liquid TEM to study biomineralization.

Since the work by Nielsen et al., the formation mechanisms of calcium carbonates in biological settings have remained poorly understood, particularly considering the role of ACC and biological environment effects. This has led to further exploration conducted using liquid TEM combined with other characterization methods to address unsolved questions within the field and shed light on $CaCO_3$ formation reactions.

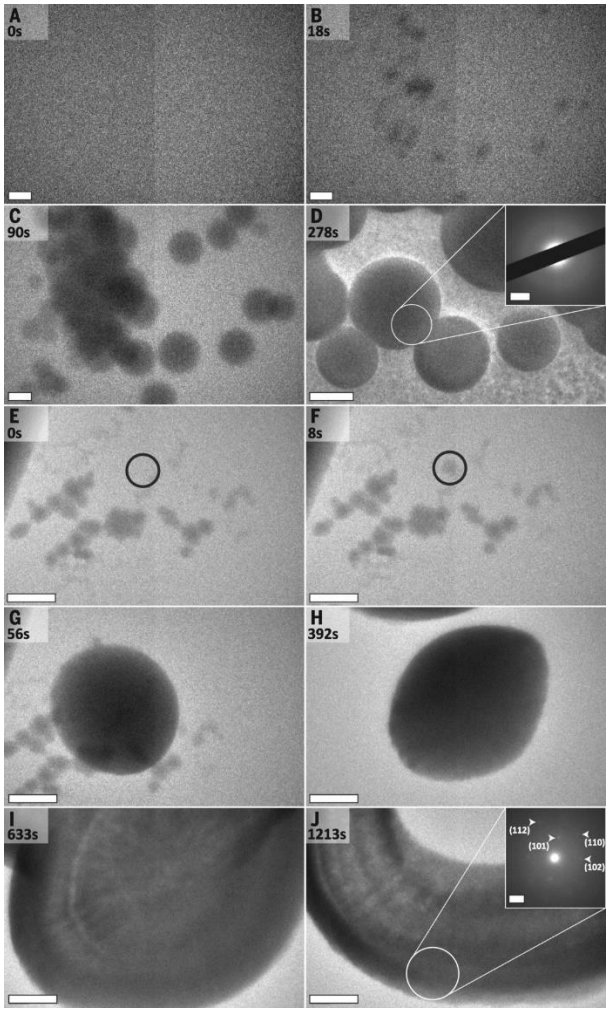

Ch. 2.4 – Figure 3. Direct formation of ACC and vaterite. *A. Frames highlighting fluid cell before nucleation and B.-D. during nucleation and growth of ACC. Diffraction analysis [inset to D.] of thinned fluid layer confirms the amorphous nature of the particles. E.-J. Frames following vaterite formation and growth. E. Gray spots already present are salt deposits that formed on the outer surface of the liquid cell window during cell assembly. In E. and F., the nucleation site of a vaterite particle is circled for clarity. G. The particle grows, H. merges with a second particle, and I., J. exhibits layering at the growth front and dissolution in the center. Diffraction analysis [inset to J.] identifies the material as vaterite. Scale bars are: A.-J. 500 nm, and [insets D., J.] 2 nm^{-1}. Solution conditions—designated in all figure legends by [$CaCl_2$]:[$NaHCO_3$]/R($CaCl_2$): R($NaHCO_3$) with concentrations in millimolar and flow rates R in microliters per minute are: A.-D. 50:50/10:0.2 and E.-J. 40:40/9:1. Times listed in all figures are relative to the beginning of the associated movie shared within the work. Image reproduced with permission from Nielsen et al.*[96] *(Copyright © 2014 American Association for the Advancement of Science).*

Focusing on early-stage $CaCO_3$ development at relatively lower supersaturation concentrations, Kimura et al. explored the role of ACC and embryos or PNCs, and their significance in $CaCO_3$ nucleation using liquid and traditional TEM means.[101] In the study, prenucleation pathways in near-equilibrium conditions were visualized, where PNCs were observed to form in ACC structures at relatively high formation rates, indicative of low

interfacial energy existing between crystals and ACC.[101] They note that PNCs may be of different polymorphs of $CaCO_3$, though observed only the formation of calcite nucleation particles passed critical radius growth thresholds.[101] In contrast, ACC phases were observed with similar composition and structure, implying the lack of distinctive polyamorphs associated with specific $CaCO_3$ polymorphs.[101]

In performing liquid TEM, there is often a disparity in results stemming from bulk solutions to those captured *in situ* in confined liquid enclosures.[97] Further, confinement is highly relevant in natural biomineralization systems, which can impact $CaCO_3$ polymorph structure stabilization.[125] To investigate the impacts of confinement on mineralization dynamics of supersaturated solutions, Kröger and Verch used liquid TEM to study $CaCO_3$ formation as a model system.[97] Based on their observations *in situ*, $CaCO_3$ precipitates (calcite) were formed spontaneously upon imaging in STEM.[97] The study speculated the calcite formation was likely to be accelerated by the electron beam in surveying other regions.[97] By combining liquid TEM findings with 2D Finite Elements simulations, their work further suggested certain ranges of liquid volume confinement led to reductions in ion concentrations, resulting in more stable precipitate formation.[97] Overall, they found that confinement in liquid TEM has a strong impact on ion transport mechanisms affecting mineralization processes.[97] In particular, ion incorporation rates based on fluidics and solution diffusion were noted to be controlling factors in phase stabilization for consideration.[97] This does not disregard findings found in the liquid TEM field studying these phenomena within confined environments; in native biomineralization systems, confinement is hypothesized to play a role in how biominerals form and has been noted to impact the $CaCO_3$ polymorph structure stabilization.[125]

Others have been working towards pushing imaging boundaries of liquid TEM in application to study $CaCO_3$ crystallization events by replacing SiN membranes with thinner film-based enclosures. Work by Dae et al. examined $CaCO_3$ formation under supersaturated conditions with dark field (DF) TEM and HRTEM with graphene enclosures.[103] Their work highlighted a sequential three-stage growth process involving nucleation, diffusion-limited growth, and Ostwald ripening with particle coalescence (Fig. 4). Real-time dynamic liquid imaging exposed the transformation of metastable aragonite which grew sequentially into stable calcite under highly supersaturated conditions.[103] In contrast to other studies, Dae et al. did not observe the formation of any ACC phase; rather, they suggested that spatial resolution may be a limiting factor in liquid TEM restricting capabilities in experiments to clarify the presence of an amorphous phase in comparison to nanocrystalline precipitation.[103]

However, the graphene thin-film enclosure used by Dae et al.[103] did not allow for solution mixing *in situ*, implying that reactions were possibly driven by electron beam interactions to induce crystallization. To address this challenge, emerging research from Kelly et al. further expanded upon liquid TEM thin-film capabilities with a new 2D layer mixing technique to study $CaCO_3$ reactions at HR.[69] Using controllable fracture of an adjunct atomically thin separation membrane within the enclosure, *in situ* mixing was induced with

the electron beam through a 2D heterostructure mixing cell, pushing the visualization of $CaCO_3$ mixing reactions to sub-nanometer resolution.[69] Using this technique, direct visualization of calcite formation was achieved where nanodroplet precursors that formed into crystalline calcite were observed, supporting non-classically proposed liquid-liquid phase separation theories leading to the formation of ACC.[69] This unique cell offers benefits not just for studying $CaCO_3$ formation and growth, but also in other mineralization systems and liquid-liquid mixing reactions, expanding thin-film liquid TEM capabilities.

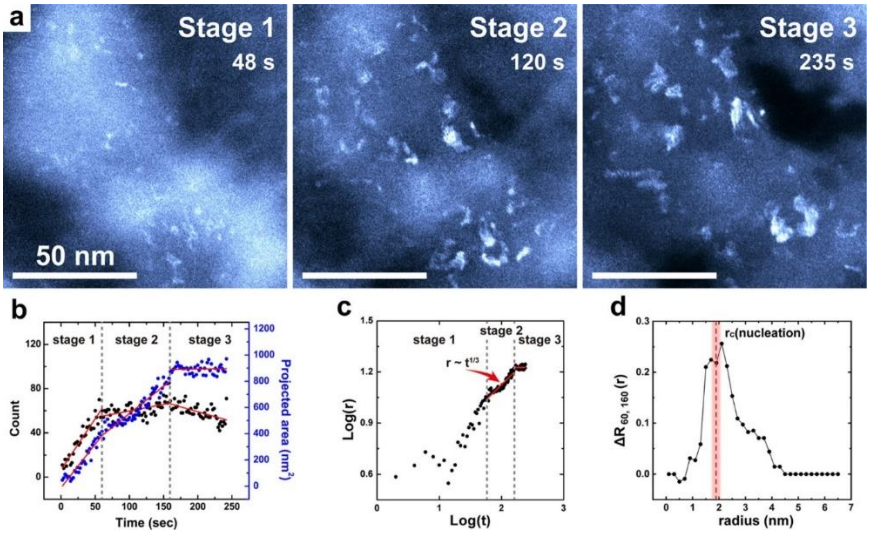

Ch. 2.3 – Figure 4. In situ dark-field liquid TEM analysis of $CaCO_3$ crystallization. *A. Time series images corresponding to each mineralization stage. B. Each black and blue dot gives the number of particles and total projected area of all precipitates as a function of irradiation time t. Based on the dynamics of mineralization, the whole process is divided into three stages: nucleation, diffusion-limited growth, and Ostwald ripening/coalescence. Red solid lines show the trends in each stage. C. Logarithm relationship between the radius r of the particles and t. D. Increase in the ratio of the number of particles larger than r during the growth step (Stage 2), $\Delta R_{60,160}(r)$. The peak indicated by the red dotted line shows the critical radius for the nucleation, r_c (nucleation). Image reproduced under the Creative Commons Attribution 4.0 International (CC BY 4.0) License from Dae et al.[103] published by the ACS Omega journal (Copyright © 2020 American Chemical Society).*

To mimic biological systems where $CaCO_3$ forms, researchers have also incorporated additives to explore the impacts of additional system variables on $CaCO_3$ formation. Research from Smeets et al. was among the first to study the nucleation and growth of $CaCO_3$ in supersaturated conditions with exposure to a matrix of polystyrene sulphonate (PSS).[98] PSS is a negatively charged polyelectrolyte known as a growth modifier for $CaCO_3$ mimetic to biomacromolecules in marine life. PSS has been shown through dry spectroscopy and imaging techniques to inhibit the crystallization of liquid ACC while promoting crystallization in solid-state.[126] However, this behaviour had not been proven with dynamic evidence, until findings from Smeets et al. demonstrated real-time metastable ACC formation *in situ*.[98] At the initial stage of mineralization, calcium ion binding to PSS led to the formation of Ca-PSS globules, an essential precursor for the formation of ACC

in biomineralization systems.[98] Subsequently, ACC nucleation was observed from the Ca-PSS globules with carbonate introduction to the enclosure, where over time with electron beam exposure crystals formed within the same regions.[98] Without the addition of PSS, direct nucleation, and growth of vaterite were observed as the predominant phase, but some calcite formation was noted.[98] Overall, these findings demonstrate ion Ca-binding in PSS-containing systems is an important factor leading to the formation of metastable ACC, directing nucleation processes within this system, and lending insight into how other acidic macromolecules may behave in analogous mineralization processes.

Similar to PSS, the highly negatively charged structure of L-aspartic acids' (LAsp) is believed to influence $CaCO_3$ formation through crystallization inhibition of liquid ACC while promoting crystallization in solid-state.[126] In this context, efforts stemming from Longuinho et al. and Ramnarain et al. investigated the process of $CaCO_3$ formation with the presence of LAsp.[99,100] The formation of Ca-rich, organic vesicle-like structures with LAsp was described – similar in behaviour to ACC droplets/globules described by Smeets et al. [98] – where $CaCO_3$ formed in association with these described vesicle structures.[99] Complimented by molecular dynamics simulation analysis, LAsp was proposed to reduce $CaCO_3$ crystal growth rates by decreasing Ca ion diffusion.[99] Follow-up works by some of these authors further expanded this research, supporting the findings with hyperpolarized solid-state nuclear magnetic resonance (DNP NMR) and density functional theory (DFT) calculations.[100] LAsp was observed to lead to the stabilization of transient precursor phases that increase the formation of individual and aggregated PNCs that transform into an ACC phase.[100] These two studies not only highlighted the key findings regarding how organic molecules influence $CaCO_3$ mineralization processes, but they also demonstrated the efficacy of complementary analytical techniques and modelling analysis to validate observations *in situ.*

Inorganic ions are also reported to impact the formation of biominerals, such as $CaCO_3$. For instance, Mg^{2+} is shown to alter $CaCO_3$ transformation pathways and is theorized to act as a stabilizer of ACC[127–129] and inhibit the crystal formation of calcite.[130,131] Recent work from Liu et al. demonstrated the influence of Mg^{2+}, sodium citrate (Na-Cit) and sodium poly-acrylate (PAA) individually as biomimetic representatives of inorganic ions, small organic molecules, and macromolecules, respectively, found in natural $CaCO_3$ biomineralization systems.[102] It was reported that Mg^{2+} at lower concentrations ($\leq$2.5 mM) increased ACC lifetimes, Na-Cit slowed calcite formation and ACC dissolution, and PAA had the same effects as both Mg^{2+} and Na-Cit, leading to dissolution-reprecipitation formation of ACC-to-calcite.[102] At higher concentrations ($\geq$5.0 mM), Mg^{2+} additions were observed to lead to shape-preserving direct transformation of ACC-to-calcite.[102] Through *in situ* and complimentary spectroscopy and molecular dynamics analyses, Mg^{2+} was found to increase hydration in the ACC phase which allowed for its direct transformation into calcite through dehydration, conserving the ACC shape, rather than through morphological changing steps.[102] This work highlights the varying effects of different additives on *in situ* $CaCO_3$ formation while also providing new rationale as to the presence of Mg in $CaCO_3$-based biominerals.

The fundamental mechanisms governing $CaCO_3$ mineralization remain poorly understood as there are many competing theories proposed under different systems. However, as first discussed in the work by Nielsen et al.[96] many different pathways likely coexist based on the *in situ* work presented in literature. Considering the number of different polymorphs of $CaCO_3$, their stabilization *in situ* may vary based on factors such as solution concentration, thermodynamic conditions, confinement, electron beam effects, and more. While select additives, both organic[98–100] and inorganic,[102] have been probed, limited research has been performed to examine the influence of other additional system elements that aid in mimicking these complex systems in nature. This leaves room for opportunity for future liquid TEM research studying the formation and growth of $CaCO_3$, a simple biomineral with complex mineralization processes behind its formation.

Calcium Phosphates

One principal component of hard tissues, such as bone and teeth, in vertebrates consists of a CaP mineral that is fundamental for the mechanical strength of the tissue.[132,133] A clear understanding of the pathways behind CaP biomineralization in healthy and pathological conditions is significant for biological and medical advancements.[4] In particular, knowledge of the mechanisms behind CaP biomineralization can inform perspectives on therapeutic targets for diseases such as atherosclerosis, dental caries, and osteoporosis[4,134,135] and strategies for treatment and repair, such as improving implant osseointegration.[136,137]

As far as the authors are aware, our recent study was the first to explore the early stages of CaP mineralization *in situ* using liquid TEM.[30] The work revealed for the first time dynamically that CaP mineralization in a simulated body fluid occurs through particle attachment,[30] using Ca-P model ratios based on established mineralization models.[138,139] Bright-field STEM captured real-time CaP nucleation and growth events with nanometer spatial resolution and documented the movement and aggregation of particulates in solution as well as the subsequent formation of polymeric branch structural assemblies (Fig. 5).[30] This observation provided novel dynamic evidence that CaP mineralizes through a more complex, non-classical crystal growth pathway involving the formation of pre-nucleation clusters that aggregate before more mature crystallization,[30] supporting the works explored at similar time-scale points using cryo TEM.[15,17] This work laid the foundation for further biomineralization research in studying CaP mineralization processes *in situ*.

New works exploring CaP crystallization *in situ* have since emerged, probing the formation of hydroxyapatite (HA). HA is a naturally occurring CaP-based mineral found prominently in bone structures and has been studied extensively in hard tissue regeneration.[140,141] Most notably, He et al. conducted a comprehensive and systematic HR *in situ* liquid TEM study of HA nucleation and mineralization process.[104] Using a biomimetic ion-rich saliva model, they revealed that the nucleation processes started with the formation of ion-

rich and ion-poor regions that subsequently led to an amorphous CaP (ACP) phase.[104] Uniquely, they observed the co-existing classical and non-classical growth pathways, involving multiphasic processes with direct agglomeration-coalescence growth of HA as well as nucleation of HA on ACP phase, respectively.[104] Agglomeration and coalescence formation mechanisms driven theoretically by the minimization of surface energy were observed as a dominant growth process for HA.[104] They note other common growth mechanisms such as Oswald ripening, island growth, and intraparticle growth, were not observed.[104] These findings demonstrate more broadly the multiphasic behaviour of biomineralization processes and allude to simultaneous mechanisms at play during these complex processes, even when the same experimental conditions are considered.

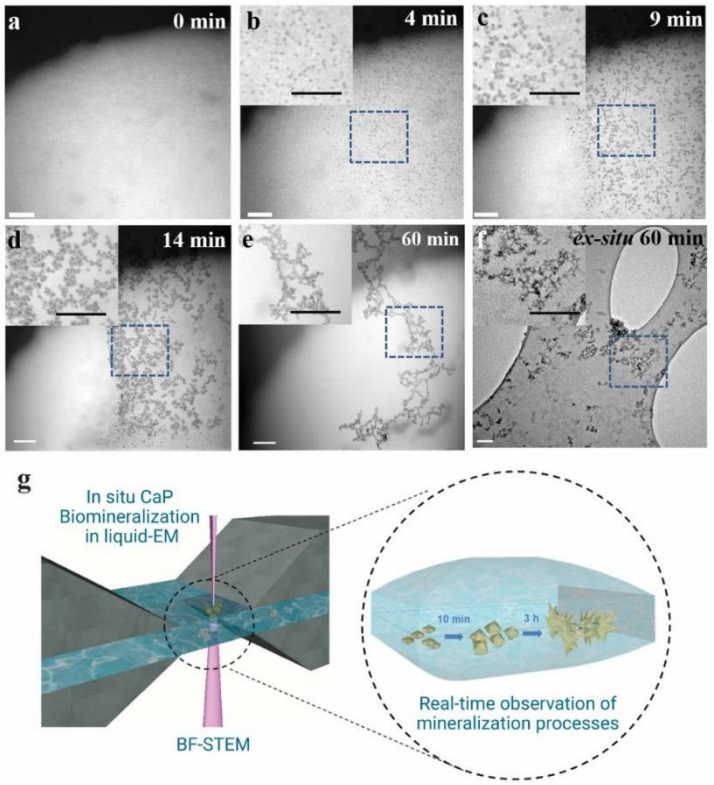

Ch. 2.3 – Figure 5. In situ exploration of CaP mineralization processes. *A.-F. In situ liquid TEM BF-STEM imaging highlighting initial nucleation and growth of CaP over 60 minutes. A.-D. Nucleation and growth of CaP particles are observed to occur, which form E. a branched particle assembly after 60 minutes, correlating to ex situ observations in F. G. Representative schematic of this in situ CaP mineralization process over time in the liquid cell assembly. Image reproduced under the Creative Commons Attribution 4.0 International (CC BY 4.0) License from Wang et al.[30] published by Communications Chemistry (Copyright © 2018 Wang et al.).*

In contrast to some *ex situ* studies performed through traditional TEM where no sign of ACP dissolution was observed during HA nucleation, He et al. demonstrated that the ACP substrates shrunk at the expense of HA growth.[104] This highlights the key capability of liquid TEM to track and identify the dynamic mineralization processes

that led to a better understanding of the role of ACP during HA mineralization and other biomineralization process pathways. Additionally, while briefly addressed, He et al. discuss that the negatively charged surface of the SiN-based window served as a functional surface that likely promoted the nucleation of HA,[104] whereas others have observed similar preferential attachment mechanisms in SiN-based liquid TEM studies at the surface.[142] While He et al. describe that these confinement effects and preferential nucleation may not be a significant concern due to liquid TEM reports of membrane bulging, this could further serve at explaining faster reaction rates observed in comparison to *ex situ*.[104]

In other CaP mineralization studies, confinement effects in liquid TEM studies are described to significantly impact biomineralization reactions, necessitating the use of complementary and *ex situ* analysis to understand wholistically reactions at play. Recent liquid TEM work from the team of De Yoreo et al. explored further the transformation from an ACP phase to HA with and without exposure to Mg^{2+}.[105] Mg^{2+} is a naturally occurring element in hard tissues that has been shown to chemically inhibit ACP crystallization, delaying the formation of HA and acting as a promoter for mineralization in bone at certain concentrations.[143] Mg^{2+} has also been reported as a stabilizer of other amorphous precursor biominerals such as ACC.[144] In comparison to the previous work described by He et al. claiming liquid TEM confinement has negligible effects on CaP mineralization,[104] this recent research from De Yoreo's team attributed the increases in ACP size within the liquid TEM system to the confinement effects.[105] Liquid TEM work was complemented by Fourier Transform Infrared Spectroscopy (FTIR) and extensive correlative *ex situ* and *post situ* studies.[105] ACP particles were described to be much larger in liquid TEM cells, even without beam exposure, than *in vitro* work, highlighting the confined environment may either slow nucleation rates or increase growth rates.[105] In discussing the role of Mg^{2+} in governing HA formation, it was thought that Mg^{2+} stabilized ACP by reducing its solubility leading to the inhibition of HA formation.[105] The stabilization of ACP led to the delayed formation of HA *in situ*, thus making the two-step dissolution-recrystallization process that transforms ACP to HA easier to be observed using liquid TEM.[105]

It was proposed that the addition of Mg^{2+} altered the transformation mechanisms from ACP to HA by structurally and/or chemically changing the ACP surface.[105] This was supported through the formation of hollowed structures, hypothesized due to the dissolution of the ACP core, visualized to form after which HA formed preferentially on its surface and then in bulk.[105] Overall, this work has broad implications regarding the confinement effects on ACP formation and biomineralization reactions in general, as well as provides better insight into the influence of HA-inhibitory additives in CaP systems. Similarly noted for $CaCO_3$ systems, in certain applications, confinement effects may be relevant to the study of natural biomineralization reactions and key to their mimetic study. For instance, in the context of mineralized tissues such as bone and dentin, biomineralization is hypothesized to occur in confinement in small liquid regions within compact tissue sections, where confinement has been demonstrated to stabilize ACP.[145] Regardless, in planning a liquid

TEM experiment, such confinement effects must be considered in scaling up liquid TEM observations to understand nanoscale *in situ* reactions observed in the context of the whole.

Previous *in vitro* TEM studies on CaP mineralization often demonstrated the formation of classic needle-like structures of HA. This morphological feature has not been observed in liquid TEM investigations until very recently by the team of Dalmônico et al.[107] In their study on exploring ACP to HA transformation, they observed the dissolution process of $Ca(OH)_2$, originating from their buffer solutions, followed by the formation of an ion-dense phase that appeared to be liquid.[107] This ion-dense phase subsequently was observed to lead to the transformation of ACP nanoparticles from this phase.[107] Most interestingly, they observed the formation of plate-like needle HA structures through three different pathways involving precursors, summarized in Fig. 6, of 1) ion-dense, high-Ca concentrated regions, 2) ACP nanoparticle attachment to existing HA particles, and 3) ACP nanoparticle aggregation, where crystallization in these cases was observed after particle elongation.[107]

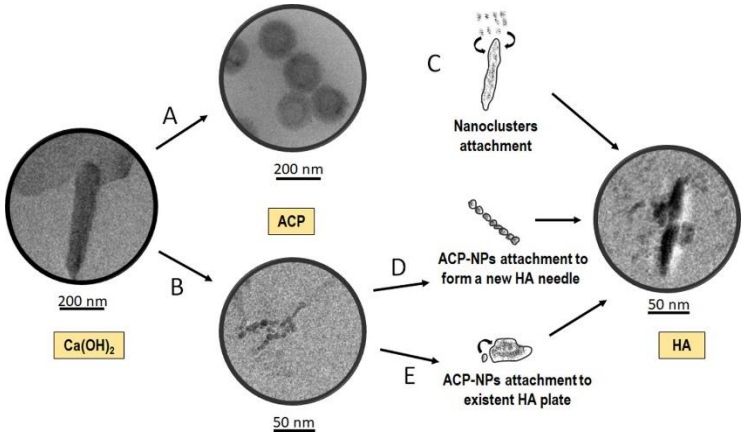

Ch. 2.3 – Figure 6. Schematic illustration summarizing different CaP phase transformations observed in situ using liquid TEM. *Image reproduced with permission from Dalmônico et al. [107] (Copyright © 2022 American Chemical Society).*

While not explicitly studying the biomineralization mechanisms of HA, recent work published by Jokisaari et al. demonstrated the crucial behaviour of HA *in situ* in water using a thin-film graphene liquid cell for HR imaging and spectroscopy analysis.[106] A challenge to studying CaP systems *in situ* with liquid TEM is the sensitivity of CaP structures to changes in pH, which can impact the stabilization of formed CaP-based compounds.[4,146] Electron beam-induced hydrolysis of water in liquid TEM can lead to local changes of pH *in situ* in aqueous solutions,[147,148] and subsequently impact CaP mineralization taking place. A peculiar finding made by Jokisaari et al. identified the critical role of HA in increasing the radiolysis resistance of water, acting as a scavenger of reactive species and raising the cumulative electron dose threshold where hydrogen bubbles are normally observed to form.[106] The work further observed the dynamic dissolution and recrystallization of HA, which was correlated to the production of H^+ ions

with electron beam interactions.[106] Overall, these observations have wider implications beyond biomineralization research whereby the outcomes of this work suggest that beam-sensitive samples in aqueous conditions could be stabilized for *in situ* liquid TEM through the addition of HA as a radical product scavenger. Exploring HA as an additive could then aid in reducing imaging artifacts and provide a means to push for HR imaging for longer periods. However, this scavenging behaviour makes studying CaP-based biomineralization systems increasingly more difficult due to considerations that must be made to reduce electron beam effects to this sensitive material and necessitate correlative means for validating observations made *in situ.* Others note that the use of buffering agents in biomineralization systems may alleviate this problem by stabilizing the pH and helping reduce electron beam effects described.[30,104]

These works represent tremendous strides toward understanding the complex mechanisms behind CaP biomineralization relevant to tissue mineralization, however, these biomineralization pathways are still not fully understood. Apart from the addition of Mg^{2+},[105] limited research has considered the influence of additional system additives and biomolecules key to representing CaP systems in a more holistic biomimetic fashion. This presents a clear opportunity for growth within the biomineralization field to further utilize novel liquid TEM techniques. Most recently, we have started to explore the addition of poly-L-aspartic acid (pAsp) as a mimic of non-collagenous proteins found in mineralized hard tissues.[108] pAsp-CaP models are well established for studying hard tissue mineralization and can lead to intrafibrillar collagen mineralization patterns mimetic of natural tissues.[19,24,138,139,149] Our latest work showed *in situ* stabilization of CaP mineralization reactions and their overall delay with pAsp addition, where ACP particles were observed to stably aggregate and form branched structures over lengthened periods.[108] Understanding how CaP systems mineralize with exposure to additives such as pAsp will lead to better replication of these natural biomineralization processes for their study, which anticipates in future to provide meaningful contributions to understanding the role of NCPs in controlling mineralization processes.

Other Mineralization Systems

While $CaCO_3$ and CaP systems are the most widely studied biomineralization systems *in situ* using liquid TEM, other calcium-based mineralization systems that have implications within the health field can be discussed. For instance, a recent work by Banner et al. has investigated the formation of calcium oxalate (CaOx), a process that is related to kidney stone formation in humans and calcium storage in plants.[116] The study highlighted the critical role of citrate, a common kidney stone inhibitor relevant to clinical research, in controlling CaOx nucleation pathways.[116] The absence of citrate had led to the coexistence of classical and nonclassical nucleation pathways in the nucleation of CaOx in saturated solutions.[116] More specifically, rhombohedral CaOx monohydrate was formed through classical means while square CaOx monohydrate formed non-classically with precursors.[116] In adding citrate, Ca solubility increased where amorphous precursors were observed to form, then dissolve, reform, and eventually lead to the formation of CaOx

dihydrate particles.[116] These dynamic observations supported by atomistic molecular dynamics simulations revealed the potential mechanisms behind the pathological formation and controlled growth of CaOx biominerals in kidney stones as well as the effectiveness of citrate as a mineralization inhibitor. This study presents essential information on the clinical application of citrate in kidney stone treatments.

Most prominently, other mineralization systems studied using liquid TEM involve research probing the formation of iron-based biominerals. Iron oxides and related chemical compounds play important roles in different geological and biological processes.[150] Notably, iron-based biominerals such as magnetite, greigite and goethite offer unique magnetic and mechanical properties within magnetotactic bacteria, chiton's teeth, and limpet's teeth.[150] Early liquid TEM work observing iron-based crystal growth processes was achieved by Li et al. which focused on studying iron oxyhydroxide nanoparticle attachment processes.[109] The study adopted HRTEM to examine liquid directed particle attachment interactions and subsequent crystal growth in these systems, where nanoparticles were observed to rotate *in situ* until a preferential crystal lattice alignment occurred.[109] The work was the first to provide real-time evidence at HR of such processes in liquid, elucidating the alignment mechanism of oxyhydroxide nanoparticle crystal growth which has wide implications for a variety of iron-based mineral assembly processes.

In health science research, ferritin biomineralization processes have recently been investigated using liquid TEM with graphene cells by Narayanan et al. Ferritin biomineralization is key for regulating iron ions within our bodies, where ferritin acts as a storage unit for iron and is involved in several physiological and pathological processes.[151] Work produced earlier by Narayanan et al. (2019) focused on studying the structure and chemistry of iron oxide cores in human heart and spleen ferritins in hydrated conditions,[115] and the latest work from Narayanan et al. visualized the formation of such iron oxides *in situ* using graphene liquid enclosures.[114] Observations at the nanometer length scale were reported for the first time showcasing template-based biomineralization processes of individual ferritin proteins, where iron ions accumulated over time.[114] Past two hours, mineralization reactions reached a latent point where progression ceased to occur. It was speculated that the halt in mineralization was attributed to cumulative electron beam damage as well as enclosure confinement.[114]

The study of magnetotactic bacteria and the formation and growth of their magnetite or greigite grain-based organelles termed magnetosomes have also emerged related to the formation of iron-based biominerals. These highly mobile Gram-negative bacteria, through a term coined magnetotaxis, utilize these magnetosomes as fixed magnets for geomagnetic navigation within their local environment.[152] The work produced by Kashyap et al.[110] used liquid TEM to explore the unique mediation processes of iron oxide nanoparticle nucleation using the Mms6 protein, otherwise known as the magnetite biomineralization protein – an acidic bacterial recombinant protein believed to play a dominant role in the formation of magnetosomes.[153,154] Kashyap et al. focused on *in situ* visualization of early

phases of nucleation of iron-based nanoparticles, mediated using an *in vitro* model involving the addition of sodium hydroxide to Mms6 protein micelles exposed to ferric chloride.[110] Their work provides the first real-time *in situ* visualization of iron-binding to negatively charged Mms6, where an amorphous iron prenucleation phase was observed to preferentially appear on micelle surfaces.[110] The study by Kashyap et al. is among the first in liquid TEM to explore a protein-based template for the formation of biomimetic minerals,[110] shedding light on how ion-binding reactions may take place within specific liquid iron-based biological systems and beyond.

In other work studying magnetotactic bacteria, Woehl et al. used a correlative approach combining liquid TEM with fluorescence microscopy.[111] Both techniques have the advantage of imaging viable, unfixed, hydrated cells, and the study was the first to examine magnetotactic bacteria in liquid conditions in TEM. A key distinction is emphasized that the cells imaged were viable before imaging, not necessarily culturable *post situ*. Woehl et al. discussed challenges in assessing whether cells are alive or not within liquid TEM and several factors, notably electron beam irradiation and confinement, which may have resulted in alterations or arresting of cellular functions as well as possible reproductive death of cells *post situ*.[111] Using magnetosomes as high-contrast particles as labels, the bacteria were easily identifiable in liquid TEM and correlated with fluorescence microscopy.[111] Low electron dose rates in thin liquid regions were attributed to the resolution of intact membranes with minimal ultrastructure damage *in situ* observed.[111]

Other works have since probed magnetotactic bacteria to study their unique magnetosomes. Prozorov et al. observed magnetotactic bacteria and magnetic nanoparticle assemblies using liquid TEM through off-axis electron holography.[112] They successfully demonstrated the ability to collect electron holograms in liquid, with sufficient signal in the low-contrast structures for reconstructions of electron wave phase shifts, as well as visualized magnetization of nanocrystals through magnetic mapping.[112] These studies present tremendous advancements in cellular imaging using liquid TEM with complementary techniques, opening the door towards *in vivo* imaging for a wide variety of biomineralizing applications. Further, these works have implications beyond the study of magnetotactic bacteria, where a variety of bacteria are studied within the biomineralization field, with microbe-mineral interactions being important within the study of habitat mineralization and for de-pollution research.[155]

Further, using thin-film graphene enclosures, Firlar et al. recently explored the nucleation and growth processes of magnetosomes in magnetotactic bacteria.[113] To induce biomineralization, specimens were grown in an iron-depleted medium and then exposed to an iron-rich solution when encapsulated in the graphene enclosure.[113] Within the work, nucleation and growth of nanoparticles resembling *in vivo* biomineralization of magnetosomes were reported, indicating the bacteria were alive and viable during TEM imaging.[113] The graphene enclosure was theorized to have led to higher tolerance to electron beam-induced radiation damage, with less liquid encapsulated and thinner membranes.[113] However, the article provided limited biological assessments *post situ* or

correlative *ex situ* to support these claims – where the formation of iron-based nanoparticles resembling magnetosomes could potentially occur in the presence of relevant template proteins and iron sources demonstrated by Kashyap et al.[110] in their *in situ* work with Mms6. Regardless, this work provided HR imaging and visualized these biomineralization reactions in the context of a whole cell structure, thus presenting tremendous strides toward how these processes may occur *in vivo* and highlighting the potential of the technique for studying whole biomineralization organisms.

These select additional studies demonstrate the versatility of the liquid TEM technique to support biomineralization-themed research. Apart from iron-based biomineralization processes and the previous calcium-based studies reviewed, there are limited liquid TEM works relating to the biomineralization field. This presents a substantial opportunity for expanding liquid TEM research, which through real-time observation of dynamic interactions could aid in answering important research questions about how biomineralization processes occur. For instance, biomineralization processes related to marine silica cycles have not yet, to our knowledge, been probed using liquid TEM, where silica biomineralization is ecologically important to several organisms such as sponges, radiolarians, and diatoms.

2.3.6. General Challenges & Considerations for Liquid TEM

While successful mineralization studies utilizing liquid TEM have been highlighted in this review, several technical challenges remain that can impose limitations on experiments. Although it is possible to perform HR liquid TEM, optimum liquid TEM imaging parameters and standardized experimental settings are yet to be established, since best practice approaches are far from being understood, especially for electron beam-sensitive matter.[41] As such, running an *in situ* liquid TEM experiment can be a daunting task for the first-time user. However, with the right background information paired with careful experimental planning to wholistically consider the system being explored, the liquid TEM technique offers a highly impactful way of exploring mechanisms behind biomineralization processes dynamically in real time.

In this context, we have summarized a general proposed workflow for liquid TEM methods for observing biomineralization events and key considerations to make along each step (Fig. 7). As shown in Figure 7, it splits up the general workflow for *in situ* biomineralization into: A. Considerations before *in situ* liquid TEM and B. Considerations for *in situ* liquid TEM acquisition. These are generalized and applied to a variety of other liquid TEM systems.

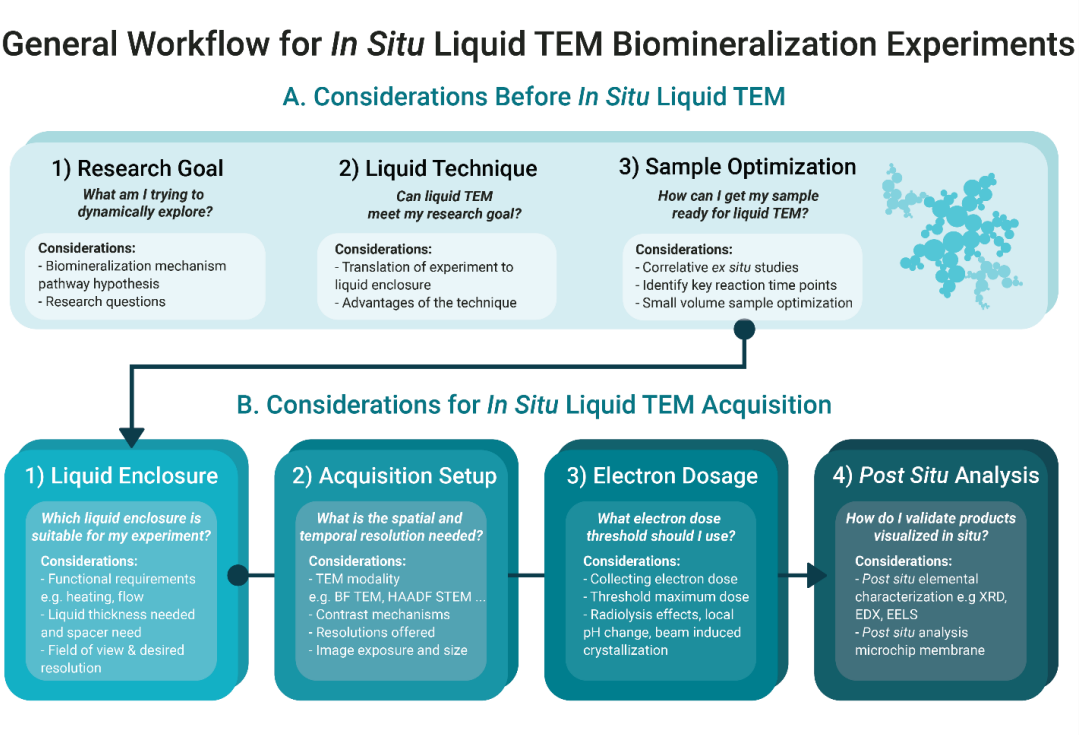

Ch. 2.3 – Figure 7. General workflow for in situ biomineralization. *A. Key considerations to make before performing in situ liquid TEM experiments. Researchers should contemplate the overall research goal of their work, how the liquid technique will be used to address these questions and optimize their experimental conditions accordingly to tune towards a liquid enclosure. B. Considerations for in situ liquid TEM acquisition. Users should reflect on the liquid enclosure they aim to use (Fig. 2), acquisition setup parameters, electron dosage, and post situ analysis.*

Considerations Before In Situ Liquid TEM

Thus far, liquid TEM research presented herein has focused on successes within the biomineralization field for performing novel *in situ* research. However, there are several challenges related to the execution of the liquid TEM technique which requires introspective inspection and planning before running the experiment to overcome these hurdles and get interpretable data. We note: Liquid TEM will not be the magic answer to all your research questions. For example, if a liquid TEM experiment is planned poorly, consumable resources, money, and time could be wasted in pursuit of an answer that may be unable to be answered using a particular liquid TEM configuration.

Importantly, before moving forward with planning liquid TEM mineralization experiments, one should establish a research goal and ask yourself (Fig. 7A.-1): *What am I trying to explore dynamically?* As in any experiment planning, specific research questions relating to the overarching research goal should be established at the beginning of the project, which are related to a research goal and tied may be tied to an established hypothesis supported by literature if applicable. As a second step, one should consider the

technique and ask (Fig, 7A.-2): *Can liquid TEM examine the events that I aim to explore/observe?* A careful translation of an experiment to a liquid enclosure should be considered as to how a system may be scaled down for liquid TEM. A potential user should also think about what advantages liquid TEM has over other techniques that would prompt them to use this method to lead to an answer to their research question. Special consideration should be made for spatial and temporal resolution needed to answer a research question and whether *in situ* methods can capture these dynamics in real-time.

Moreover, as discussed earlier in this review, confinement within small liquid volume enclosures can influence mineralization reactions, where others have reported confinement impacts on nucleation rates and the stabilization of larger ACP particles in solution in comparison to bulk *in vitro* studies.[97,105] This should further be considered in scaling down to the liquid TEM level. For instance, one can imagine that larger samples and assembly processes ranging from several microns in size or more may further be impacted by a thin-liquid TEM enclosure. Strong and well-understood *in vitro* models should be established before a liquid TEM study to translate a biomineralization reaction trying to be mimicked *in situ.* Compounding variables can add additional factors that influence observations *in situ;* dividing a hypothesized reaction into steps with levels of control can aid in the interpretation of liquid TEM results and validate findings later on. Using an established biomimetic *in vitro* model can potentially lead to well-informed observations with optimized experimental conditions that can be scaled up from liquid cells to make meaningful contributions to the field of biomineralization.

A relevant challenge with liquid TEM strategies is acquisition data tends to be more qualitative than quantitative. For *in situ* liquid TEM research, there is often a lack of confidence in reported results where small sample sizes are considered as often experiments show limited repeatability.[156] Observations can give information on size, composition, homogeneity, distribution, etc., but as enclosures are not reusable and are relatively expensive in addition to EM time, it is difficult to study a wide variety of samples with statistical significance. For performing liquid TEM studies, it is thus essential to consider sample optimization before *in situ* studies and ask (Fig. 7A.-3): *How can I get my sample ready for liquid TEM?* Challenges with collecting quantitative data using liquid TEM are often overcome through correlative *ex situ* means to understand reactions that may take place and validate observations made *in situ* later. In correlative studies, larger sample sizes are typically more feasible, serving for quantitative validation and identifying important reaction time points to probe *in situ*. Sample optimization through correlative means can further help in understanding how confinement in liquid TEM may impact a reaction in comparison to bulk *in vitro* studies. Additionally, as demonstrated, the use of complementary correlative techniques can also be informative in understanding reactions occurring *in situ* using liquid TEM for biomineralization research and their validation.[97,102,104,111] Several of the published studies reviewed within this work support their research claims through correlative means, be it through *ex situ* analysis with spectroscopy methods such as EELS and/or EDX, correlative techniques including FTIR

and thermogravimetric analysis (TGA), or computational-based estimations such as molecular dynamic simulations.

Considerations for In Situ Liquid TEM

At the start of performing *in situ* liquid TEM research, an enclosure must be chosen, and a researcher should answer (Fig. 7B.-1): *Which liquid TEM enclosure is suitable for my experiment?* As described within this review, several different enclosure options have been used in literature, generally summarized in Fig. 2 for TEM while other methods for SEM including RTILs and WETSEM capsules were discussed.

Many factors can influence the selection of an enclosure, such as functional requirements, liquid thickness needs on specimen size, as well as field of view and desired resolution. Considerations for selecting an appropriate enclosure are discussed earlier in this review, particularly focusing on the selection of SiN-based versus thin-film enclosures for liquid TEM. From literature survey on liquid TEM studies related to the biomineralization field, enclosure methods are summarized in Table 1 where SiN-based commercial holders are among those widely used within the community to date. One possible reason for the wide acceptance of SiN holders is the quicker process for commercialization and slower adoption of thin-film assemblies in biomineralization research. SiN-based commercial holders can meet some of the functional requirements needed to replicate physiological conditions within a biological environment, with options for heating and flow, while functional thin-film enclosures with flow and mixing capabilities have only recently been explored experimentally.[69,74]

Another deciding factor in selecting enclosures relates to the amount of liquid that is typically encapsulated and resolution limitations based on enclosure setup. Liquid thickness combined with the contributing thickness of membrane windows has been one of the biggest limiting factors in imaging resolution in liquid TEM, as the resolution is reduced with electron scattering.[42] With the advent of thinner membrane windows and thinner liquid layers encapsulated in enclosures, this problem has been better addressed in literature, though remains a challenge for biomineralization research. Routinely, thin-film enclosures encapsulate much less liquid – often resulting in isolated liquid pockets rather than a continuous liquid layer – in comparison to commonly used SiN-based enclosures. The liquid pockets provide thinner imaging regions and thus lead to higher resolution in imaging.[49,51,72] The use of thin-film enclosures can also help reduce artifacts from window bowing from high vacuum conditions experienced in SiN-based assemblies that can contribute to thicker liquid layers.[157] However, these thin liquid layers can limit solution mobility and confinement effects may further be experienced. In comparison, thicker layers offered in SiN-based holders can provide more liquid in encapsulation and an improved ability to enclose larger biological specimens, which may be necessary to visualize biomineralization reactions over time and reduce confinement effects. However, thicker imaging regions can lead to increased beam scattering and decreased resolution.[157,158] With thicker liquid layers, Brownian motion and liquid movement may be more prominent.

This can cause blurring in imaging and biases towards larger, less mobile particles and agglomerates.[84,85]

Acquisition setup is also a key element to consider, where users should ask (Fig. 7B.-2): *What is the spatial and temporal resolution needed?* In TEM, a high-energy beam is transmitted through a specimen to get an image; this can be done through a broad beam in TEM or through rostering with a small probe in STEM. Different TEM modalities are available, such as BF TEM and HAADF STEM, which have been successfully applied within liquid EM paired with several analytical techniques such as diffraction, EELS and EDX.[42] Each technique provides unique insight into material behaviour, with different contrast mechanisms and optimizing in collection conditions required. Choosing the right modality could be vital for *in situ* validation and the observation of a particular phenomenon. It is outside of the scope of this paper to cover the physical considerations behind acquisition and different TEM modalities, though we recommend readers consult the book *Liquid Cell Electron Microscopy* edited by Frances Ross[159] as well as Williams and Carter's book on *Transmission Electron Microscopy*[160] to gain insight on choosing appropriate acquisition conditions.

Acquisition parameters are also important for collecting and determining framerates that are needed to capture a reaction taking place. Fast, instantaneous reactions that occur within seconds will need to be captured with a high framerate enabling camera while slow reactions occurring over long periods may need to be imaged serially at low framerates to reduce electron exposure and reduce dataset sizes. Advances in aberration-corrected electron optics, the advent of high-speed and sensitive direct electron detectors, and light-element-sensitive analytical instrumentation, and their wider availability, are further leading into exciting new avenues for fast-frame, HR, and low-dose *in situ* imaging.[161] Others within the liquid TEM field have used automated acquisition tools paired with direct electron detectors to conduct high-throughput, low-dose biological imaging to collect sufficient views of specimens to reconstruct its 3D structure using single-particle analysis.[31,32] The availability and suitability of each such technique may depend on current resources available within an imaging facility as well as sample-specific acquisition needs.

Generally, liquid TEM involves complex observations which necessitate a holistic approach to understanding the influence of compounding system variables. Notably, related directly to acquisition setup and determining spatial resolution and temporal imaging needs, one of the biggest challenges in liquid TEM includes considerations related to the electron beam and its effects.[42,162] The electron beam can both destroy samples or, if well monitored, can be used to help as a catalysis to initiate and drive reactions at faster rates.[28,51,74] Inelastic electron scattering can further lead to several physical and chemical changes, leading to imaging artifacts.[163] Researchers should seek to understand (Fig. 7B.-3): *What electron dose threshold should I use?* To get a better understanding of the reactions at play in liquid TEM, researchers must consider how the electron beam interacts with the solution, the sample within the solution, and the membrane, to further understand what the sample is being exposed to and mitigate its effects. However, this is no easy task

and standardized operation procedures and workflow practices to consider remain a current challenge within the liquid TEM community.[28,157]

Electron beam and sample interactions can cause radiolysis and ionization processes to occur which leads to the formation of reactive radiolytic products, dependent on electron flux and cumulative dose.[157] These products influence the local chemical environment and must ultimately be considered when interpreting the results of *in situ* experiments. System pH and temperature changes that may arise could impact mineralization events. For instance, work from Koutsoukos et al. studying the crystallization of CaP noted that changing composition ratios has a direct impact on acidity and solubility.[146] Further work showed different pH stability ranges of different CaP-based compounds.[4] Temperature changes alter the synthesis and stabilization of different calcium carbonate polymorphs.[164] While often overlooked, recent works by Birk et al. highlighted the necessity of considering local beam-induced changes in temperature and pH for liquid TEM research.[148,165]

Thus, to make these considerations and monitor environmental changes *in situ* from the electron beam, the *in situ* community has identified electron flux, or dose rate, and cumulative electron dose as critical parameters for reporting to improve experiment reproducibility and validate results.[28] The total electron dose *D* is typically estimated through the following equation:

$$D = \frac{I_p t}{eA} \quad (1)$$

Where I_p is the probe current, t is the exposure time, *A* is the area exposed to the electron beam, and *e* is the elementary charge.[28] Wu et al. further described that electron dose rate is typically estimated in three main manners: 1) using a known conversion factor of signal intensity to electron count (k_e) obtained for a camera, 2) measuring *Ip* using a pAmp Faraday cup built in the tip of a holder or mounted in the microscope, and 3) using a fluorescent screen read-out.[28,166]

Considering the electron flux and cumulative electron dose, the schematic presented in Fig. 8 is a summary of possible solutions to mitigate electron irradiation damage influencing liquid TEM research.[157] A general solution provided in all cases is to reduce the electron dose.[157] Works produced by Egerton and colleagues should further be consulted for understanding radiation damage in EM modalities and the mitigation of electron beam effects.[167–170]

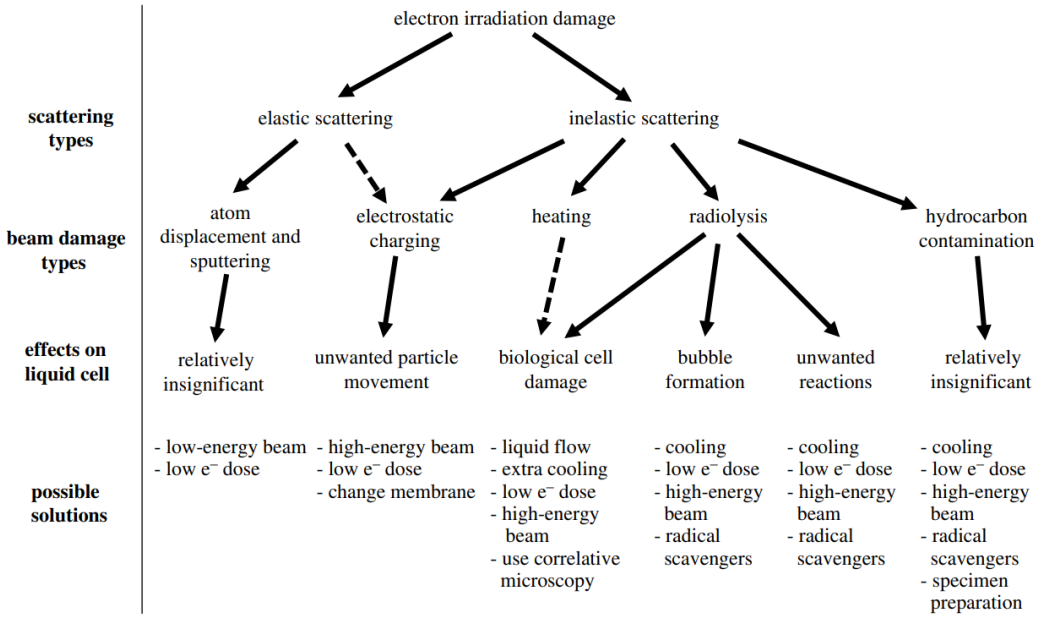

Ch. 2.3 – Figure 8. Electron beam damage summary. *Schematic created by Pu et al. showing different types of electron beam damage and their effects on liquid cell TEM (dotted lines indicate relatively insignificant contribution). Image reproduced under the Creative Commons Attribution 4.0 International (CC BY 4.0) License from Pu et al. [157] published by Royal Society Open Science (Copyright © 2020 Pu et al.).*

In setting up a liquid TEM experiment, it is important to consider the resolution required, which is proportional to the electron dose – where a scaling law implies reducing the dose leads to lower resolution.[28,167,171,172] Users need to identify what spatial and temporal resolution is needed for their liquid TEM experiment, rather than what maximum resolution is achievable, to minimize radiation damage. Moreover, there exists a limiting electron dosage, where, after a certain threshold, samples are critically exposed. In such an instance, mineralization events may be dominantly controlled by electron beam interactions, experience critical amounts of damage, and/or amorphize. Researchers have summarized that limiting dosage thresholds can be estimated by 1) diffraction pattern disappearance with exposure[28,173] or 2) Fourier transferred signal intensity reduction, which reduces exponentially with respect to electron dose.[28,174] Others have also recommended that electron dose be validated by taking a series of images at different conditions to understand the influence of electron dosage, electron flux, as well as beam energies.[28]

Last of all, after *in situ* liquid TEM, one remaining question that should be considered in experimental workflow includes (Fig. 7B.-4): *How do I validate products visualized in situ?* For liquid TEM experiments which can often be challenging and costly to replicate results in a statistically relevant way, considerations must be made to correlatively understand what was observed *in situ* using *post situ* or *post mortem* means. Typically, this will involve disassembling the liquid enclosure after an experiment and performing TEM analysis on dry products on a window membrane, where products can be observed at higher

resolution without the liquid layer and concern of impacting an *in situ* reaction with longer electron beam exposures. Often, higher-intensity analytical chemical techniques that may have been avoided *in situ*, such as EELS, will be probed *post situ* to confirm elements presented in products.[30] Other correlative characterization means could be used, such as SEM, FTIR, and X-Ray diffraction analysis.

2.3.7. Outlook & Concluding Remarks

Biomineralization processes are essential for life on Earth. In this review, the liquid TEM technique itself is introduced and research utilizing *in situ* liquid TEM techniques relevant to biomineralization has been summarized, demonstrating the significant impact of this technology on the field. A range of exciting applications using the method was reviewed; from studying Ca to Fe-based minerals, many are using this technique to probe biologically-relevant mineralization reactions occurring in liquid with real-time and at nanometer resolution – complimenting timestamp-based traditional and cryo-TEM methods to establish mineralization theories. Moreover, for those interested in expanding their research capabilities with this technique, we summarized liquid TEM experimental details found in biomineralization studies (Table 1) and presented an experimental workflow (Fig. 7) as a reference to overcome the technical challenges discussed, notably related to liquid layer confinement and beam effects, acting as a foundational resource to achieve better quality liquid TEM data.

The liquid TEM field is approaching a point where methods are better established, and experimental workflows have significantly improved since the field was established twenty years ago.[33,159] Emerging technical advances such as the possibility to perform liquid TEM tomography,[45] thin-film enclosures with sub-nanometer resolution and mixing capabilities,[69] smart dose and sample tracking software to streamline acquisition,[175] fast framerate low-dose direct-electron detectors,[26] and automated acquisition tools,[32] are transforming the field, leading us into uncharted research territories.

However, the liquid TEM technique is yet to be widely adopted within the biomineralization field, where many of the works reviewed within this article stem from collaborations involving only a few key researchers using this novel technique. Reflecting on Table 1 which summarized liquid TEM experimental details, standardized reporting metrics still need to be established within the liquid TEM community related to enclosure setup and acquisition details. For instance, while electron dose rates are typically provided, especially for more recent articles, few shared details on the cumulative electron doses experienced by samples during imaging, which are essential to understanding damage threshold limits, understanding electron beam effects, and planning future studies in similar mineralization systems. For improvement, researchers should strive towards sharing clear, detailed information on experimental parameters to standardize these experiments. Guiding principles outlined by Wilkinson et al. for standardization reporting and data access, i.e. the Findability, Accessibility, Interoperability, and Reusability (FAIR) Guiding Principles,[176] should be adopted to remove barriers to using these novel techniques.

Considering the plethora of mineralization systems and species investigated within the biomineralization field, there is a clear opportunity to utilize this technique more to investigate these processes dynamically in a liquid environment. To date, simpler mineralization systems have dominated what has been published using liquid TEM, where the majority of the processes are Ca or Fe based. To our knowledge, no research has been published involving, for instance, silica mineralization, relevant to marine life. Additionally, limited works have considered the introduction of biologically relevant additives, such as proteins (e.g. NCPs) which are hypothesized to inhibit crystallization in biological systems, leaving the opportunity for the utilization of liquid TEM. In future, we anticipate the expansion of current and emerging liquid TEM methods to lead to transformative discoveries within the field of biomineralization, providing complimentary real-time dynamic insight on what may be happening in biological systems – *revealing secrets behind life itself.*

Declaration of Interests

The authors declare that they have no known competing financial interests or personal relationships that could have appeared to influence the work reported in this paper.

Acknowledgements

The authors greatly acknowledge financial support provided by the Canadian Institutes of Health Research Project Grant Program (PJT 180575, E.D.S. and K.G.) as well as by the Natural Sciences and Engineering Research Council of Canada (NSERC) Discovery Grant program (RGPIN-2020-05722), Canada Research Chairs program (K.G.), & the Vanier Canada Graduate Scholarship program (L.-A.D.).

Conflicts of Interest

The authors declare no conflict of interest.

Author Contributions

Conceptualization: Liza-Anastasia DiCecco, Kathryn Grandfield
Methodology: Liza-Anastasia DiCecco, Kathryn Grandfield, Deborah F. Kelly
Data curation: Liza-Anastasia DiCecco
Funding acquisitions and/or supervision: Kathryn Grandfield, Eli D. Sone, Deborah F. Kelly
Writing: Liza-Anastasia DiCecco, Tengteng Tang
Review and editing: Liza-Anastasia DiCecco, Tengteng Tang, Kathryn Grandfield, Eli D. Sone, Deborah F. Kelly

References

[1] J. G. Hardy et al., *Prog Polym Sci* 2010, *35*, 1093.
[2] E. Beniash, *Wiley Interdiscip Rev Nanomed Nanobiotechnology* 2011, *3*, 47.
[3] S. Weiner et al., *Rev Mineralogy Geochem* 2003, *54*, 1.
[4] S. V. Dorozhkin et al., *Angewandte Chemie Int Ed* 2002, *41*, 3130.
[5] H. Kurihara et al., *Mar. Biol.* 2012, *159*, 2819.
[6] S. Li et al., *Environ Sci Technol* 2016, *50*, 1157.
[7] S. Goffredo et al., *Nat Clim Change* 2014, *4*, 593.
[8] P. Roschger et al., *Curr Osteoporos Rep* 2014, *12*, 338.
[9] G. Boivin et al., *Osteoporosis Int* 2003, *14*, 19.
[10] X. Wang et al., *Acs Biomater Sci Eng* 2017, *3*, 49.
[11] X. Wang et al., *Adv Mater Interfaces* 2018, *5*, 1800262.
[12] H. Kempf et al., *Frontiers Cell Dev Biology* 2021, *9*, 759702.
[13] J. F. Collingwood et al., *J Phys Conf Ser* 2005, *17*, 54.
[14] J. F. Collingwood et al., *J Alzheimer's Dis* 2008, *14*, 235.
[15] W. J. E. M. Habraken et al., *Nat Commun* 2013, *4*, 1507.
[16] P. J. M. Smeets et al., *Proc National Acad Sci* 2017, *114*, E7882.
[17] A. Dey et al., *Nat Mater* 2010, *9*, 1010.
[18] M. J. Olszta et al., *Connect Tissue Res* 2009, *44*, 326.
[19] F. Nudelman et al., *J Struct Biol* 2013, *183*, 258.
[20] J. J. D. Yoreo et al., *Science* 2015, *349*, aaa6760.
[21] D. Qin et al., *Front Chem* 2022, *10*, 834503.
[22] L. B. Gower et al., *J Cryst Growth* 2000, *210*, 719.
[23] S. J. Homeijer et al., *Cryst Growth Des* 2010, *10*, 1040.
[24] M. J. Olszta et al., *Mater Sci Eng R Reports* 2007, *58*, 77.
[25] N. de Jonge et al., *Nat Nanotechnol* 2011, *6*, 695.
[26] D. F. Kelly et al., *Curr. Opin. Struct. Biol.* 2022, *75*.
[27] K. He et al., *J Phys Condens Matter* 2019, *31*, 103001.
[28] H. Wu et al., *Adv Mater* 2020, *32*, 2001582.
[29] Z. Xu et al., *Materials* 2023, *16*, 2026.
[30] X. Wang et al., *Commun Chem* 2018, *1*, 80.
[31] G. Jonaid et al., *Adv Mater* 2021, *33*, 2103221.
[32] L.-A. DiCecco et al., *J Vis Exp* 2022, e63856.
[33] M. J. Williamson et al., *Nat Mater* 2003, *2*, 532.
[34] C. Lei et al., *J Dent Res* 2021, 002203452110538.
[35] J. P. Patterson et al., *Accounts Chem Res* 2017, *50*, 1495.
[36] R. F. Thompson et al., *Methods* 2016, *100*, 3.
[37] E. Kellenberger et al., *J Microsc-oxford* 1992, *168*, 181.
[38] S. B. Surman et al., *J Microbiol Meth* 1996, *25*, 57.
[39] A. Katsen-Globa et al., *Scanning* 2016, *38*, 625.
[40] C. G. Golding et al., *Sci Rep-uk* 2016, *6*, 26516.
[41] T. H. Moser et al., *Micron* 2019, *119*, 8.
[42] F. M. Ross, *Science* 2015, *350*, aaa9886.

[43] D. B. Peckys et al., *Mrs Bull* 2020, *45*, 754.
[44] L. Kong et al., *Research Square - Preprint V1* 2022, DOI 10.21203/rs.3.rs-1298112/v1.
[45] W. J. Dearnaley et al., *Nano Lett* 2019, *19*, 6734.
[46] G. M. Jonaid et al., *Microsc Microanal* 2022, 1.
[47] C. F. Reboul et al., *Sci Adv* 2021, *7*, eabe6679.
[48] K. L. Jungjohann et al., *Microsc Microanal* 2012, *18*, 621.
[49] J. Park et al., *Nano Lett* 2015, *15*, 4737.
[50] Q. Chen et al., *Nano Lett* 2013, *13*, 4556.
[51] J. M. Yuk et al., *Science* 2012, *336*, 61.
[52] M. J. Dukes et al., *J Vis Exp* 2013, 50936.
[53] D. F. Parsons, *Science* 1974, *186*, 407.
[54] V. R. Matricardi et al., *Science* 1972, *177*, 268.
[55] S. W. Hui et al., *Science* 1974, *184*, 77.
[56] E. Kennedy et al., *Acs Nano* 2016, *10*, 2669.
[57] R. Serra-Maia et al., *Acs Nano* 2021, *15*, 10228.
[58] J. E. Evans et al., *Micron* 2012, *43*, 1085.
[59] J. T. van Omme et al., *J Mater Chem C* 2020, *8*, 10781.
[60] H. Fan et al., *Acs Nano* 2021, *15*, 17895.
[61] J. Yang et al., *J Phys Chem C* 2017, *121*, 7435.
[62] G.-Z. Zhu et al., *J Phys Chem C* 2014, *118*, 22111.
[63] M. G. Burke et al., *Ultramicroscopy* 2017, *176*, 46.
[64] J. Æ. Hyllested et al., *Ultramicroscopy* 2021, *221*, 113178.
[65] Y. A. Wu et al., *Acs Nano* 2016, *10*, 3738.
[66] E. S. Pohlmann et al., *Nano Lett* 2015, *15*, 2329.
[67] L. R. Parent et al., *J Am Chem Soc* 2017, *139*, 17140.
[68] P. Blach et al., *J Vis Exp* 2020, e61458.
[69] D. J. Kelly et al., *Adv Mater* 2021, *33*, 2100668.
[70] H. Cho et al., *Nano Lett* 2016, *17*, 414.
[71] S. Keskin et al., *Nano Lett* 2018, *18*, 7435.
[72] M. Textor et al., *Nano Lett* 2018, *18*, 3313.
[73] X. Gao et al., *Adv. Funct. Mater.* 2022, *32*, 2202502.
[74] G. Dunn et al., *Acs Nano* 2020, *14*, 9637.
[75] K.-L. Liu et al., *Lab Chip* 2008, *8*, 1915.
[76] J.-C. Kuo et al., *Acs Sustain Chem Eng* 2022, *10*, 464.
[77] S. Giorgio et al., *Gold Bull* 2008, *41*, 167.
[78] A. M. Donald, *Nat Mater* 2003, *2*, 511.
[79] T. W. Hansen et al., *Mater Sci Tech Ser* 2010, *26*, 1338.
[80] A. Bogner et al., *Ultramicroscopy* 2005, *104*, 290.
[81] A. Kolmakov, in *Liquid Cell Electron Microscopy* (Ed: F. Ross), 2016, pp. 78–105.
[82] A. S. Al-Asadi et al., *Microsc Microanal* 2015, *21*, 765.
[83] S. Thiberge et al., *Proc National Acad Sci* 2004, *101*, 3346.
[84] C. Lorenz et al., *Int J Occup Env Heal* 2010, *16*, 406.
[85] K. Tiede et al., *Water Res* 2009, *43*, 3335.

[86] J. Kraus et al., *Nanoscale* 2014, *6*, 14394.
[87] L. DiCecco et al., *Chembiochem* 2021, *22*, 2488.
[88] T. Welton, *Chem Rev* 1999, *99*, 2071.
[89] J. S. Wilkes et al., *J Chem Soc Chem Commun* 1992, *0*, 965.
[90] S. Kuwabata et al., *Chem Lett* 2006, *35*, 600.
[91] T. Tsuda et al., *Microscopy* 2020, *69*, 183.
[92] B. E. J. Lee et al., *Chembiochem* 2021, *22*, 571.
[93] L.-A. DiCecco et al., *Micron* 2021, 103192.
[94] T. Tsuda et al., *Biophysical Rev* 2018, *10*, 927.
[95] E. H. Hayakawa et al., *Plos One* 2013, *8*, e85467.
[96] M. H. Nielsen et al., *Science* 2014, *345*, 1158.
[97] R. Kröger et al., *Mineral-basel* 2018, *8*, 21.
[98] P. J. M. Smeets et al., *Nat Mater* 2015, *14*, 394.
[99] M. M. Longuinho et al., *Crystengcomm* 2022, *24*, 2602.
[100] V. Ramnarain et al., *J Am Chem Soc* 2022, *144*, 15236.
[101] Y. Kimura et al., *Faraday Discuss* 2022, *235*, 81.
[102] Z. Liu et al., *Proc National Acad Sci* 2020, *117*, 3397.
[103] K. S. Dae et al., *Acs Omega* 2020, *5*, 14619.
[104] K. He et al., *Sci Adv* 2020, *6*, eaaz7524.
[105] B. Jin et al., *Cryst Growth Des* 2021, *21*, 5126.
[106] J. R. Jokisaari et al., *Nanotechnology* 2021, *32*, 485707.
[107] G. M. L. Dalmônico et al., *Cryst Growth Des* 2022, *22*, 4828.
[108] L.-A. DiCecco et al., *Microsc Microanal* 2022, *28*, 1818.
[109] D. Li et al., *Science* 2012, *336*, 1014.
[110] S. Kashyap et al., *Acs Nano* 2014, *8*, 9097.
[111] T. J. Woehl et al., *Sci Rep-uk* 2014, *4*, 6854.
[112] T. Prozorov et al., *J Roy Soc Interface* 2017, *14*, 20170464.
[113] E. Firlar et al., *Nanoscale* 2019, *11*, 698.
[114] S. Narayanan et al., *Acs Biomater Sci Eng* 2020, *6*, 3208.
[115] S. Narayanan et al., *Nanoscale* 2019, *11*, 16868.
[116] D. J. Banner et al., *Adv Funct Mater* 2021, *31*, 2007736.
[117] R. D. Hodges et al., *Nature* 1967, *216*, 609.
[118] J. W. Morse et al., *Chem Rev* 2007, *107*, 342.
[119] A. Trailokya et al., *J Assoc Physicians India* 2017, *65*, 100.
[120] J. Perić et al., *Thermochim Acta* 1996, *277*, 175.
[121] J. H. E. Cartwright et al., *Angew. Chem. Int. Ed.* 2012, *51*, 11960.
[122] L. Addadi et al., *Adv. Mater.* 2003, *15*, 959.
[123] M. Jehannin et al., *J Am Chem Soc* 2019, *141*, 10120.
[124] H. H. Teng et al., *Science* 1998, *282*, 724.
[125] C. J. Stephens et al., *Adv. Funct. Mater.* 2010, *20*, 2108.
[126] J. Ihli et al., *Adv. Funct. Mater.* 2013, *23*, 1575.
[127] D. Wang et al., *Proc National Acad Sci* 2009, *106*, 21511.
[128] J. Tao et al., *Proc National Acad Sci* 2009, *106*, 22096.
[129] S. Raz et al., *Adv. Mater.* 2000, *12*, 38.

[130] E. Loste et al., *J Cryst Growth* 2003, *254*, 206.
[131] F. C. Meldrum et al., *J Cryst Growth* 2001, *231*, 544.
[132] L. C. Palmer et al., *Chem Rev* 2008, *108*, 4754.
[133] Y.-R. Zhang et al., *Int J Oral Sci* 2014, *6*, 61.
[134] C.-W. (Jeff) Wang et al., *Curr Osteoporos Rep* 2016, *14*, 284.
[135] N. Alexopoulos et al., *Nat Rev Cardiol* 2009, *6*, 681.
[136] V. C. Mendes et al., *Biomaterials* 2007, *28*, 4748.
[137] S. R. Paital et al., *Mater Sci Eng R Reports* 2009, *66*, 1.
[138] A. S. Deshpande et al., *Cryst Growth Des* 2008, *8*, 3084.
[139] A. J. Lausch et al., *Adv Funct Mater* 2013, *23*, 4906.
[140] W. E. Brown et al., *Annu Rev Mater Sci* 1976, *6*, 213.
[141] V. S. Kattimani et al., *Bone Tissue Regen Insights* 2016, *7*.
[142] T. J. Woehl et al., *Nano Lett* 2014, *14*, 373.
[143] J. Zhang et al., *Adv Healthc Mater* 2019, *8*, 1901030.
[144] Y. Politi et al., *Chem Mater* 2010, *22*, 161.
[145] B. Cantaert et al., *Chem European J* 2013, *19*, 14918.
[146] P. Koutsoukos et al., *J Am Chem Soc* 1980, *102*, 1553.
[147] N. M. Schneider et al., *J Phys Chem C* 2014, *118*, 22373.
[148] B. Fritsch et al., *Arxiv* 2022, DOI 10.48550/arxiv.2209.05331.
[149] B. D. Quan et al., *J Roy Soc Interface* 2018, *15*, 20180269.
[150] D. Faivre et al., *Angew. Chem. Int. Ed.* 2015, *54*, 4728.
[151] M. A. Knovich et al., *Blood Rev* 2009, *23*, 95.
[152] R. P. Blakemore, *Annu Rev Microbiol* 1982, *36*, 217.
[153] N. Ginet et al., *Plos One* 2011, *6*, e21442.
[154] A. Arakaki et al., *J Biol Chem* 2003, *278*, 8745.
[155] L. C. Staicu et al., *Front Microbiol* 2021, *12*, 796374.
[156] T. H. Moser et al., *Sci Adv* 2018, *4*, eaaq1202.
[157] S. Pu et al., *Roy Soc Open Sci* 2020, *7*, 191204.
[158] N. de Jonge et al., *Ultramicroscopy* 2010, *110*, 1114.
[159] F. M. Ross, Ed. , *Liquid Cell Electron Microscopy*, Cambridge: Cambridge University Press, 2016.
[160] D. B. Williams et al., *Transmission Electron Microscopy*, 2009.
[161] R. Ramachandramoorthy et al., *Acs Nano* 2015, *9*, 4675.
[162] G. Zhu et al., *Micron* 2019, *118*, 35.
[163] T. J. Woehl et al., *Ultramicroscopy* 2013, *127*, 53.
[164] J. Chen et al., *Powder Technol* 2009, *189*, 64.
[165] B. Fritsch et al., *Nanoscale Adv* 2021, *3*, 2466.
[166] D. R. G. Mitchell et al., *Microsc Res Techniq* 2015, *78*, 886.
[167] R. F. Egerton, *Ultramicroscopy* 2013, *127*, 100.
[168] R. F. Egerton et al., *Micron* 2004, *35*, 399.
[169] R. F. Egerton, *Micron* 2019, *119*, 72.
[170] R. F. Egerton, *Ultramicroscopy* 2021, *229*, 113363.
[171] N. de Jonge et al., *Nat Rev Mater* 2019, *4*, 61.
[172] N. de Jonge, *Ultramicroscopy* 2018, *187*, 113.

[173] B. E. Bammes et al., *J Struct Biol* 2010, *169*, 331.
[174] S. B. Hayward et al., *Ultramicroscopy* 1979, *4*, 201.
[175] M. D. Dukes et al., *Microsc Microanal* 2022, *28*, 108.
[176] M. D. Wilkinson et al., *Sci Data* 2016, *3*, 160018.

Chapter 3: Ionic Liquid Treatment for Efficient Sample Preparation of Hydrated Bone for Scanning Electron Microscopy

3.1 Section Introduction (Objective i)

SEM has been used for years in the characterization of mineralized tissues such as bone, particularly useful for its spatial resolution and spectroscopy capabilities. However, conventional preparation methods for bone necessitate lengthy steps to stabilize structures for imaging in a high-vacuum SEM environment, involving typically dehydration, fixation, and/or embedding steps that can risk altering native structures. As outlined in the objectives, in Chapter 3 a new liquid SEM protocol involving RTILs, also referred to as molten or fused salts, was explored for bone as an alternative solution to these conventional preparation methods. SEM preparation involving different low-vapour, highly conductive RTILs was optimized for the treatment of hydrated, unfixed healthy and pathological bone structures. An optimal RTIL treatment was established using a 10 % v/v [BMI][BF4] aqueous-based method which led to successful imaging in both SE and BSE mode with minimal electron beam charging effects even in EDX analysis. In comparison to conventional preparation means, this RTIL-based method reduced bone SEM preparation time by nearly ten-fold and was observed to better preserve natural bone structures. Overall, this research contributes a highly efficient new liquid SEM method for preparing bone and other biomaterials, having wide implications for the field of liquid EM.

Authors: **Liza-Anastasia DiCecco**, Andrew D'Elia, Cheryl C. Quenneville, Leyla Soleymani, Kathryn Grandfield.

Publication: This work is published with a full citation provided as follows:

DiCecco, L.-A., D'Elia, A., Quenneville, C., Soleymani, L., and Grandfield, K. Ionic liquid treatment for efficient sample preparation of hydrated bone for scanning electron microscopy. 2022. *Micron,* Vol 15 (103192). DOI: 10.1016/j.micron.2021.103192

Reprinted from the above-listed citation, with permission from *Micron.* Copyright © 2021 Elsevier Ltd.

Micron 153 (2022) 103192

Contents lists available at ScienceDirect

Micron

journal homepage: www.elsevier.com/locate/micron

Tutorial

Ionic liquid treatment for efficient sample preparation of hydrated bone for scanning electron microscopy

Liza-Anastasia DiCecco [a], Andrew D'Elia [a], Cheryl Quenneville [b,c], Leyla Soleymani [b,d], Kathryn Grandfield [a,b,*]

[a] Department of Materials Science and Engineering, McMaster University, Hamilton, ON, Canada
[b] School of Biomedical Engineering, McMaster University, Hamilton, ON, Canada
[c] Department of Mechanical Engineering, McMaster University, Hamilton, ON, Canada
[d] Department of Engineering Physics, McMaster University, Hamilton, ON, Canada

ARTICLE INFO

Keywords:
Bone
Ionic liquids
Mineralization
Biological imaging
Scanning electron microscopy

ABSTRACT

This study presents a new protocol for preparing bone samples for scanning electron microscopy (SEM) using a room temperature ionic liquid (RTIL) treatment method. RTIL-based solutions can be adopted as an alternative to lengthy and laborious traditional means of preparation for SEM due to their unique low-vapour pressure and conductive properties. Applied to biological samples, RTILs can be used quickly and efficiently to observe hydrated, unfixed structures in typical SEM systems. This first-time feasibility study of the optimization of this protocol for bone was explored through various SEM modalities using two distinct ionic liquids, 1-ethyl-3-methylimidazolium tetrafluoroborate ([EMI][BF_4]) and 1-butyl-3-methyl imidazolium tetrafluoroborate ([BMI][BF_4]), at varying concentrations of 5, 10, and 25 % v/v in aqueous solution through an addition-based method. Based on qualitative observations in the SEM, a 60-second solution addition treatment of 10 % v/v [BMI][BF_4] performed the best in imaging hydrated, unfixed bone samples, resulting in minimal charge buildup and no solution pooling on the surface. The treatment was applied effectively to a variety of bone samples, notably flat and polished, as well as highly topographical bone fracture surfaces of both healthy and osteoporotic human bone samples. In comparison to conventionally dehydrated bone, the RTIL treatment better preserved the natural bone structure, resulting in minimal microcracking in observed structures.

1. Introduction

In biological imaging communities, bone has been a topic of high interest in scanning electron microscopy (SEM) for well over half a century (Shah et al., 2019). The study of bone's complex hierarchical structure using SEM can elicit key details on bone sample health (Milovanovic et al., 2018), disease mechanisms (Dempster et al., 1986), failure mechanisms (Braidotti et al., 2000; Hiller et al., 2003), bone ingrowth behaviour for orthopedic implant applications (Shah et al., 2016), and much more. However, due to restrictions on the high vacuum state of typical SEM systems, conventional preparation methods typically including fixation, dehydration and conductive coating, are required to make structural observations on bone features. While these methods aid in preserving bone structure for long-term study, they also risk altering the natural morphologies present in these tissues (Kellenberger et al., 1992; Li et al., 2017; McKee et al., 1991; Utku et al., 2008). Moreover, bone is a non-conductive material, which presents other challenges for SEM imaging, such as charging.

As such, researchers are exploring alternative methods of sample preparation to observe biological materials in their natural hydrated states through SEM. Recently, the use of room temperature ionic liquids (RTILs) has risen in popularity as a sample treatment method for this purpose. RTILs are ionic salts that exist in the liquid state at room temperature, composed of ions and short-lived ionic pairs (Welton, 1999). Apart from their liquid nature, two particularly important aspects of RTILs include their high conductivity and low vapour pressure (Hagiwara and Ito, 2000), which make them highly applicable in SEM. This allows for samples to be treated by RTILs and be imaged in their natural hydrated, unfixed state. Kuwabata et al. were the first to show that RTILs can be observed in high vacuum SEM and experience limited charge buildup during observation (Kuwabata et al., 2006). A wide range of biological samples have been observed following similar

* Corresponding author at: McMaster University, 1280 Main Street West, Hamilton, ON, L8S 4L7, Canada.
E-mail address: kgrandfield@mcmaster.ca (K. Grandfield).

https://doi.org/10.1016/j.micron.2021.103192
Received 8 September 2021; Received in revised form 22 November 2021; Accepted 23 November 2021
Available online 27 November 2021
0968-4328/© 2021 Elsevier Ltd. All rights reserved.

treatments since (Golding et al., 2016; Komai et al., 2014; Lee et al., 2021; Lu et al., 2019; Tsuda et al., 2011). Notably, hydrophilic RTILs have been shown in several instances to be more effective in imaging hydrated biological samples in comparison to hydrophobic RTILs (Arimoto et al., 2008; Ishigaki et al., 2011a).

An RTIL-based preparation technique can be used as a facile, relatively inexpensive treatment option for biological samples in lieu of time-consuming traditional sample preparation methods required for typical SEM configurations. For bone samples, conventional SEM preparation methods can be lengthy and laborious (Binkley et al., 2020; Tedesco et al., 2017). Figs. 1 and 2 can be used for comparing the proposed RTIL treatment pathway for bone to traditional preparation methodologies for SEM observation. In conventional methodologies, fixation and dehydration steps can take upwards of 40 h per sample. Considering equipment availability and lab working hours, it can take weeks to fully prepare a bone sample for SEM observation. This is not considering embedding in resin and staining processes – which can increase the time required for sample preparation (Chissoe et al., 1995; Reznikov et al., 2013). In contrast, RTIL treatments can be employed to observe bone within hours, allowing for quicker sample turn-around time and improved productivity. Two distinct RTIL treatment methods can be identified in literature: 1) immersion, where samples are immersed in solution, and 2) addition, where the RTIL solution is added directly to samples and potentially drained via membrane filtering (DiCecco et al., 2021). In general, the immersion method is more effective for large biological samples (over millimetre size in thickness) while an addition-based method is preferred for smaller specimens (Tsuda and Kuwabata, 2020). Effectively, if an additional method cannot suitably coat your samples based on its thickness or overall size, an immersion method should be considered. RTIL treatment exposure times may vary to allow for sufficient penetration of the sample and is often dependent on sample size, the type of biological sample, and the solution used (Tsuda et al., 2011), though generally, this treatment is less than 10 min (DiCecco et al., 2021; Tsuda and Kuwabata, 2020).

Limited works have explored this technique to study mineralized tissues, and—to our knowledge—none have used this technique to observe human bone. In works produced by Abe et al., RTIL treatment is shown to be effective for SEM observation of mineralized, hard tissue shellfish samples, achieving a similar resolution to images produced using Pt/Pd sputtering techniques (Abe et al., 2012). This work also highlighted the capacity of RTILs to be used in conjunction with elemental analyses, such as energy-dispersed fluorescent X-ray spectroscopy (EDS) (Abe et al., 2012). The successful utilization of RTIL-based SEM preparation protocols applied to stiff, porous wooden structures to study their natural composite hierarchical structure and topographical features (Kanbayashi and Miyafuji, 2016; Lu et al., 2019) provides insight on the potential of these techniques in studying bone – a similarly organic, porous composite material with complex hierarchical features (Binkley and Grandfield, 2017). This suggests that similarly-adopted RTIL treatments can be used to investigate hydrated, unfixed bone structures with polished or highly topographical surfaces in SEM.

Herein, we investigated RTIL sample preparation methodologies and SEM imaging conditions for hydrated bone tissues using two different RTILs at various concentrations. This first-of-its-kind work presents a simple and effective protocol to image hydrated, unfixed bone samples in the SEM and with EDS analysis capabilities. The study focuses on bone from the femoral neck as a clinically relevant region of interest, where applications of this proposed protocol are highlighted for healthy cortical and trabecular bone, as well as for flat and topographical fracture surfaces of diseased tissue, such as osteoporotic bone. This work bridges the gap between bone research and RTIL-methods developed in chemistry, showing the potential of using this novel non-conventional SEM preparation method for the analysis of mineralized bone tissue.

2. Materials and methods

2.1. Bone preparation

This research and sample acquisition was approved by the Hamilton Integrated Research Ethics Board (HiREB 2015-0990-T). Bone sections were procured from the proximal femur, at the femoral neck, of three fresh-frozen human cadaveric femurs (Table 1), which were cleaned of all exterior soft tissue. Each sample had an associated T-score, a common clinical measure of osteoporosis determined by dual energy x-ray absorptiometry (DEXA) imaging to analyze bone mineral density (Kanis et al., 2008). T-scores of $\leq$ -2.5 indicate osteoporosis and very low mineral density, while scores between -1.0 and -2.5 are considered osteopenic with moderately low mineral density and scores $\geq$ -1.0 are indicative of healthy bone mineral density (Kanis et al., 2008). Samples from the femoral neck of a healthy bone specimen featuring both trabecular and cortical sections were used to optimize the RTIL protocol.

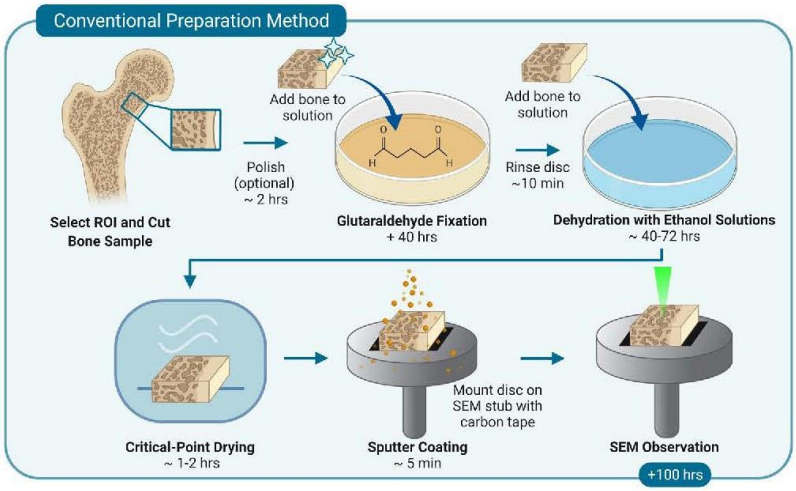

Fig. 1. Illustration of conventional SEM preparation methods used for bone with time of each step approximated (estimation for bone specimens 1 cm^3 or larger). Note that staining and embedding procedures would further lengthen the preparation time.

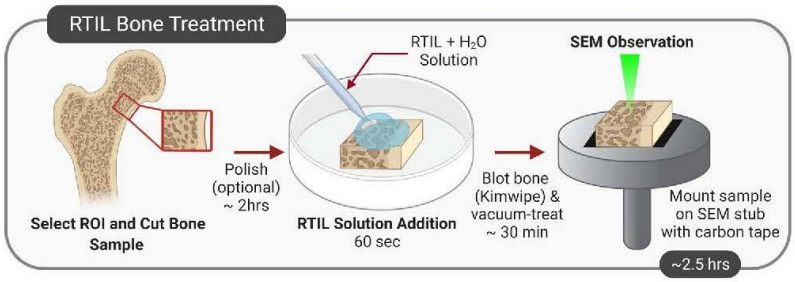

Fig. 2. Schematic illustrating the specific RTIL treatment process used in this work for SEM imaging of hydrated, unfixed bone samples.

Table 1
Summary of human bone specimen information imaged in this study.

Bone Description & Type	Anatomical Location	Sex	Age	Total T-Score	Neck T-Score
Healthy femur	Femoral neck, intact site (superior half cross-section)	F	70	−1.0	−1.1
Osteoporotic femur	Femoral neck, intact site (interior half cross-section)	F	99	−2.6	−3.2
Osteoporotic femur, fractured in the study featured in ref. (Jazinizadeh et al., 2020)	Femoral neck, fracture site (superior half cross-section)	F	76	−3.0	−4.6

This protocol was then adopted for the investigation of unfractured and fractured osteoporotic bone.

To prepare bone for this study, large bone sections were cut at the base of the femoral neck with a handsaw, perpendicular to the neck axis at the inferior aspect. The bone was further sectioned into smaller pieces using a water-cooled, diamond-edged precision low-speed saw (Buehler, Illinois, USA). Specimens were kept frozen at −21 °C and were thawed for a minimum of twelve hours prior to sectioning. Samples were hand-ground and polished using an incremental grit scheme with 400, 800, 1200, and 2400 grit emery paper and a final 0.5 μm diamond suspension on a polishing pad (Buehler, Illinois, USA). All samples were treated with the same preparation scheme, apart from the fractured bone samples which were not ground and polished. The resulting samples were approximately 1 cm × 1 cm × 0.5 cm in size, containing both cortical and trabecular bone structures.

As a control, healthy bone samples were also prepared using conventional methods, where samples were subjected to the same polishing scheme and subsequently dehydrated through a graded series of ethanol in aqueous solution (50, 70, 70, 90, 90, 100, 100 %) for six hours at each stage. Incubation time for dehydration is based on the size of the sample, where shorter dehydration periods can be adapted due to the size sectioned samples considered (Helfrich and Ralson, 2012) (for samples larger than 1 cm^2 our team recommends periods of 12–24 hours for dehydration). Samples were ultrasonically cleaned in pure ethanol, air dried, and sputter-coated with 10 nm gold using a Precision Etching Coating System (PECS II) coater (Gatan Inc., CA, USA) before observation.

2.2. RTIL application methods

Prior to RTIL treatment, prepared bone samples were ultrasonically cleaned in ultra-pure Milli-Q water. The two hydrophilic RTILs investigated were 1-ethyl-3-methylimidazolium tetrafluoroborate and 1-butyl-3-methyl imidazolium tetrafluoroborate (Sigma-Aldrich Canada Co, Oakville, CA) referred to as [EMI][BF_4] and [BMI][BF_4], respectively. The treatment considered for these samples was an addition-based method (Fig. 2) where varying concentrations of 5, 10, & 25 % v/v RTIL in ultra-pure Milli-Q water were applied to samples. [BMI][BF_4] and [EMI][BF_4] are two of the most widely used hydrophilic RTILs in SEM observation of biological specimens in literature and the concentrations used in this study were founded on the review of analogous biological specimens such as wood and crustaceans (DiCecco et al., 2021). In detail, solutions were prepared with the appropriate concentration and heated by submerging in a 40 °C water bath for 60 s before application to bone to reduce the viscosity and improve their ability to spread onto samples. For treatment, 100 μl of RTIL solution was pipetted onto bone samples for a 60 s exposure time, providing full coverage of the sides and top surfaces of the samples, after which excess solution was gently blotted away using precision wipes (Kimwipes). Samples were then mounted onto standard 12.7 mm diameter sized aluminum SEM stubs with double-sided carbon tape and aluminum tape. Before imaging, samples were placed in a desiccator under vacuum for 30 min to further eliminate excess liquid.

2.3. SEM imaging

Bone samples were imaged using a tungsten filament equipped JEOL 6610 L V SEM (JEOL, Tokyo, Japan) SEM and backscattered electron (BSE) images were acquired. Microscope parameters including accelerating voltage and vacuum modes were optimized for best imaging results. An electron beam accelerating voltage of 15 kV was found to be optimal for imaging, where limited charging and no visible electron-burning of the tissue were experienced. Both low-vacuum imaging at 30 Pa and conventional high-vacuum mode ranging from 10^{-4}–10^{-5} Pa in session were investigated, with a consistent working distance of 10 mm. Elemental maps were collected by EDS with an Oxford Instruments X-Max 20 mm^2 area Silicon Drift EDS Detector (SDD) (Oxford Instruments, Oxford, UK) at 15 kV. EDS was performed in low-vacuum mode post-calibration using pure silicon and aluminum specimens as standards. EDS maps were analyzed and exported using the Oxford Instruments AZtec 3.3 software. Images were assessed and compared on a qualitative basis, where factors such as charging, liquid pooling, spatial resolution, and ease of imaging were considered together in identifying an ideal treatment.

3. Results and discussion

3.1. Effect of RTIL selection and concentration

Despite the low conductivity of bone tissue, little to no charging artifacts were observed following RTIL treatment in images acquired at a relatively high acceleration voltage of 15 kV, suggesting that RTILs impart adequate conductivity to the sample surface. Images of healthy bone taken in low vacuum mode are shown in Fig. 3 to demonstrate the

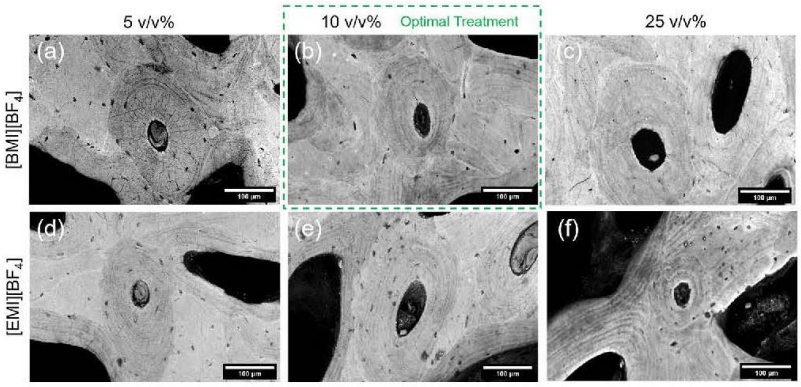

Fig. 3. BSE SEM images of healthy bone taken in low-vacuum conditions. Samples were treated with 5, 10, or 25 % v/v of [BMI][BF_4] (a-c) or [EMI][BF_4] (d-f) in water for 60 s. All images show osteons in a central location of each image surrounded by concentric lamellae bone centralized around a harversian canal. At higher concentrations of 25 % v/v, fine details in the bone structure were obscured while liquid pooling was also observed on the structure. The 10 % v/v had limited issues with charging and could be used readily for high resolution in both low and high-vacuum conditions, thus performed optimally within the treatments explored.

effectiveness of the two RTILs at concentrations of 5, 10 and 25 % v/v. Throughout the RTIL optimization process, the 10 % v/v [BMI][BF_4] treatment had the best performance overall during SEM imaging when considering the mitigation of liquid pooling (Fig. S1) and charging effects (Fig. S2) as well as qualitative imaging quality in both high and low vacuum schemes.

At concentrations of 25 % v/v, both RTIL treatments showed signs of liquid pooling on the sample surface, which resulted in a loss of resolution, and, in secondary electron (SE) mode, the appearance of liquid pooling artifacts (Fig. S1). RTIL solution pooling on a sample surface can greatly impact the quality of SEM imaging, especially when observing highly topographical samples in SE mode. This can lead to the loss of sharp and/or fine morphological features and potentially hide topographical features from being detected. Pooling typically occurs when using concentrated RTILs due to their viscous nature (Arimoto et al., 2008; Yanaga et al., 2012).

Although pooling was observed infrequently during imaging, it was found that BSE mode could still be used to observe these regions. The depth of the BSE signal likely allowed for key features to be resolved, despite the liquid layer, permitting the observation of underlying bone structures. Thus, within certain thicknesses, liquid pooling has minimal influence on the resolution of bone features in BSE mode due to the depth of signal origin; however, excess pooling can obscure features and lead to poor quality SEM images (Fig. S1).

Samples treated with 5 % v/v [EMI][BF_4] exhibited some charging effects, resulting in notable imaging artifacts such as noise and distortions from scanning (Fig. S2). Similar artifacts were noted for the 5 % v/v [BMI][BF_4] and 10 % v/v [EMI][BF_4] treatments in high vacuum trials, particularly on trabecular bone segments. In other works, similar charging trends are noted for biological samples imaged at lower RTIL concentrations, where excess surface charging has been found when below-optimal concentrations due to insufficient conductivity (Ishida et al., 2016; Yanaga et al., 2012). For both RTILs, the 10 % v/v treatment performed well in high and low vacuum and had mitigated pooling and charging effects; however, the [EMI][BF_4] scheme was observed to leave contaminants in isolated regions of the sample surface. Therefore, overall, treatment with [BMI][BF_4] resulted in universally higher quality SEM images than those imaged using [EMI][BF_4] and thus the 10 % v/v [BMI][BF_4] was found the most optimal in the testing schemes considered. While commercially purchased high purity [EMI][BF_4] (=>99 %) was used in the unpurified state herein, further purification means could help mitigate contaminants and to yield improved imaging results (Tsuda et al., 2011; Tsuda and Kuwabata, 2020).

Similar to how many other conductive coatings behave, it is important to note that the authentic structure of the sample could be obscured by the RTIL-treatment itself. While charging was noted in the [BMI][BF_4] 5 % v/v scheme (Fig. S2), there are features with higher contrast in the [BMI][BF_4] 5 % v/v scheme (Fig. 3(a)) which are more muted in the [BMI][BF4] 10 % v/v scheme (Fig. 3(b)). Correlative imaging methods are thus important to validate the authenticity of the imaging method, further discussed in section 3.4.

3.2. RTILS for imaging cortical bone and trabecular bone

With all treatment schemes, osteons in cortical bone can be clearly identified at the centre of each image in Fig. 3 as circular features composed of concentric layers of lamellae bone centralized around a haversian canal that contains blood vessels (Kini and Nandeesh, 2012). Lacunae, the sites housing bone cells called osteocytes, appear as blacker contrast smaller ellipsoidal shapes and can be resolved within the osteonal layers as well as the interstitial bone at all RTIL concentrations. Conventionally, the advantage of BSE SEM of bone is to distinguish regions of varying mineral content qualitatively or quantitatively by greyscale intensity (Roschger et al., 1998). In cortical bone, variations in mineral density can be readily observed between osteons and interstitial bone surrounding osteons. Interstitial bone, which is generally the oldest least remodelled bone tissue, tends to have higher mineralization densities and thus appears brighter in BSE mode in comparison to remodelled newer osteons, which typically have lower mineral amounts and appear darker (Milovanovic et al., 2018; Shah et al., 2019; Skedros et al., 2005). This is particularly evident in the central osteons features in Fig. 3. – all representing nearly fully circular, and therefore secondary, osteons created during bone remodelling (Kini and Nandeesh, 2012).

Fig. 4 highlights higher magnification images of both cortical and trabecular bone that could be achieved using the 10 % v/v [BMI][BF_4] treatment in low vacuum, where a haversian canal in cortical bone is shown in Fig. 4 (a,b) while trabecular bone is featured in Fig. 4 (c,d). Lacunae osteocyte networks can be observed in the bone structures of the samples in Fig. 4 (b) and (d), while finer micro-scale features of the bone can be resolved. Considering trabecular segments, charging artifacts can be challenging to mitigate in un-embedded trabecular bone segments even using conventional preparation methods. The higher porosity of trabecular bone results in free-floating unmounted bone fragments that interfere with the beam and subsequently create imaging challenges due to difficulty establishing a conductive path to ground the incoming electron beam in un-embedded samples (Boyde et al., 1986; Boyde and Jones, 1996). However, they were effectively observed using the 10 % v/v [BMI][BF_4] treatment (Fig. 4 (c,d)), where lamellar hemi-osteons and lacunae where osteocytes reside can clearly be distinguished.

3.3. Application to osteoporotic bone

The application of 10 % v/v [BMI][BF4] can readily be used to

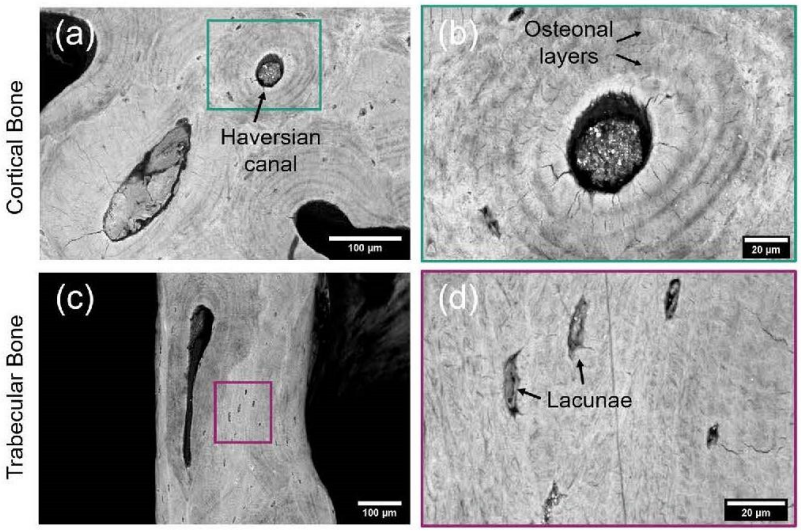

Fig. 4. BSE SEM images of healthy bone in low-vacuum conditions treated with 10 % v/v [BMI][BF4]. Both cortical bone (a,b) with visible harversian canals and trabecular bone (c,d) were easily imaged with this concentration. At higher magnification (b,d) both osteonal and lamellar bone as well as lacunae where osteocytes are located are visible. Minimal cracks are observed.

observe a variety of healthy or pathological bone tissues in both low and high vacuum SEM conditions. Figs. 5 and 6 highlight the high vacuum imaging capabilities in secondary electron (SE) and BSE modes of this method, showing that RTILs facilitate imaging of both polished (Fig. 5) and fractured (Fig. 6) osteoporotic bone. The imaging illustrates that the optimized RTIL treatment can be used to i) observe samples in high vacuum modes, ii) study fractured or highly topographical bone specimens, & iii) efficiently and quickly observe diseased bone such as osteoporotic bone in SEM.

Fig. 5 shows high-resolution images of an osteon in osteoporotic cortical bone. Osteonal lamellae can be easily observed, measured, and counted using images captured from this preparation technique. This helps show the versatility of this protocol, which can readily be applied to a variety of different bone and mineralized tissues for their study in SEM. Comparing Fig. 5 to 4 (a,b), it is noted that similar imaging quality could be resolved in both high and low vacuum conditions, where

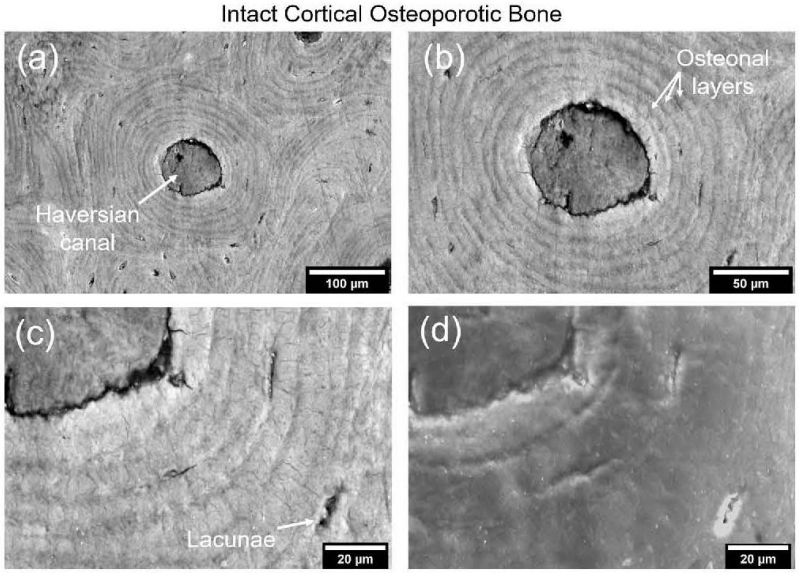

Fig. 5. RTIL 10 % v/v [BMI][BF_4] treated intact, unfractured osteoporotic cortical bone samples, showing in (a-c) BSE SEM images and (d) SE SEM of image of (c), all in high vacuum condition. Clear bone structural microfeatures can be distinguished such as a haversian canal at the center of (a,b) and circumferential osteonal layers can be distinguished, showing similar imaging quality in comparison to low vacuum observation in Fig. 4(a,b).

Fig. 6. SE SEM images of RTIL 10 % v/v [BMI][BF_4] treated fractured osteoporotic trabecular bone in high vacuum condition at successively higher magnification (a-c). Fine structural fracture surface and topography can be resolved with minimal charging effects.

similar structural microfeatures of bone can be resolved through BSE mode. However, due to the nature of the high-vacuum condition and more efficient detection modality, the structure can be resolved in better detail in the high-vacuum condition overall.

In BSE mode, contrast is dominated by atomic number, where heavy elements appear brighter. Thus, structural contrast is gained due to the hierarchical structure of bone, which is principally composed of inorganic calcium-rich mineral (heavier component = brighter), organic components such as cells and collagen as well as unbound water (both higher components = darker). In comparison, SE mode contrast is dominated by topography in the structure, thus Fig. 4 (d) of the polished bone does not have the same visibility of these structures. Limited charging was noted in high-vacuum mode in SE, however, we noted not all edge-related charge accumulation could be mitigated, exemplified by the lacunae visualized in the lower right corner of Fig. 4 (d).

Fig. 6 exemplifies the applications of RTILs in investigating highly topographical samples such as fracture surfaces to elucidate fracture mechanisms and modes of failure in nonconductive materials such as bone. For such bone segments, which may be over >1cm^3 in size, their preparation through conventional means is lengthy (highlighted by Fig. 1) and may influence the morphologies being observed (Kellenberger et al., 1992; Li et al., 2017; McKee et al., 1991; Utku et al., 2008). Here, the RTIL method presents a key method that can be used quickly and efficiently in lieu of conventional means to observe large fracture segments, without involving fixation and dehydration steps. It is noted that the RTIL treatment may penetrate the fractured bone and potentially obscure features. Using SE and BSE modalities to complement each other in surveying fracture surfaces can help distinguish any obscurities cause by the solution treatment itself to validate observations.

3.4. Comparison to dehydrated bone

To evaluate the effectiveness of the optimal 10 % v/v [BMI][BF_4] treatment against conventional methods, healthy bone specimens with cortical and trabecular segments were sectioned, dehydrated, and sputter-coated with gold. The samples were left unfixed to better compare to the unfixed RTIL treated samples. The conventionally prepared sample imaged in high vacuum BSE and SE mode is shown with both cortical and trabecular bone in Fig. 7.

Distinct differences between the RTIL and conventionally treated samples can be noted. Microcracks are observed in greater number in the conventionally prepared dehydrated samples. While some cracks may be naturally occurring, it is suspected that most are artifacts from sample preparation methods. Microcracks are commonly a result of preparation methods such as polishing and dehydration steps (Shah et al., 2019). Given that all bone samples were ground and polished following the same procedure, it is suspected that most of these cracks are a direct result of dehydration, as minimal cracks are observed in Fig. 4 for the 10 % v/v [BMI][BF_4] treated sample. This indicates that the RTIL application process may be used to effectively mitigate sample damage in high-resolution imaging, which may not be possible with conventional preparations that involve dehydration and harsh chemical fixation.

The additional microcracks made the structure more prominently affected by bright-edge charging effects not mitigated through gold coating. This effect arises from escaping surface electrons when imaged in SE modality (Seiler, 1983). In comparison, SE imaging from Fig. 5(d) with the 10 % v/v [BMI][BF_4] treatment shows mitigation of this effect with minimal cracking. Similar RTIL treatments in SEM have been found to successfully mitigate edge-effect charging of biological samples with sharp edges and/or pointed features such as basidiospores and protists (Ishida et al., 2016; Yanaga et al., 2012).

3.5. RTIL treatment and elemental analysis

Another essential utility of RTIL-based application methods is its potential to allow for EDS analysis on hydrated bone samples. Fig. 8 demonstrates that EDS analysis can be applied to healthy bone in low-vacuum mode using the 10 % v/v [BMI][BF_4] preparation as an

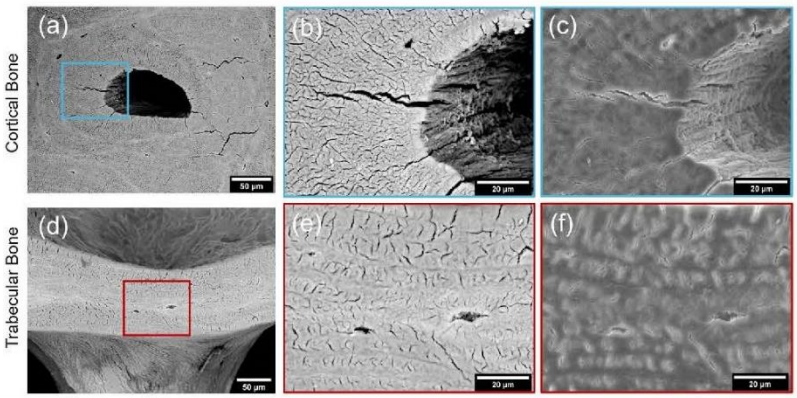

Fig. 7. BSE SEM images of healthy dehydrated bone in high-vacuum conditions, highlighting both cortical bone (a,b) and trabecular bone (d, e), with SE SEM images featured in (c,f). Inset on (a) represents the edge of a lacunae and (d) inset highlights two lacunae. Similar to Fig. 4, fine structural details can be distinguished such as osteonal and lamellar bone as well as osteocyte lacunae; however, the structure has been significantly impacted by dehydration and microcracks are more prominent in comparison to the RTIL scheme, making them more susceptible to edge-effect charging in SE mode.

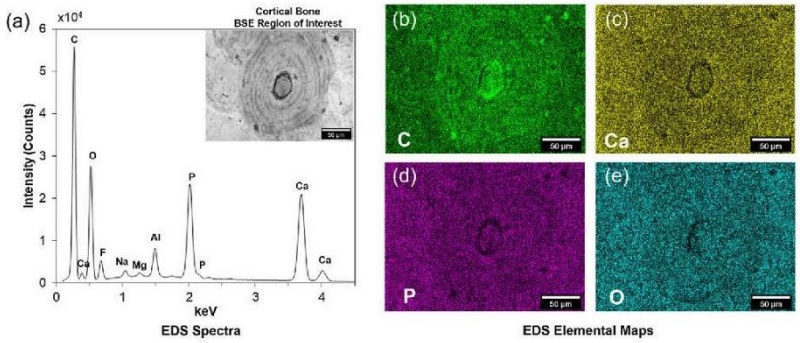

Fig. 8. EDS analysis applied in imaging healthy cortical bone in low-vacuum mode using the 10 % v/v [BMI][BF_4] (a) EDS spectra collected during analysis, with BSE image inset highlighting the cortical region of interest considered, where distinct peaks are noted for C, Ca, P, O, Na, F, and Mg; trace amounts of N, Si, Cl and S were also noted. Corresponding EDS elemental maps for characteristic elements present in bone structures (b) C, (c) Ca, (d) P, and (e) O, are shown.

example. An osteon is shown in the healthy bone in Fig. 8 (a), which was selected as a region of interest with known differences in bone mineral density for EDS analysis. Given that bone is a natural composite material composed primarily of calcium phosphate hydroxyapatite crystals, organic components, and unbound water, it was expected that C, Ca, P, and O would be key detectable elements in the structure and that higher density mineralized regions would have higher amounts of Ca and P (Clarke, 2008; Milovanovic et al., 2018; Shah et al., 2019; Skedros et al., 2005).

A typical EDS spectrum collected during analysis is shown in Fig. 8 (a), where distinct peaks are noted for C, Ca, P, O, Na, F, and Mg; trace amounts of N, Si, Cl and S were also noted. Elemental detection of fluorine is attributed to the [BMI][BF_4] RTIL, where boron could have also been expected to be able to be detected though likely its peak was unable to be distinguished due to the strong nearby by carbon peak in the spectra. Fig. 8 (b–e) depicts elemental mappings of the major constituents C, Ca, P, and O. Higher detection of Ca and P outside of the central osteon and a higher detection of C within this full osteon demonstrate the lower mineral to matrix composition, which is known to be associated with newly remodelled osteons compared to older or interstitial bone (Milovanovic et al., 2018; Skedros et al., 2005). This finding corroborates qualitative BSE imaging, Fig. 8 (a) (inset), which by its darker contrast indicates the central osteon has a lower mineral density.

It has been suggested reporting Ca:P ratios in lieu of wt% of each component as a reliable measure of composition in bone (Zaichick and Tzaphlidou, 2002). In this consideration for the region analyzed in Fig. 8 (a), a ratio of 1.9 Ca:P can be reported. This aligns well with median Ca:P values that were reported for cortical bone in the femoral neck summarized by Zaichick and Tzaphlidou (2002) and is slightly off from the expected 1.67 Ca:P ratio for stoichiometric hydroxyapatite.

Several effects could influence the results obtained from EDS analysis, such as noise in the spectra from detection and SEM imaging conditions as well as the RTIL treatment itself. Abe et al. noted in their work that higher accumulated regions of the RTIL treatment can lead to a lack of penetration of the electron beam to a region of interest and lead to a lack of signal detection, where they used a 5 kV electron beam (Abe et al., 2012). This effect can be mitigated by using a higher kV beam to get higher penetration within the sample and an optimal RTIL treatment that reduces RTIL pooling, as done in our work here with a 15 kV beam and the optimal 10 % v/v [BMI][BF_4] treatment. However, the underlying effect of the RTIL on the surface remains a presence in the spectra, as exemplified by the strong F peak in Fig. 8 (a), which is not normally present in bone in such amount. One advantage to such an RTIL treatment is the F peak present does not have an overlapping peak with P, which both common Pt and Au coatings for bone can have with their M level characteristic X-rays peaks (Goldstein et al., 2018). This can lead to challenges in the interpretation of concentration of P in characterization and its detection more challenging in conventional preparation schemes using Pt or Au sputter coatings.

3.6. Potential pitfalls and challenges

Despite the quick turn-around time for preparing samples with RTILs, the treatment is temporary. After 6–7 days, RTIL-treated SEM samples can begin to show signs of debris accumulation, carbon deposition, and charging effects (Ishigaki et al., 2011b, 2011c; Lee et al., 2021). Samples may also begin to degrade or foul, depending on the sample. This is a clear disadvantage of RTIL-based SEM compared to conventional methods, which typically include a fixation step to prevent sample degradation; however, the scheme may still be applied to fixed samples which could help preserve their structure for longer. Careful storage in a closed system such as a desiccator has been shown to mitigate these contamination effects up to one month, after which the RTIL treatment must be reapplied (Ishigaki et al., 2011a). Hypothetically, re-application would be possible to sustain fixed samples for longer periods for imaging. Limited work explores the effectiveness of re-applying RTILs to further treat samples, however, which raises caution for its reapplication considering the effects of consecutive RTIL treatment on sample structure and quality.

A possible concern with using [EMI][BF_4] and [BMI][BF_4] RTILs is the formation of HF by-products through potential degradation mechanisms involving aqueous [BF4] , particularly at elevated temperatures (Freire et al., 2010; Radosavljević et al., 1979). Tsuda et al. (2014) theorized that using [EMI][BF_4] and [BMI][BF_4] in aqueous solution for SEM treatment led to the formation of HF, which they discussed may have decreased the size of superabsorbent polymer particles observed in their work, as well as drastically changed their particle surface morphologies. In the work presented here, we noted no signs of degradation in the bone samples studied during SEM imaging. Due to the high affinity of HF towards calcium, which typically attacks bone structures and leads to calcium depletion (Bertolini, 1992), it would be expected that noticeable degradation may have occurred if significant amounts of HF had formed. Thus, the risk of HF-related damage is believed to be negligible under the imaging conditions and RTIL concentrations used in this study.

The success of this RTIL-based imaging protocol has permitted the efficient observation of hydrated bone samples, in the absence of any specialized equipment or complicated preparation steps. The work poses several implications to the bone imaging community – exploring new preparation methods to observe hydrated natural tissues quickly and efficiently. This work offers attractive alternatives for studying the

hierarchical structure of bone and other mineralized tissues, providing a new method to perform correlative observations of their features. Current methodologies require steps that may inadvertently compromise the natural structure of bone tissue, namely dehydration and fixation (Kellenberger et al., 1992; Li et al., 2017; McKee et al., 1991; Utku et al., 2008). This calls into question the validity and reliability of data collected using these methods.

The other state-of-the-art approach for retaining bone structure during imaging is cryo-preservation (Kerschnitzki et al., 2016; Mahamid et al., 2011, 2010). This methodology preserves the hydrated structure of bone, mitigating issues described that arise from conventional preparation involving dehydration. Moreover, cryo-EM methods can produce clearer images due to the limited amount of electron scatter in vitrified liquids in comparison to liquids in their native state (Patterson et al., 2017). However, once vitrified, similar densities of soft materials and the vitrified mediums can reduce Z-contrast in imaging and lower the signal-to-noise ratio (He et al., 2019). However, the cryo-EM vitrification process and sample preparation require extensive experience and a relatively expensive suite of equipment to achieve impeccable results in comparison to the simply applied RTIL method presented in this work.

In summary, we demonstrate that RTIL treatment presents a feasible method to study the hierarchical structure of bone. While there exists apprehension to the application of such liquid-based SEM preparation techniques (DiCecco et al., 2021), our present work, and the plethora of other works on biological materials (Golding et al., 2016; Komai et al., 2014; Kuwabata et al., 2006; Lee et al., 2021; Lu et al., 2019; Tsuda et al., 2011), gives further confidence to this technique.

4. Conclusions

This work highlights a new methodology to study bone in its natural, hydrated state through SEM imaging using an RTIL-based treatment method. The optimization of this treatment was explored using [EMI][BF_4] and [BMI][BF_4] RTILs at 5, 10, and 25 % v/v in aqueous solution at varying imaging conditions. The described protocol is simple, efficient, and can be quickly applied to fresh bone samples as an alternative SEM preparation method to lengthy and laborious conventional means. Moreover, the RTIL treatment is suggested to better preserve natural bone structure, resulting in minimal cracking as observed in comparison to traditional preparation schemes involving dehydration. An optimal treatment identified in this work involved a 60-second application method with 10 % v/v [BMI][BF_4] treatment for hydrated, unfixed bone. The described protocol was used to observe polished and fractured surfaces of bone in both high and low vacuum mode SEM, with acceleration voltages of 15 kV, and in both SE and BSE imaging modes. Minimal charging effects were observed using this treatment and we showed that it was still possible to perform elemental analysis, such as EDS, on RTIL-treated bone. This proof-of-concept work highlights the versatility and feasibility of this technique for observing a variety of healthy and pathological mineralized bone samples for wide-ranging applications. This work lays the foundation for the biological community to continue to explore RTIL-based techniques in the study of natural and hydrated tissues.

Author contributions

Conceptualization: Liza-Anastasia DiCecco, Kathryn Grandfield.
Methodology: Liza-Anastasia DiCecco, Andrew D'Elia.
Data curation: Liza-Anastasia DiCecco.
Formal analysis: Liza-Anastasia DiCecco, Andrew D'Elia.
Funding acquisitions and supervision: Kathryn Grandfield, Leyla Soleymani, Cheryl Quenneville
Writing- first draft: Liza-Anastasia DiCecco.
Review and editing: Liza-Anastasia DiCecco, Andrew D'Elia, Leyla Soleymani, Cheryl Quenneville, Kathryn Grandfield.

Data availability

No data was used for the research described in the article.
Data is available upon request to the corresponding author.

Declaration of Competing Interest

The authors report no declarations of interest.

Acknowledgements

Financial support provided by the Natural Sciences and Engineering Research Council of Canada (NSERC) Discovery Grant program (RGPIN-2020-05722), Canada Research Chairs program (LS and KG), the Vanier Canada Graduate Scholarship (Vanier CGS, L-AD) program and McMaster Engineering Big Ideas Grant is greatly acknowledged. Electron microscopy was performed at the Canadian Centre for Electron Microscopy (also supported by NSERC and other government agencies). Illustrations in this work highlighting the process pathways were created with BioRender.com.

Appendix A. Supplementary data

Supplementary material related to this article can be found, in the online version, at doi:https://doi.org/10.1016/j.micron.2021.103192.

References

Abe, S., Hyono, A., Machida, Y., Watari, F., Yonezawa, T., 2012. Conductivity preparation by choline lactate ethanol solution for SEM observation: both hard and soft tissues in living matter. Nano Biomed 4, 18–23. https://doi.org/10.11344/nano.4.18.

Arimoto, S., Sugimura, M., Kageyama, H., Torimoto, T., Kuwabata, S., 2008. Development of new techniques for scanning electron microscope observation using ionic liquid. Electrochim. Acta 53, 6228–6234. https://doi.org/10.1016/j.electacta.2008.01.001.

Bertolini, J.C., 1992. Hydrofluoric acid: a review of toxicity. J. Emerg. Med. 10, 163–168. https://doi.org/10.1016/0736-4679(92)90211-b.

Binkley, D.M., Grandfield, K., 2017. Advances in multiscale characterization techniques of bone and biomaterials interfaces. ACS Biomater. Sci. Eng. 4, 3678–3690. https://doi.org/10.1021/acsbiomaterials.7b00420.

Binkley, D.M., Deering, J., Yuan, H., Gourrier, A., Grandfield, K., 2020. Ellipsoidal mesoscale mineralization pattern in human cortical bone revealed in 3D by plasma focused ion beam serial sectioning. J. Struct. Biol. 107615. https://doi.org/10.1016/j.jsb.2020.107615.

Boyde, A., Jones, S.J., 1996. Scanning electron microscopy of bone: instrument, specimen, and issues. Microsc. Res. Techn. 33, 92–120. https://doi.org/10.1002/(sici)1097-0029(19960201)33:2<92::aid-jemt2>3.0.co;2-0.

Boyde, A., Maconnachie, E., Reid, S.A., Delling, G., Mundy, G.R., 1986. Scanning electron microscopy in bone pathology: review of methods, potential and applications. Scanning Microsc. 1537–1554.

Braidotti, P., Bemporad, E., D'Alessio, T., Sciuto, S.A., Stagni, L., 2000. Tensile experiments and SEM fractography on bovine subchondral bone. J. Biomech. 33, 1153–1157. https://doi.org/10.1016/s0021-9290(00)00074-9.

Chissoe, W.F., Vezey, E.L., Skvarla, J.J., 1995. The use of osmium-thiocarbohydrazide for structural stabilization and enhancement of secondary Electron images in scanning electron microscopy of pollen. Grana 34, 317–324. https://doi.org/10.1080/00173139509429065.

Clarke, B., 2008. Normal bone anatomy and physiology. Clin. J. Am. Soc. Nephrol. 3, S131–S139. https://doi.org/10.2215/cjn.04151206.

Dempster, D.W., Shane, E., Horbert, W., Lindsay, R., 1986. A simple method for correlative light and scanning electron microscopy of human iliac crest bone biopsies: qualitative observations in normal and osteoporotic subjects. J. Bone Miner. Res. 1, 15–21. https://doi.org/10.1002/jbmr.5650010105.

DiCecco, L., D'Elia, A., Miller, C., Sask, K.N., Soleymani, L., Grandfield, K., 2021. Electron microscopy imaging applications of room temperature ionic liquids in the biological field: a review. Chembiochem 22, 2488–2506. https://doi.org/10.1002/cbic.202100041.

Freire, M.G., Neves, C.M.S.S., Marrucho, I.M., Coutinho, J.A.P., Fernandes, A.M., 2010. Hydrolysis of tetrafluoroborate and hexafluorophosphate counter ions in imidazolium-based ionic liquids †. J. Phys. Chem. 114, 3744–3749. https://doi.org/10.1021/jp903292n.

Golding, C.G., Lamboo, L.L., Beniac, D.R., Booth, T.F., 2016. The scanning electron microscope in microbiology and diagnosis of infectious disease. Sci. Rep.-UK 6, 26516. https://doi.org/10.1038/srep26516.

Goldstein, J.I., Newbury, D.E., Michael, J.R., Ritchie, N.W.M., Scott, J.H.J., Joy, D.C., 2018. Scanning Electron Microscopy and X-Ray Microanalysis. Springer, New York NY.

Hagiwara, R., Ito, Y., 2000. Room temperature ionic liquids of alkylimidazolium cations and fluoroanions. J. Fluorine Chem. 105, 221–227. https://doi.org/10.1016/s0022-1139(99)00267-5.

He, K., Shokuhfar, T., Shahbazian-Yassar, R., 2019. Imaging of soft materials using in situ liquid-cell transmission electron microscopy. J. Phys. Condens. Matter 31, 103001. https://doi.org/10.1088/1361-648x/aaf616.

Helfrich, M.H., Ralson, S.H. (Eds.), 2012. Bone Research Protocols, Methods in Molecular Biology. Springer Science+Business Media. https://doi.org/10.1007/978-1-61779-415-5.

Hiller, L.P., Stover, S.M., Gibson, V.A., Gibeling, J.C., Prater, C.S., Hazelwood, S.J., Yeh, O.C., Martin, R.B., 2003. Osteon pullout in the equine third metacarpal bone: effects of ex vivo fatigue. J. Orthop. Res. 21, 481–488. https://doi.org/10.1016/s0736-0266(02)00232-2.

Ishida, H., Gobara, Y., Kobayashi, M., Suzaki, T., 2016. Use of ionic liquid for scanning electron microscopy of protists. Int. J. New Technol. Res. 2, 43–46.

Ishigaki, Y., Nakamura, Y., Takehara, T., Kurihara, T., Koga, H., Takegami, T., Nakagawa, H., Nemoto, N., Tomosugi, N., Kuwabata, S., Miyazawa, S., 2011a. Comparative study of hydrophilic and hydrophobic ionic liquids for observing cultured human cells by scanning electron microscopy. Microsc. Res. Tech. 74, 1104–1108. https://doi.org/10.1002/jemt.21001.

Ishigaki, Y., Nakamura, Y., Takehara, T., Nemoto, N., Kurihara, T., Koga, H., Nakagawa, H., Takegami, T., Tomosugi, N., Miyazawa, S., Kuwabata, S., 2011b. Ionic liquid enables simple and rapid sample preparation of human culturing cells for scanning electron microscope analysis. Microsc. Res. Tech. 74, 415–420. https://doi.org/10.1002/jemt.20924.

Ishigaki, Y., Nakamura, Y., Takehara, T., Shimasaki, T., Tatsuno, T., Takano, F., Ueda, Y., Motoo, Y., Takegami, T., Nakagawa, H., Kuwabata, S., Nemoto, N., Tomosugi, N., Miyazawa, S., 2011c. Scanning electron microscopy with an ionic liquid reveals the loss of mitotic protrusions of cells during the epithelial–mesenchymal transition. Microsc. Res. Tech. 74, 1024–1031. https://doi.org/10.1002/jemt.20989.

Jazinizadeh, F., Mohammadi, H., Quenneville, C.E., 2020. Comparing the fracture limits of the proximal femur under impact and quasi-static conditions in simulation of a sideways fall. J. Mech. Behav. Biomed. Mater. 103, 103593 https://doi.org/10.1016/j.jmbbm.2019.103593.

Kanbayashi, T., Miyafuji, H., 2016. Microscopic characterization of tension wood cell walls of Japanese beech (Fagus crenata) treated with ionic liquids. Micron 88, 24–29. https://doi.org/10.1016/j.micron.2016.05.007.

Kanis, J.A., McCloskey, E.V., Johansson, H., Oden, A., Melton, L.J., Khaltaev, N., 2008. A reference standard for the description of osteoporosis. Bone 42, 467–475. https://doi.org/10.1016/j.bone.2007.11.001.

Kellenberger, E., Johansen, R., Maeder, M., Bohrmann, B., Stauffer, E., Villiger, W., 1992. Artefacts and morphological changes during chemical fixation. J Microsc.-Oxford 168, 181–201. https://doi.org/10.1111/j.1365-2818.1992.tb03260.x.

Kerschnitzki, M., Akiva, A., Shoham, A.B., Assecher, Y., Wagermaier, W., Fratzl, P., Addadi, L., Weiner, S., 2016. Bone mineralization pathways during the rapid growth of embryonic chicken long bones. J. Struct. Biol. 195, 82–92. https://doi.org/10.1016/j.jsb.2016.04.011.

Kini, U., Nandeesh, B.N., 2012. Physiology of bone formation, remodeling, and metabolism. In: Fogelman, I., Gnanasegaran, G., van der Wall, H. (Eds.), Radionuclide and Hybrid Bone Imaging. Springer-Verlag, Berlin Heidelberg, pp. 29–57. https://doi.org/10.1007/978-3-642-02400-9_2.

Komai, F., Okada, K., Inoue, Y., Yada, M., Tanaka, O., Kuwabata, S., 2014. SEM observation of wet lily pollen grains pretreated with ionic liquid. J. Jpn. Soc. Hortic. Sci. 83, 317–321. https://doi.org/10.2503/jjshs1.mi-008.

Kuwabata, S., Kongkanand, A., Oyamatsu, D., Torimoto, T., 2006. Observation of ionic liquid by scanning electron microscope. Chem. Lett. 35, 600–601. https://doi.org/10.1246/cl.2006.600.

Lee, B.E.J., DiCecco, L., Exir, H., Weck, A., Sask, K.N., Grandfield, K., 2021. Simultaneous visualization of wet cells and nanostructured biomaterials in SEM using ionic liquids. Chembiochem 22, 571–576. https://doi.org/10.1002/cbic.202000552.

Li, Y., Almassalha, L.M., Chandler, J.E., Zhou, X., Stypula-Cyrus, Y.E., Hujsak, K.A., Roth, E.W., Bleher, R., Subramanian, H., Szleifer, I., Dravid, V.P., Backman, V., 2017. The effects of chemical fixation on the cellular nanostructure. Exp. Cell Res. 358, 253–259. https://doi.org/10.1016/j.yexcr.2017.06.022.

Lu, B.-J., Li, J.-R., Tai, H.-C., Cai, W., Tseng, H.-H., Hsieh, Y.-T., 2019. A facile ionic-liquid pretreatment method for the examination of archaeological wood by scanning electron microscopy. Sci. Rep.-UK 9, 13253. https://doi.org/10.1038/s41598-019-49773-y.

Mahamid, J., Aichmayer, B., Shimoni, E., Ziblat, R., Li, C., Siegel, S., Paris, O., Fratzl, P., Weiner, S., Addadi, L., 2010. Mapping amorphous calcium phosphate transformation into crystalline mineral from the cell to the bone in zebrafish fin rays. Proc. Natl. Acad. Sci. 107, 6316–6321. https://doi.org/10.1073/pnas.0914218107.

Mahamid, J., Sharir, A., Gur, D., Zelzer, E., Addadi, L., Weiner, S., 2011. Bone mineralization proceeds through intracellular calcium phosphate loaded vesicles: a cryo-electron microscopy study. J. Struct. Biol. 174, 527–535. https://doi.org/10.1016/j.jsb.2011.03.014.

McKee, M.D., Nanci, A., Landis, W.J., Gotoh, Y., Gerstenfeld, L.C., Glimcher, M.J., 1991. Effects of fixation and demineralization on the retention of bone phosphoprotein and other matrix components as evaluated by biochemical analyses and quantitative immunocytochemistry. J. Bone Miner. Res. 6, 937–945. https://doi.org/10.1002/jbmr.5650060907.

Milovanovic, P., Scheidt, Avom, Mletzko, K., Sarau, G., Püschel, K., Djuric, M., Amling, M., Christiansen, S., Busse, B., 2018. Bone tissue aging affects mineralization of cement lines. Bone 110, 187–193. https://doi.org/10.1016/j.bone.2018.02.004.

Patterson, J.P., Xu, Y., Moradi, M.-A., Sommerdijk, N.A.J.M., Friedrich, H., 2017. CryoTEM as an advanced analytical tool for materials chemists. Accounts Chem. Res. 50, 1495–1501. https://doi.org/10.1021/acs.accounts.7b00107.

Radosavljević, S., Šćepanović, V., Stević, S., Milojković, D., 1979. Effect of boric acid on tetrafluoroborate ion hydrolysis in solutions of tetrafluoroboric acid. J. Fluorine Chem. 13, 465–471. https://doi.org/10.1016/s0022-1139(00)83094-8.

Reznikov, N., Almany-Magal, R., Shahar, R., Weiner, S., 2013. Three-dimensional imaging of collagen fibril organization in rat circumferential lamellar bone using a dual beam electron microscope reveals ordered and disordered sub-lamellar structures. Bone 52, 676–683. https://doi.org/10.1016/j.bone.2012.10.034.

Roschger, P., Fratzl, P., Eschberger, J., Klaushofer, K., 1998. Validation of quantitative backscattered electron imaging for the measurement of mineral density distribution in human bone biopsies. Bone 23, 319–326. https://doi.org/10.1016/s8756-3282(98)00112-4.

Seiler, H., 1983. Secondary electron emission in the scanning electron microscope. J. Appl. Phys. 54, R1–R18. https://doi.org/10.1063/1.332840.

Shah, F.A., Snis, A., Matic, A., Thomsen, P., Palmquist, A., 2016. 3D printed Ti6Al4V implant surface promotes bone maturation and retains a higher density of less aged osteocytes at the bone-implant interface. Acta Biomater. 30, 357–367. https://doi.org/10.1016/j.actbio.2015.11.013.

Shah, F.A., Ruscsák, K., Palmquist, A., 2019. 50 years of scanning electron microscopy of bone—a comprehensive overview of the important discoveries made and insights gained into bone material properties in health, disease, and taphonomy. Bone Res. 7, 15. https://doi.org/10.1038/s41413-019-0053-z.

Skedros, J.G., Holmes, J.L., Vajda, E.G., Bloebaum, R.D., 2005. Cement lines of secondary osteons in human bone are not mineral-deficient: new data in a historical perspective. Anatomical Rec. Part Discov. Mol. Cell Evol. Biol. 286A, 781–803. https://doi.org/10.1002/ar.a.20214.

Tedesco, J., Lee, B.E.J., Lin, A.Y.W., Binkley, D.M., Delaney, K.H., Kwiecien, J.M., Grandfield, K., 2017. Osseointegration of a 3D printed stemmed titanium dental implant: a pilot study. Int. J. Dent. 2017, 1–11. https://doi.org/10.1155/2017/5920714.

Tsuda, T., Kuwabata, S., 2020. Electron microscopy using ionic liquids for life and materials sciences. Microscopy 69, 183–195. https://doi.org/10.1093/jmicro/dfaa013.

Tsuda, T., Nemoto, N., Kawakami, K., Mochizuki, E., Kishida, S., Tajiri, T., Kushibiki, T., Kuwabata, S., 2011. SEM observation of wet biological specimens pretreated with room-temperature ionic liquid. Chembiochem 12, 2547–2550. https://doi.org/10.1002/cbic.201100476.

Tsuda, T., Mochizuki, E., Kishida, S., Iwasaki, K., Tsunashima, K., Kuwabata, S., 2014. SEM observation of hydrous superabsorbent polymer pretreated with room-temperature ionic liquids. PLoS One 9, e91193. https://doi.org/10.1371/journal.pone.0091193.

Utku, F.S., Klein, E., Saybasili, H., Yucesoy, C.A., Weiner, S., 2008. Probing the role of water in lamellar bone by dehydration in the environmental scanning electron microscope. J. Struct. Biol. 162, 361–367. https://doi.org/10.1016/j.jsb.2008.01.004.

Welton, T., 1999. Room-Temperature Ionic Liquids. Solvents for Synthesis and Catalysis. Chem. Rev. 99, 2071–2084. https://doi.org/10.1021/cr980032t.

Yanaga, K., Maekawa, N., Shimomura, N., Ishigaki, Y., Nakamura, Y., Takegami, T., Tomosugi, N., Miyazawa, S., Kuwabata, S., 2012. Use of ionic liquid in fungal taxonomic study of ultrastructure of basidiospore ornamentation. Mycol. Prog. 11, 343–347. https://doi.org/10.1007/s11557-011-0794-6.

Zaichick, V., Tzaphlidou, M., 2002. Determination of calcium, phosphorus, and the calcium/phosphorus ratio in cortical bone from the human femoral neck by neutron activation analysis. Appl. Radiat. Isot. 56, 781–786. https://doi.org/10.1016/s0969-8043(02)00066-0.

Chapter 3: Supplemental Figures

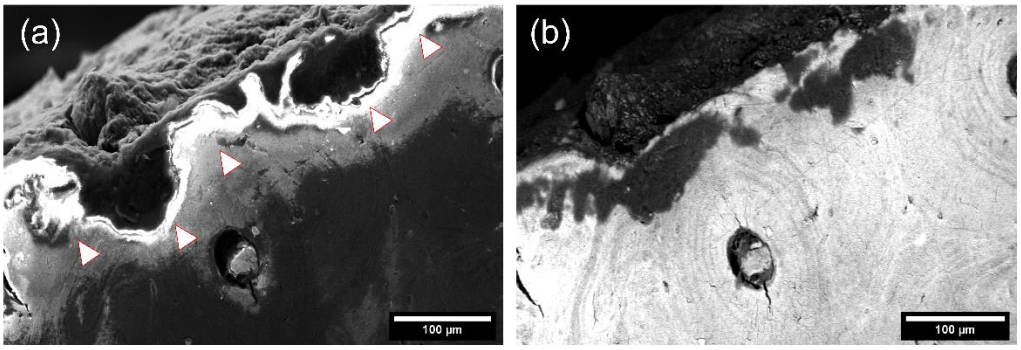

Ch. 3 – Figure S1. *SEM of healthy bone imaged with a 25 v/v% of [BMI][BF_4] treatment in (a) SE and (b) BSE mode. RTIL solution pooling is noted on the edge of the sample (interface indicated by triangles), which obscures the underlying features of the bone and results in poorer quality SEM images. It is noted that this influence is more noticeable in SE mode than in BSE mode, where edge charging better highlights the liquid interface.*

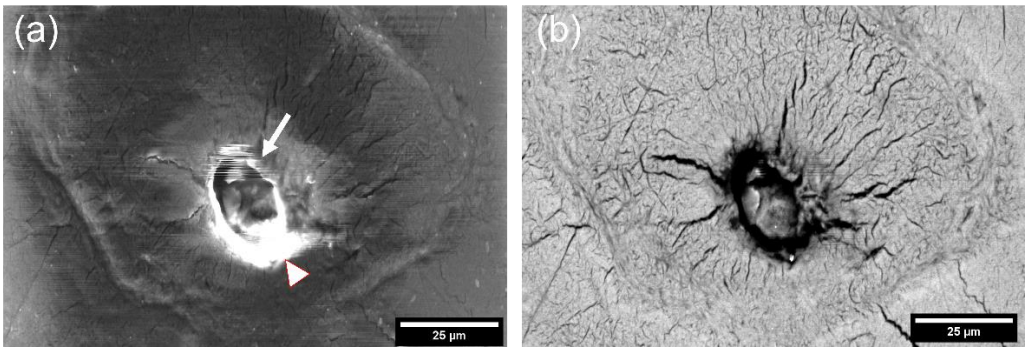

Ch. 3 – Figure S2. *SEM of healthy bone imaged with a 5 v/v% of [EMI][BF_4] treatment in (a) SE and (b) BSE mode. Charging effects are noted (triangle) which resulted in noise and distortions (arrow) from scanning in SEM imaging.*

Chapter 4: Advancing High-Resolution Imaging of Virus Assemblies in Liquid and Ice

4.1 Section Introduction (Objective ii)

Within the structural biology field, cryo TEM is considered the gold standard characterization technique for characterizing small biological specimens. However, cryo TEM captures specimens in ice, where the dynamic and flexible nature of biological structures are limited. With the advent of new liquid TEM techniques, there is a desire to pair the two methods to combine HR cryo with liquid dynamic imaging to expand insights into complex structures. Considering the ongoing COVID-19 pandemic, there is emerging pressure to gain dynamic insights into virus structures for the development of new therapeutics and the fight against future pandemic pathogens. As outlined in the objectives, in Chapter 4 new methods for HR liquid biological TEM of virions were developed. This involved the use of a commercial liquid TEM holder as well as a newly developed thin-film liquid TEM enclosure. Combined with automated acquisition tools and low-dose direct electron detection, high-resolution structural features in the range of ~3.5 Å – 10 Å were able to be resolved using single-particle analysis and the enclosures were established as a correlative complementary tool for cryo TEM. Particularly, the development of a new thin-film liquid TEM enclosure was highlighted as a facile and affordable tool to perform liquid TEM and its assembly demonstrated within this video article, broadening the accessibility of the technique. Overall, this research contributes to the improvement of structural biology single-particle methods in liquid and ice for virus studies – helping give the field new resources for studying these elusive disease culprits.

Authors: **Liza-Anastasia DiCecco***, Samantha Berry, GM Jonaid, Maria Solares, Liam Kaylor, Jennifer Gray, Carol Bator, William J. Dearnaley, Michael Spilman, Madeline J. Dressel-Dukes, Kathryn Grandfield, Sarah M. McDonald Esstman, Deborah F. Kelly.

Publication: This work is published with a full citation provided as follows:

DiCecco, L.-A.*, Berry, S.*, Jonaid, G.*, Solares, M.J., Kaylor, L., Gray, J.L., Bator, C., Dearnaley, W.J., Spilman, M., Dressel-Dukes, M.J., Grandfield, K., McDonald Esstman, S. M., and Kelly, D.F. Advancing high-resolution imaging of virus assemblies in liquid and ice. 2022. *Journal of Visualized Experiments*, 2022 Jul (185). DOI: 10.3791/63856 [Invited]

* *Indicates equal contribution.*

Reprinted from the above-listed citation, with permission from *JoVE.* Copyright © 2022 MyJoVE Corporation.

jove JOURNAL OF VISUALIZED EXPERIMENTS
17 Sellers Street
Cambridge, MA 02139
tel. +1.617.945.9051
www.JoVE.com

Standard Manuscript Template

Advancing high-resolution imaging of virus assemblies in liquid and ice

Liza-Anastasia DiCecco[1,2*], Samantha Berry,[1*], GM Jonaid[1,3*], Maria Solares[1,4], Liam Kaylor[1,4], Jennifer Gray[5], Carol Bator[6], William J. Dearnaley[1], Michael Spilman[7], Madeline J. Dressel-Dukes[8], Kathryn Grandfield[2], Sarah M. McDonald Esstman[9], and Deborah F. Kelly[1,5,6**]

[1.] Department of Biomedical Engineering, Pennsylvania State University, University Park, PA, 16802, USA.

[2.] Department of Materials Science and Engineering, McMaster University, Hamilton, ON, L8S 4L8, Canada

[3.] Bioinformatics and Genomics Graduate Program, Huck Institutes of the Life Sciences, Pennsylvania State University, University Park, PA, 16802, USA.

[4.] Molecular, Cellular, and Integrative Biosciences Graduate Program, Huck Institutes of the Life Sciences, Pennsylvania State University, University Park, PA, 16802, USA.

[5.] Materials Research Institute, Pennsylvania State University, University Park, PA, 16802, USA.

[6.] Huck Institutes of the Life Sciences, Pennsylvania State University, University Park, PA, 16802, USA.

[7.] Applications team, Direct Electron, LP, San Diego, CA 92128, USA

[8.] Application Scientist, Protochips, Inc., Morrisville, NC 27560, USA

[9.] Department of Biology, Wake Forest University, Winston-Salem, NC 27109, USA

* These authors contributed equally to the work.

** Correspondence to: Deborah F. Kelly, Pennsylvania State University, University Park, PA, USA; email: Debkelly@psu.edu ; phone: (814) 865-8242

KEYWORDS: Transmission Electron Microscopy (TEM), Liquid-EM, Cryo-EM, Adeno-associated Virus, SARS-CoV-2, Rotavirus double-layered particles (DLPs), Structural Biology

SHORT ABSTRACT: Here we describe protocols to prepare virus assemblies suitable for Liquid-EM and Cryo-EM analysis at the nanoscale using transmission electron microscopy.

LONG ABSTRACT: Interest in liquid-Electron Microscopy (liquid-EM) has skyrocketed in recent years as scientists can now observe real-time processes at the nanoscale. It is extremely desirable to pair high-resolution cryo-EM information with dynamic observations as many events occur at rapid timescales – in the millisecond range or faster. Improved knowledge of flexible structures can also assist in the design of novel reagents to combat emerging pathogens, such as SARS-CoV-2. More importantly, viewing biological materials in a fluid environment provides a unique glimpse of their performance in the human body. Here we present newly developed methods to investigate the nanoscale properties of virus assemblies in liquid and vitreous ice. To accomplish this goal, we used well-defined samples as model systems. Side-by-side comparisons of sample preparation methods and representative structural information are presented. Sub-nanometer features are shown for structures resolved in the range of ~3.5 Å – 10 Å. Other recent results that support this complementary framework include dynamic insights of vaccine candidates and antibody-based therapies imaged in liquid. Overall, these correlative applications advance our ability to visualize molecular dynamics, providing a unique context for their use in human health and disease.

INTRODUCTION:

Biomedical research improves our understanding of human health and disease through the development of new technologies. High-resolution imaging is transforming our view of the nanoworld – permitting us to study cells and molecules in exquisite detail[1–5]. Static information of dynamic components such as soft polymers, protein assemblies or human viruses reveals only a limited snapshot of their complex narrative. To better understand how molecular entities operate, their structure and function must be jointly investigated.

Recent advances in the production of materials such as atomically thin graphene or silicon-based microchips provide new opportunities for real-time structure-function analysis using transmission electron microscopes (TEMs). These materials can create hermetically sealed chambers for live EM imaging[6–11]. The new field of liquid-EM, the room temperature correlate to cryo-EM, provides unprecedented views of hard or soft materials in solution, allowing scientists to simultaneously study the structure and dynamics of their specimen. Liquid-EM applications include real-time recordings of therapeutic nanoparticles interacting with cancer stem cells as well as changes in the molecular intricacies of viral pathogens[12–14].

Just as methodological advances spurred the "resolution revolution" in the cryo-EM field, new techniques and methods are needed to extend the use of liquid-EM as a high-throughput tool for the scientific community. The overall goal of the methods presented here is to streamline liquid-EM specimen preparation protocols. The rationale behind the developed techniques is to employ new microchip designs and autoloader devices, suitable for both liquid- and cryo-EM data

collection (Fig. 1)[7,14–17]. The assemblies are mechanically sealed using standard grid clips for automated instruments, like the Titan Krios (Thermo Fisher Scientific) which can accommodate multiple samples per session or a Talos F200C TEM (Thermo Fisher Scientific) (Fig. 2). This methodology expands the use of high-resolution imaging beyond standard Cryo-EM applications demonstrating broader purposes for real-time materials analysis.

In the current video article, we present protocols for preparing virus assemblies in liquid with and without commercially available specimen holders. Using the Poseidon Select system (Protochips, Inc.), we show that thin liquid specimens provide structural information comparable with Cryo-EM samples, as well as dynamic insights. We also demonstrate methods for preparing liquid specimens using autoloader tools for high-throughput routines. The *major advantage over other techniques* is that automated specimen production allows the user to quickly assess their samples for optimum thickness and electron dosage prior to data collection. This screening technique quickly identifies ideal areas for real-time recordings in liquid or ice[12,14,18,19]. For purposes of 3D structure determination, liquid-EM may compete with the long-establish cryo-EM methods implemented in cryo-EM. Readers employing conventional TEM or cryo-EM technologies may consider using liquid-EM workflows to provide new, dynamic observations of their samples in a manner that complements their current strategies.

PROTOCOL:

1. **Load the Poseidon Select System for Liquid-EM**

   1.1) Clean the silicon nitride (SiN) microchips (Protochips, Inc.) by incubating each chip in 150 ml of acetone for 2 minutes then 150 ml of methanol for 2 minutes. Allow chips to dry under laminar air flow.

   1.2) Plasma clean the dried chips using a glow-discharge instrument such as a Pelco EasiGlow (Ted Pella, Inc.) operating under standard conditions for 45 seconds using Argon gas.

   1.3) Load a dry base microchip into the tip of Poseidon Select specimen holder. Add ~0.2 µL of sample solution to the base chip. Following a 1 - 2 minutes incubation step, add the top chip to the wet bottom chip containing the sample.

   1.3) Clamp the assembly together to form a hermetically sealed enclosure, held in place mechanically by 3 brass screws.

   1.4) Upon sealing the assembly, the tip of the holder is pumped to 10^{-6} Torr using a turbo-pumped dry pumping station (Gatan, Inc.). The holder is now ready to be inserted into the TEM.

2. Produce Microchip Sandwich Assemblies

2.1) Different SiN or silicon dioxide (SiO) microchips (Simpore Inc.) can be used directly from the shipped gel packs. Carbon-coated gold grids may also be used directly as supplied (Electron Microscopy Sciences).

2.2) Plasma clean the microchips and EM grids using a Pelco EasiGlow (Ted Pella, Inc.) operating under standard conditions for 45 seconds using Argon gas.

2.3) Add ~2 μL of sample solution to a glow-discharged microchip placed on a gel pack. Excess solution may be removed with Whatman #1 filter paper. Following a 1 - 2 minutes incubation step, add the glow-discharged carbon grid to the wet microchip containing the sample.

2.4) Clamp the assembly together using a single-tilt specimen holder or autoloader grid clips at room temperature to form a hermetically sealed enclosure.

3. Imaging Specimens using a Transmission Electron Microscope

Liquid-EM imaging – Talos F200C

3.1) Load the specimen holder into the Talos F200C TEM equipped with a field-emission gun (FEG) and operating at 200 kV.

3.2) Turn on the gun and adjust the eucentric height of the microscope stage with respect to the specimen by using the wobbler function, tilting the sample from -15° to +15° in the column. This procedure adjusts the stage in the Z-direction to accommodate the sample thickness. This step also helps ensure an accurate magnification during image recording.

3.3) Images may be recorded as long-framed movies using the *In Situ* software package integrated with a DirectView direct detector (Direct Electron) having a pixel spacing of 6 μm. Individual images may also be recorded using the SerialEM software package[20], implementing automated imaging routines. Images are recorded under low-dose conditions using the DirectView detector at magnifications ranging from 28,000x - 92,000x and 40 frames per second. Exposure times (0.25 – 1 second) are adjusted to minimize beam damage to the specimen.

3.4) Use a defocus range of -1 – 4 μm at the specified magnification. If thick solution is encountered, use higher defocus values or select a different region of interest.

3.5) To ensure solution is present in the samples throughout the imaging session, focus the electron beam until bubbles are formed in a sacrificial area not used for data collection.

Cryo-EM imaging – Titan Krios

3.6) Load the clipped EM grids (Quantifoil) or microchip sandwiches into the Titan Krios TEM equipped with a FEG and operating at 300 kV.

3.7) Turn on the gun and adjust the eucentric height of the microscope stage, using a similar procedure described for the Talos F200C.

3.8) Individual images are recorded using the EPU software system (Thermo Fisher Scientific) integrated within the microscope system while implementing automated imaging routines. Images are recorded under low-dose conditions using the Falcon 3EC direct detector (Thermo Fisher Scientific) having a pixel spacing of 14 μm at a magnification of 59,000x and 40 frames per second.

3.9) Use a defocus range of -1 – 4 μm at the specified magnification. If thick layers of vitreous ice are encountered, use higher defocus values or select a different region for data collection.

4. Data analysis and 3D structure comparisons

Adeno-associated virus (AAV) in liquid and vitreous ice

4.1) Movies for AAV particles in liquid and ice were processed using RELION-3.08[21] and cryoSPARC 2.14.2[22]. Motion correction was performed using MotionCor2 v1.2.3.

4.2) Once corrected, the auto-picking tool in the RELION software package was used to extract AAV particles. Box sizes were 330 pixels for liquid specimens and 350 pixels for ice specimens.

4.3) Initial reconstructions with C1 symmetry were calculated using the RELION 3D initial model routine and for comparison using the *ab-initio* model options in the cryoSPARC software package. In RELION, a regularization parameter of *T=4* was used along with a pixel size of 1.01 Å for liquid specimens and 1.13 Å for ice specimens. A mask value of 300 Å was used throughout the refinement procedures.

4.4) Further refinement was performed in cryoSPARC with imposed I1 symmetry, yielding multiple EM maps. The highest resolution achieved was ~3.22 Å (liquid) and 3.37 Å (ice). Resolution estimates were based on the gold-standard Fourier shell correlation (FSC) criteria. Particle equivalency implementing icosahedral symmetry was 16,800 (liquid) and 15,240 (ice).

4.5) The final maps were masked at ~250 Å and examined using the Chimera software package[23,24]. In Figure 3, slices are shown in increments of ~5 nm.

4.6) Capsid protein (VP1) subunits from the liquid-EM and cryo-EM maps were extracted and compared. Dynamic changes in liquid structures were quantified and visualized using the Morph map function in Chimera.

SARS-CoV-2 sub-viral assemblies in liquid

4.7) Movies were processed using RELION-3.08. Drift and beam-induced motion were corrected using MotionCor2 v1.2.3 and CTFFIND4 was used to correct for the contrast transfer function (CTF) of the microscope.

4.8) The auto-picking tool in RELION was used to select viral assemblies using a box size of 800 pixels. For computational efficiency, extracted particles were rescaled to 256 pixels.

4.9) An initial model was obtained using C1 symmetry in RELION with a regularization parameter of *T=2* and 1.66 Å pixel size. No masking was applied at this step.

4.10) Additional 3D refinement was performed using C2 symmetry, yielding a final map resolved at 8.25 Å according to gold standard FSC criteria. Using C2 symmetry, the particle equivalency was 2,674.

4.11) The final EM map was visualized using Chimera with slices incremented at 25 nm in Figure 4.

Rotavirus double-layered particles (DLPs) in vitreous ice

4.12) Movies for rotavirus DLPs in ice were processed using cryoSPARC 2.14.2. Motion correction was performed using MotionCor2 v1.2.3 and Patch CTF Estimation was used to correct the images.

4.13) The template-based auto-picking tool in cryoSPARC was used to extract DLPs with a box size of 950 pixels down-sampled by ¾ to a box size of 712 for computing purposes

4.14) Initial models were calculated using *ab-initio* options and C1 symmetry in cryoSPARC. Refinement parameters included a pixel size of 1.47 Å and a mask value of 800 Å that was used during subsequent refinement procedures.

4.15) Additional refinement routines were performed in cryoSPARC while imposing I1 symmetry, yielding a final map of 10.15-Å resolution according to the gold-standard FSC criteria. Particle equivalency implementing icosahedral symmetry was 123,000.
4.16) The final maps were masked at ~750 Å and visualized using the Chimera software package. In Figure 5, slices are shown in increments of ~10 nm.

REPRESENTATIVE RESULTS:

A Talos F200C TEM operating at 200 kV was used for all liquid-EM imaging experiments and a Titan Krios operating at 300 kV was used for all cryo-EM data collection. Representative images and structures of multiple viruses are presented to demonstrate the utility of the methods across various test subjects. Here, we employed recombinant adeno-associated virus subtype 3 (AAV), SARS-CoV-2 sub-viral assemblies derived from the patient serum (RayBiotech, Inc.), and simian rotavirus double-layered particles (DLPs), SA11 strain. First, we demonstrated structural comparisons of the same AAV sample (1 mg/mL) imaged in liquid buffer solution (50 mM HEPES, pH, 7.5; 150 mM NaCl; 10 mM $MgCl_2$; 10 mM $CaCl_2$) and in vitreous ice (Fig. 3A-C). The liquid-EM samples were prepared using SiN-based microchips and the Poseidon Select system (Protochips, Inc). The cryo-EM samples were prepared using standard holey carbon grids (Quantifoil) and vitrified using a Mark IV Vitrobot (ThermoFisher Scientific). Resulting virus structures had similar overall diameters of ~25 nm. A comparison of individual VP1 capsid protomers also showed consistent features in both liquid and ice EM maps (Fig. 3D). One difference between the liquid-EM and cryo-EM data was that additional dynamic structures were observed in liquid that were not present in the cryo-EM results (Fig. 3E)[12].

Next, we examined deactivated SARS-CoV-2 samples (0.25 mg/mL) prepared in buffer solution (50 mM HEPES, pH, 7.5; 150 mM NaCl; 10 mM $MgCl_2$; 10 mM $CaCl_2$) using a new microchip sandwich technique[7,14]. The new technique employs SiN-based microchips (Simpore, Inc) along with carbon-coated gold grids (Electron Microscopy Sciences). In this preparation, the liquid sample was sandwiched between the two substrates (Fig. 2A-C). Sandwiched specimens were clamped with a single-tilt specimen holder or autoloader clips commonly used in cryo-EM sample preparation. Samples can be viewed immediately in the TEM or stored at 4 °C for up to one week, depending upon the stability of the biological specimen. The appearance of bubbling in the liquid samples ensures the presence of the liquid layer. Liquid thickness can be measured using EF-TEM protocols as previously described.[12] SARS-CoV-2 sub-viral assemblies in liquid appeared to have high visible contrast with respect to the surrounding liquid (Fig. 4 A, B). Class averages and slices through the 8.25-Å structure showed internal features within the particles comprised of protein subunits and the viral RNA genome (Fig. 4C).

Finally, we analyzed rotavirus DLPs (3 mg/mL; 50 mM HEPES, pH, 7.5; 150 mM NaCl; 10 mM $MgCl_2$; 10 mM $CaCl_2$) in vitreous ice by manually flash-freezing microchip sandwich preparations. The same sandwich technique used to produce liquid-EM samples was employed for frozen-hydrated specimens. Sandwiches were sealed with autoloader grid clips and examined using the Titan Krios under standard conditions. Low-magnification views of the frozen specimens showed little to no cubic or hexagonal ice contamination and regions of densely packed DLPs were observed throughout the viewing windows (Fig. 5A, B). Images were collected using automated routines implemented in the EPU package. Class averages and slices through the 10.15-Å map revealed stable features consistent with viral protein components and the double-stranded RNA genome (Fig. 5D, E). The contrast difference between the DLPs and the ice background was not as visibly strong in the cryo-EM images compared with the liquid-EM samples. While we are still

working to determine the cause of this interesting effect, it is worth noting the difference as liquid-EM may offer future advantages for the imaging community.

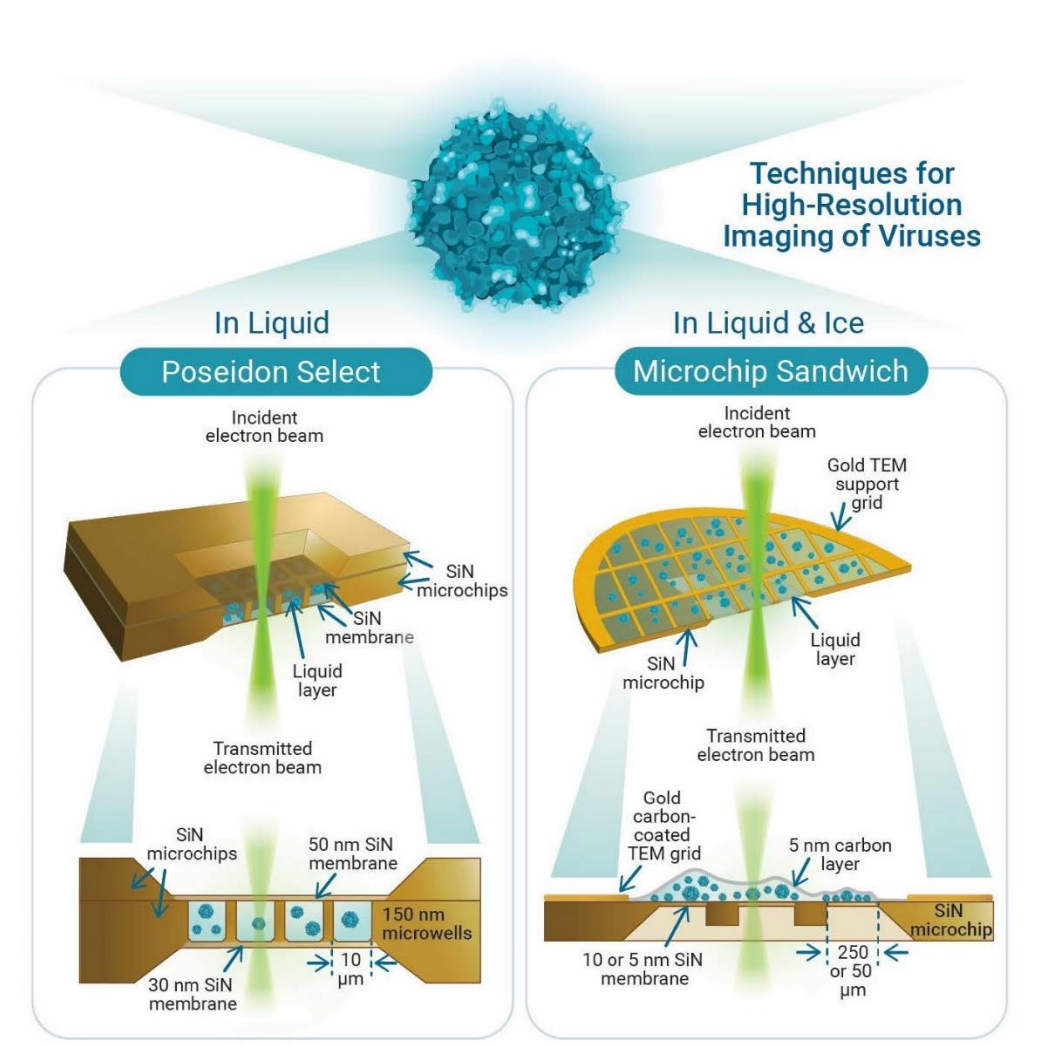

Figure 1. Techniques used for high-resolution imaging of viruses in liquid and in ice. The two workflows highlight different Liquid-EM sample preparation methods. The left panel shows a schematic representation of the Poseidon Select system. The SiN base microchip includes an array (500 µm x 100 µm) of integrated microwells (10 µm x 10 µm) that are ~ 150 nm in-depth with a ~30 nm-thick membrane. The right panel presents a schematic of the microchip sandwich technique, which can be used for both liquid-EM and cryo-EM research. The sandwich assemblies use a SiN microchip paired with a carbon-coated gold TEM grid. A cross-section of the assembly indicates nine imaging windows ranging from 250 µm x 250 µm to 50 µm x 50 µm in size with membrane thicknesses of 10 nm or 5 nm, respectively. The carbon support film is ~5 nm thick.

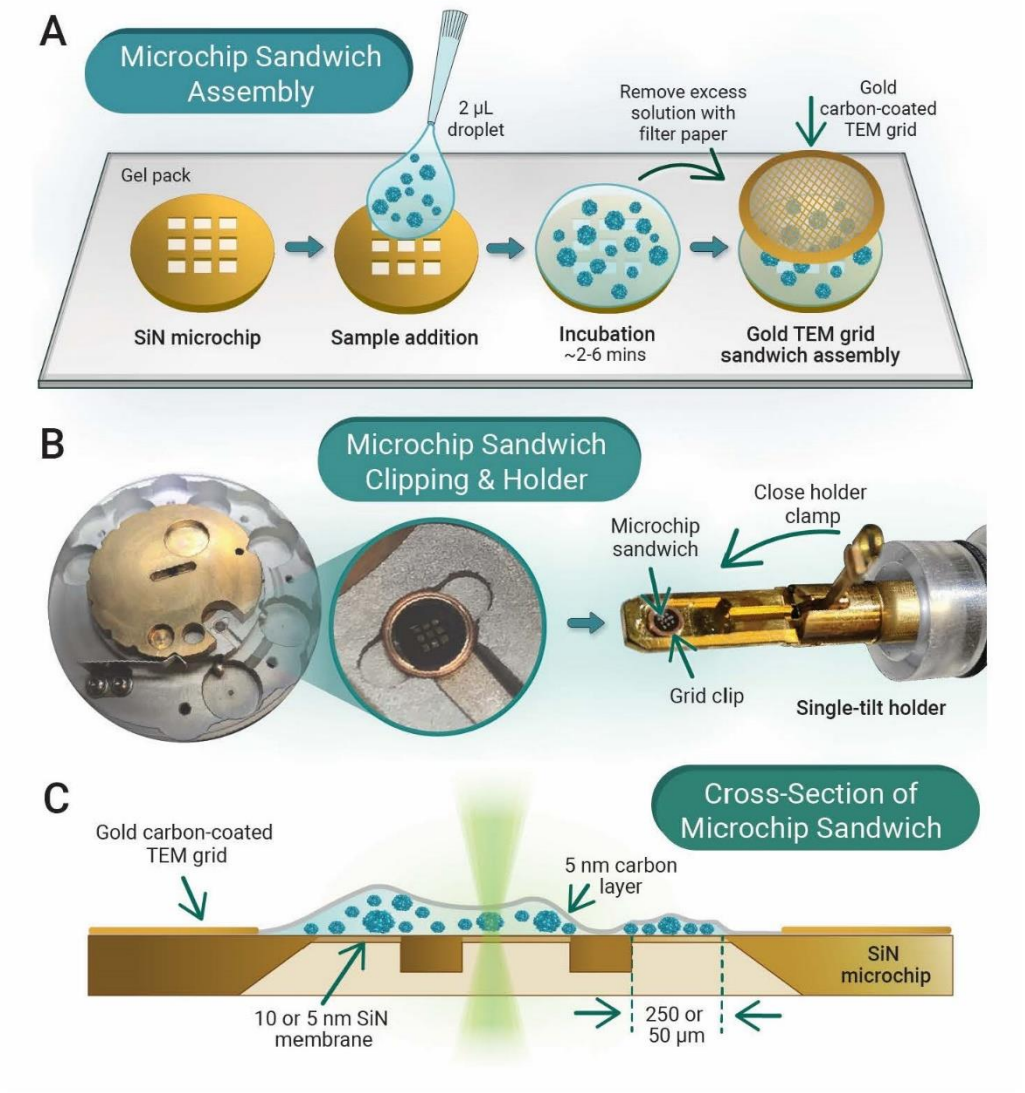

Figure 2. The microchip sandwich technique for liquid-EM and cryo-EM. (A) The microchip sandwich assembly uses a SiN microchip (Simpore, Inc.) paired with a carbon-coated gold TEM grid. A glow-discharged microchip is placed on a gel pack and virus samples are added to the microchip. After a brief incubation period, excess solution is removed, and the sandwich is sealed with the TEM grid. **(B)** The microchip sandwich is sealed in a clipping device at room temperature and can be loaded directly into a single-tilt TEM holder or a TEM autoloader system. **(C)** Cross-section drawings of the microchip sandwich assembly highlight the dimensions of the microchips and carbon layer.

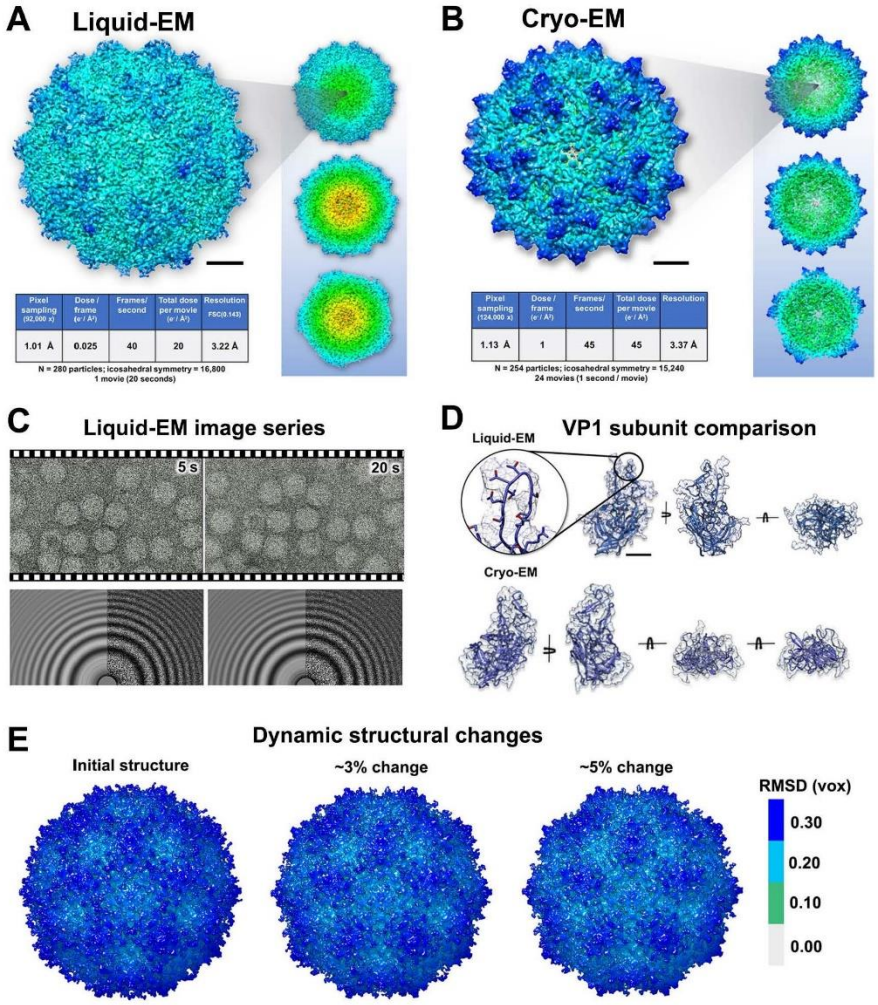

Figure 3. Comparison of liquid-EM and cryo-EM structures of AAV. (A) Structure of AAV in solution (3.22 Å resolution) with colored radial densities showing 5-nm slices through the map. Scale bar is 5 nm. Imaging metrics are for data acquisition using the DirectView direct detector. **(B)** Structure of AAV imaged in ice (3.37 Å resolution) with colored radial densities represent 5-nm slices through the structure. Scale bar is 5 nm. Imaging metrics are for data acquisition using the Falcon 3EC direct detector. **(C)** A region of interest shows 5-second and 20-second time points along with Fourier transforms calculated at different time points. Left side shows CTF estimates, right side shows the experimental data. **(D)** Rotational views of the AAV VP1 subunit extracted from the liquid and ice structures. The segments were interpreted using the crystal structure (PDB code 3KIC, A chain[25]). Scale bar is 10 Å. **(E)** Dynamic values in the liquid structures generated using the morph map function in Chimera. From left to right, structures show conformational changes with a corresponding ~5% diameter change, measured using EM data. RMSD values in voxels indicate changes according to the color scale. *Adapted from Jonaid et al. (2021)*[12].

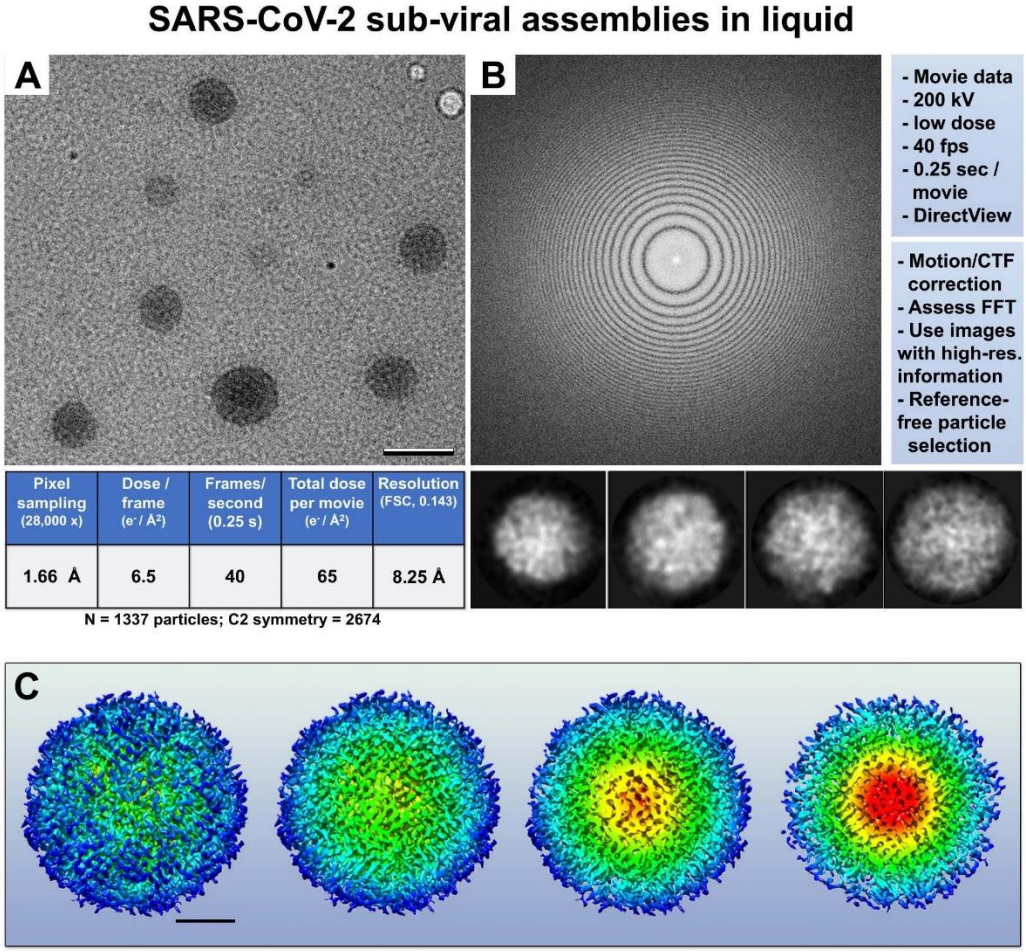

Figure 4. SARS-CoV-2 sub-viral assemblies prepared in liquid using the microchip sandwich technique. (A) Image of SARS-CoV-2 sub-viral assemblies isolated from serum fractions from COVID-19 patients (RayBiotech, Inc.). Imaging metrics are for data acquisition using the DirectView direct detector. White bubbles in the top right corner of the image are a visual indicator that liquid is present in the sample. Scale bar is 100 nm. **(B)** Calculated Fourier transform of the image shows high-resolution information in reciprocal space with little to no drift in the corresponding image. Class averages show unique features in the viral assemblies contained in solution. **(C)** An EM reconstruction of the sub-viral assemblies (8.25 Å resolution) is shown with colored radial densities at 5-nm slices through the map. Scale bar is 25 nm. *Adapted from Jonaid et al. (2021)*[12].

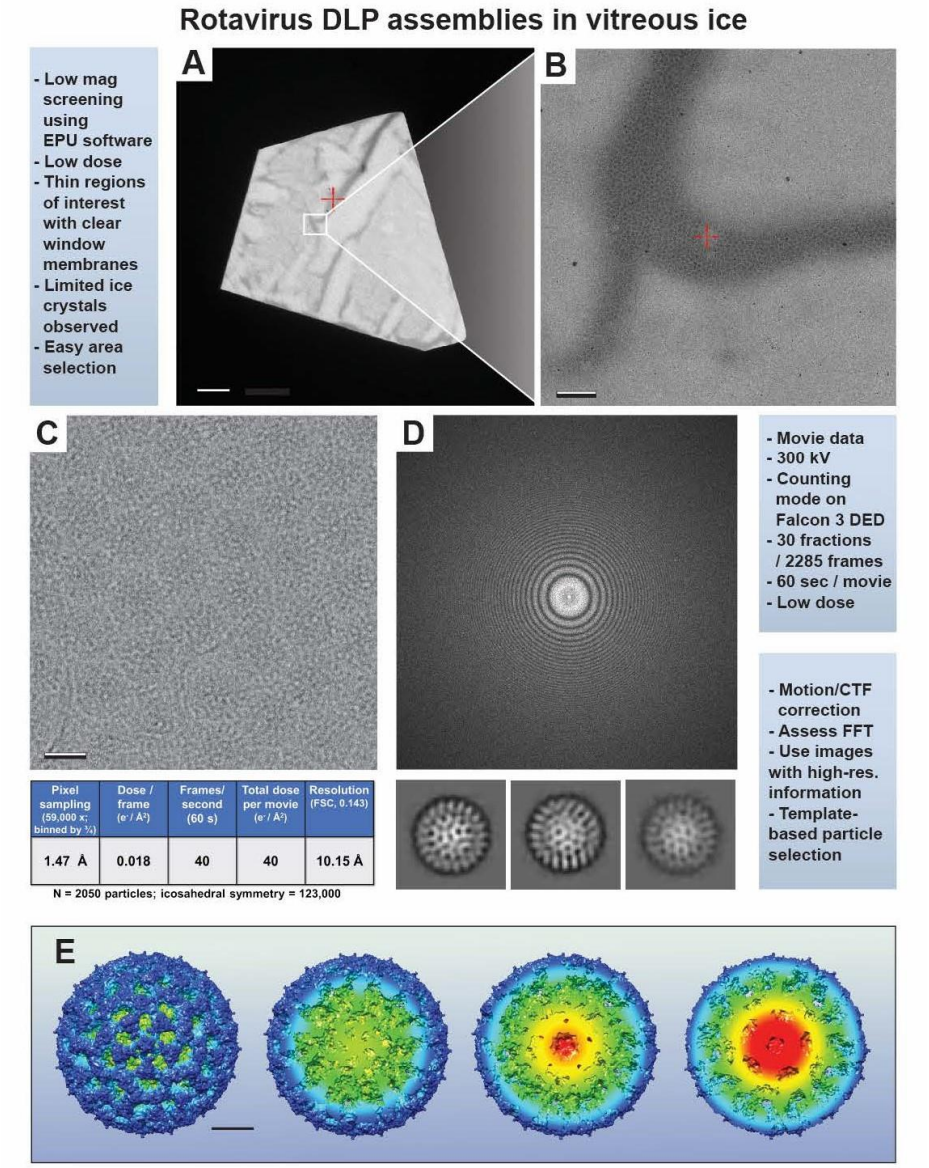

Figure 5. Rotavirus DLPs prepared in liquid using the microchip sandwich technique. (A, B) Low magnification screening steps using EPU software. Limited ice crystals were observed, and window membranes were thin and clear, simplifying area selection for data acquisition. Scale bar in (A) is 5 µm and in (B) 500 nm. **(C)** Movies were acquired using the Falcon 3EC direct electron detector in counting mode according to the indicated imaging metrics. Scale bar is 50 nm. **(D)** Fourier transform information indicates high-resolution information present in the data and class averages show strong features in the icosahedral lattice. **(E)** An EM reconstruction of the DLPs (10.15 Å resolution) is shown with colored radial densities at 10-nm slices through the map. Scale bar is 15 nm.

DISCUSSION:

Here we present new opportunities to streamline current liquid-EM workflows by using new automated tools and technologies adapted from the cryo-EM field. *Applications involving the new microchip sandwich technique are significant with respect to other methods because they enable high-resolution imaging analysis in liquid or vitreous ice*. One of the *most critical steps in the protocol* is producing specimens with the ideal liquid thickness to visualize exquisite details at the nanoscale level. Ideal regions of interest are identified at lower magnifications by screening the entire sample prior to implementing high-throughput routines for automated data collection. Should identified regions in liquid or ice specimens contain beam-damage artifacts or appear too thick to identify individual particles that are visually crisp, they should be excluded from data collection. Limitations in high-resolution data acquisition include beam-induced movement and Brownian motion in the liquid samples. Cryo-EM methods aim to minimize motion in biological samples, however, motion correction methods are computationally robust at mitigating these resolution-limiting factors. If the liquid samples present long-range drift and thermal instability, thinner samples may be prepared by removing excess solution during sample preparation steps to decrease the thickness of the liquid layers.

Molecular crowding among virus particles may result when samples are used at high concentrations. If there are multiple regions with overlapping particles in a manner that limits robust data collection, the input sample should be reduced in concentration prior to sample preparation. Having a suitable sample concentration is a *crucial step in the protocols*. Images that contain an excess of particles will complicate downstream image processing procedures. For purified virus particles, an adequate concentration range is between 0.3 – 3 mg / mL, depending on the dimensions and molecular weight of the sample. Larger viruses (~100 nm diameter or greater) typically require higher concentrations than do smaller viruses (~25 nm diameter or lesser) for the success of the technique. Another factor to consider is the level at which the particles of interest adhere to the glow-discharged microchips. If the virus sample does not adhere well to the surface, a greater concentration may be needed to adequately prepare specimens for Liquid-EM or Cryo-EM. Alternatively, the sample can instead be applied to the carbon-coated gold grid with the microchip serving as the lid of the enclosure. Should these procedures fail to recruit sufficient particles for data collection procedures, affinity capture methods may present a viable option[26–28].

The use of certain additives such as detergents, glycerol, polyethylene glycols, and high levels of sucrose or glucose should be minimized or avoided for liquid-EM imaging. These reagents may introduce artifacts in the images as well as create excessive bubbling, hydrolysis products and free radicals due to beam damage. Such effects lead to muted features in the imaged particles and ultimately limit structural resolution. One way to remove these reagents if they are used in biochemical preparations is through extensive dialysis into a buffer solution lacking the additives. These reagents will need to be tested and used on a case-by-case basis. Moreover, once sufficient specimens have been produced using the microchip sandwich technique, they may be imaged right away or stored at 4 °C until ready to examine. Storage times depend upon sample stability.

Overall, using liquid-EM in combination with cryo-EM permits researchers to examine biological systems with complementary imaging tools. The newly developed microchip sandwich technique yields consistent samples for TEM imaging in liquid or ice. The technique also provides a simple means for researchers to prepare and view specimens without the need for a commercial sample holder or vitrification system. In combination with automated imaging protocols, large amounts of data on the order of thousands of images per session may be acquired per specimen. The pioneering work of Parsons and colleagues[29–33] laid the foundational groundwork for producing biological specimens in liquid enclosures. The protocols presented here describe how state-of-the-art tools can now provide an exciting means to visualize biological macromolecules through new eyes. Future applications that are expected to result from mastering these techniques, when paired with high-performance computing, are real-time mechanistic insights for understanding structure-function relationships in 3D. We anticipate the liquid-EM field may elevate research on novel viruses that pose a threat to human health, perhaps even contributing to pandemic preparedness measures. In summary, the use of these protocols should permit scientists and engineers to better study dynamic processes at atomic detail, across a large variety of samples encompassing life sciences, medicine and materials research.

DISCLOSURES

- The authors declare that they have no competing financial interests.
- The author, Madeline J. Dressel-Dukes, is an employee of Protochips, Inc. and Michael Spilman is an employee of DirectElectron.

ACKNOWLEDGEMENTS

The authors acknowledge Dr. Luk H. Vandenberghe (Harvard Medical School, Department of Ophthalmology) for providing purified AAV-3. This work was supported by the National Institutes of Health and the National Cancer Institute [R01CA193578, R01CA227261, R01CA219700 to D.F.K.].

REFERENCES

1. Deng, W. *et al.* Assembly, structure, function and regulation of type III secretion systems. *Nat Rev Microbiol* 15, 323–337 (2017).

2. Oikonomou, C. M., Chang, Y.-W. & Jensen, G. J. A new view into prokaryotic cell biology from electron cryotomography. *Nat Rev Microbiol* 14, 205–220 (2016).

3. Murata, K. & Wolf, M. Cryo-electron microscopy for structural analysis of dynamic biological macromolecules. *Biochimica Et Biophysica Acta Bba - Gen Subj* 1862, 324–334 (2018).

4. DiMaio, F. *et al.* Atomic accuracy models from 4.5 Å cryo-electron microscopy data with density-guided iterative local refinement. *Nat Methods* 12, 361–365 (2015).

5. Frank, J. *et al.* A model of protein synthesis based on cryo-electron microscopy of the E. coli ribosome. *Nature* 376, 441–444 (1995).

6. Dukes, M. J., Gilmore, B. L., Tanner, J. R., McDonald, S. M. & Kelly, D. F. In situ TEM of Biological Assemblies in Liquid. *J Vis Exp* 50936 (2013) doi:10.3791/50936.

7. Dearnaley, W. J. *et al.* Liquid-Cell Electron Tomography of Biological Systems. *Nano Lett* 19, 6734–6741 (2019).

8. Park, J. *et al.* Direct Observation of Wet Biological Samples by Graphene Liquid Cell Transmission Electron Microscopy. *Nano Lett* 15, 4737–4744 (2015).

9. Chen, Q. *et al.* 3D Motion of DNA-Au Nanoconjugates in Graphene Liquid Cell Electron Microscopy. *Nano Lett* 13, 4556–4561 (2013).

10. Yuk, J. M. *et al.* High-Resolution EM of Colloidal Nanocrystal Growth Using Graphene Liquid Cells. *Science* 336, 61–64 (2012).

11. Wang, X., Yang, J., Andrei, C. M., Soleymani, L. & Grandfield, K. Biomineralization of calcium phosphate revealed by in situ liquid-phase electron microscopy. *Commun Chem* 1, 80 (2018).

12. Jonaid, G. *et al.* High-Resolution Imaging of Human Viruses in Liquid Droplets. *Adv Mater* 33, 2103221 (2021).

13. Pohlmann, E. S. *et al.* Real-Time Visualization of Nanoparticles Interacting with Glioblastoma Stem Cells. *Nano Lett* 15, 2329–2335.

14. Jonaid, G. M. *et al.* Automated Tools to Advance High-Resolution Imaging in Liquid. *Microsc Microanal* 1–10 (2022) doi:10.1017/s1431927621013921.

15. Varano, A. C. *et al.* Customizable Cryo-EM Chips Improve 3D Analysis of Macromolecules. *Microsc Microanal* 25, 1310–1311 (2019).

16. Alden, N. A. *et al.* Cryo-EM-On-a-Chip: Custom-Designed Substrates for the 3D Analysis of Macromolecules. *Small* 15, 1900918 (2019).

17. Tanner, J. R. *et al.* Cryo-SiN – An Alternative Substrate to Visualize Active Viral Assemblies. *J Anal Mol Techniques* 1, (2013).

18. Solares, M. J. *et al.* Microchip-Based Structure Determination of Disease-Relevant p53. *Anal Chem* 92, 15558–15564 (2020).

19. Casasanta, M. A. *et al.* Microchip-based structure determination of low-molecular weight proteins using cryo-electron microscopy. *Nanoscale* 13, 7285–7293 (2021).

20. Mastronarde, D. N. Advanced Data Acquisition From Electron Microscopes With SerialEM. *Microsc Microanal* 24, 864–865 (2018).

21. Scheres, S. H. W. RELION: Implementation of a Bayesian approach to cryo-EM structure determination. *J Struct Biol* 180, 519–530 (2012).

22. Punjani, A., Rubinstein, J. L., Fleet, D. J. & Brubaker, M. A. cryoSPARC: algorithms for rapid unsupervised cryo-EM structure determination. *Nat Methods* 14, 290–296 (2017).

23. Pettersen, E. F. *et al.* UCSF Chimera—A visualization system for exploratory research and analysis. *J Comput Chem* 25, 1605–1612 (2004).

24. Goddard, T. D., Huang, C. C. & Ferrin, T. E. Visualizing density maps with UCSF Chimera. *J Struct Biol* 157, 281–287 (2007).

25. Lerch, T. F., Xie, Q. & Chapman, M. S. The structure of adeno-associated virus serotype 3B (AAV-3B): Insights into receptor binding and immune evasion. *Virology* 403, 26–36 (2010).

26. Sharma, G. *et al.* Affinity grid-based cryo-EM of PKC binding to RACK1 on the ribosome. *J Struct Biol* 181, 190–194 (2013).

27. Kiss, G. *et al.* Capturing Enveloped Viruses on Affinity Grids for Downstream Cryo-Electron Microscopy Applications. *Microsc Microanal* 20, 164–174 (2014).

28. Degen, K., Dukes, M., Tanner, J. R. & Kelly, D. F. The development of affinity capture devices—a nanoscale purification platform for biological in situ transmission electron microscopy. *Rsc Adv* 2, 2408–2412 (2012).

29. Hui, S. W. & Parsons, D. F. Electron Diffraction of Wet Biological Membranes. *Science* 184, 77–78 (1974).

30. Hui, S. W., Parsons, D. F. & Cowden, M. Electron Diffraction of Wet Phospholipid Bilayers. *Proc National Acad Sci* 71, 5068–5072 (1974).

31. Parsons, D. F., Matricardi, V. R., Moretz, R. . C. & Turner, J. N. Electron Microscopy and Diffraction of Wet Unstained and Unfixed Biological Object. *Advances in Biological and Medical Physics* 15, 161–270 (1974).

32. Parsons, D. F. Structure of Wet Specimens in Electron Microscopy. *Science* 186, 407–414 (1974).

33. Matricardi, V. R., Moretz, R. C. & Parsons, D. F. Electron Diffraction of Wet Proteins: Catalase. *Science* 177, 268–270 (1972).

Chapter 4: Supplemental – Materials List

jove

Materials List for

Advancing High-Resolution Imaging of Virus Assemblies in Liquid and Ice

Liza-Anastasia DiCecco*[1,2], Samantha Berry*[1], G. M. Jonaid*[1,3], Maria J. Solares[1,4], Liam Kaylor[1,4], Jennifer L. Gray[5], Carol Bator[6], William J. Dearnaley[1], Michael Spilman[7], Madeline J. Dressel-Dukes[8], Kathryn Grandfield[2], Sarah M. McDonald Esstman[9], Deborah F. Kelly[1,5,6]

[1]Department of Biomedical Engineering, Pennsylvania State University [2]Department of Materials Science and Engineering, McMaster University [3]Bioinformatics and Genomics Graduate Program, Huck Institutes of the Life Sciences, Pennsylvania State University [4]Molecular, Cellular, and Integrative Biosciences Graduate Program, Huck Institutes of the Life Sciences, Pennsylvania State University [5]Materials Research Institute, Pennsylvania State University [6]Huck Institutes of the Life Sciences, Pennsylvania State University [7]Applications team, Direct Electron [8]Application Scientist, Protochips, Inc. [9]Department of Biology, Wake Forest University

*These authors contributed equally

Corresponding Author

Deborah F. Kelly
Debkelly@psu.edu

Citation

DiCecco, L.A., Berry, S., Jonaid, G.M., Solares, M.J., Kaylor, L., Gray, J.L., Bator, C., Dearnaley, W.J., Spilman, M., Dressel-Dukes, M.J., Grandfield, K., McDonald Esstman, S.M., Kelly, D.F. Advancing High-Resolution Imaging of Virus Assemblies in Liquid and Ice. *J. Vis. Exp.* (185), e63856, doi:10.3791/63856 (2022).

Date Published

July 20, 2022

DOI

10.3791/63856

URL

jove.com/video/63856

Materials

Name	Company	Catalog Number	Comments
Acetone	Fisher Scientific	A11-1	1 Liter
Autoloader clipping tool	ThermoFisher Scientific	N/A	Also SubAngstrom supplier
Autoloader grid clips	ThermoFisher Scientific	N/A	top and bottom clips
Carbon-coated gold EM grids	Electron Microcopy Sciences	CF400-AU-50	400-mesh, 5-nm thickness
COVID-19 patient serum	RayBiotech	CoV-Pos-S-500	500 microliters of PCR+ serum
Methanol	Fisher Scientific	A412-1	1 Liter
Microwell-integrad microchips	Protochips, Inc.	EPB-42A1-10	10x10-mm window arrays
TEMWindows microchips	Simpore Inc.	SN100-A10Q33B	9 large windows, 10-nn thick
TEMWindows microchips	Simpore, Inc.	SN100-A05Q33A	9 small windows, 5-nm thick
Top microchips	Protochips, Inc.	EPT-50W	500 mm x 100 mm window
Whatman #1 filter paper	Whatman	1001 090	100 pieces, 90 mm
Equipment			
DirectView direct electron detector	Direct Electron		6-micron pixel spacing
Falcon 3 EC direct electron detector	ThermoFisher Scientific		14-micron pixel spacing
Gatan 655 Dry pump station	Gatan, Inc.		Pump holder tip to 10^{-6} range
Mark IV Vitrobot	ThermoFisher Scientific		state-of-the-art specimen preparation unit
PELCO easiGlow, glow discharge unit	Ted Pella, Inc.		Negative polarity mode
Poseidon Select specimen holder	Protochips, Inc.		FEI compatible;specimen holder
Talos F200C TEM	ThermoFisher Scientific		200 kV; Liquid-TEM

Copyright © 2022 JoVE Journal of Visualized Experiments

Titan Krios G3	ThermoFisher Scientific		300 kV; Cryo-TEM
Freely available software	**Website link**		**Comments (optional)**
cryoSPARC	https://cryosparc.com/		other image processing software
CTFFIND4	https://grigoriefflab.umassmed.edu/ctffind4		CTF finding program
MotionCorr2	https://emcore.ucsf.edu/ucsf-software		
RELION	https://www3.mrc-lmb.cam.ac.uk/relion/index.php?title=Main_Page		
SerialEM	https://bio3d.colorado.edu/SerialEM/		
UCSF Chimera	https://www.cgl.ucsf.edu/chimera/		molecular structure analysis software package

Copyright © 2022 JoVE Journal of Visualized Experiments

Chapter 5: Liquid Transmission Electron Microscopy for Probing Collagen Biomineralization

5.1 Section Introduction (Objective iii)

For mineralized tissues such as bone, collagen biomineralization processes are essential for their formation and maintenance. However, while studied extensively in research, the mineralization mechanisms behind these nanoscale processes are highly debated with many different contributing theories proposed in literature based on time-stamped observations. Liquid TEM provides a new way for theories behind collagen mineralization to be tested through real-time visualization. As outlined in the objectives, in Chapter 5 the newly developed thin-film enclosure featured in Chapter 4 was applied to study collagen biomineralization processes. A murine-derived collagen mineralization model was used with a CaP and pAsp solution to promote intrafibrillar mineralization. Using the liquid enclosure, HR details of collagen mineralization processes were revealed in liquid conditions, where direct electron detector automated acquisition provided high-throughput, low-dose imaging capabilities. Dynamic interactions were however not captured within this enclosure, theorized to be a result of confinement effects, lack of heating functionality, and cumulative beam damage. However, the first-time liquid TEM imaging of collagen mineralization progression provided unparalleled resolution into the natively hydrated structures. Amorphous precursors were noted in early mineralization while at more mature mineralization crystalline mineral platelets were observed along fibril lengths. Overall, this work contributes a new, facile liquid imaging approach that can be used for exploring collagen biomineralization and other biological systems, expanding our understanding of complex biological processes.

Authors: **Liza-Anastasia DiCecco**, Ruixin Gao, Deborah F. Kelly, Eli D. Sone, Kathryn Grandfield.

Publication: This work is to be submitted in 2023.

Liquid Transmission Electron Microscopy for Probing Collagen Biomineralization

Liza-Anastasia DiCecco[1], Ruixin Gao[2], Jennifer L. Gray[3], Deborah F. Kelly[3-5], Eli D. Sone[2,6,7], Kathryn Grandfield[1,8*]

[1] Department of Materials Science and Engineering, McMaster University, Hamilton, ON, Canada
[2] Institute of Biomedical Engineering, University of Toronto, Toronto, ON, Canada
[3] Materials Research Institute, Pennsylvania State University, University Park, PA, USA.
[4] Department of Biomedical Engineering, Pennsylvania State University, University Park, PA, USA.
[5] Center for Structural Oncology, Pennsylvania State University, University Park, PA, USA.
[6] Faculty of Dentistry, University of Toronto, Toronto, ON, Canada
[7] Department of Materials Science and Engineering, University of Toronto, Toronto, ON, Canada
[8] School of Biomedical Engineering, McMaster University, Hamilton, ON, Canada

* Co-corresponding author:
Prof. Kathryn Grandfield
McMaster University
1280 Main Street West
Hamilton, Ontario L8S 4L7, Canada
Email: kgrandfield@mcmaster.ca

* Co-corresponding author:
Prof. Eli D. Sone
University of Toronto
184 College Street
Toronto, Ontario M5S 3E4, Canada
Email: eli.sone@utoronto.ca

Keywords: Liquid Electron Microscopy; Collagen Mineralization; Calcium Phosphate; Polyaspartic Acid; Hard Tissues

5.2. Abstract

Collagen biomineralization is foundational to hard tissue assembly. While studied extensively, collagen mineralization processes are not fully understood as the majority of theories are derived from electron microscopy (EM) in static, dehydrated, or frozen conditions, unlike the liquid environment where mineralization occurs dynamically. Herein, novel liquid transmission EM (TEM) strategies are presented, where collagen mineralization was explored in hydrated liquid conditions for the first time. Custom thin-film enclosures were employed to visualize the mineralization of reconstituted collagen fibrils in a calcium-phosphate and polyaspartic acid solution to promote intrafibrillar mineralization. TEM highlighted that at early time points, precursor mineral particles attached to collagen and progressed to crystalline mineral platelets aligned with fibrils at later time points. This aligns with current theories and validates this liquid TEM approach. This work provides a new liquid imaging approach for exploring collagen biomineralization, advancing toward understanding disease pathogenesis and remineralization strategies for hard tissues.

Liquid Transmission Electron Microscopy for Probing Collagen Mineralization

5.3. Introduction

Biomineralization is key to the formation and maintenance of mineralized tissues found in the musculoskeletal system of vertebrates, such as bones and teeth[1]. Bone is a biocomposite made primarily of calcium phosphate (CaP) mineral phase, known as hydroxyapatite, an organic phase consisting mainly of type I collagen and non-collagenous proteins (NCPs), and water.[2] Notably, the distribution and extent of CaP among collagen fibrils are fundamental to the mechanical strength of mineralized tissues.[3,4] Understanding the pathways behind collagen mineralization in tissues is thus significant for medical advancements; both to shed light on disease pathogenesis, such as periodontitis and osteoporosis, and to provide new insights for designing regenerative materials and treatment pathways.[5–7]

Although collagen biomineralization has been studied extensively,[8–14] it is yet to be fully understood and well-controlled synthetically. Type I collagen is found prominently in hard tissues and formed of a triple helix of peptide chains rich in amino acids glycine, proline, and hydroxyproline.[15] The Type I collagen molecule is approximately 300 nm in length and 1.23 nm in width and in mineralized tissues like bone, they bundle together into fibrils with a repeating periodicity[11] of 67 nm, with characteristic gap and overlap zones of 40 nm and 27 nm, respectively.[8,11] These gap and overlap zones play a key role in biomineralization, where CaP mineral nucleates preferentially within gap regions,[9,16–18] but can also grow outwards into overlap regions.[9,11,18] The unique structure of these fibrils combined with the presence of NCPs are believed to actively contribute to the biomineralization of collagen.[9] A significant portion of mineral can be found between (interfibrillar) and outside (extrafibrillar) of collagen fibrils as well.[12,19,20]

For tissue regeneration applications, imitating this complex biomineralization behaviour of native collagen is key for engineering synthetic biomaterial models of similar structure, composition, and mechanical properties to facilitate tissue restoration.[7] This has been achieved *in vitro* with the use of organic macromolecules to replace the role of NCPs in templating mineral formation.[9] One such additive includes polyaspartic acid (pAsp), a synthetic mimic of NCPs believed to facilitate intrafibrillar collagen mineralization found in native mineralized tissues.[21,22] pAsp is an established additive in *in vitro* collagen mineralization models, where its highly disordered structure is theorized to act as a nucleation inhibitor of CaP in solution.[9,23,24] One theory suggests that pAsp sequesters mineral precursor, forming a negatively charged structure that interacts with the positively charged gap-zone C-terminus to mediate intrafibrillar mineralizatio.[26]

Limited by the technologies available to probe it directly, questions still remain on how this process fundamentally takes place, notably: where is the mineral mainly located? And how does it transform and get there in the first place? To date, traditional and cryogenic (cryo) transmission electron microscopy (TEM) modalities have dominated the

characterization of nanoscale collagen mineralization processes and helped elicit crucial theories of their mechanistic pathways.[9,11,25–32] This research has led to tremendous strides within the collagen mineralization field, specifically involving the discovery of non-traditional CaP crystallization theories involving precursor phases unlike traditional ion-by-ion pathways.[32] However, these TEM methods cannot visualize structures in the liquid state, representative of how they exist within the human body. Within collagen, water is an integral part of its structure, where water migration from dehydration or osmotic stresses can lead to structural alterations such as shrinkage.[33] It can be inferred that the state and amount of water in collagen therefore influences structural observations made at the nanoscale. Moreover, sample preparation for TEM can lead to structural alterations arising from artifacts such as shrinking and ice-induced crystal formation that may influence nanoscale observations.[34–37]

Thus, capturing mineralization processes in a liquid state is key to understanding and interpreting mineralization pathways. Liquid TEM, the room temperature correlate to cryo TEM, is a relatively new imaging technique that can provide high-resolution (HR) and real-time information of hydrated biological states.[38–46] While cryo TEM routinely provides HR imaging, recent technical breakthroughs in acquisition strategies and thin films enclosures are pushing liquid TEM imaging resolution to comparable levels with the additional benefit of retaining hydration.[45] Liquid imaging is often performed in one of two ways: with a commercial liquid TEM holder, or by encapsulation methods. Neither approach has been used previously to observe collagen mineralization processes.

Herein, liquid TEM techniques were used in a facile manner to probe collagen mineralization. A hybrid silicon nitride (SiN)-thin film enclosure was used with a simple two-step assembly process (Fig. 1), where collagen in solution was added to the enclosure, hermetically sealed, screened in a light microscope and loaded into the TEM. This method, adapted from the protocol described by DiCecco et al. for virus imaging[47], was highly repeatable – with an over 70% estimated encapsulation success rate, facile – taking only 10 mins to prepare, and affordable – accessible to use without specialized equipment.

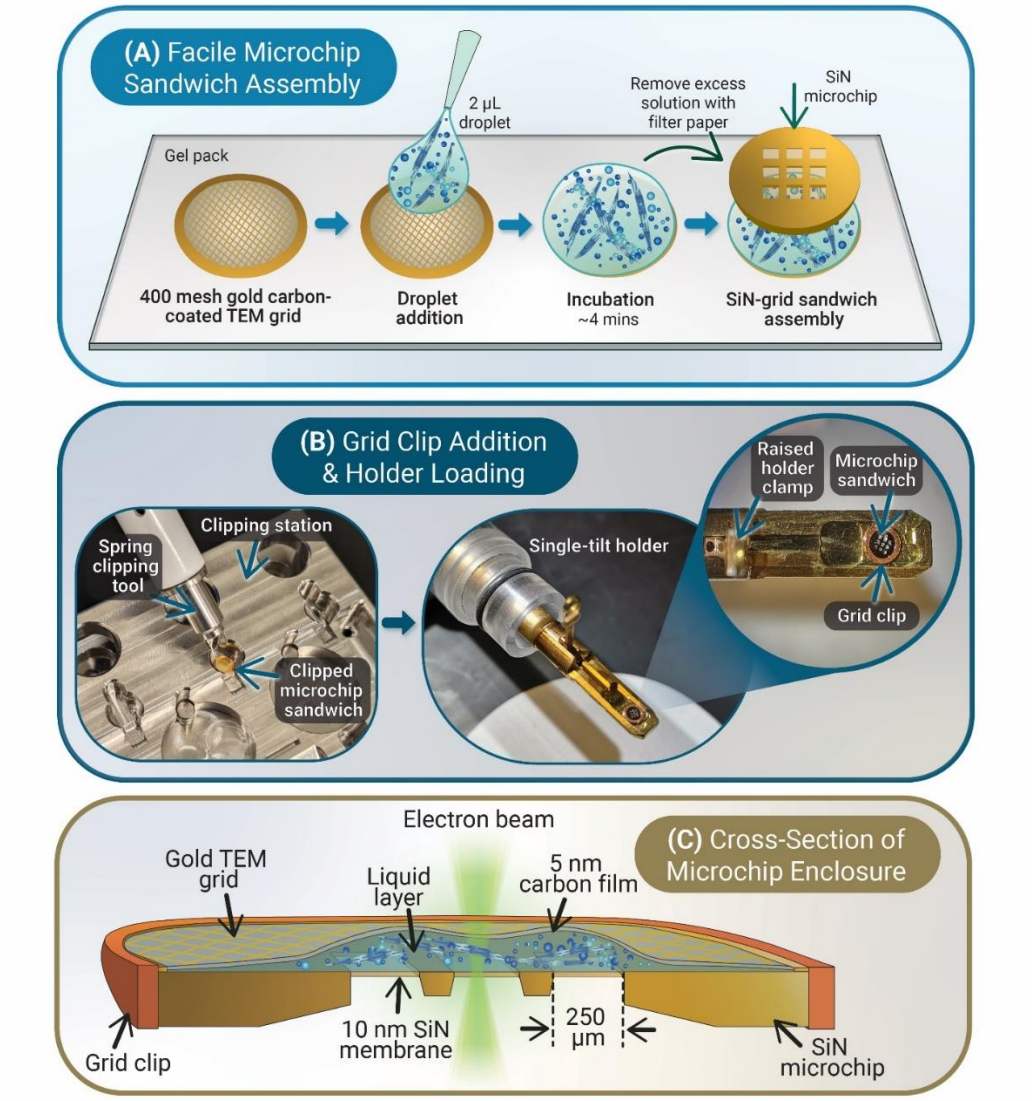

Ch. 5 – Figure 1. Microchip sandwich enclosure for liquid TEM of calcium phosphate-based collagen fibril mineralization processes. A. *Assembly of liquid enclosure method from left to right, where 2 µL of mineralization solution is deposited onto a plasma-cleaned carbon-coated 400 mesh gold TEM grid, incubated for 4 minutes, and then excess solution is removed before assembling the enclosure by adding a SiN microchip on top to create a SiN-grid sandwich.* ***B.*** *The SiN-grid sandwich enclosure is hermetically sealed using a cryo-autoloader grid clip, then stored or imaged immediately using a single-tilt TEM holder.* ***C.*** *Cross-section of the microchip enclosure, highlighting the thin film of the 5 nm carbon and 10 nm SiN membranes.*

5.3. Results & Discussion

A rat tail tendon source was used to extract reconstituted collagen fibrils for mineralization and imaging, described in greater detail in the supplemental methods (Fig. S1). CaP-based

solutions with pAsp were used to drive collagen mineralization, which have successfully mimicked intrafibrillar mineralization similar to bone *in vitro*.[22] A 25 µg/ml concentration of pAsp (Mw 14 kDa; Alamanda Polymers, Huntsville, AL, USA) was used, where full mineralization of collagen fibrils (~0.1 mg/ml) has been observed to occur within 18 hrs. Solutions were mineralized in bulk at 37°C and sampled using liquid TEM at time points of 4, 7, 15.5, and 18 hours, rather than mineralized within the enclosures in an attempt to mitigate long-term confinement effects described in literature.[48] Automated low-dose image acquisition, automated focusing, frame averaging and direct electron detectors, detailed further in supplemental information, are some of the technological strategies implemented to enable imaging.

Within a 4-hour mineralization period, two representative collagen stages were detected, with unmineralized regions dominating the mineralized (Fig. 2). Along less mineralized collagen fibrils both small and large higher-contrast globular particle aggregates were noted (Fig. 2A-B) and confirmed to be amorphous by SAED (Fig. 2B-Inset). This is indicative that the particles may be amorphous CaP (ACP) precursors. Mineral precursor aggregates have been identified in collagen models involving pAsp by works by Olszta et al.[24] and Deshpande and Berniash[23] with theories proposing a polymer-induced liquid precursor or involving particle attachment, respectively. Nudelman et al. theorize that collagen works together with pAsp to inhibit apatite formation and promote ACP infiltration observed in HR cryo TEM studies involving horse tendon-derived collagen.[25] They note clusters of charged amino acids in gap and overlap zones form nucleation sites that facilitate ACP transformation into aligned mineral apatite platelets.[25] Others studying compact turkey tendon collagen mineralization models theorize diffusive behaviour of mineral ions, where mineral precursors first integrate into the intrafibrillar space transversely and propagate in the longitudinal direction of fibrils to form mineral platelets.[26]

While regions were observed with particles attached to fibrils with this work, a caveat is that these observations cannot rule out the presence of crystalline-based and/or ion-dense liquid precursors elsewhere in the bulk sample. However, without the presence of collagen, the same CaP mineralization solutions combined with pAsp at 25 µg/ml resulted in the formation of ACP precursor mineral phases in the form of branched polymeric assemblies or globular particle aggregates (Fig. S2). This observation aligns with assemblies visualized in similar CaP-pAsp-based systems, where works by Quan and Sone show that pAsp molecules increase crystallization inhibition effects by stabilizing ACP while recent *in situ* studies showed the formation of such assemblies through liquid TEM methods.[21,43]

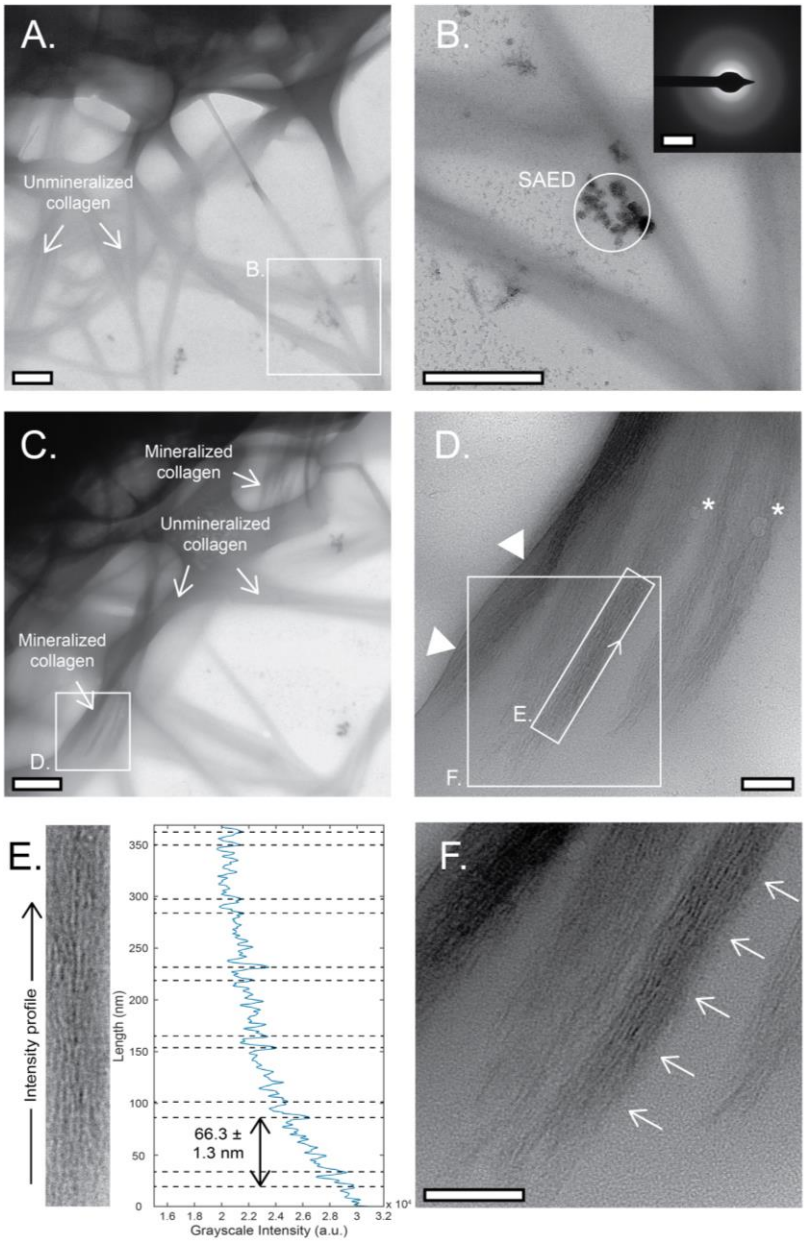

Ch. 5 – Figure 2. Representative BF TEM micrographs of hydrated mineralized collagen fibrils mineralized after 4 hrs in the presence of pAsp. ***A.*** *Lower magnification image highlights highly mineralized (darker contrast) and nearby regions of unmineralized collagen fibrils (box) under hydrated conditions.* ***B.*** *Higher magnification image showing an intermediate phase of collagen mineralization where smaller mineral aggregates were seen in solution and attached to the fibrils.* ***Inset – B:*** *SAED of these mineral aggregates show that they are amorphous in nature.* ***C.*** *A separate low magnification region where sections of unmineralized and mineralized collagen fibrils are shown.* ***D.*** *Higher magnification region where mineral platelets were observed in the hydrated collagen fibrils, where a liquid waterfront (triangles) and bubbles (stars) validate the hydration of this region.* ***E.*** *Grayscale intensity plot profile from the rectangular box in D. shows faint collagen banding patterns that repeat at intervals of 66.3 ± 1.3 nm, highlighted visually in* ***F.*** *(arrows). Scale bars: A.-C. 500 nm, Inset-B. 5 nm^{-1}, D. and F. 100 nm.*

In other regions at 4 hours, select fibrils show signs of more mature mineralization, with mineral platelets formed along fibril lengths (Fig. 2D-F). This is expected as the fibrils will not all mineralize simultaneously based on their heterogeneous distribution in suspension and variations in bundle sizes. The presence of mineral platelets at the 4-hour period demonstrates the active role of collagen in mineralization with pAsp, as the same solution without collagen at 4 hrs forms ACP polymeric branched structures as opposed to needle-like mineral platelets (Fig. S2). Faint collagen banding patterns that repeat locally at intervals of 66.3 ± 1.3 nm are shown in Fig. 2E, highlighted with better clarity in Fig. 2F (arrows). This local measurement is slightly lower than values obtained by Quan et al. reported as 68.0 ± 0.2 nm from cryo TEM of unmineralized collagen fibrils derived from rat tail tendon.[31] This difference is expected due to contractile stresses that arise during mineralization and result in shrinkage.[31,33,49]

Similar trends were noted in correlative 4-hour collagen biomineralization study in dehydrated conditions (Fig. S3), where SAED results show the presence of a CaP apatite crystalline phase with diffraction pattern (DP) rings for planes (002), (211), and (004) observed (Fig. S3D-Inset). The (002) and (004) DP arcs in reciprocal space aligned with that of the collagen in real space, indicative of apatite *c-axis* alignment to the long axis of the fibril (Fig. S3D-Inset). However, even with sample rinsing, under dehydrated TEM preparation methods (Fig. S1C) salt residue was noted (Fig. S3A,B). Salt accumulation was not noted in hydrated conditions however – pointing towards the importance of having a fully hydrated view of biomineralized samples.

At later time-points, after the 7-hour mineralization period, similar regions with various stages of mineralization were observed (Fig. 3). In Fig. 3A, bubbles (upper right) exemplify hydration in densely packed collagen region. Unlike many graphene liquid cells that feature isolated liquid pockets[50], continuous liquid layers in grid squares appear to be achieved. Figure 3B focuses on a collagen fibril that exhibits signs of early mineralization, surrounded by unmineralized fibrils seen at lower magnification (Fig. 3A). Particulate matter was also noted in solution and on collagen fibrils (Fig. 3B, triangles). To visualize the region with higher resolution, DED acquisition was also performed (Fig. 3C) in parallel to CETA camera imaging. Here, high-frame-rate 40 fps 4K videos were captured on the Direct-View camera at an electron dose rate of 45 e/Å^{2}s (1 second exposure). Videos were frame averaged by processing with motion correction using cryoSPARC 2.14.2[51] with MotionCor2 v1.2. DED acquisition shows, with high contrast, the presence of plate-like mineral features aligned along the collagen fibril among what appears to be amorphous darker contrast regions (Fig. 3C). SAED highlights faint diffraction patterns, the start of fine mineral platelets forming (Fig. 3C-Inset), though these are on a predominantly amorphous background without a distinguishable preferential orientation, as seen by images. Cryo TEM observations by Nudelman et al. show that collagen mineralization progresses by the infiltration of ACP and later the formation of apatite mineral platelets arises from ACP regions, with a similar intermediate platelet-ACP region noted.[25]

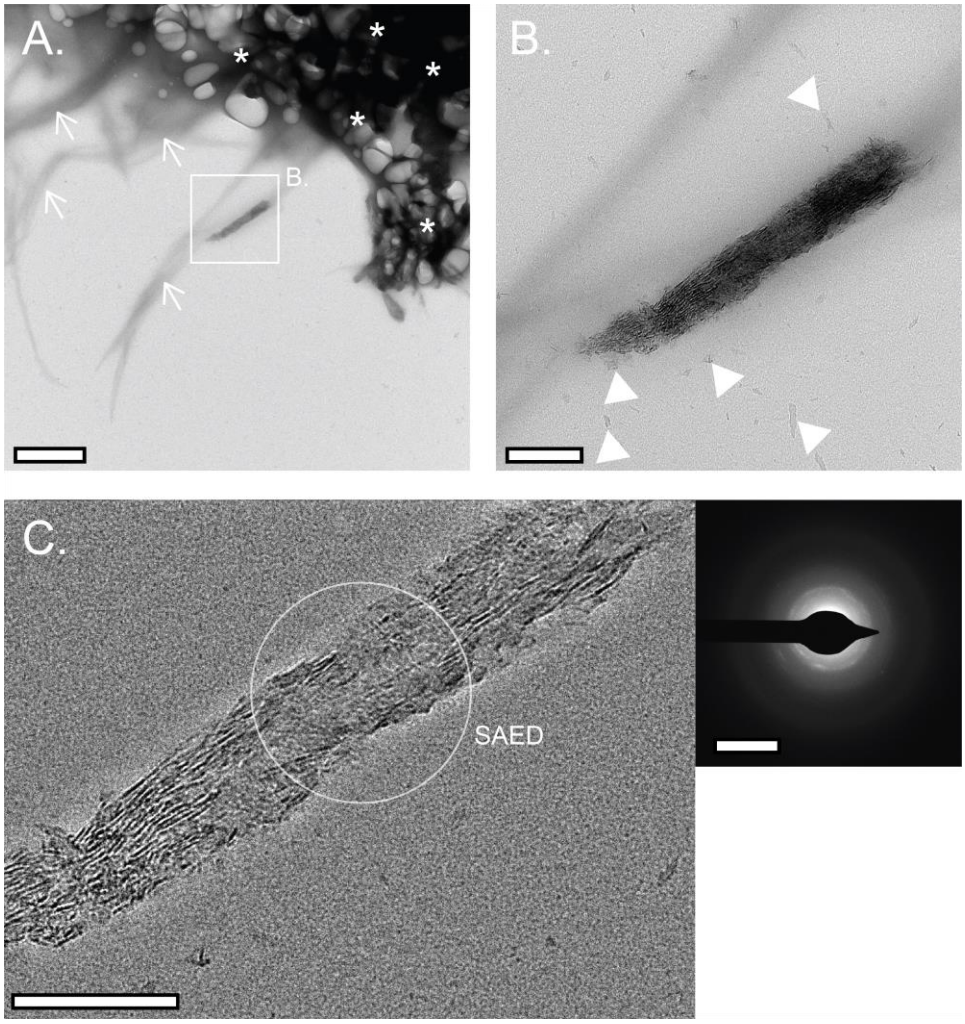

Ch. 5 – Figure 3. Representative BF TEM micrographs of hydrated mineralized collagen fibrils mineralized after 4 hours in the presence of pAsp. A. *Low magnification imaging highlights a mineralized region (box) with nearby unmineralized fibrils (arrows) and thicker clusters of less well-dispersed fibrils (stars). Bubbles (in starred regions) indicate the imaging area is hydrated.* ***B.*** *Higher magnification image showing an intermediate phase of collagen mineralization wherein smaller mineral aggregates were seen in solution and attached to the featured fibril (arrowheads).* ***C.*** *DED acquisition (frame-averaged 4K 40 fps movie, 1-sec exposure) shows plate-like mineral features resolved clearly with high contrast in the hydrated fibril in select regions along its length.* ***Inset - C:*** *SAED shows the intermediate apatite crystallization phase wherein thin and faint arcs without preferred orientation are observed on an amorphous background. Scale bars: A. 1 µm, B. and C. 200 nm, Inset-C. 5 nm^{-1}.*

The fibril featured in Fig. 3B-C is only partially mineralized, with the transverse direction showing signs of mineralization across its width, while the longitudinal direction is mineralized only in the specific segment shown in Fig. 3B-C, though it extends further (Fig. 3A). This indicates active mineralization was ongoing before encapsulation for TEM imaging. The ends of this mineralized region seem partially mineralized, suggesting mineralization is still occurring at these mineralization fronts – progressing outwards,

along the length of the fibril. This parallels the mineralization model proposed by Macías-Sánchez et al.[26] whereby using a compact turkey-tendon collagen model, mineralization is said to occur first transversely across a fibril width and then proceeds longitudinally.

Nearly mature fully-mineralized collagen arose after longer times, with a representative period of 15.5 hours in Figure 4. Stable bubbles demonstrate the hydrated nature of these specimens (Fig. 4A). At a higher magnification region, discrete mineral platelets were observed aligned with their *c-axis* to the fibril length (Fig. 4B). Again, DED acquisition shows clear platelets aligned with collagen banding, suggesting the possibility of intrafibrillar mineralization (Fig. 4C). On the SAED, (002), (211), and (004) rings were noted with (002) and (004) arcs aligned to fibrils in real space (Fig. 4C-Inset1,2), confirming the presence of apatite with preferred *c-axis* along the fibril length. Imaging of the mature 18hr collagen mineralization period (Fig. S4) further supports that the enclosure membranes and liquid environment have limited influence on interpreting SAED patterns.

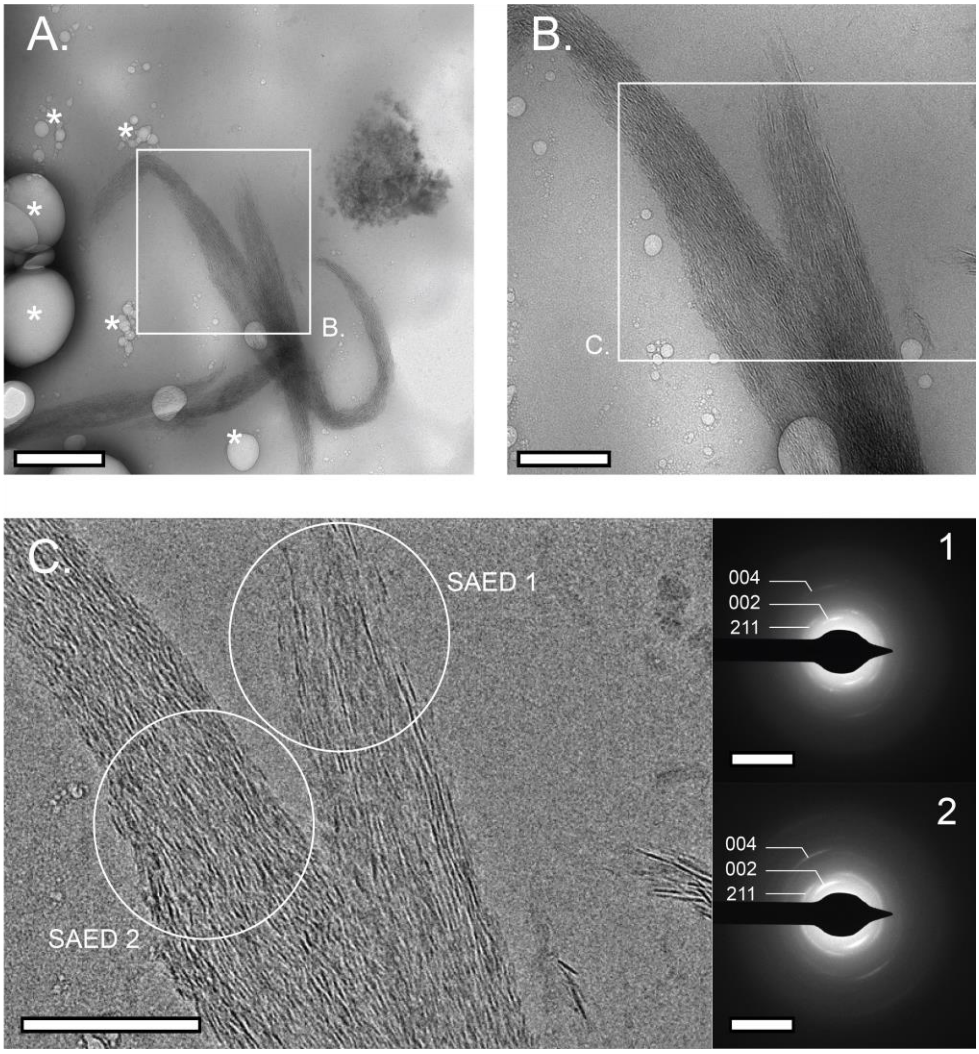

Ch. 5 – Figure 4. Representative BF TEM micrographs of hydrated mineralized collagen fibrils after 15.5 hours in the presence of pAsp. ***A.*** *Low magnification imaging highlights visible mineralized collagen fibrils (box). Bubbles (stars) indicate the imaging area is hydrated.* ***B.*** *Higher magnification image shows a region with distinctive mineral platelets visualized to be aligned along the length of the collagen fibrils featured.* ***C.*** *DED acquisition (frame-averaged 4K 40 fps movie, 1-sec exposure) shows at higher resolution the clear definition of these platelets.* ***Insets 1,2 – C:*** *SAED shows 002), (211), and (004) rings corresponding to CaP-based apatite crystals. The (002) and (004) arc alignments are indicative that the crystalline apatite is preferentially oriented with its c-axis parallel to the long axis of the collagen fibrils. Scale bars: A. 500 nm, B. and C. 200 nm, Insets-C. 5 nm^{-1}.*

Collagen fibrils and their aggregates were challenging to image in liquid TEM. First, they are quite large for liquid TEM enclosures, with ranges in size from twenty to hundreds of nanometers in diameter, which also corresponds to sample thickness.[52] Moreover, collagen fibrils distribute heterogeneously in solution and tend to aggregate. This poses a challenge for commercial liquid TEM holders that use rigid SiN membranes, where the large collagen fibrils would act as spacers – leading to thick liquid layers that limit the

resolution and/or uneven membrane stresses that lead to rupture.[42] While affordable graphene thin-film liquid TEM enclosures are now often used and result in thinner liquid layers for HR imaging,[53–58] their assembly can be complex with multiple steps and the handling of fragile graphene susceptible to cracking.[55,59] Moreover, only small amounts of liquid are captured within these assemblies, where liquid pockets enveloping samples are often achieved rather than continuous liquid layers.[59] The effect of the lack of liquid on mineralization kinetics would likely be substantial. The hybrid carbon-SiN membrane liquid TEM thin-film enclosure used herein (Fig. 1) proved to be effective in imaging these large samples with continuous liquid layers while automated tools and direct electron detector acquisition allowed for high-throughput HR imaging at low dose.

While this exciting new strategy holds promise for studying biomineralization reactions in hydrated conditions, a limitation was that dynamic events could not be captured with this imaging strategy. This is theorized due to the following three factors, discussed herein, which must be considered in the future: i) confinement effects, ii) lack of heating functionality of the enclosure, and iii) cumulative beam damage.

Firstly, based on qualitative changes observed in liquid contrast, it is likely that the carbon TEM-grid film 'blankets' the collagen structures, where near the fibrils the collagen itself acts as a local spacer but away from the fibrils the liquid thins out. Confinement of mineralized solutions in small liquid volumes is known to affect mineralization, namely by influencing nucleation rates and leading to larger ACP precursors in comparison to bulk volumes.[41,48] By using a bulk mineralization solution and probing at defined time points, some long-term confinement effects may have been avoided in this work. Further, the thin liquid layers and encapsulation may have provided more of a 2D, rather than 3D, space for mineralization where collagen fibrils and large particles were immobilized within the enclosure. Similar observations have been made in carbon-based thin-film liquid cells of larger biological samples such as bacteria, which are described as being wrapped in the film with limited movement,[60] while smaller samples, such as adeno-associated virus[45] and platinum nanocrystal growth in solution,[61] have been reported to exhibit dynamic motion in such enclosures.

Secondly, the current enclosure has no heating functionality to mimic physiological conditions in which collagen biomineralization occurs at 37°C. Thermodynamics play a key role in calcium phosphate mineral nucleation and particle growth rates, as summarized in detail by Sorokina et al.[62] Energy transferred thermodynamically into a system by heat contribute to the control of nucleation and growth, affect the diffusion of mineralization products, and influence the thermodynamic stability of pre-nucleation and ACP phases present in the system.[62] Considering the colder vacuum TEM environment, this may have delayed mineralization within the enclosures, nearly halting reactions from progressing and limiting dynamics.

Last of all, electron beam sensitivity of the solution and cumulative beam dose damage contribute to challenges related to capturing dynamic mineralization processes. In this

mineralization system, the use of buffers stabilized to a pH of 7.4 is hypothesized to aid in reducing chemically active species[38] while in mineralized fibrils apatite acts as a scavenger of radiolysis species to increase electron beam dose damage thresholds.[63] However, in thicker liquid regions where small particle motion was observed during screening, beam sensitivity of the solution caused near-instant bubbling (Fig. S5A). Such bubbles form from H+ ions arising from beam irradiation during imaging of beam-sensitive solutions and in thick regions that require a higher beam intensity to resolve formed products.[63,64] Automated imaging through SerialEM helped overcome these barriers to mitigate beam exposure during sample screening, though beam-sensitive regions still posed problems for longer video acquisitions needed to capture dynamics. Cumulative doses of approximately 250 e/Å^2 were detected to lead to severe structural beam damage in mineralized fibrils (Fig. S5B). Moser et al.[64] report that structural damage such as shrinking occurring in biological cell samples as low as 4 e/Å^2 while structural damage caused by bubbling in cryo TEM occurred in ranges between 300-400 e/Å^2.

5.4. Conclusion

This work demonstrates a facile method to visualize collagen mineralization in liquid TEM for the first time. A new hybrid SiN-thin film liquid TEM enclosure hermetically sealed with a clip was presented which encapsulated collagen fibrils in thin, continuous liquid layers for imaging. Automated acquisition and direct electron detection provided high-throughput, low-dose, HR imaging of collagen in liquid. In addition, automated imaging helped in increasing acquisition efficiently in screening samples and identifying regions of interest, while mitigating unnecessary electron beam exposure prior to acquisition.

Using these imaging techniques, various stages of mineralization were captured in liquid: an amorphous mineral phase was noted attached to unmineralized fibrils at initial time points, then amorphous and crystalline mineral platelets co-existed, and finally, distinctive nanoscale mineral platelets that aligned with their c-axis along the collagen fibrils were revealed, and confirmed through SAED to be a crystalline apatite. These observations parallel and complement the findings of others under dry or cryo conditions, [9,11,25–31] validating this liquid TEM technique as a feasible tool to apply to the investigation of complex real-time mineralization processes. This work highlights a significant leap forward by introducing a facile liquid TEM characterization tool to view native hydrated specimens with nanoscale features – important for understanding collagen mineralization and foundational to the clinical study of mineralized tissues and their repair.

ASSOCIATED CONTENT

SUPPORTING INFORMATION.

The following supporting information is available free of charge:
- Supporting Information document containing Methods and Methods section as well as Supplemental Figures (PDF format).

AUTHOR INFORMATION

Co-corresponding Author

Prof. Kathryn Grandfield, Department of Materials Science and Engineering, McMaster University; School of Biomedical Engineering, McMaster University, Hamilton, L8S 4L7 Ontario, Canada, https://orcid.org/0000-0002-0188-9580; Email: kgrandfield@mcmaster.ca

Co-corresponding Author

Prof. Eli D. Sone, Department of Materials Science and Engineering, University of Toronto, Institute of Biomedical Engineering, University of Toronto, Faculty of Dentistry, University of Toronto, Toronto, M5S 3E4 Ontario, Canada, https://orcid.org/0000-0001-7087-473X; Email: eli.sone@utoronto.ca

Notes

The authors declare no competing financial interest and no conflicts of interest.

Author Contribution

Conceptualization: Liza-Anastasia DiCecco, Ruixin Gao, Eli Sone, Kathryn Grandfield
Methodology: Liza-Anastasia DiCecco, Ruixin Gao, Deborah F. Kelly
Data curation: Liza-Anastasia DiCecco, Deborah F. Kelly
Formal analysis: Liza-Anastasia DiCecco, Ruixin Gao, Deborah F. Kelly, Eli Sone, Kathryn Grandfield
Funding acquisitions and supervision: Deborah F. Kelly, Eli Sone, Kathryn Grandfield
Writing: Liza-Anastasia DiCecco, Eli Sone, Kathryn Grandfield
Review and editing: Liza-Anastasia DiCecco, Ruixin Gao, Deborah F. Kelly, Eli Sone, Kathryn Grandfield

Acknowlegements

Financial support is greatly acknowledged from the Canadian Institutes of Health Research Project Grant (to E.D.S. and K.G. grant no. PJT 180575), and several programs of the Natural Sciences and Engineering Research Council of Canada (NSERC): Discovery Grant Program (to K.G. grant no. RGPIN-2020-05722), Canada Research Chairs Program (to K.G.; Tier II Chair in Microscopy of Biomaterials and Biointerfaces), and Vanier Canada Graduate Scholarship (to L.-A.D.). Electron microscopy was performed at the Canadian Centre for Electron Microscopy and the Pennsylvania State University Materials Research Centre and Huck Institutes of the Life Sciences. Carol Barter from Pennsylvania State

University is kindly acknowledged for their electron microscopy technical support and guidance.

References

[1] H. A. Lowenstam et al., *On Biomineralization*, Oxford University Press, 1989.
[2] U. Kini et al., in *Radionuclide and Hybrid Bone Imaging* (Eds: I. Fogelman et al.), Springer-Verlag Berlin Heidelberg, 2012, pp. 29–57.
[3] L. C. Palmer et al., *Chem Rev* 2008, *108*, 4754.
[4] Y.-R. Zhang et al., *Int J Oral Sci* 2014, *6*, 61.
[5] S. V. Dorozhkin et al., *Angewandte Chemie Int Ed* 2002, *41*, 3130.
[6] C.-W. (Jeff) Wang et al., *Curr Osteoporos Rep* 2016, *14*, 284.
[7] A. J. Lausch et al., *Adv Funct Mater* 2018, *28*, 1804730.
[8] A. J. Hodge et al., in *Aspects of Protein Structure* (Ed: G.N. Ramachandran), Academic Press, New York, 1963, pp. 289–300.
[9] F. Nudelman et al., *J Struct Biol* 2013, *183*, 258.
[10] S. R. Stock, *Calcif Tissue Int* 2015, *97*, 262.
[11] W. J. Landis et al., *J Struct Biol* 1993, *110*, 39.
[12] E. A. McNally et al., *Plos One* 2012, *7*, e29258.
[13] J. P. R. O. Orgel et al., *Proc National Acad Sci* 2006, *103*, 9001.
[14] J. P. R. O. Orgel et al., *Structure* 2001, *9*, 1061.
[15] B. Brodsky et al., *Matrix Biol* 1997, *15*, 545.
[16] S. F. Jackson, *Proc Royal Soc Lond Ser B - Biological Sci* 1957, *146*, 270.
[17] R. A. Robinson et al., *Anatomical Rec* 1952, *114*, 383.
[18] W. Traub et al., *Proc National Acad Sci* 1989, *86*, 9822.
[19] H. P. Schwarcz et al., *Bone* 2020, *135*, 115304.
[20] X. Su et al., *Bone* 2003, *32*, 150.
[21] B. D. Quan et al., *J Roy Soc Interface* 2018, *15*, 20180269.
[22] A. J. Lausch et al., *Adv Funct Mater* 2013, *23*, 4906.
[23] A. S. Deshpande et al., *Cryst Growth Des* 2008, *8*, 3084.
[24] M. J. Olszta et al., *Mater Sci Eng R Reports* 2007, *58*, 77.
[25] F. Nudelman et al., *Nat Mater* 2010, *9*, 1004.
[26] E. Macías-Sánchez et al., *Adv Funct Mater* 2022, *32*, 2200504.
[27] H. P. Schwarcz et al., *J Struct Biol* 2014, *188*, 240.
[28] B. E. J. Lee et al., *Adv Biology* 2021, *5*, 2100657.
[29] N. Reznikov et al., *Acta Biomater* 2014, *10*, 3815.
[30] N. Reznikov et al., *Science* 2018, *360*, eaao2189.
[31] B. D. Quan et al., *Bone* 2015, *77*, 42.
[32] W. J. E. M. Habraken et al., *Nat Commun* 2013, *4*, 1507.
[33] A. Masic et al., *Nat Commun* 2015, *6*, 5942.
[34] R. F. Thompson et al., *Methods* 2016, *100*, 3.
[35] M. D. McKee et al., *J Bone Miner Res* 1991, *6*, 937.
[36] E. Kellenberger et al., *J Microsc-oxford* 1992, *168*, 181.

[37] C. G. Golding et al., *Sci Rep-uk* 2016, *6*, 26516.
[38] X. Wang et al., *Commun Chem* 2018, *1*, 80.
[39] P. J. M. Smeets et al., *Nat Mater* 2015, *14*, 394.
[40] M. H. Nielsen et al., *Science* 2014, *345*, 1158.
[41] B. Jin et al., *Cryst Growth Des* 2021, *21*, 5126.
[42] H. Wu et al., *Adv Mater* 2020, *32*, 2001582.
[43] L.-A. DiCecco et al., *Microsc Microanal* 2022, *28*, 1818.
[44] W. J. Dearnaley et al., *Nano Lett* 2019, *19*, 6734.
[45] G. Jonaid et al., *Adv Mater* 2021, *33*, 2103221.
[46] D. F. Kelly et al., *Curr. Opin. Struct. Biol.* 2022, *75*.
[47] L.-A. DiCecco et al., *J Vis Exp* 2022, e63856.
[48] R. Kröger et al., *Mineral-basel* 2018, *8*, 21.
[49] H. Ping et al., *Science* 2022, *376*, 188.
[50] J. Park et al., *Acs Nano* 2021, *15*, 288.
[51] A. Punjani et al., *Nat Methods* 2017, *14*, 290.
[52] D. A. D. Parry et al., *Proc Royal Soc Lond Ser B Biological Sci* 1978, *203*, 305.
[53] Q. Chen et al., *Nano Lett* 2013, *13*, 4556.
[54] J. Park et al., *Nano Lett* 2015, *15*, 4737.
[55] P. Blach et al., *J Vis Exp* 2020, DOI 10.3791/61458.
[56] P. M. G. Deursen et al., *Adv Funct Mater* 2020, *30*, 1904468.
[57] I. N. Dahmke et al., *Acs Nano* 2017, *11*, 11108.
[58] C. Wang et al., *Adv Mater* 2014, *26*, 3410.
[59] M. Textor et al., *Nano Lett* 2018, *18*, 3313.
[60] E. Firlar et al., *Nanoscale* 2019, *11*, 698.
[61] J. M. Yuk et al., *Science* 2012, *336*, 61.
[62] L. V. Sorokina et al., *Emergent Mater* 2021, *4*, 1205.
[63] J. R. Jokisaari et al., *Nanotechnology* 2021, *32*, 485707.
[64] T. H. Moser et al., *Micron* 2019, *119*, 8.

Chapter 5: Supplemental Information

5.5. Materials and Methods

5.5.1. Collagen Fibrillogenesis

Collagen was extracted from a rat-tail tendon model as a close structural mimic to type I collagen found in mineralized tissues within the human body.[1,2] Collagen fibrillogenesis and crosslinking of this model are further elaborated in works by Lausch et al.[3] Briefly, extracted rat tail tendons were dissolved at 1 mg/mL in 0.5 M acetic acid. Then, the solution was diluted 1:1 by distilled water (diH_2O) and the pH was adjusted to 5.0 with 1 M NaOH, which was incubated for 2 hours in a water bath at 35°C before collecting collagen fibrils.

Collected collagen fibrils were fixed using glutaraldehyde over an 18-hr fixation period with 0.08% glutaraldehyde in an aqueous solution (Electron Microscopy Sciences, Hatfield, PA, USA). Samples were subsequently dialyzed against diH_2O for 2 days with frequent water replacements to halt system reactions and remove glutaraldehyde and acetic acid from the system.

5.5.2. Collagen Mineralization

An overview of key experimental details within this and the following subsections of the materials and methods is provided in Fig. S1. Reconstituted collagen fibrils were mineralized based on procedures adapted from published work by the team of Despande and Beniash,[4] where a calcium phosphate-based system is used. Mineralization was prepared by mixing equal volumes of collagen fibrils in diH_2O at a concentration of approximately 0.4 mg/mL with the following aqueous-based solutions, all buffered to a pH of 7.4 at 37°C using 1 M of hydrochloric acid: 9 mM $CaCl_2$ in 50 mM Tris, 4.2 mM K_2HPO_4 in 50 mM Tris, and 100 mM Tris–500 mM NaCl (Tris-NaCl). Poly-L-aspartic acid (pAsp) sodium salt (pAsp 100 – Mw 14 kDa; Alamanda Polymers, Huntsville, AL, USA) was dissolved into the Tris-NaCl solution such that a desired concentration of 25 µg/ml of pAsp would be achieved in the final solution. All mineralization solutions, except the collagen suspension, were filtered through a 0.2 µm acrodisc syringe filter before incorporation. After mixing, the final mineralization solution consisted of 125 mM NaCl, 1.7 mM $CaCl_2$, 9 mM Na_2HPO_4, 50 mM Tris, and a concentration of 25 µg/ml of pAsp and an approximate concentration of 0.1 mg/mL of collagen fibrils. Prepared solutions were mineralized at 37°C in a water bath set with a probe-controlled hot plate and gentle mixing of 100 rpm. All reagents described were purchased from Sigma Aldrich and dissolved in Milli-Q diH_2O, except for the pAsp which was purchased Alamanda Polymers as noted.

For liquid TEM, mineralization periods of 4, 7, 15.5, and 18 hrs were probed to capture early to mature mineralization phases within collagen fibrils. For correlative studies of the mineralization solution without collagen fibrils featured in the supplemental material, the

solution was prepared in the same manner with simply diH_2O added instead of the collagen fibril suspension.

5.5.3. Liquid Enclosure TEM: Sample Preparation and Acquisition

Figure 1 of the main body of this article highlights schematically the two-step assembly process of the liquid enclosure used in this work, adapted from the protocol described in DiCecco et al.[5] The hybrid SiN-thin film enclosure used is composed of two pieces: a 2.9 mm diameter silicon nitride microchip with nine membrane windows (sizes: (8) 250x250 µm + (1) 250x500 µm) with a membrane thickness of 10 nm (SiMPore Inc., West Henrietta, NY, USA) on one side and a gold 400 mesh TEM grid with a 5 nm carbon film (Electron Microscopy Sciences) on the other, clamped together by copper grid clip used for cryo-TEM autoloaders (ThermoFisher Scientific, MA, USA). Before loading, all TEM grids and SiN microchips were plasma glow discharged for 2 cycles of 45 seconds with a plasma current of 15 mA using a Pelco EasiGlow instrument (Ted Pella, Inc. Redding, CA, USA).

To form the enclosure, 2 µL of the liquid collagen solution was deposited onto the carbon side of a TEM grid resting on a gel pack holder (Fig. 1A). The grid was then incubated for 4 minutes to allow collagen to settle. During this time, the samples were screened under a light microscope to confirm collagen deposition. Following this, excess solution was removed with the edge of a piece of Whatman #1 filter paper (Sigma-Aldrich Canada Co., Oakville, ON, Canada), and the sample was enclosed by the addition of the SiN microchip (Fig. 1A) on top. Early attempts at collagen deposition onto SiN highlighted that collagen removed itself easily from the membranes, while the carbon-coated TEM grid kept samples stable on the surface and was thus used. The assembly was hermetically sealed with a copper grid clip, traditionally used for cryo TEM autoloaders (Fig. 1B). Prior to insertion in the TEM, the enclosure was inspected using a light microscope to ensure there were no cracks in the SiN microchip and that collagen fibrils were visible.

For correlative dry TEM samples presented within the supplemental of this study, 2 µL of a liquid mineralization sample was deposited onto a copper 400 mesh TEM grid with either a continuous or lacy 5 nm carbon film (Electron Microscopy Sciences) for reactions with or without collagen, respectively. These samples were then incubated for 4 minutes and then dipped into methanol to halt any further mineralization reactions and rinse away excess products arising from drying.

A single-tilt TEM holder was used for bright field (BF) TEM imaging using a Talos F200C or X series TEM (ThermoFisher Scientific, MA, USA), both operated at a voltage of 200 kV and equipped with a Direct-View direct electron detector (Direct Electron, CA, USA) and/or a CETA camera. For liquid TEM, the SerialEM software[6] (University of Colorado, Boulder, CO, USA) was used to facilitate high-throughput acquisition through automation using both the CETA camera and Direct-View detector. [5]Automated sample screening using SerialEM provided low-dose, low-magnification window-membrane maps, which

supported quick sample screening and the selections of regions of interest (ROIs) for imaging. This offered quick screening capabilities of the entire microchip sandwich for ROIs, limiting beam exposure to the sensitive samples. Within each TEM grid square captured, ROIs for imaging were either selected manually or chosen through a grid square of points for serial acquisition, where SerialEM automated focusing was used to adjust acquisition parameters adjacent to an ROI to mitigate its beam exposure to an ROI.

Electron dosage was varied between 40-55 e/Å^2 per acquisition. When considered, direct electron (DE) movies were acquired at 40 fps, with 1 s exposure at an approximate rate of 45 e/Å^{2}s. These DE movies were frame averaged to provide images featured within this work with motion correction using cryoSPARC 2.14.2[7] with MotionCor2 v1.2.3. Selective area electron diffraction (SAED) was achieved using either 10 µm or 40 µm sized apertures which covered an approximate diameter of 125 nm or 250 nm in the real image, respectively. Indexing for SAED polycrystalline patterns for CaP-apatite was done by analyzing concentric ring patterns belonging to the polycrystalline structures captured using the ImageJ software. From these measurements of the calibrated camera acquisitions, interplanar spacing was calculated and compared to reference CaP-based crystal structures. Regions with distinguishable ring patterns were compared to a hydroxyapatite crystallography base reference[8] – as expected for mineral platelets present in mineralized collagen fibrils within regions investigated.

5.5.4. Line Scan Analysis

When referenced, the periodicity of collagen fibrils was investigated using grayscale intensity analysis using the ImageJ software package “Plot Profile” function. Here, the fibril considered is featured in Figure 2 with 6 distinguishable periods noted. This region was considered for line grayscale intensity profiling along the c-axis of the collagen fibril, with an applied averaging line width of approximately 47.7 nm (300 px). Local graph maximum and minimum points were identified using MATLAB, where a custom smoothing algorithm[9] was applied for local peak identification using pseudo-Gaussian smoothing (4 passes of the same sliding average) applied to 5 data points at a time. The periodicity of the collagen fibril was calculated based on the appearance of a local maximum present, visually associated with collagen banding patterns, found at repeating patterns of the grayscale intensity plots.

5.6. Supplemental Images

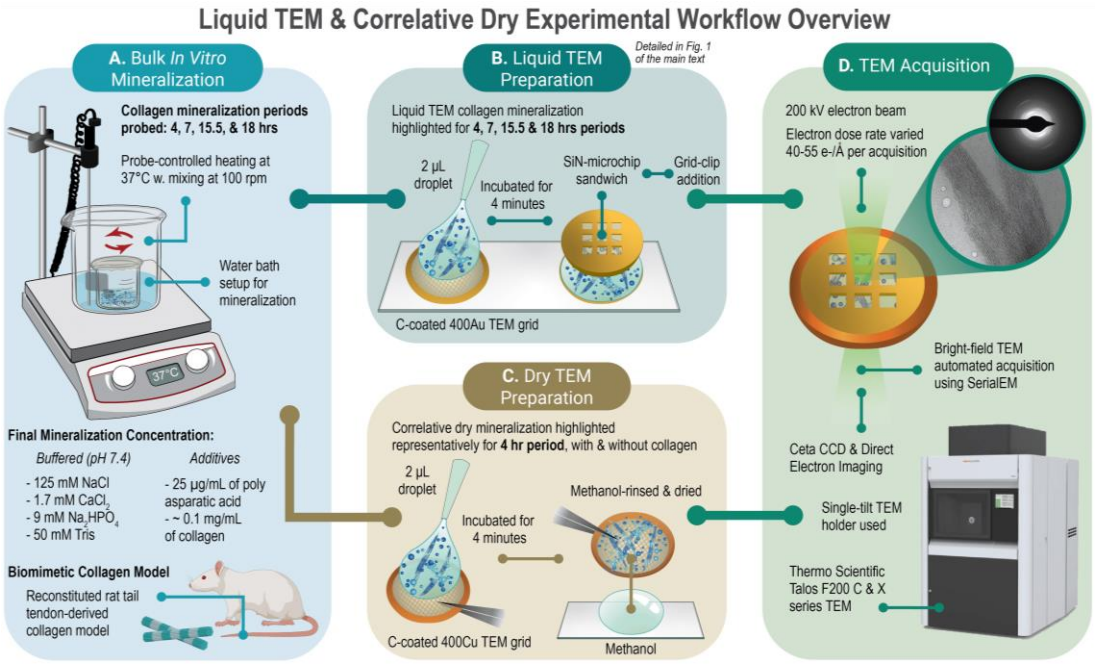

Ch. 5 – Figure S1. Liquid *TEM and Correlative Dry Experimental Workflow Overview.* A. *Summary of mineralization conditions and setup considered for the study, where collagen mineralization periods of 4, 7, 15.5, and 18 hrs were considered for liquid TEM.* **B.** *Summary of liquid TEM sandwich enclosure preparation, explained in greater detail within Fig. 1 of the main text.* **C.** *Correlative dry TEM preparation method highlighted for the supplemental results featured with and without collagen for the 4-hr mineralization period.* **D.** *Overview of key TEM acquisition parameters. The murine schematic in A. was created with Biorender.com.*

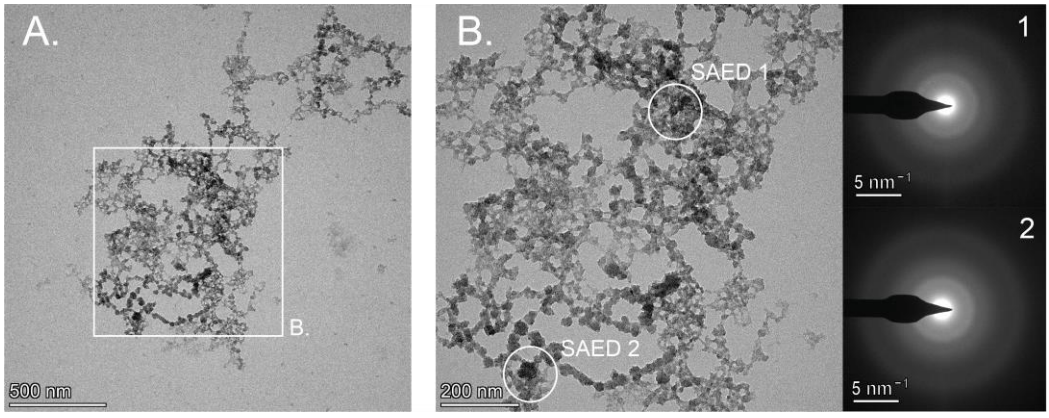

Ch. 5 – Figure S2. Representative correlative ex situ BF TEM micrographs of dry CaP products mineralized after 4 hrs in the presence of pAsp without collagen. A. *Lower magnification image highlights larger mineral aggregates that formed within the solution.* ***B.*** *Higher magnification image shows branched spherical mineral assemblies.* ***Insets 1, 2 – B:*** *SAED of regions marked in B. show the amorphous nature of mineral aggregates.*

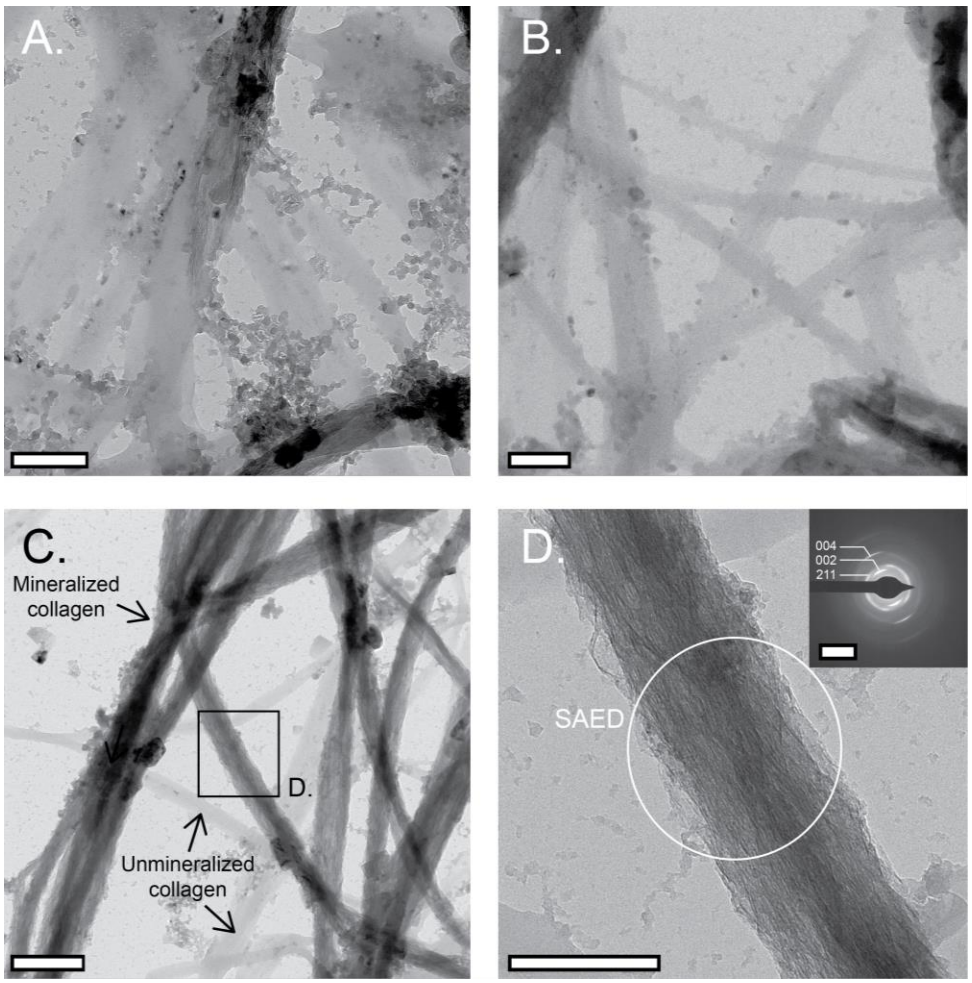

Ch. 5 – Figure S3. Representative correlative BF TEM micrographs of dry mineralized collagen fibrils after 4 hrs in the presence of pAsp. A.-B. *Representative regions consisting primarily of unmineralized fibrils at an intermediate phase of collagen mineralization where small mineral aggregates can be seen around and attached to the fibrils. Despite rinsing, salt residue from mineralization buffers is noted to possibly adhere to the fibrils – a drawback to this traditional dry-based preparation method.* ***C.*** *Another region highlights an area in which both unmineralized and mineralized collagen fibrils can be seen* ***D.*** *Higher magnification region where mineral can be observed along the length of the collagen fibril.* ***Inset – D:*** *SAED show the (002), (211), and (004) rings corresponding to CaP-based apatite crystals, where (002) and (004) arcs alignment indicate that these mineral platelets are preferentially oriented with its c-axis parallel to the long axis of the collagen fibrils. Scale bars: A., B., and D. 200 nm, C. 500 nm.*

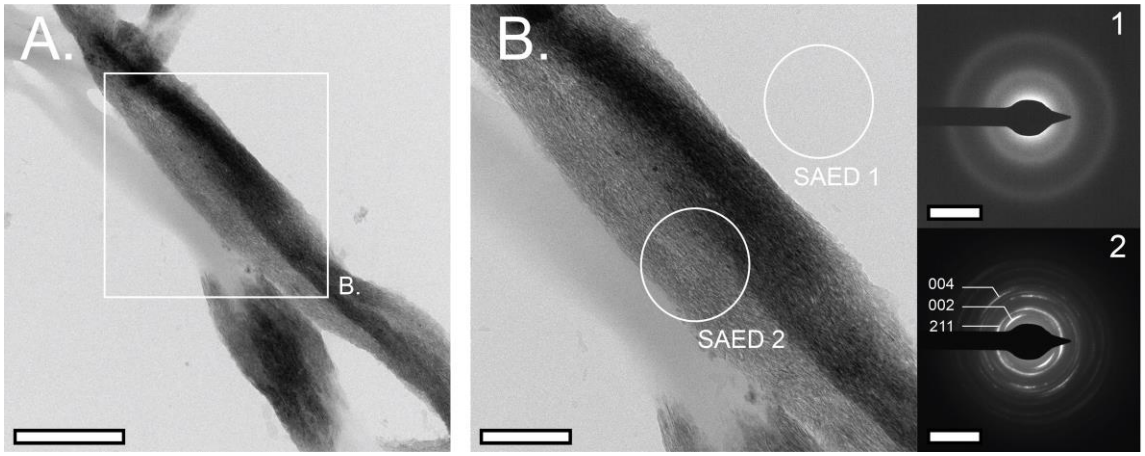

Ch. 5 – Figure S4. Representative BF TEM micrographs of hydrated mineralized collagen fibrils mineralized for 18 hrs, showing minimal influence of the enclosure on SAED interpretation. A.-B. *Low to high magnification imaging highlights highly mineralized collagen fibrils, with mineral (darker contrast) appearing along the fibril length.* ***Inset 1– B:*** *SAED of the substrate in the region without collagen shows the amorphous nature of the SiN and carbon film membranes.* ***Inset 2 – B:*** *SAED show the (002), (211), and (004) rings corresponding to CaP-based apatite crystals, where (002) and (004) arcs alignment indicate that these mineral platelets are preferentially oriented with its c-axis parallel to the long axis of the collagen fibrils. These patterns are noted clearly within the region, despite the apparent thickness of this collagen fibril bundle, indicating that the SiN and carbon film membranes are thin enough to obtain clear diffraction patterns of hydrated specimens with limited influence on signal detection. Scale bars: A. 500 nm, B. 200 nm, Insets-B. 5 nm^{-1}.*

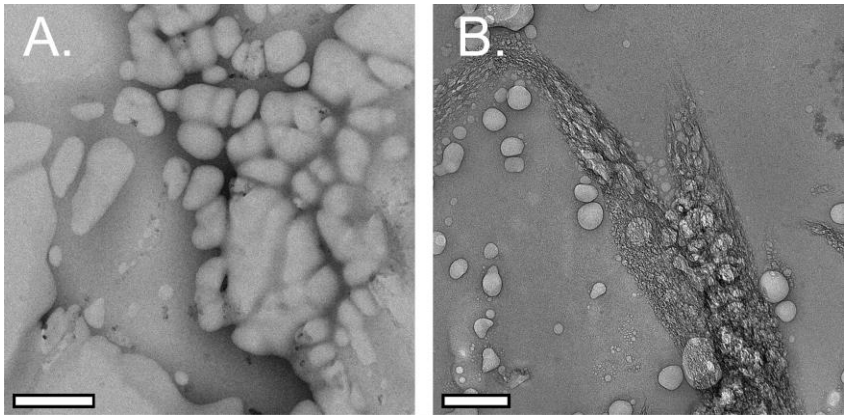

Ch. 5 – Figure S5. Representative regions of thicker liquid and bubbling artifacts in 15.5 hr collagen mineralization sample. A. *BF TEM micrograph of thicker liquid region showing instantaneous bubbling on imaging of the solution, highlighting challenges with beam sensitivity and related resolution limitation caused by liquid mobility within thick regions in this liquid TEM imaging.* ***B.*** *Overview image of the region of interest featured in Figure 4 of the main text after continuous imaging and severe beam damage, occurring after a cumulative electron dose of approximately 250 e/Å^2. Scale bars: A. 500 nm. B. 200 nm.*

References

[1] A. J. Lausch et al., *Adv Funct Mater* 2018, *28*, 1804730.
[2] B. D. Quan et al., *J Roy Soc Interface* 2018, *15*, 20180269.
[3] A. J. Lausch et al., *Adv Funct Mater* 2013, *23*, 4906.
[4] A. S. Deshpande et al., *Cryst Growth Des* 2008, *8*, 3084.
[5] L.-A. DiCecco et al., *J Vis Exp* 2022, e63856.
[6] D. N. Mastronarde, *Microsc Microanal* 2018, *24*, 864.
[7] A. Punjani et al., *Nat Methods* 2017, *14*, 290.
[8] "Ca-hydroxyapatite (Ca5[PO4]3[OH] rt) Crystal Structure: Datasheet from 'PAULING FILE Multinaries Edition – 2022' in SpringerMaterials," can be found under https://materials.springer.com/isp/crystallographic/docs/sd_1802016, n.d.
[9] T. O'Haver, "Fast Smoothing Function," can be found under https://www.mathworks.com/matlabcentral/fileexchange/19998-fast-smoothing-function, 2017.

Chapter 6: Towards Understanding Dynamics Behind Collagen Mineralization Through In Situ Liquid TEM – Trials and Tribulations

6.1 Section Introduction (Objective iii)

Determining the mechanisms behind collagen mineralization processes presents many medical benefits to society, whereby an improved understanding of these pathways can help identify better treatments for hard tissue diseases such as osteoporosis as well as aid in tissue regeneration research involving implants. However, the dynamic mechanisms behind these processes have yet to be visualized, where our current understanding of these processes is enumerated from dry or frozen time-stamp states of these reactions. As outlined in the objectives, Chapter 6 sought to explore the dynamics behind these processes using liquid TEM and attempted to overcome the functional limitations described in Chapter 5. A similar collagen mineralization model from Chapter 5 was used in Chapter 6, involving a murine-derived collagen model with a CaP and pAsp solution to promote intrafibrillar mineralization. Successful acquisition of dynamic nanoscale processes was captured using a commercial liquid TEM holder mimicking physiological conditions at 37°C to study dynamic mineralization reactions. Uniquely, I present evidence of the coexistence within this model of two amorphous precursor phases, potentially involving polymer-induced liquid as well as particle attachment mineralization mechanisms. However, several liquid TEM challenges remain, particularly beam sensitivity and distribution, which pose limits on what can currently be captured, though provides many exciting avenues in future to explore this system. Overall, this work contributes to a new understanding of potential mechanisms behind collagen mineralization involving ACP phases which interplay with one another as well as demonstrates the potential of liquid TEM for biomineralization research.

Authors: **Liza-Anastasia DiCecco**, Ruixin Gao, Eli D. Sone, Kathryn Grandfield.
Publication: This work is to be submitted in 2023.

Towards Understanding Dynamics Behind Collagen Mineralization Through *In Situ* Liquid TEM – Trials and Tribulations

Liza-Anastasia DiCecco[1], Ruixin Gao[2], Eli D. Sone[2-4*], Kathryn Grandfield[1,5*]

[1] Department of Materials Science and Engineering, McMaster University, Hamilton, ON, Canada
[2] Institute of Biomedical Engineering, University of Toronto, Toronto, ON, Canada
[3] Faculty of Dentistry, University of Toronto, Toronto, ON, Canada
[4] Materials Science and Engineering, University of Toronto, Toronto, ON, Canada
[5] School of Biomedical Engineering, McMaster University, Hamilton, ON, Canada

* Co-corresponding author:
Prof. Kathryn Grandfield
McMaster University
1280 Main Street West
Hamilton, Ontario L8S 4L7, Canada
Email: kgrandfield@mcmaster.ca

* Co-corresponding author:
Prof. Eli Sone
University of Toronto
184 College Street
Toronto, Ontario M5S 3E4, Canada
Email: eli.sone@utoronto.ca

Keywords: Liquid Transmission Electron Microscopy; Collagen Mineralization; Calcium Phosphate; Polyaspartic Acid; Mineralized Tissues

6.2. Abstract

Collagen is one of the major constituents of mineralized tissues. Understanding its biomineralization mechanisms can aid in the improvement of regenerative biomaterials and inform new treatment pathways for diseases. While studied extensively, collagen mineralization is yet to be fully understood. Several competing theories exist based on time-stamped observations using conventional transmission electron microscopy (TEM) means. But – complementary real-time dynamic observations are needed for validation. Liquid TEM, an emerging technique used to observe nanoscale reactions in near-native liquid environments, is explored as an alternative to probe dynamic collagen mineralization at physiological temperatures in real-time for the first time. To elucidate early to mature mineralization behaviour, an established biomimetic rat-tail tendon reconstituted collagen mineralization *in vitro* model is used, featuring poly-aspartic acid (pAsp) as a mimic of non-collagenous proteins to mediate collagen mineralization. Evidence of two amorphous mineral precursors were noted in liquid, where at early mineralization an ion-dense mineral phase was observed while at later stage mineralization dynamic results show particle attachment at a mineralization front. This may suggest that two mechanisms interplay the two phases interplay in collagen biomineralization processes in the presence of pAsp. Technical limitations to the liquid TEM technique, notably impacts of collagen heterogeneity and electron beam sensitivity, are summarized. We aspire sharing trials and tribulations in a transparent manner will bridge technical knowledge gaps and guide others seeking to use liquid TEM. This work lays a foundation for studying collagen mineralization *in situ* and brings us closer to understanding how it occurs.

Towards Understanding Dynamics Behind Collagen Mineralization Through *In Situ* Liquid TEM – Trials and Tribulations

6.3. Introduction

Collagen is one of the most abundant proteins in the human body and forms the structural units responsible for the differentiated properties of connective tissues. Type I collagen molecules, formed of a triple helix of peptide chains rich in amino acids glycine, proline and hydroxyproline, are most prominently found in mineralized tissues such as bone.[1,2] Its molecule is approximately 300 nm in length and 1.23 nm in width, where in human bone they bundle together to form fibrils with a stacked repeating periodicity of characteristic gap and overlap regions on average of 67 nm.[3,4] As one of the major constituents of hard tissues, the study of collagen structure and mineralization pathways is key to improving biomaterial design for hard-tissue regenerative medicine applications and for helping inform new treatment pathways of related diseases such as osteoporosis and dental caries.[5–9] Notably, the mechanical properties of bone are attributed to the extent and distribution of calcium phosphate (CaP) based mineral, typically hydroxyapatite (HAP), among collagen fibrils.[10,11] An in-depth understanding of how CaP mineralizes with respect to collagen hence offers significant possibilities for clinical advances.

Decades of research and advances in characterization techniques have led to transformative findings and theories on how collagen biomineralization may occur,[3,4,12–16] however, the mechanisms behind these processes have remained elusive. While it is generally accepted that high mineral-dense matrix vesicles start primary mineralization in bone, secondary mineralization over time involving the formation, refinement and organization of CaP-based mineral platelets among collagen is widely disputed.[1,12,17] A combination of non-collagenous proteins (NCPs) and the distinct structure of collagen molecules and formed fibrils are believed to regulate the initiation and growth of CaP biomineralization.[12] It is theorized that gap and overlap zones fulfill an important role in collagen mineralization, where preferential intrafibrillar CaP mineral nucleation has been observed in gap regions[12,18–20] that seem to grow in excess outwards into overlap regions[3,12,20]. Apart from intrafibrillar regions, mineral has also been reported to be found outside (extrafibrillar) and amid (interfibrillar) collagen fibrils.[14,21,22]

Biomimetic *in vitro* models have been used to elucidate the influence of various systematic factors contributing to complex collagen biomineralization processes.[12] One such successful mimic in collagen mineralization models has included the use of polyaspartic-L-acid (pAsp) as a substitute for NCPs found in natural mineralized collagenous tissues.[12,23] Research performed by Olszta et al[24] and Deshpande and Berniash[25] were among the first to use this additive in mineralization solutions to induce intrafibrillar mineralization *in vitro*, mimetic of what occurs in native hard tissues.

Current theories indicate that pAsp acts as a nucleation inhibitor, stabilizing CaP systems and delaying mineralization events due to its highly charged, aspartate-rich, disordered structure.[12,23–27] The size of aspartate-rich sequences of pAsp impact mineralization, where work by Quan and Sone suggests that larger pAsp molecules increase crystallization inhibition effects, decreasing the growth rates of amorphous CaP (ACP) and ultimately leading to its stabilization.[23] It has also been suggested that pAsp sequesters mineral ions or precursors in solution[24,25] and that its negative charge interacts with the positive C-terminus of collagen gap-zones, delaying extrafibrillar mineralization and leading to the mediation of intrafibrillar mineralization.[26] Through this interaction with pAsp, mechanistically CaP apatite minerals are hypothesized to form through the action of either: 1) the formation of a polymer-induced liquid precursor (PILP), otherwise described as an ion-dense highly hydrated ACP phase, that infiltrates into collagen fibrils by capillary action to then form apatite,[24] or 2) the binding of pAsp to collagen, leading to the sequestering of supersaturation of mineral ions locally, particle attachment, and then direct mineralization into collagen fibrils.[25] Regardless, despite being extensively studied, these theories have yet to be validated through *in situ* observation and remain contended.

Commonly, traditional and cryogenic (cryo) transmission electron microscopy (TEM) methods have been used to explore collagen biomineralization mechanisms and reveal structural insights into these pathways, eliciting key theories on their mineralization.[12,23–26,28–34] These techniques provide a high-resolution (HR) avenue to probe nanoscale mineralization events, however, they only capture time-stamp observations in a dry or frozen state. Water is integral to the collagen structure, where its displacement can lead to structural alterations such as shrinkage.[35] Thus, to validate theories behind these interactions, real-time dynamic liquid imaging is required to visualize these nanoscale processes. With the advent of improved manufacturing in microchip fabrication and enclosure methods, liquid TEM is an emerging technique that can visualize nanoscale organic-inorganic interactions in near-native liquid state environments, in real-time and at resolutions encroaching those similarly achieved through conventional and cryo TEM means.[36–44] Liquid TEM could be a key correlative means to validate established theories on the complex mechanisms behind collagen mineralization with real-time resolution, but technical challenges to date have restricted the visualization of such dynamics. Recently, our team demonstrated that thin-film liquid TEM enclosures can be used to study HR collagen mineralization steps in hydrated conditions, although dynamic reactions were not captured as described in Chapter 5. Overall, the samples have been challenging to image in liquid; collagen is beam-sensitive, fibril aggregations impose excess stress onto viewing membranes, as well as act as spacers leading to local thick liquid layers, confinement in thin films restricts particle mobility, and mineralization is sensitive to local environmental conditions – discussed in detail in Chapter 5.

Herein, dynamic collagen mineralization events in liquid at physiological temperatures are shown for the first time. This work sheds light on collagen mineralization mechanisms by overcoming technical challenges experienced prior with the implementation of the liquid TEM experimental configurations summarized in Figure 1. A previously established *in vitro* rat tail tendon-derived reconstituted collagen model mineralized with exposure to CaP and pAsp is consulted as a mimic of Type I collagen found in bone.[9,23,45] Early collagen mineralization periods were explored using a Protochips Poseidon liquid TEM holder with heating at 37°C to mimic conditions in the body using a silicon nitride (SiN_X) based enclosure (Fig. 1A). The Poseidon holder was also used to explore correlative mineralization solutions *in situ* without the addition of collagen using a microwell configuration (Fig. 1B). Observations from experiments presented seem to point towards a combination of both proposed theories from literature for collagen mineralization. A significant caveat to liquid TEM remains its low repeatability for capturing these events and thus qualitative observations must be paired with correlative experimental methods. Trials and tribulations related to overcoming issues with repeatability and efforts to make this liquid TEM configuration work for collagen-based systems are shared. Ultimately, the novel liquid TEM techniques presented are not aimed to replace current characterization methods but rather offer real-time dynamic complementary insight to help validate theories arising from time-stamp observations, providing researchers with unparalleled opportunities to probe mineralization reactions. This work provides a foundation to move the field forward toward improving upon our liquid TEM capabilities to capture nanoscale inorganic-organic reactions and providing new means to unravel the intricacies behind how collagen mineralization occurs.

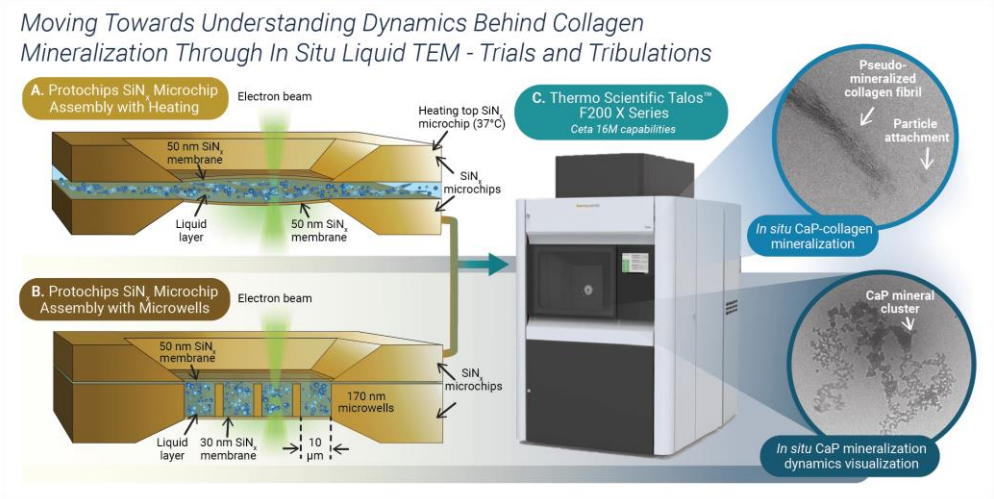

***Ch. 6 – Figure 1. Overview of liquid TEM enclosures used to capture mineralization dynamics**. **A.** Protochips SiN_x microchip assembly with heating used to observe collagen mineralization dynamics with exposure to CaP and pAsp. **B.** Protochips SiN_x microchip assembly featuring representative microwells used to probe mineralization reactions of the CaP-pAsp solution without the addition of collagen. **C.** Talos F200X is used for liquid TEM acquisition, equipped with a CETA 16M camera. Schematics not drawn to scale.*

6.4. Materials & Methods

6.4.1. Collagen Preparation

To study collagen biomineralization processes, a biomimetic rat-tail tendon reconstituted collagen mineralization *in vitro* model was used. The model closely mimics the structurally Type I collagen found in hard tissues in the human body.[9,23] The work described by Lausch et al. [9] describes the model collagen fibrillogenesis and crosslinking preparation in greater detail while Quan et al.[34] performs structural characterization on the structures.

To summarize the technique, rat tail tendons were surgically extracted from and then dissolved at 1 mg/mL in 0.5 M acetic acid. The solution was then diluted 1:1 by distilled water (diH_2O) and pH was adjusted to 5.0 using 1 M NaOH. After a 2-hour incubation period at 35°C in a water bath, collected collagen fibrils were fixed for 18 hours using a 0.08% glutaraldehyde aqueous solution (Electron Microscopy Sciences, Hatfield, PA, USA). After this crosslinking process, to remove excess glutaraldehyde and acetic acid as well as cease further system reactions, the collagen fibrils were dialyzed against diH_2O for 2 days with frequent water replacements.

6.4.2. Mineralization Experiments

Mineralization experiments were conducted based on an adaption to established procedures using a calcium phosphate-based system published by Despande and Beniash[25]. The aqueous-based mineralization solutions were prepared by mixing equal volumes of: prepared collagen fibrils in diH_2O at a concentration of approximately 0.4 mg/mL, 9 mM $CaCl_2 \cdot 2H_2O$ in 50 mM Tris, 4.2 mM K_2HPO_4 in 50 mM Tris, and 100 mM Tris–500 mM NaCl (Tris-NaCl). Prior to mixing, pAsp sodium salt (Mw 14 kDa; Alamanda Polymers, Huntsville, AL, USA), referred to as pAsp100, was dissolved into the Tris-NaCl solution to achieve a final solution concentration of 50 µg/ml for collagen mineralization experiments and 25 µg/ml for experiments without collagen. Except for the collagen solution, all other mineralization reagents were buffered to a pH of 7.4 at 37°C using 1M of hydrochloric acid and filtered through a 0.2 µm acrodisc syringe filter before use. For mineralization experiments without collagen fibrils, diH_2O was substituted in equal volume to the collagen fibril suspension.

Prepared solutions were mineralized at 37°C in a water bath set with a probe-controlled hot plate and gentle mixing of 100 rpm. All solutions for the experiments described were mineralized first *in vitro* and sampled at periods of interest for either *in situ* liquid TEM or *ex situ* correlative analysis. This was done to avoid long-term mineralization *in situ* under confinement, where mineralization in small liquid volumes has been reported to influence nucleation rates and lead to larger ACP particles in solution.[39,46,47] In between

transportation and setup periods, mineralization solutions were stored on ice to minimize reaction progression. All reagents were purchased from Sigma Aldrich and dissolved in Milli-Q diH_2O unless otherwise specified.

6.4.3. Liquid TEM Enclosure and Dry Sample Preparation

Liquid TEM experiments were performed using the Poseidon Select (Protochips, Morrisville, NC, USA) liquid TEM holder, a commercially available holder with *in situ* heating functionality. An exploded view of all of its components and the general liquid sample addition process and assembly process flow are shown in Figure 2.

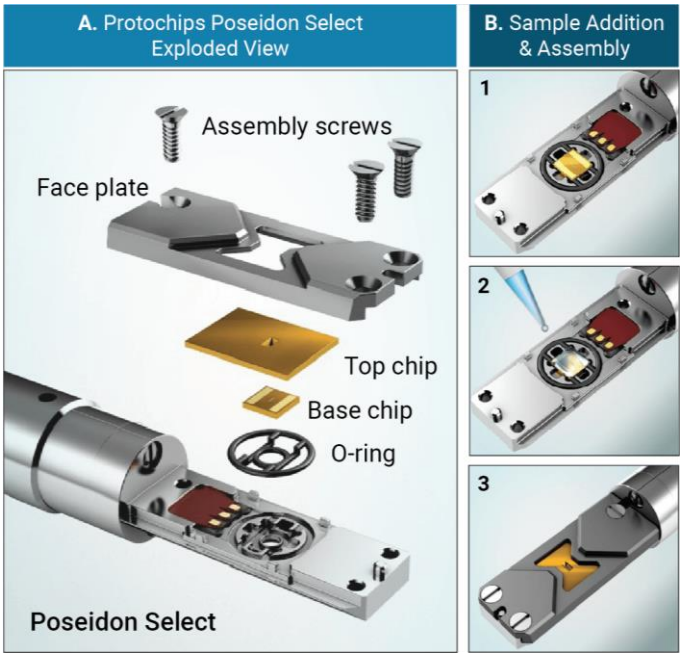

Ch. 6 – Figure 2. Protochips Poseidon Select assembly. A. *Exploded view of the holder, highlighting the top and bottom SiN_X microchips or E-chips that are sealed together through the addition of a face plate.* ***B.*** *Sample addition and assembly process shown for the holder, where 1) the small base E-chip is inserted into the O-ring in the open configuration of the holder then 2) liquid solution is drop-casted onto it and 3) the top large E-chips is added to the face place is screwed to seal the assembly.*

For liquid TEM collagen mineralization experiments featured, EPB-55A bottom SiN_X microchips, or E-chips referred to by Protochips, were paired with EHT-45ZZ top heating SiN_X E-chips. Both microchips have a 550 µm × 50 µm membrane window size. For these experiments, E-chips were arranged in a parallel configuration to maximize the field of view for experimentation to find regions of interest. During acquisition, the sample solution was heated to 37°C using the holder's *in situ* heating functionality.

For mineralization experiments without collagen added, EPT-42A top microwell E-chips with an 8 × 16 array of 10 μm × 10 μm, 170 nm-deep microwells were used paired with ECB-39A bottom E-chips, which had 400 μm × 200 μm and 300 μm × 90 μm membrane window sizes, respectively. For this configuration, E-chips were aligned perpendicularly to each other, leaving an effective viewing membrane window area of 200 μm × 90 μm. The perpendicular alignment provides higher stability to the assembly and mitigates bulging at the sacrifice of a larger viewing area. The microwells used in this assembly create small, isolated liquid pockets for running multiple experiments simultaneously to each other while mitigating beam effects from overspilling from one microwell to the next.[36,43] The microwells also have supports within the membrane through sections separating microwells, which contribute to a more rigid membrane that can lead to reduced bulging and a more uniform liquid layer within microwells.

E-chips were cleaned following the standard operating procedure recommended by Protochips to remove their photoresist protective layer. This involved a two-minute acetone then methanol wash, with approximately 50 mL of each solution, after which compressed air-dried E-chips were plasma cleaned with a Solarus Gatan Plasma System under 30 kW power conditions for two minutes with a Ne, H_2, and Ar gas combination (Gatan, Inc., Pleasanton, CA, USA). To form the liquid enclosure (Fig. 2B), variable amounts of mineralization solution, between 1-2 μL, were deposited onto the bottom E-chip and incubated for 2 minutes. Excess solution was removed using the edge of a piece of filter paper before adding the top E-chip and sealing the liquid TEM holder assembly, all done with screening using a light optical microscope (LOM). Prior to TEM imaging, the sealed liquid TEM holder was leak checked using a custom-designed vacuum pump station based on the HiCUBE™ Eco turbo pump platform (Pfeiffer Vacuum, Inc., Aßlar, Germany).

Following *in situ* liquid TEM experimentation, the holder was disassembled, and E-chips were removed, dipped in methanol to halt mineralization reactions from further progressing and clean samples of excess mineralization products, and then air-dried for *post situ* analysis. Correlative *ex situ* analysis was conducted using the same *in vitro* bulk mineralization solutions used for *in situ* testing at similar periods. *Ex situ* samples were drop-casted onto carbon-coated 400 mesh Cu TEM grids (Electron Microscopy Sciences, Hatfield, PA, USA) in 2 μL amounts. Liquid samples were allowed to incubate onto the grids for 2 minutes and then gently rinsed in a series of methanol droplets and allowed to air dry before imaging.

6.4.4. TEM Acquisition and Analysis

TEM acquisition was performed Talos 200X TEM (ThermoFisher Scientific, Waltham, MA, USA) equipped with an X-FEG source operated at 200kV in bright-field (BF) mode

with a CETA 16M camera. For *post situ* and *ex situ* correlative analysis, either the Poseidon Inspection single-tilt (Protochips, Morrisville, NC, USA) or a standard single-tilt (ThermoFisher Scientific, Waltham, MA, USA) holder was used. A 100 μm objective lens was used for low-dose beam exposure liquid TEM acquisition, with electron flux or dose rates varying between 0.40-6.5 $e^-/Å^2s$ in dynamic video mode and 0.40-10 $e^-/Å^2s$ otherwise for standard imaging. This electron dose rate aligns with acceptable ranges identified within mineralization systems involving CaP[36] and $CaCO_3$[37] as a safe threshold with limited beam-induced crystallization effects, having similar thresholds to low-dose cryo TEM if short exposures are considered.[48] Rates were measured using a recently calibrated fluorescent screen. Beam size was locked during imaging such that it would not vary during magnification to reduce sudden changes in beam dosage during screening and sample screening was further minimized throughout acquisitions. For acquisition, an exposure time of 1 second per frame was chosen using the Velox software (ThermoFisher Scientific, Waltham, MA, USA) with a 1-sec delay between acquired frames. All videos provided in the supplemental information were exported at a sped-up framerate of 10 fps, where elapsed time is featured in the upper left of each video in the minute:second configuration. When used, selective area electron diffraction (SAED) patterns were acquired using either a 10 or 40 μm sized aperture which provided an area coverage of an approximate diameter of 125 or 250 nm, respectively, in real space. SAED indexing was accomplished by analyzing concentric rings present in polycrystalline structures using the ImageJ software. Radii measurements from the camera-calibrated acquisitions were used to calculate the interplanar spacing and then compared to a hydroxyapatite (HA) crystallography base reference[49] – the expected present mineral phase in mineralized collagen fibrils.

Scanning TEM (STEM) mode using a high-angle annular dark field (HAADF) detector was used for *post situ* analysis. Electron energy loss spectroscopy (EELS) was conducted using a CMOS detector (Thermo Fisher Scientific) for EELS acquisition at an energy dispersion of 0.3 eV/channel and with a convergence semi-angle of 10.5 mrad. Dual EELS was used to simultaneously collect spectra from both core-loss and low-loss regimes. The acquisition region had a pixel size of 1.2 m and was collected with an exposure time of 0.005 s, where the total acquisition time was 21 min and 31 s in the region analyzed. EELS spectra were analyzed using Digital Micrograph Suite (GMS) 3.4.3 (Gatan, Inc., Pleasanton, CA, USA). Spectra collected were processed using principal component analysis (PCA) for denoising through the GMS PCA denoising option, based on the work of Lucas et al.[50] For maps collected, a power Law background subtraction modelling approach was taken. Elemental maps for Ca were generated from signals extracted within the corresponding peak energy window of PCA-analyzed spectra after background subtraction.

6.4.5. Grayscale Intensity Line Scan Analysis

Grayscale intensity line scan analysis was used to investigate collagen periodicity using the ImageJ software package and then analyzed in MATLAB. When implemented for Fig. 8, the "Plot Profile" function in ImageJ function was used for 7 whole distinguishable periods within the collagen fibril observed. Line scanning was done profiling along the long axis of the collagen fibril, with a line width averaging approximately 89.8 nm (280 px). Using MATLAB, a custom smoothing algorithm[51] was applied to the collected data using pseudo-Gaussian smoothing (4 passes of the same sliding average) applied to 5 data points at a time. The software was also used to identify local graph maxima and minima points to correlate with the line scan region to calculate the periodicity of the patterns present at repeating intervals.

6.5. Results & Discussion

6.5.1. CaP-pAsp *In Situ* Mineralization in Liquid TEM

To better understand *in situ* collagen mineralization reactions, the CaP-pAsp mineralization solution was investigated firstly on its own using *in situ* liquid TEM measures with the use of isolated microwells. In this set of experiments, a lower concentration of 25 μg/ml pAsp was used as a correlate to previously published work by Quan et al.[23] While studied extensively through time-stamped observations, limited research, except preliminary results of our own,[41] has explored this CaP-pAsp system dynamically in liquid.

Two representative early mineralization time points of approximately 2 and 4 hours were explored, where dynamic mineralization reactions were observed (Fig. 3). At the 2-hour mineralization point, small nucleation products and particles are seen (arrows, Fig. 3A). As mineralization progressed in different microwells, assumed to be isolated from each other and representative of different experiments running in parallel, branching and growth of particle assemblies occurred at approximately a 2.5-hour point (Fig. 3B, Video S1). To reduce electron beam dose, the long-term observation of CaP mineral assembly growth was prioritized over the observation of nucleation and growth mechanisms which require a higher magnification and dose. Thus, a low dose rate of 0.4 e^-/A^2s was selected to provide sufficient resolution to observe particles over time while simultaneously mitigating beam effects. Under these exposure rates, where Videos S1 and S2 have cumulative doses of approximately 400 e^-/A^2 and 800 e^-/A^2, respectively, the solution appeared stable. Beam-induced crystallization and sample degradation were not readily observed when comparing microwells that were exposed to the electron beam for relatively long periods in comparison to those that were left 'untouched' by the beam and only quickly screened for validation.

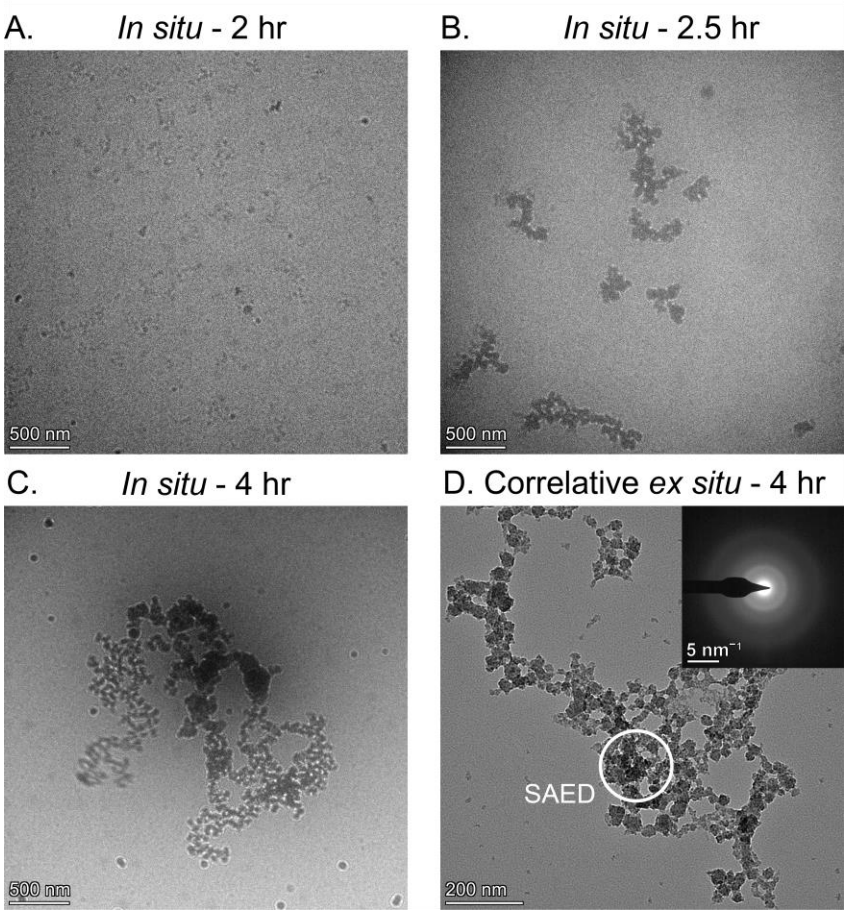

Ch. 6 – Figure 3. In situ liquid and ex situ dry BF TEM of CaP mineralization at early time points, mineralized in the presence of pAsp in a microwell system. A. *Initial survey region where arrows denote the presence of nucleation products formed in solution after mineralizing for 2 hours.* ***B.*** *In a new microwell, at the 2.5-hour mark, small particle clusters are observed and are seen attaching (Video S1).* ***C.*** *At the 4-hour mineralization point, larger branched aggregates are visualized to move in solution (Video S2).* ***D.*** *Correlative ex situ dry mineralization of the same solution captures similar CaP products which have formed, where selected area diffraction (inset) highlights the products are still amorphous after 4 hours of mineralization.*

At the 4-hour mineralization point, larger mineral aggregates were observed to grow over time and form branched assemblies (Fig. 3C, Video S2). Correlative *ex situ* mineralization results at the same period highlight similar-sized branched assemblies, where representative SAED confirms that the products formed are ACP in nature (Fig. 3D). In keyframes from Video S2 shown in Fig. S1, white triangles point out regions of the aggregate shown in Fig. 3C that transform over time. The regions of interest seem to transition from a dense phase to a more discretized branch-like particle aggregates with distinctive beads or globular particles. This could be further paralleled to the work from Olszta et al[24] and the formation of an ion-dense ACP PILP phase in the native liquid environment. However, the lower resolution of this reaction due to the low electron dose

rates used cannot, with certainty, validate this theory. Moreover, considering the size of the aggregate visualized and its partial mobility, products may be affected by the confinement of the liquid microwell and be partially adhered to the membrane window.

Post situ analysis of the sample after *in situ* mineralization for 6 hours (sample from Fig. 3C) is shown in Figure 4. Using the HAADF-STEM modality, EELS confirmed that the branched particle assemblies visualized were Ca-based, where the Ca-$L_{2,3}$ edge could be identified in the products, while the surrounding region without products was absent of this signal (and representative of the SiNx membrane itself) (Fig 3C,D). Correlative *ex situ* 6-hour mineralization results highlight the formation of large aggregates of similar polymeric branch morphology, wherein these structures were observed to be nearly amorphous (Fig. S2A). Without the addition of pAsp to inhibit crystallization, structures mineralized in this solution are expected to form crystalline apatite much quicker.[23,52] Figure S2B shows a correlative *ex situ* 5.5 hr mineralization period without the addition of pAsp to exemplify its role; a large, crystallized apatite structure is shown with no signs of polymeric branch structures when pAsp is not added (Fig. S2B).

These findings are consistent with the expected role of pAsp in solution. The mineral products visualized *in situ* at both 2 and 4 hr time points can be compared to the works of Quan and Sone using the same CaP mineralization solution buffers and pAsp concentration analyzed under dry conditions.[23] Similar branched polymeric bead assemblies were achieved in their experiments at 2 and 4-hour time points, where pAsp is attributed to a delay in apatite formation from Ca^{2+} ion-selective electrode measurements.[23] Similarly, cryo TEM observations, however without the presence of pAsp, have clearly demonstrated the formation of branched polymer assemblies before CaP crystalline mineral formation.[52] Prior *in situ* observations have also shown this behaviour, where nucleation and growth of similar branched assemblies, formed without the addition of pAsp, occurred within 20 minutes of mineralization with continued branching and growth observed within 60 minutes.[36] Polymeric branches and aggregated spherical particles in these systems without pAsp were visualized within earlier ranges of 2-60 minutes,[36,52] showing the comparative delay of mineralization events in 2-6 hour time points within the work presented here when pAsp is present. These findings and preliminary mineralization experiments set the stage for conducting *in situ* mineralization experiments in the same solution in the presence of collagen.

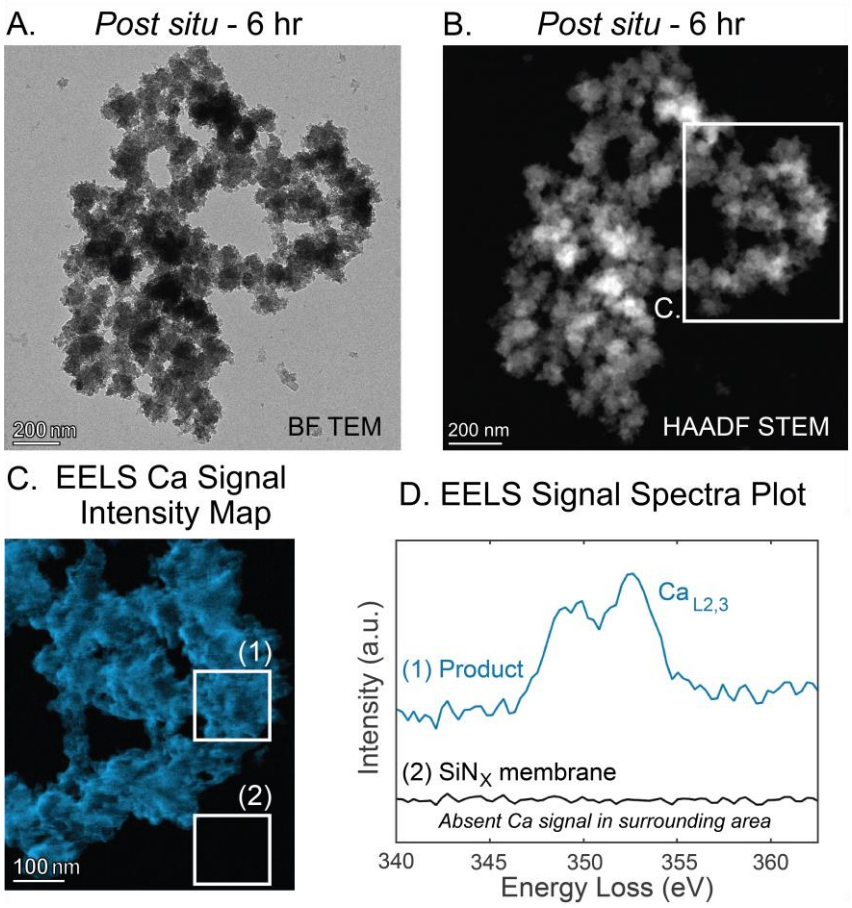

Ch. 6 – Figure 4. Post situ dry S/TEM of CaP particle products, mineralized for approximately 6 hours in the presence of pAsp. A. *BF TEM and* ***B.*** *HAADF STEM imaging of representative product on the SiN_x membrane. The box enclosed in B,* ***C.*** *shows an extracted post situ EELS Ca signal intensity map where in blue higher signal of Ca were detected.* ***D.*** *Extracted EELS signal spectra from the regions identified in the enclosed boxes in C. demonstrate that the in situ phase formed were Ca-based products where the Ca-$L_{2,3}$ edge is identified, while the surrounding region without products was absent of this signal (representative of the SiN_x membrane itself).*

6.5.2. Early Collagen Minearalization in Liquid TEM

Liquid TEM methods with heating at 37°C to mimic physiological conditions in the body were successfully applied to capture dynamic collagen mineralization reactions in solution from early (diffuse polymeric structures, limited CaP mineral platelets) to more mature (highly contrasted mineralized structures, CaP platelets aligned along fibrils) phase mineralization. As early as a 4-hour mineralization period, signs of mature mineralization have been observed within this collagen model from Chapter 5. Collagen fibrils do not mineralize simultaneously with each other within this system, attributed to their

heterogeneous suspension in solution, differences in surface area, solution exposure *in vitro*, and aggregation effects – as expected even within the body.

At early collagen mineralization periods, the majority of fibrils have diffuse contrast and have limited mineral platelets observed within their structures, demonstrated by the 2.5 hr mineralization period in Fig. 5. These regions were highly unstable during liquid TEM imaging, where solution bubbling was seen almost instantly at low electron dose rates of 2 e^-/A^2s or less. On magnification (Fig. 5B), short-beam exposures of an approximate cumulative dose of 10 e^-/A^2 showed already an increase in bubble sizes and a change in contrast of the fibril, eliciting potential electron damage to the collagen fibril. Recent literature suggests that HA, the common CaP-mineral phase in mature mineralization, can act as a scavenger of radiolysis species and thus lead to increased electron beam dose damage thresholds.[53] Likely this may explain the much higher beam sensitivity of the system at early mineralization points where mineral apatite is not yet observed – where more mature mineralization periods, discussed later, experienced higher beam damage tolerances.

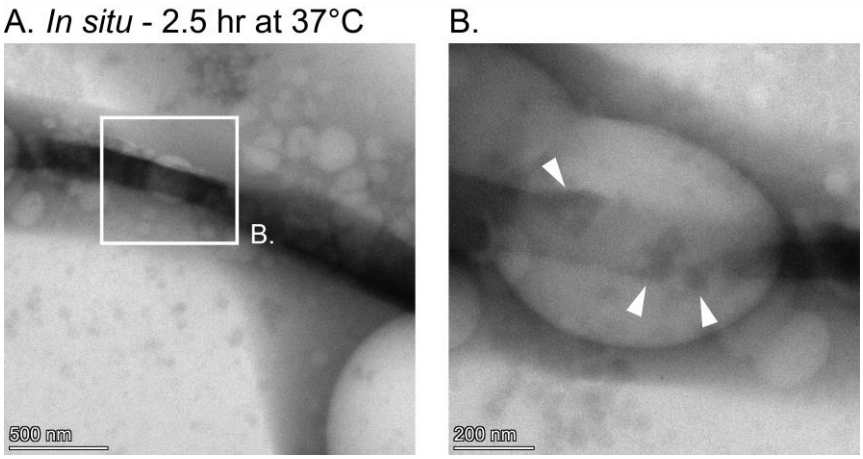

Ch. 6 – Figure 5. In situ liquid BF TEM of hydrated collagen fibrils, mineralized for approximately 2.5 hours in the presence of pAsp. A. *Low-magnification image of a hydrated region of interest, where a collagen fibril bundle is shown. Bubbles formed instantaneously on imaging within this region, highlighting the instability of the solution at this time point during liquid TEM even with low-dose screening measures with a rate of approximately 2 e^-/A^2s.* ***B.*** *High magnification of visualized fibril from region enclosed in B., where aggregates of unknown phase appear around and attached to the collagen (triangles).*

Considering challenges with beam sensitivity at this early mineralization stage, dynamic observations that elucidate mineralization initiation have yet to be captured using liquid TEM in this system. The magnified region in Fig. 5B where bubbles expanded with beam exposure did however lead to a partly thinner area on the fibril exposing particulate matter of an unknown phase (arrows, Fig. 5B). This seems to be attached to the fibril and could be visualized in the surrounding region, though it could not be fully resolved due to the

beam sensitivity and formation of bubbles on continued imaging. Thus, it is difficult to distinguish whether this is an agglomeration of particles or potentially an ion-dense PILP phase.

Similarly, correlative *ex situ* dry imaging of a 2.5-hour mineralized sample (Fig. 6A) shows diffuse low contrast in fibrils characteristic of early mineralization, where most fibrils are not fully mineralized and have minimal contrast. Darker regions represent areas that have accumulated mineral products and/or have started to mineralize. Representative areas shown in Fig. 6B-G highlight similar regions to Fig. 5 with particles attached and surrounding collagen fibrils. These regions appear to have less defined particulate structures, with no large polymeric structures but rather a diffuse phase decorated with small higher contrast particles. SAED shows these structures to be amorphous, with no diffraction rings or points noted (Fig. 6D, G). From the mineralization, times observed here and the reported CaP crystallization inhibition role of pAsp,[23] products observed *in situ* here seem to be an ACP precursor mineral phase to collagen mineralization. The structures seen *in situ* and *ex situ*, supported by the *in situ* observations in the absence of collagen presented in 3.1, seem to be potentially analogous to the ACP PILP collagen mineralization theory proposed by Olszta et al.[24]

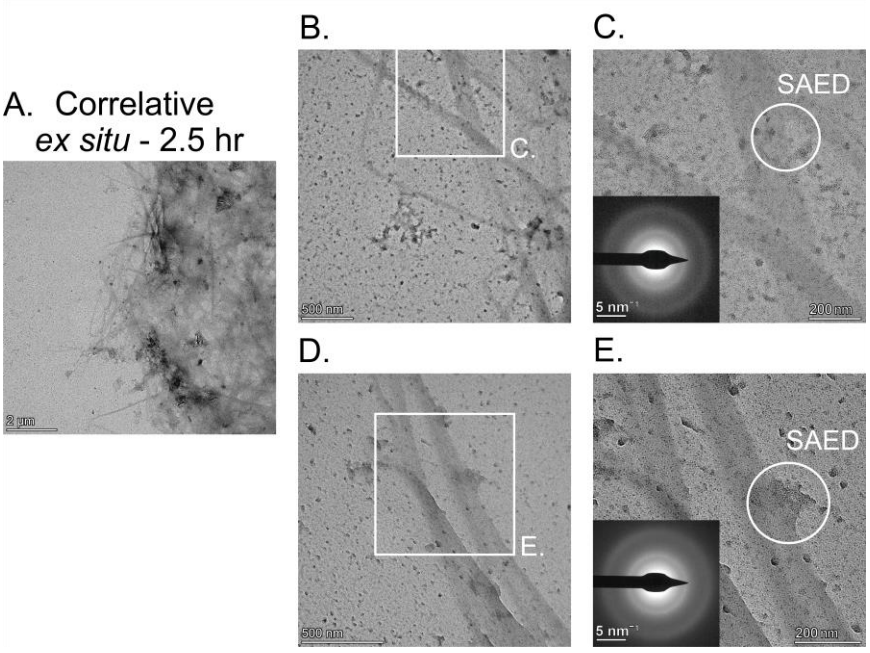

Ch. 6 – Figure 6. Representative correlative ex situ BF TEM of dry collagen fibrils, mineralized for approximately 2.5 hours in the presence of pAsp. A. *Low-magnification image of survey region, where collagen fibrils seen are bundled on a dry carbon-coated TEM grid.* ***B.-G.*** *Variable magnifications of representative collagen fibrils with mineral products dispersed within the region.* ***Insets - D., G.*** *SAED patterns indicate that adhered particles are likely amorphous.*

6.5.3. Dynamic Collagen Mineralization in Liquid TEM

Later stage collagen mineralization progression after 6 hrs is shown in Fig. 7, where collagen had darker contrast and mineral platelets were visualized. Dynamic particle attachment events were captured towards the end of a collagen fibril at its mineralization front *in situ* (Fig. 7B-G, Video S3 and S4). The video captures the dynamic formation of a mineral aggregate in solution near the collagen fibril mineralization front, tracked by the white arrow in Fig. 7E-G, which then attaches to the fibril. Additionally, a mineral aggregate already attached to the fibril is shown that seems to attract other particles in solution and integrate/flatten itself along the fibril, where a needle-like mineral structure appears adjacently (triangle, Fig. 7G). Seeing such a reaction *in situ* points towards the pAsp-involving particle attachment theory for collagen mineralization suggested by Deshpande and Berniash.[25] Others have theorized that once mineralization occurs across the transverse direction of a collagen fibril through spherulitic growth, it progresses from mineralization fronts longitudinally along fibril lengths.[28] Provided the *in situ* dynamics visualized at the 6-hour point (Fig. 7) and results presented in sections 3.1 and 3.2, there is a possibility of the interplay between PILP and particle attachment theory mechanisms that contribute together to collagen mineralization. But – the interpretation of these observations in Fig. 7 must be dissected further.

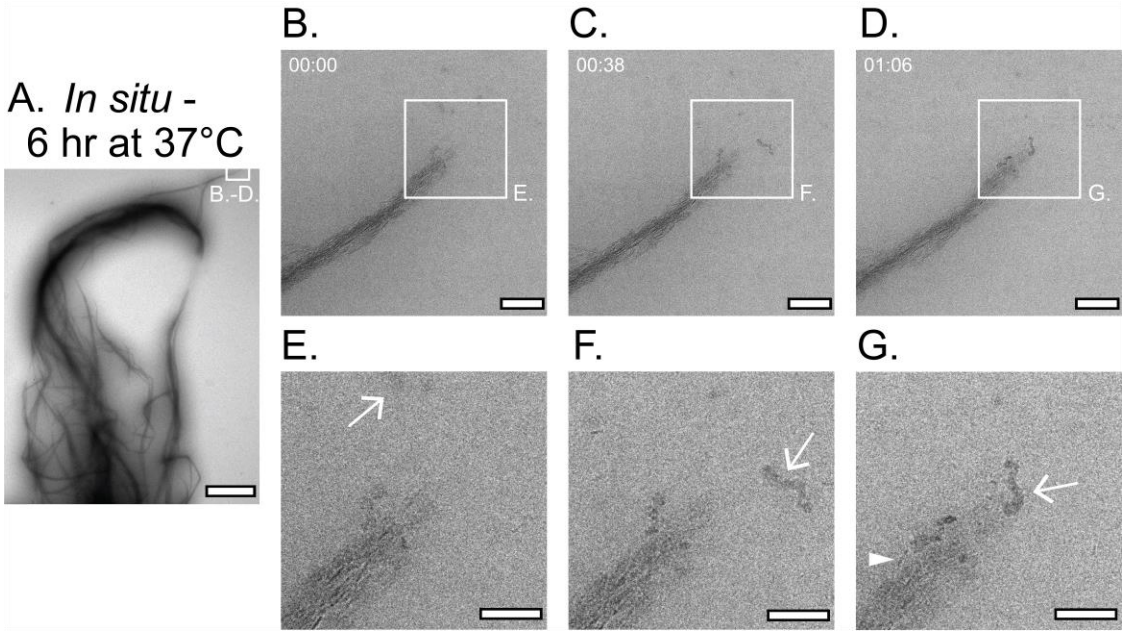

Ch. 6 – Figure 7. In situ liquid BF TEM imaging of dynamic hydrated collagen mineralization events at 37°C, mineralized for approximately 6 hours in the presence of pAsp. A. *Overview of the hydrated region of interest with a heterogeneous distribution of collagen fibrils.* ***B.-D.*** *Elapsed time progression (collection min:sec shown in the upper*

left corner) snapshot views of dynamic particle attachment events toward the end of a collagen fibril at its mineralization front (Video S3). ***E.-G.*** *Magnified view of the reaction, where a white arrow tracks the formation and movement of a particle assembly attaching to the collagen mineralization front in situ while the white triangle highlights the apparition of a needle-like structure after particle attachment (Video S4). Scale bars: A. 5 μm, B.-D. 200 nm, and E.-G. 100 nm.*

Although seeing this reaction take place may lead to 'believing', a caveat to the interpretation of these *in situ* using liquid TEM observations must be discussed: beam sensitivity. As the achievable resolution is sensitive to electron dose exposure,[40] a fine balance is needed between having a high enough electron dose rate to visualize nanoscale reactions taking place while not pushing this rate too high to destroy the sample too quickly. Tuning this balance can be done by observing changes in image quality/information with limiting beam-damage dosage thresholds using live monitoring of diffraction pattern disappearance or Fast Fourier Transform (FFT) signal intensity change, with beam exposure.[40,54,55] The review by Wu et al. nicely summarizes further approaches to take in performing liquid TEM for soft biological matter in consideration of beam effects in greater detail for reference.[40] While low-beam dose rates were carefully used, screening was kept to a minimum to reduce exposure, and solutions were buffered to aid in reducing chemically active species as theorized in literature,[36] electron beam damage could not be fully avoided in this system *in situ*. The electron beam may have induced the formation of products under beam exposure and/or accelerated reaction rates.[47,56] This re-emphasizes the importance of conducting *ex situ* observations in parallel, as done in this work.

Moreover, collagen as a biological material and matrix polymer is a soft, beam-sensitive material. CaP minerals are also formed of lighter elements and are inherently beam sensitive. Combined, these components were unstable during imaging, making *in situ* repeatability extremely challenging. The reactions taken place in Fig. 7 were only successfully captured in video in one instance. Within the region in Fig. 7, after 34 acquisition frames at an electron dose rate of 6.5 e^-/A^2s, signs of beam damage were observed which progressed and led to severe degradation (Video S5). The upper damage threshold of this system is estimated to be a cumulative dose of 442 $e/Å^2$, where severe structural damage occurred after this range. In another region with a dose rate of 3.5 $e^-/Å^2s$, severe degradation occurred almost immediately on electron beam exposure past a cumulative dose of approximately 119 $e/Å^2$ (Fig. S3, Video S6). Mineral products were seen around the collagen fibril and near the mineralization front in Fig. S3, but dynamic mineralization interactions could not be captured there or in other areas as fibrils experienced expansion and degradation processes quickly after acquisition (Fig. S3, Video S6).

Insight into processes viewed *in situ* must be paired with correlative complementary characterization methods for validation such as *post situ* (after *in situ* liquid imaging) and *ex situ* (without beam exposure) experimentation. Representative *post situ* observation results of the 6-hour collagen mineralization point (Fig. 7) after mineralizing for 1 hour *in situ* are shown in Fig. 7. Regions could not be located that were similar to the key frames shown in Fig. 7, though particulate matter was seen around and attached to collagen fibrils throughout their lengths. Similar observations were made in correlative *ex situ* 6-hour mineralization (Fig. S4). The dry *post situ* sample, now without a thick liquid layer, showed more clearly the presence of nanoscale CaP apatite mineral platelets along the collagen fibrils (Fig. 8A, B). SAED highlight the (002), (211), and (004) planes associated with crystalline CaP apatite, where arcs (002) and (004) indicate the preferential *c-axis* orientation of the crystals along the long axis of the collagen fibrils, indicative of intrafibrillar mineralization (Fig. 8B-Inset). Banding patterns of the repeating collagen structure were resolved *post situ* (Fig. 8B) where grayscale intensity plot profiling shows a repeating pattern of 67.1 nm with a standard deviation of 0.8 nm (Fig. 8C). These values align with results obtained by Quan et al. of unmineralized rat tail tendon derived reconstituted collagen with banding intervals on average to be 68.0 +/- 0.2 nm from cryo TEM imaging,[34] with the slightly lower average values achieved herein expected from shrinkage arising from contraction in mineralization.[35] Since the same mineralization solution without collagen would form large ACP polymeric branch structures (Fig. 4, Fig. S2A) rather than ordered plate-like mineral platelets along the long-axis of collagen fibrils (Fig. 7 and 8) at similar mineralization periods, the collagen fibril itself must then play an active role in forming crystalline mineral products within this CaP-pAsp system.

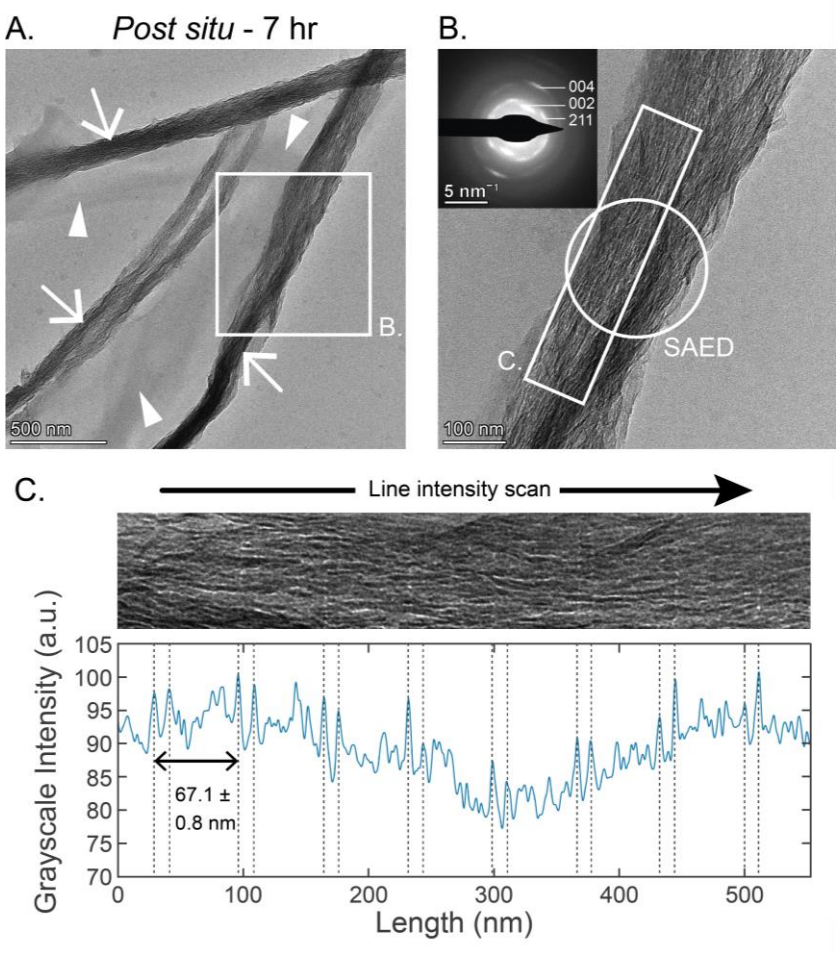

Ch. 6 – Figure 8. Post-situ BF TEM of dry collagen fibrils, mineralized for approximately 7 hours in the presence of pAsp. A. *Low magnification imaging highlights the distribution of regions of mineralized (arrows) and unmineralized (triangles) collagen fibrils.* ***B.*** *Higher magnification imaging of a mineralized collagen fibril shows the presence of mineral platelets with collagen banding patterns noted.* ***C.*** *SAED patterns of the region highlight the (002), (211), and (004) rings corresponding to the CaP-based apatite crystals, with arcs (002) and (004) indicating the preferential orientation of the crystal c-axis' along the long axis of the collagen fibrils.* ***D.*** *Grayscale intensity plot profile from the region enclosed in B. displays a magnified view of collagen banding patterns, repeating at intervals of 67.1 nm with a standard deviation of 0.8 nm.*

6.5.4. Technical Challenges, Limitations, and Future Considerations

There are several technical complexities involving using liquid TEM that limit the interpretation of these results and lead to future considerations. Two main challenges faced in collecting results within this collagen mineralization system are discussed herein which primarily included: 1) collagen heterogeneity and 2) electron beam sensitivity. Trials and tribulations to yield dynamic observations are further discussed, while future considerations are highlighted for those interested in performing similar experiments.

Collagen Heterogeneity

First, imaging the collagen fibrils proved to be challenging based on their heterogeneity and size ranges, which vary between twenty to hundreds of nanometers in diameter.[57] This is large for liquid TEM samples. In many instances, specimens would aggregate in solution and lead to uneven stresses on E-chips, resulting in a rupture on assembly or within the vacuum leak-check stage. Protochips offers E-chips with built-in spacers ranging from 50 nm to 5 μm to help control liquid thickness within a system and ensure a uniform liquid layer is achieved based on sample size to mitigate this. However, the spacers required to accommodate a larger thickness, like collagen fibrils, are generally over 150 nm and lead to significantly thick liquid layers on viewing membranes that limit resolution capabilities – making observing nanoscale CaP mineralization mechanisms of low-contrast collagen fibrils extremely challenging. Within these experiments, no spacer was used in these trials to keep liquid layers thin and reduce electron scattering, where larger fibril aggregates likely served as spacers themselves. Considering experiments to date, the success rate of enclosing a collagen sample without rupture and achieving images in the TEM is estimated to be 1/10, but this did not guarantee a good region of interest for capturing reactions or that collagen was found within membrane windows – making running these experiments time-consuming and expensive.

Moreover, heterogeneous collagen fibril aggregates can act as spacers between the SiN_X membranes, where such large specimens lead to thick, resolution-limiting liquid layers.[40] This is observed in a separate 6-hour mineralization trial presented in Fig. 9 where no spacer was used. Signs of mature mineralization with higher contrast fibrils with mineral platelets are present, though less diffuse unmineralized fibrils are not able to be resolved within the region (Fig. 9). Regions of higher density of collagen fibrils appear significantly darker (stars, Fig. 9A), where it is assumed locally that the collagen is acting as a spacer and contributing to thicker liquid regions based qualitatively on mass-thickness contrast. This is expected due to sample size and associated liquid thickness effects in BF TEM.[43,58] While plate-like mineral structures could be resolved in select regions where the liquid layer appeared thinner due to higher intensity brightness (Fig. 9B,C), these areas appeared muted and resolution of such features was challenging in the thicker liquid.

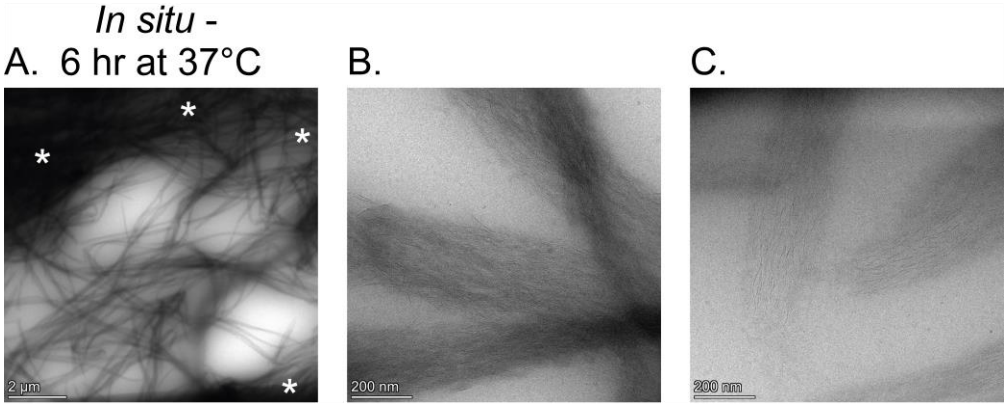

Ch. 6 – Figure 9. In situ liquid BF TEM of hydrated collagen fibrils at 37°C, mineralized for approximately 6 hours in the presence of pAsp. A. *Overview of the hydrated region with a heterogeneous distribution of collagen fibrils, where regions with a higher density of fibrils appear darker (stars).* ***B.,C.*** *Representative imaging of collagen in the mineralization solution, where needle-like mineral platelets were observed but overall features appear muted through the thick liquid layer.*

Ruptures and thick liquid layers from the heterogeneous collagen fibrils were somewhat avoided through careful specimen solution deposition during the liquid TEM preparation (Fig. 2B). Light optical microscopy (LOM) screening was used to ensure large aggregates were removed with a pipette or filter paper before assembly while removing excess solution. LOM screening served another failure-reducing purpose during preparation: to ensure that collagen was deposited across the viewing area. At times, collagen would not be distributed across the membrane window or would dewet from the membrane when the excess solution was removed or on assembly. This led to trials with no collagen within the viewing membranes in liquid TEM. LOM aided to verify the presence of collagen on membrane windows; if no collagen was seen, additional liquid sample was deposited. This is the reason why a parallel E-Chip configuration was used to maximize viewing area and hence increase the odds of collagen fibrils being captured *in situ.* This is at the sacrifice of a more rigid membrane structure that would be more resistant to rupture and bulging that would otherwise be obtained using a perpendicular E-Chip configuration with a smaller viewing area. Significantly fewer fibril aggregates were encapsulated in comparison in Fig. 7 implementing LOM screening and the deposition method described, resulting in regions with less fibril density and assumed thinner liquid layers based on resolution capabilities and brightness in BF TEM.

Running *post situ* analysis brought to light other challenges with collagen heterogeneity. *Post situ,* a methanol rinse was used to clean and halt mineralization reactions, which could further displace specimens. Fibrils risked delamination and displacement from SiN_X E-chip membranes on liquid TEM enclosure opening and during the *post situ* methanol rinse.

Thus, collagen and mineralization products were unlikely to remain in the same location as observed *in situ*, limiting the ability to revisit this region *post situ.*

While this discussion has provided methods to improve the success throughput of enclosures for liquid TEM research studying heterogeneous collagen fibrils, widely applicable to other mineralization systems and heterogeneous samples, it is warned that these large structures with the tendency to aggregate and dewet from SiN_x membranes remain challenging to image, requiring time and resource investment to move forward in making observations using liquid TEM.

Electron Beam Sensitivity and Beam Effects

The second and perhaps more prominent challenge with these liquid experiments is the electron beam sensitivity of this system and the potential for beam-induced effects to influence findings. Within experiments presented herein, electron dose rates varying between 0.40-6.5 $e^-/Å^2s$ in dynamic video mode and 0.40-10 $e^-/Å^2s$ otherwise for standard imaging were used. As mentioned in the methods section, these rates align with acceptable ranges identified within mineralization systems involving CaP[36] and $CaCO_3$[37] as a safe threshold with limited beam-induced crystallization effects. They also align with similar thresholds to low-dose cryo TEM if short exposures are considered.[48]

Still, it was noted *in situ* that the observation of long-term collagen mineralization reactions was impeded by electron beam irradiation that led to severe damage to samples over time. Section 3.2 reports that for early mineralization periods, cumulative doses of approximately 10 $e^-/Å^2$ lead to increases in bubble sizes as well as changes in contrast in the polymeric collagen, indicative of beam damage (Fig. 5). Section 3.3 reports higher range cumulative dose values between 119-445 $e^-/Å^2$ resulting in severe fibril damage (Videos S5 and S6), suggesting in comparison that a higher degree of mineralization may contribute to increased electron beam damage thresholds. Recent work by Jokisaari et al. suggests that HA, the common CaP-mineral structural formed in mineral platelets described within mature mineralization, can act as a scavenger of radiolysis species and thus lead to increased electron beam dose damage thresholds.[53] An increase in the resistance of water against radiolysis of approximately twentyfold when HA was introduced in their graphene-based liquid TEM enclosure, where no stable hydrogen bubbles were found for electron dose rates below a 170 $e^-/Å^2s$ threshold compared to in water alone was a mere 9 $e^-/Å^2s$ threshold was shown.[53] This may explain differences in beam dose tolerances in regions previously discussed in the 6-hour mineralization system versus the 2.5-hour sample, where also consideration of sample distribution and liquid layer thickness could contribute. Thus, the same damage threshold cannot be applied across collagen fibrils experiments and will vary on sample mineralization progress and distribution and must be optimally and conservatively chosen for each experiment.

Moreover, unlike many *in situ* liquid TEM reactions published, collagen mineralization reactions take place over long periods, often lasting hours with some tissue models taking days. As observed within this work, beam exposure within seconds can cause permanent damage to the structures, affecting subsequent reactions even when low electron doses are used, limiting the ability to image such samples over long periods. Such beam interactions can affect local temperature and chemistry *in situ*[59,60] – where temperature and pH also have been reported to play a significant role in CaP mineral nucleation and growth.[61] Thus, unlike other liquid TEM experiments where a region of interest may be revisited and reimaged, this limits the ability to perform liquid TEM over long periods in the same area.

This provides only the capability of viewing snapshots of reactions such as that shown in Fig. 7, limiting observations over time and introducing the need to validate with correlative TEM. Moreover, while microfluidic liquid flow is often introduced to relieve *in situ* of radiolysis products and replenish regions of interest with fresh solutions,[62,63] this was not implemented with mineralization systems explored herein. As collagen and CaP mineral products can easily dewet from SiN_x membranes and form aggregates, as described earlier, they could also do so under flow conditions and likely clog microfluidic lines. Second, this would ideally require a heated external pump capable of maintaining an *ex situ* reservoir solution at consistent temperatures, currently not commercially available. Thus, while microfluidic liquid flow could be a better mimic for the human body and would mitigate some effects from electron dose, this could not be implemented in trials that were operationally safe for the liquid TEM holder or reliable without external liquid reservoir heating.

In the future, the advent of low-electron dose imaging and automated tools, used extensively in cryo TEM fields, and new software options for sample and acquisition metadata tracking, e.g. Protochips AXON platform,[64] will be key for promoting faster high-resolution liquid TEM acquisition with better control over electron beam effects.[44,65] Electron beam effects may further be mitigated in future research by introducing a scavenging element, such as graphene, shown in literature to effectively scavenge reactive radical species in solution.[66,67] Care must be made to ensure that such additives do not significantly interfere with these sensitive mineralization processes. Lastly, to avoid continued effects from radiolysis product buildup and possible long-term confinement effects, as reported previously in literature in CaP[39] and $CaCO_3$[46] systems to impact mineralization and ACP stabilization, bulk mineralization solutions should be sampled at multiple periods of interest as done herein. Nonetheless, considering the multiscale hierarchy of mineralized tissues,[68] understanding how these reactions scale up must further be investigated to correlate *in situ* nanoscale observations to macroscale tissue regeneration events. Light microscopy methods paired with novel liquid-SEM means, such as WETSEM[69] or room-temperature ionic liquids,[70,71] offer further opportunities to

correlatively study mineralization processes with direct imaging through hydrated multiscale means.

6.6. Conclusion

Liquid TEM is a powerful tool to shed light on real-time dynamic processes. In this work, the first dynamic and physiological temperature liquid TEM videos capturing collagen mineralization from a CaP-pAsp mineralization solution are presented. Using *in situ* liquid TEM, early to more mature collagen mineralization periods were probed in near-native conditions. Evidence of both ACP PILP and particle attachment processes were seen in early and later mineralization, respectively, suggesting the two mechanisms contribute to collagen mineralization in the presence pAsp and may operate at different stages of mineralization. These first-time experiments in liquid present considerable leaps in technique development and demonstrate the feasibility of studying collagen mineralization dynamically by liquid TEM. These findings and our ensuing honest discussion on trials and tribulations will help bridge technical knowledge gaps and guide others seeking to study collagen mineralization processes or similar inorganic-organic interfaces *in situ* using liquid TEM. Ultimately, this work shares new technical breakthroughs in the characterization of complex mineralization reactions, bringing us ultimately one step closer to answering: *how does biomineralization occur?*

Acknowledgements

Financial support provided by the Natural Sciences and Engineering Research Council of Canada (NSERC) (grant no. RGPIN-2020-05722) and by the Canadian Institutes of Health Research (grant no. PJT 180575) are greatly acknowledged. Further financial support provided by NSERC for the Canada Research Chairs Program (K.G.; Tier II Chair in Microscopy of Biomaterials and Biointerfaces), and Vanier Canada Graduate Scholarship (L.-A.D.), are acknowledged. Electron microscopy was performed at the Canadian Centre for Electron Microscopy (also supported by NSERC and other government agencies). Special thanks go out to Dr. Deborah F. Kelly from Pennsylvania State University for their electron microscopy support and guidance.

Author Contributions

Conceptualization: Liza-Anastasia DiCecco, Ruixin Gao, Eli Sone, Kathryn Grandfield
Methodology: Liza-Anastasia DiCecco, Ruixin Gao
Data curation: Liza-Anastasia DiCecco
Formal analysis: Liza-Anastasia DiCecco, Ruixin Gao, Eli Sone, Kathryn Grandfield
Funding acquisitions and supervision: Eli Sone, Kathryn Grandfield
Writing: Liza-Anastasia DiCecco, Eli Sone, Kathryn Grandfield
Review and editing: Liza-Anastasia DiCecco, Ruixin Gao, Eli Sone, Kathryn Grandfield

References

[1] H. P. Wiesmann et al., *Int Rev Cytol* 2004, *242*, 121.
[2] B. Brodsky et al., *Matrix Biol* 1997, *15*, 545.
[3] W. J. Landis et al., *J Struct Biol* 1993, *110*, 39.
[4] A. J. Hodge et al., in *Aspects of Protein Structure* (Ed: G.N. Ramachandran), Academic Press, New York, 1963, pp. 289–300.
[5] S. V. Dorozhkin et al., *Angewandte Chemie Int Ed* 2002, *41*, 3130.
[6] L. He et al., *J Struct Biol* 2019, *207*, 115.
[7] C.-W. (Jeff) Wang et al., *Curr Osteoporos Rep* 2016, *14*, 284.
[8] N. Alexopoulos et al., *Nat Rev Cardiol* 2009, *6*, 681.
[9] A. J. Lausch et al., *Adv Funct Mater* 2018, *28*, 1804730.
[10] L. C. Palmer et al., *Chem Rev* 2008, *108*, 4754.
[11] Y.-R. Zhang et al., *Int J Oral Sci* 2014, *6*, 61.
[12] F. Nudelman et al., *J Struct Biol* 2013, *183*, 258.
[13] S. R. Stock, *Calcif Tissue Int* 2015, *97*, 262.
[14] E. A. McNally et al., *Plos One* 2012, *7*, e29258.
[15] J. P. R. O. Orgel et al., *Proc National Acad Sci* 2006, *103*, 9001.
[16] J. P. R. O. Orgel et al., *Structure* 2001, *9*, 1061.
[17] Y. Bala et al., *Bone* 2010, *46*, 1204.
[18] S. F. Jackson, *Proc Royal Soc Lond Ser B - Biological Sci* 1957, *146*, 270.
[19] R. A. Robinson et al., *Anatomical Rec* 1952, *114*, 383.
[20] W. Traub et al., *Proc National Acad Sci* 1989, *86*, 9822.
[21] H. P. Schwarcz et al., *Bone* 2020, *135*, 115304.
[22] X. Su et al., *Bone* 2003, *32*, 150.
[23] B. D. Quan et al., *J Roy Soc Interface* 2018, *15*, 20180269.
[24] M. J. Olszta et al., *Mater Sci Eng R Reports* 2007, *58*, 77.
[25] A. S. Deshpande et al., *Cryst Growth Des* 2008, *8*, 3084.
[26] F. Nudelman et al., *Nat Mater* 2010, *9*, 1004.
[27] B. Cantaert et al., *J Mater Chem B* 2013, *1*, 6586.
[28] E. Macías-Sánchez et al., *Adv Funct Mater* 2022, *32*, 2200504.
[29] W. J. Landis et al., *J. Struct. Biol.* 1993, *110*, 39.
[30] H. P. Schwarcz et al., *J Struct Biol* 2014, *188*, 240.
[31] B. E. J. Lee et al., *Adv Biology* 2021, *5*, 2100657.
[32] N. Reznikov et al., *Acta Biomater* 2014, *10*, 3815.
[33] N. Reznikov et al., *Science* 2018, *360*, eaao2189.
[34] B. D. Quan et al., *Bone* 2015, *77*, 42.
[35] A. Masic et al., *Nat Commun* 2015, *6*, 5942.
[36] X. Wang et al., *Commun Chem* 2018, *1*, 80.
[37] P. J. M. Smeets et al., *Nat Mater* 2015, *14*, 394.
[38] M. H. Nielsen et al., *Science* 2014, *345*, 1158.
[39] B. Jin et al., *Cryst Growth Des* 2021, *21*, 5126.
[40] H. Wu et al., *Adv Mater* 2020, *32*, 2001582.

[41] L.-A. DiCecco et al., *Microsc Microanal* 2022, *28*, 1818.
[42] W. J. Dearnaley et al., *Nano Lett* 2019, *19*, 6734.
[43] G. Jonaid et al., *Adv Mater* 2021, *33*, 2103221.
[44] D. F. Kelly et al., *Curr. Opin. Struct. Biol.* 2022, *75*, DOI 10.1016/j.sbi.2022.102426.
[45] A. J. Lausch et al., *Adv Funct Mater* 2013, *23*, 4906.
[46] R. Kröger et al., *Mineral-basel* 2018, *8*, 21.
[47] G. Zhu et al., *Micron* 2019, *118*, 35.
[48] H. Friedrich et al., *Angewandte Chemie Int Ed* 2010, *49*, 7850.
[49] "Ca-hydroxyapatite (Ca5[PO4]3[OH] rt) Crystal Structure: Datasheet from 'PAULING FILE Multinaries Edition – 2022' in SpringerMaterials," can be found under https://materials.springer.com/isp/crystallographic/docs/sd_1802016, n.d.
[50] G. Lucas et al., *Micron* 2013, *52*, 49.
[51] T. O'Haver, "Fast Smoothing Function," can be found under https://www.mathworks.com/matlabcentral/fileexchange/19998-fast-smoothing-function, 2017.
[52] W. J. E. M. Habraken et al., *Nat Commun* 2013, *4*, 1507.
[53] J. R. Jokisaari et al., *Nanotechnology* 2021, *32*, 485707.
[54] B. E. Bammes et al., *J Struct Biol* 2010, *169*, 331.
[55] S. B. Hayward et al., *Ultramicroscopy* 1979, *4*, 201.
[56] T. J. Woehl et al., *Mrs Bull* 2020, *45*, 746.
[57] D. A. D. Parry et al., *Proc Royal Soc Lond Ser B Biological Sci* 1978, *203*, 305.
[58] H. Wu et al., *Small Methods* 2021, *5*, 2001287.
[59] B. Fritsch et al., *Nanoscale Adv* 2021, *3*, 2466.
[60] B. Fritsch et al., *Arxiv* 2022, DOI 10.48550/arxiv.2209.05331.
[61] L. V. Sorokina et al., *Emergent Mater* 2021, *4*, 1205.
[62] E. A. Ring et al., *Microsc Microanal* 2010, *16*, 622.
[63] X.-Y. Yu et al., *Microfluid Nanofluid* 2013, *15*, 725.
[64] M. D. Dukes et al., *Microsc Microanal* 2022, *28*, 108.
[65] L.-A. DiCecco et al., *J Vis Exp* 2022, e63856.
[66] H. Cho et al., *Nano Lett* 2016, *17*, 414.
[67] S. Keskin et al., *Nano Lett* 2018, *18*, 7435.
[68] D. M. Binkley et al., *Acs Biomater Sci Eng* 2017, *4*, 3678.
[69] C. Lorenz et al., *Int J Occup Env Heal* 2010, *16*, 406.
[70] L.-A. DiCecco et al., *Micron* 2021, 103192.
[71] L. DiCecco et al., *Chembiochem* 2021, *22*, 2488.

Chapter 6: Supplemental Figures

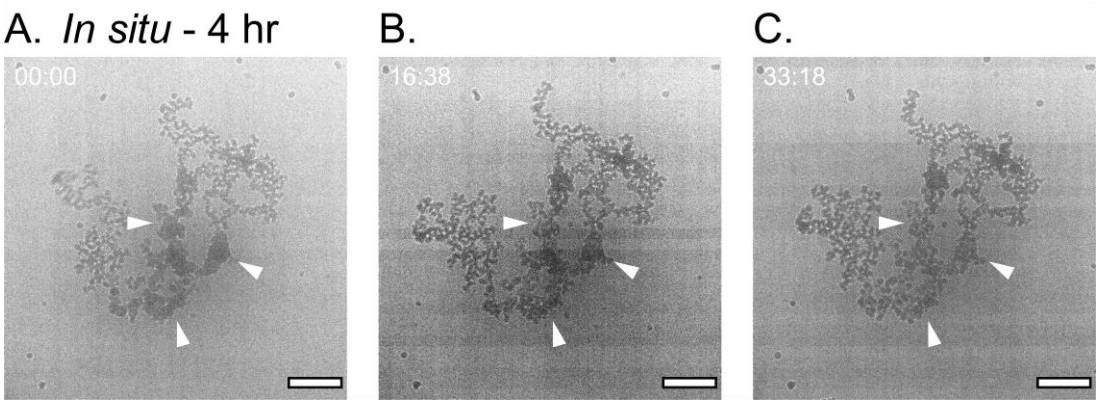

Ch. 6 – Figure S1. ***In situ liquid BF TEM of dynamic hydrated CaP mineralization events, mineralized for approximately 4 hours in the presence of pAsp (Video S2). A.-C****. Snapshot of representative frames (collection min:sec shown in the upper left corner) of dynamic CaP mineralization events, referenced in Fig. 3C of the main text. White triangles show regions that transform over time from a seemingly dense phase to branch-like particulate aggregates. Scale bars are 500 nm.*

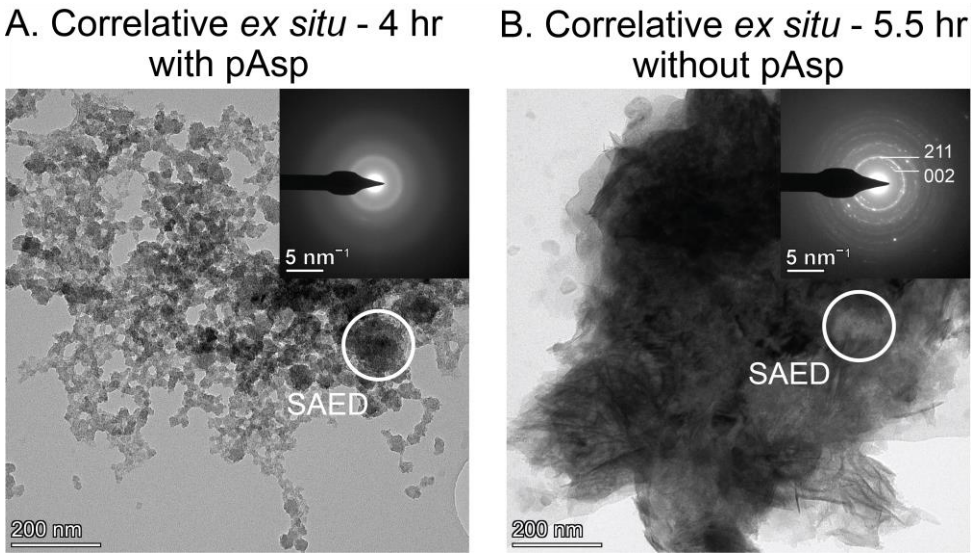

Ch. 6 – Figure S2. Representative correlative ex situ BF TEM of dry CaP mineralization products, mineralized with and without the presence of pAsp*. A. Correlative ex situ 6-hour mineralization point with pAsp where SAED (inset) highlights that the mineral branched assemblies are nearly amorphous in nature. B. Correlative ex situ 5.5-hour mineralization point without pAsp where structures were significantly larger and had a much higher degree of crystallinity from SAED (inset), where polycrystalline ring patterns of the (002) and (211) planes are highlighted representative of CaP apatite.*

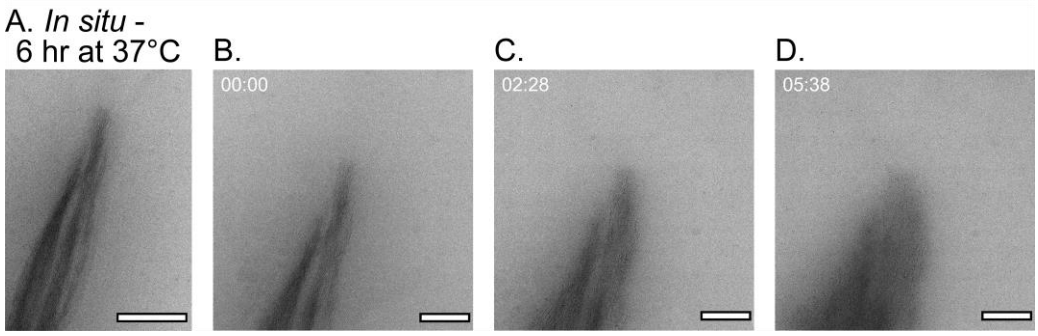

Ch. 6 – Figure S3. In situ liquid BF TEM imaging of beam-dose related damage of hydrated collagen fibril, mineralized for approximately 6 hours in the presence of pAsp. A. *Similar area of interest to Fig. 5, showing the mineralization front of a collagen fibril.* ***B.-D.*** *Elapsed time progression (collection time min:sec shown in the upper left corner) highlighting snapshots of the fibril with beam exposure over time at an electron dose rate of 3.5 e^-/A^2s (Video S6). Scale bars: A. 500 nm and B.-D. 300 nm.*

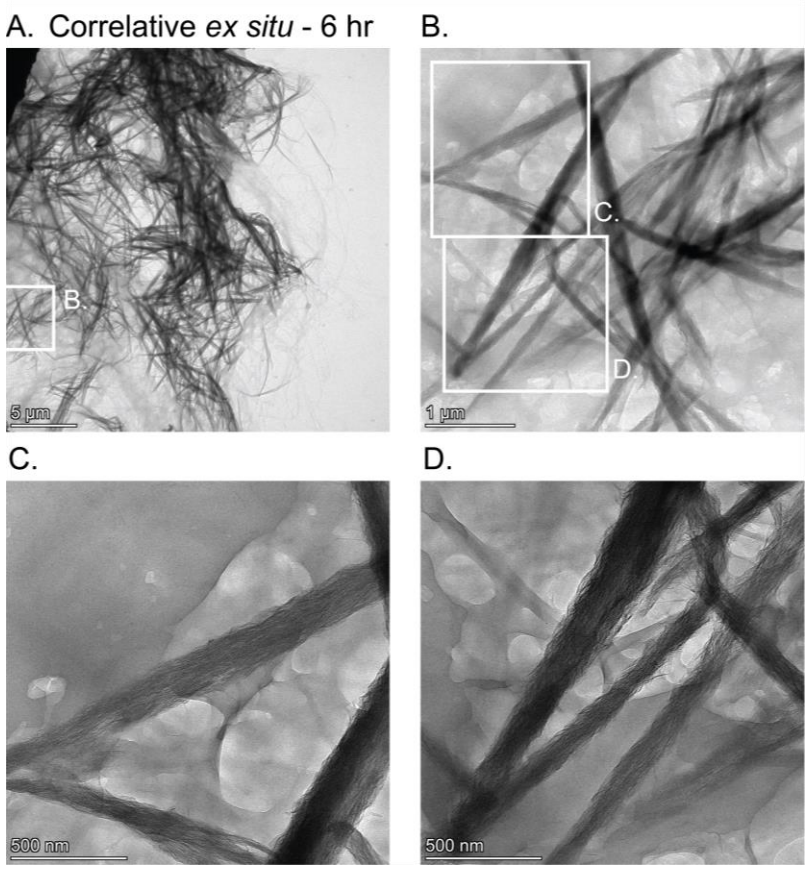

Ch. 6 – Figure S4. Ex situ BF TEM of dry collagen fibrils, mineralized for approximately 6 hours in the presence of pAsp. A. *Low magnification view of fibrils, where a mix of mineralized (darker contrast) and unmineralized (lighter and more diffuse contrast) regions can be noted.* ***B.*** *Representative region showing mineralized fibrils among unmineralized structures in the background.* ***C., D.*** *Higher magnification imaging shows the presence of mineral platelets aligned along the long axis of the fibrils.*

Chapter 7: Conclusions & Future Work

In this thesis, liquid EM techniques have been demonstrated to be a powerful tool which can assist in studying biological samples and their dynamic processes *in situ*, ultimately helping *answer life science questions using materials science approaches.* The research workflow presented, adapting in complexity from static microscale to dynamic nanoscale liquid EM, was key for the characterization of hydrated specimens in biomimetic conditions.

7.1. Key Findings and Contributions

7.1.1. Exploring Room Temperature Ionic Liquids to Facilitate Biological SEM

In Chapter 3, RTILs are *explored* to facilitate biological SEM, particularly for mineralized tissues such as bone in healthy and pathological conditions. The work contributes a simple and efficient workflow for liquid-SEM using RTILs for bone that was demonstrated to better preserve bone structures by avoiding traditional, lengthy SEM preparation schemes involving dehydration. An optimal ionic liquid treatment was established using a 10 % v/v [BMI][BF_4] aqueous-based method for studying hierarchical structures of bone which led to minimal electron beam charging effects even in EDX analysis. Overall, this provides a foundation for the use of RTIL-based SEM techniques for the study of hard tissues, widely applicable to a variety of biological materials.

Future work: In future, this technique is anticipated to be key for the study of inorganic-organic implant-bone interfaces, which are susceptible to separation and other preparation-related artifacts for traditional SEM involving dehydration, fixation, and embedding.[1,2] As exemplified in Chapter 3 and further summarized in literature in Chapter 2.1, these preparation-related artifacts for polished and bulk bone samples may be avoided through the implementation of the hydrated RTIL scheme by avoiding traditional preparation methods altogether. Moreover, recent work from my team highlights RTIL liquid SEM imaging visualizing hydrated cells on nanostructured surfaces,[3] demonstrating the potential utility of the technique to visualize hydrated cells within bone at a nanotextured interface. This could aid in expanding our understanding of implant-bone interfaces and ultimately contribute to the characterization and improvement of osseointegration processes. Additionally, there have yet to be FIB-SEM applications to my knowledge that have involved hydrated RTIL-treated biological samples. Bone as a hard tissue presents an excellent candidate for attempting hydrated FIB-SEM using RTILs, which could push the liquid EM field to 3D characterization capabilities to understand native hydrated biomaterials.

7.1.2. Developing New Methods for High-Resolution Liquid Biological TEM

In Chapter 4, I elaborated on technical protocols for performing correlative HR imaging of virions in both liquid and in ice, where notably a new thin-film liquid TEM enclosure method is *developed* and presented upon. Leveraging automated tools and direct electron detection capabilities, it is demonstrated through single-particle analysis in liquid and cryo conditions that similar resolutions may be achieved – where 3D reconstructions were able to resolve sub-nanometer structural features in the range ~3.5 Å – 10 Å.

This new liquid TEM enclosure is facile to assemble (with a video procedure provided within the article) and I highlight that samples can be stored for months in the hermetically sealed clipped enclosure. An advantage to the enclosure includes that it can be used with most TEM holders and requires limited specialized tools for assembly – contributing to the field a more inexpensive and accessible way to perform liquid TEM. I also note another contribution to this field which is demonstrated includes that this enclosure can be flash-frozen using liquid nitrogen, where screened encapsulated frozen samples were noted to have limited ice crystals present and could produce HR structural reconstructions of particles. Overall, I highlight that these complementary characterization tools are expanding our capabilities at studying biological specimens in hydrated environments, relevant to our current COVID-19 climate and understanding the complex behaviour behind pandemic pathogens.

Future work: As noted in Chapter 2.2, technical advances in direct electron detection for acquisition are anticipated to be an exciting future avenue for biological imaging with high-speed, highly sensitive acquisition capabilities key for maximizing signal-to-noise ratios at low-dose electron exposure. These technical advances paired together with automated programs that allow for high-throughput sample screening and automated acquisition techniques, such as SerialEM and EPU used in Chapter 4, anticipate leading the push for the "real-time resolution revolution" as an emerging future for liquid EM of biological specimens – leading someday to visualize HR molecular dynamics *in situ* in real-time.

7.1.3. Applying Novel Liquid-TEM Methods to Dynamic Biomineralization Systems

In Chapter 5, I *applied* the novel liquid TEM enclosure developed in Chapter 4 successfully to the study of collagen mineralization processes in hydrated conditions. HR resolution details were revealed in thin-liquid regions, where direct electron detector automated acquisition is attributed to high-throughput, low-dose imaging capabilities within this work. Within the biomimetic model consulted in liquid conditions, precursor amorphous mineral phases were noted in early phases of mineralization while at later progressions distinctive crystalline, nanoscale mineral platelets were visualized aligned along collagen fibrils. The complementary study of these processes in liquid paralleled with observations found in literature,[4–12] demonstrates the key potential of this facile liquid TEM enclosure method as a characterization tool within the field of biomineralization. However, dynamic mineralization reactions were not captured using this liquid encapsulation method. This

was discussed with support from literature to be likely a result of confinement effects, lack of heating functionality, and cumulative beam damage.

Overcoming the functional challenges described in Chapter 5, within Chapter 6 dynamic collagen mineralization reactions were successfully acquired using a commercial liquid TEM holder mimicking physiological conditions at 37°C. Uniquely, using this liquid technique, I present evidence of the coexistence of two different ACP precursors discussed separately in literature in CaP-pAsp collagen mineralization models, notably collagen-adhered PILP[13] and particle structures.[14] This suggests that the two mechanisms, discussed separately and often debated in literature, may interplay within collagen biomineralization processes – contributing to a new understanding of the potential mechanisms behind how collagen mineralizes. Chapter 6 also enumerates several challenges related to performing and interpreting *in situ* mineralization studies where I highlight two key technical challenges within research: 1) electron beam sensitivity and beam effects and 2) collagen heterogeneity. Overall, this research contributes new tools to study biological structures and complex reactions at the nanoscale in hydrated conditions.

Future Work: With the advent of novel spacers and new MEMS designs to functionalize thin-liquid EM enclosures,[15–19] in future, I aspire that thin-film enclosures can be adapted to accommodate more liquid to visualize 3D mineralizing dynamics at HR with heating to better mimic physiological conditions. Moreover, another future avenue includes the potential of this technique to be used for tomography with similar microchip assemblies.[20,21] Tomography through liquid EM is anticipated to be key to revealing the hydrated ultrastructure of mineralized collagen and to studying more broadly hard tissues – sans fixation, freezing, and embedding. The advent of real-time fast-tomography methods for beam-sensitive samples through video acquisition instead of incremental angular changes,[22,23] opens the doors to visualizing 3D liquid EM biological dynamics live. This represents an exciting albeit challenging future direction for the future of liquid EM which could transform our understanding of biological specimens and materials.

References:

[1] K. Grandfield et al., *Adv Mater Sci Eng* 2012, *2012*, 1.
[2] F. A. Shah et al., *Acta Biomater* 2018, *84*, 1.
[3] B. E. J. Lee et al., *Chembiochem* 2021, *22*, 571.
[4] F. Nudelman et al., *J Struct Biol* 2013, *183*, 258.
[5] F. Nudelman et al., *Nat Mater* 2010, *9*, 1004.
[6] E. Macías-Sánchez et al., *Adv Funct Mater* 2022, *32*, 2200504.
[7] H. P. Schwarcz et al., *J Struct Biol* 2014, *188*, 240.
[8] B. E. J. Lee et al., *Adv Biology* 2021, *5*, 2100657.
[9] N. Reznikov et al., *Acta Biomater* 2014, *10*, 3815.
[10] N. Reznikov et al., *Science* 2018, *360*, eaao2189.
[11] B. D. Quan et al., *Bone* 2015, *77*, 42.
[12] W. J. Landis et al., *J Struct Biol* 1993, *110*, 39.

[13] M. J. Olszta et al., *Mater Sci Eng R Reports* 2007, *58*, 77.
[14] A. S. Deshpande et al., *Cryst Growth Des* 2008, *8*, 3084.
[15] J. Park et al., *Acs Nano* 2021, *15*, 288.
[16] G. Jonaid et al., *Adv Mater* 2021, *33*, 2103221.
[17] S. Pu et al., *Roy Soc Open Sci* 2020, *7*, 191204.
[18] D. F. Kelly et al., *Curr. Opin. Struct. Biol.* 2022, *75*.
[19] J. T. van Omme et al., *J Mater Chem C* 2020, *8*, 10781.
[20] W. J. Dearnaley et al., *Nano Lett* 2019, *19*, 6734.
[21] L. Kong et al., *Res Square* 2022, DOI 10.21203/rs.3.rs-1298112/v1.
[22] H. Vanrompay et al., *Ultramicroscopy* 2021, *221*, 113191.
[23] T. M. Craig et al., *Nanoscale* 2023, *15*, 5391.